Hot-melt extrusion with poorly soluble drugs

Inaugural-Dissertation

zur

Erlangung des Doktorgrades der

Mathematisch-Naturwissenschaftlichen Fakultät

der Heinrich-Heine-Universität Düsseldorf

vorgelegt von

Jessica Albers

aus Essen

Juni 2008

Aus dem Institut für Pharmazeutische Technologie und Biopharmazie

der Heinrich-Heine-Universität Düsseldorf

Gedruckt mit der Genehmigung der

Mathematisch-Naturwissenschaftlichen Fakultät der

Heinrich-Heine-Universität Düsseldorf

Referent: Prof. Dr. P. Kleinebudde

Korreferent: Prof. Dr. J. Breitkreutz

Tag der mündlichen Prüfung: 27.06.2008

Table of contents

Abbreviations

a	acidic	LJ	Lennard Jones
A	surface area	MD	Molecular dynamics
A	amorphous	MP	melting point [°C]
ACE	acetaminophen	MW	molecular weight
aPMMA	amino-polymethylmethacrylate	n	number of experiments, sample size
aPMMA*	ethyldimethylamine	NAP	naproxen
a.u.	arbitrary units	NF	National Formulary
b	basic	OXC	oxcarbazepine
BCS	Biopharmaceutical Classification System	P	partition coefficient
		P	PVP VA64® (COP)
C	Coulomb [kJ/mol]	P	Coulomb/Lennard Jones ratio
C	crystalline		
CAF	caffeine	PEG	polyethylene glycol
CD	cyclodextrine	PEN	pentoxyfylline
CEL	celecoxib	Ph. Eur.	European Pharmacopeia
const	constant	pK_a	-log acidity constant
COP	copovidone	PVA	polyvinyl alcohol
Cps	counts per second	PVP	polyvinylpyrrolidone
c_s	saturation solubility [mg/L]	R^2	coefficient of determination
c_t	concentration at time t [mg/L]	resp.	respectively
		RH	relative humidity [%]
D	diameter	rpm	revolutions per minute
D	diffusion coefficient	RT	room temperature
DSC	differential scanning calorimetry	S	solubility
		SD	standard deviation
E	Eudragit® E (aPMMA)	SDS	sodium dodecyl sulphate
^endo	endothermic peak	SEM	scanning electron microscopy
ETO	etofylline		
F	conveying	T 2nd	temperature at second heat scan [°C]
FT-IR	Fourier-transform infrared spectroscopy		
GFA	conveying element	T_g	glass transition temperature [°C]
GFF	conveying element		
GFM	combing mixer element	T_m	melting temperature [°C]
h	thickness of diffusion boundary layer	UV	ultraviolet
		V	volume [cm³]
H_f	heat of fusion [J/g]	var	varied
HB_{acc}	hydrogen bond acceptor	V_m	molar volume
HB_{don}	hydrogen bond donor	vdW	van der Waals
Hbond	hydrogen bond	w	weight fraction
HME	hot-melt extrusion	w/w	weight / weight
HPC	hydroxypropyl cellulose	XRPD	x-ray powder diffraction
HPMC	hydroxypropyl methyl-cellulose	δ	solubility parameter
		$δ_d$	partial solubility parameter for dispersion interaction
HPMCAS	hydroxypropyl methyl-cellulose acetate succinate		
I	isomalt (ISO)	$δ_h$	partial solubility parameter for hydrogen bonding
IBU	ibuprofen		
ICH	International conference on harmonization	$δ_p$	partial solubility parameter for polar interaction
i.e.	id est	$δ_{total}$	total solubility parameter
ISO	isomalt	$δ_v$	combined solubility parameter
JPE	Japanese Pharmaceutical Excipients		
		$Δδ$	difference between two solubility parameters
K	Kollicoat® IR (PEG-PVA)		
KB	kneading block	ρ	density [g/cm³]
L/D	length to diameter ratio	Θ	angle X-ray diffraction
LID HCl	lidocaine hydrochloride	USP	United States Pharmacopeia

1 Introduction

1.1 Bioavailability of poorly water-soluble drugs

The bioavailability is a measurement of the extent of a therapeutically active drug that reaches the systemic circulation and is available at the site of action. The bioavailability is mainly controlled by the delivery of the drug as determined by its pharmaceutical formulation, the solubility, and the permeability through the gut wall. In addition, the bioavailability can be decreased through decomposition of the drug in the gastrointestinal tract, by formation of non-absorbable complexes, by metabolization, or by premature elimination. These limitations can be influenced by physiological parameters of the gastrointestinal tract or the physicochemical properties of the drug and the formulation.

It is estimated that about 40% of all new chemical entities have poor bioavailability because of low aqueous solubility. This percentage still increases due to combinatorial chemistry and the impact of lipophilic receptors (Kerns 2001).

1.2 Reasons for poor aqueous solubility

The solubility of a substance is influenced by its physical and chemical properties with similar molecules having similar activities. This principle called structure-activity relationship was applied by Meylan and Howard to estimate the octanol-water partition coefficient (P) and the aqueous solubility (S) of drugs. They established a database (Meylan & Howard 1995) and derived from it an equation (Equation 1), which describes the aqueous solubility of a substance (Meylan & Howard 2000). For the estimation of logP values they developed a new fragment constant approach and included correction factors (fi), which were derived from the differences between the logP estimates from atoms alone and the measured logP values. They found out, that the melting point (MP) and the octanol-water partition coefficient as measures for the endeavour to crystallize and for the lipophilicity respectively, influence decisively the solubility of a drug.

$$\log S = -1.03 \log P - 0.011(MP - 25) + 0.34 + \Sigma fi$$
$$(n = 1450; R^2 = 0.97; fi = factor)$$

Equation 1: Calculation of the solubility of a substance; S = solubility, P = partition coefficient; MP = melting point; Σfi = summation of all correction factors

A concentration of 10 μg/mL is often given as a critical value for poor solubility (Shah et al. 1989). With a solubility below this value, problems in pharmacokinetics are likely to occur.

Schamp (2002) developed an equation for the prediction of solubility problems of drugs. According to this approach, the solubility drops below the critical concentration 10 μg/mL, if the sum of logP and MP/100 exceeds the value 4.5. One logP unit and a ΔT of 100 K for the melting point respectively, change the solubility by a factor of 10.

In addition to the solubility, the dose of a drug has to be taken into account also. At a very low dose the poor aqueous solubility of a drug does not always have a negative effect on the bioavailability. In such cases it is important to determine the dose-solubility volume (dose/c_s) (Amidon et al. 1995, Dressman et al. 2001). The calculated value determines the volume necessary to completely dissolve the drug.

1.3   Ways of solubility enhancement

In general, there are both chemical and physical ways to improve the solubility of a drug. The formations of soluble salts, like ibuprofen-lysinate instead of ibuprofen, or prodrugs, for instance sulfamoyl sulfonate prodrugs, are chemical tools, which are often found in pharmaceutical formulations. Physical methods to improve the dissolution rate can be derived from the equation by Noyes and Whitney (Noyes & Whitney 1897):

$$\frac{dc}{dt} = \frac{A \cdot D \cdot (c_s - c_t)}{V \cdot h}$$

Equation 2: Equation according to Noyes and Whitney

In this equation dc/dt is the dissolution rate, A is the surface area, D is the diffusion coefficient of the compound, c_s is the solubility of the compound in the dissolution medium, c_t is the concentration of drug in the medium at time t, V is the volume of the medium, and h is the thickness of the diffusion boundary layer adjacent to the surface of the dissolving compound. According to this equation there are two main possibilities of improving the dissolution rate of a drug by physical influence. First, A can be increased by micronizing the compounds or changing the surface properties, thus, increasing the wettability of the particles. The second method is to increase the apparent c_s by changing to modifications with higher energetic states or by addition of solubility enhancing excipients.

In an early stage of development the solubility of a poorly water-soluble drug can be changed by chemical methods, like salt selection, prodrug formation, or change of the modification (Figure 1.1). If the chemical design of the drug is brought to a close, formulation approaches

have to be undertaken. The simplest way to enhance the solubility is to micronize the poorly soluble drug through pin, ball or jet milling. A property, which is accompanied by the increase of the surface area, is the increase of wettability which can be realized by the use of surfactant in the formulation. If these standard formulation approaches fail, advanced approaches need to be used. Depending on the pharmaceutical dosage form, several methods are available (Figure 1.1).
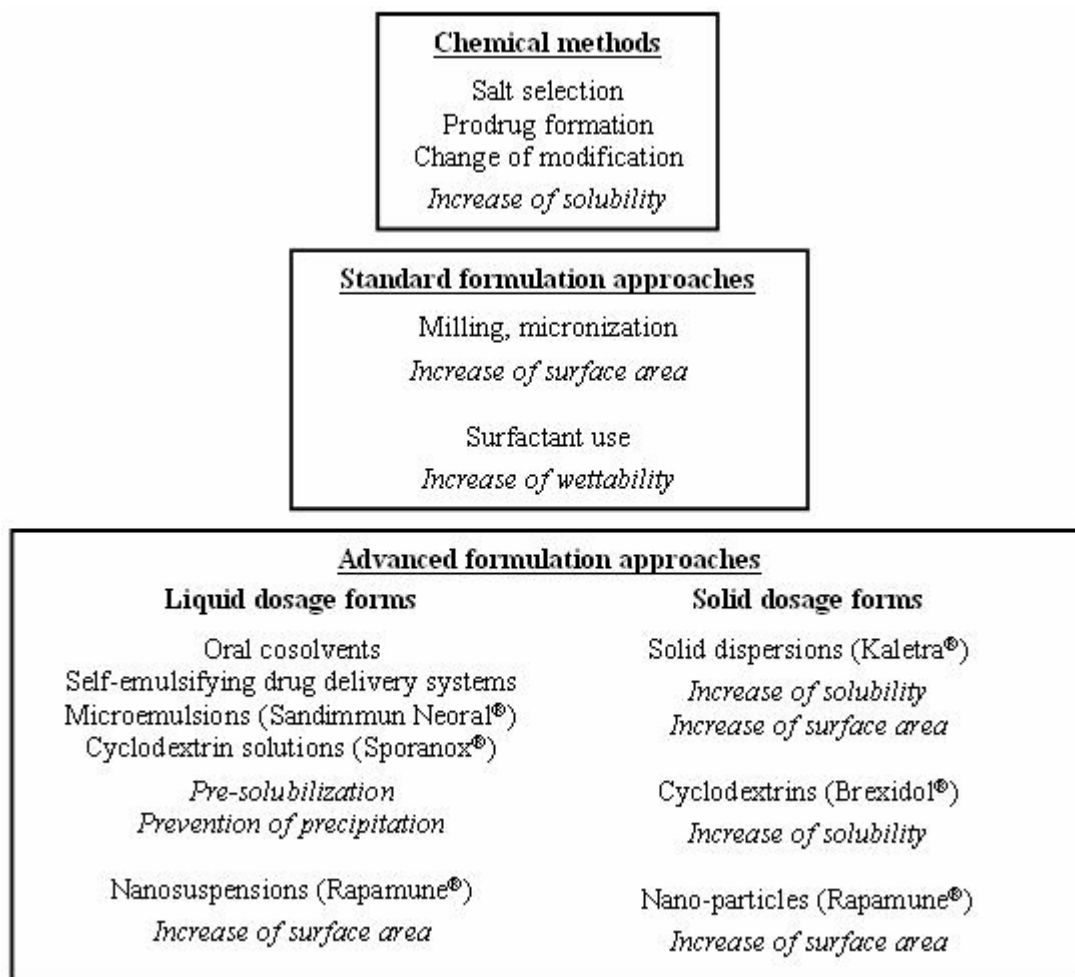
Figure 1.1: Strategies for solubility enhancement of poorly water-soluble drugs

Two main strategies can be observed in enhancing the solubility of poorly water-soluble drugs. On the one hand, the drug is pre-solubilized in a liquid dosage form, like in self-emulsifying drug delivery systems or microemulsions. When such formulations are released into the lumen of the gut, they disperse to form a fine emulsion, so that the drug remains in solution. Thus, the dissolution step, which often limits the rate of absorption of the drug, can be avoided (Pouton 1997, Constantinides 1995). On the other hand, the drug is transferred into its amorphous state, or dispersed on a molecular basis in solid dosage forms, maximizing

the surface area that comes into contact with the medium during dissolution. Thus, the solubility of the drug is improved, but the drug is not prevented of precipitation.

Solid dispersion formulations show a great variety relating to the state of the solid dispersions and the technique to produce them (Chiou & Riegelman 1971, Sethia & Squillante 2003). This is demonstrated by the number of products present on the market: Certican[®] tablets (everolimus / HPMC), Cesamet[®] tablets (nabilone / PVP), Gris-PEG[®] tablets (griseofulvin / PEG), Isoptin[®] SR-E (verapamil / HPC / HPMC), Nivadil[®] tablets (nivaldipine / HPMC), ProGraf[®] capsules (tacrolimus / HPMC), Rezulin[®] tablets (troglitazone / PVP), Sporanox[®] capsules (itraconazole / HPMC).

Nano-particles can be produced by high pressure homogenization, wet ball milling or precipitation and can be incorporated into tablets for oral delivery (Mueller 2001). Cyclodextrin formulations are quite common complexation aids to enhance solubility. Cyclodextrins are molecules with a great variety resulting in about 100 different CD-derivatives commercially available (Szente 1999).

However, the most frequent strategy for increasing the dissolution rate is the improvement of solubility through advanced formulation approaches. The method of solid dispersion formulation has been used in this work on solubility enhancement and will, therefore, be addressed in greater detail in the following chapters.

2 Outline and goal of this work

The main objective of this thesis was to establish the hot-melt extrusion technique for solubility enhancement. In this context attention was focussed on the elucidation of the mechanism of drug release from melt embeddings, the understanding of physico-chemical processes taking place during hot-melt extrusion, the prediction of drug carrier miscibility, and the thermodynamical stability of those systems. Specific aims were:

-To develop a formulation for improving solubility of a poorly water-soluble drug

In a first step various excipients were examined for suitability as solubility enhancers in melt embedding processes. To find suitable carriers, different tools like solubility parameter calculation, theory of Gordon-Taylor, differential scanning calorimetry, hot stage microscopy, and intrinsic dissolution were employed. The behaviour of the molten samples was compared to the behaviour of the respective physical mixtures to examine the effect of the melting process. Furthermore, it was evaluated whether the coevaporation technique results in similar products as the hot-melt extrusion technique.

-To optimize the hot-melt extrusion technique for solubility enhancement of a poorly soluble drug and to prove the applicability of the technique for different carriers and drugs

The hot-melt extrusion process, which was chosen as technique for melt embedding, had to be optimized regarding process parameters like screw configuration, die plate design, temperature setup and formulation parameters like drug carrier fitting, and drug load. The influence of process parameters and formulation on the resulting products was investigated. Physical and chemical processes taking place in the melt embeddings were analyzed with differential scanning calorimetry, Fourier-transform infrared spectroscopy, and X-ray powder diffraction.

-To elucidate the mechanism of solubility enhancement in hot-melt extruded products

The solid state of the extrudates was evaluated with differential scanning calorimetry, X-ray powder diffraction, and scanning electron microscopy and was correlated with the in-vitro dissolution behaviour. The mechanism of drug release from melt embeddings was elucidated with the help of solid state characteristics and the interpretation of the dissolution process.

-To find rules to predict the miscibility of drugs and carriers and to correlate these predictions with the hot-melt extrusion process

As the miscibility of drug and carrier plays a decisive role in melt embedding, tools for the prediction of miscibility were developed. These approaches were based on the chemical understanding of interactions occurring in melt embedding and the chemical and physical characteristics of basic materials, physical mixtures and molten products. Tools to investigate these characteristics and interactions involved solubility parameter calculation, molecular dynamics simulations, and thermoanalytical characterization.

-To solve stability problems and avoid recrystallization during dissolution

A main objective in melt embeddings is the thermodynamic stability of the products. Therefore, a great part of this study deals with the stability of melt embeddings and the inhibition of recrystallization on mechanical input, storage, and dissolution.

-To produce solid dosage forms

The formation of solid dosage forms from melt embeddings is a great challenge, since the characteristics of the material are different from those usually applied to the production of solid dosage forms. As the dissolution rate in those systems is mainly controlled by the solid state characteristics of the drug, mechanical influences during processing have to be taken into account.

3 General issues

3.1 Solid dispersions as a method of solubility enhancement

Solid dispersions are defined as the dispersion of one or more active ingredients in an inert carrier or matrix at solid state, prepared by the melting, solvent or melting-solvent method (Chiou & Riegelman 1970). Solid dispersion is the general term for several categories which can be characterized as follows (Table 3.1):

Table 3.1: Classification of solid dispersions according to Maegerlein (2005)

	glassy solid solution	solid solution	glass suspension	eutectic		amorphous precipitation
phases	1	1	2	2	2	2
drug	molecularly dispersed	molecularly dispersed	amorphous	crystalline	crystalline	amorphous
carrier	amorphous	crystalline	amorphous	amorphous	crystalline	crystalline

According to Chiou and Riegelman (1970), a solid solution, as against a liquid solution, is made up of a solid solute dissolved in a solid solvent. In a glassy solid solution the solute molecules are dispersed molecularly within a glassy solvent, in a solid solution molecules are dispersed within a crystalline solvent. In such systems the drug's particle size has been reduced to its absolute minimum. Glass suspensions consist of two phases: the amorphous carrier and the drug either in the amorphous or the crystalline state. In a eutectic, both, the carrier and the drug, occur in the crystalline state. Like glass suspensions amorphous precipitations have two phases, whereas in this case the drug is present in the amorphous and the carrier in the crystalline form.

Solid dispersions can be prepared either by the solvent or the melting method or by a combination of the two. In the solvent method drug and carrier are dissolved in a common solvent, which is evaporated under vacuum, resulting in solid dispersions. Tachibani and Nakumara (1965) were the first to implement this method to produce solid dispersions. With the melting method, which was first used by Sekiguchi and Obi (1961), drug and carrier are molten and cooled through a common method to obtain solid dispersions.

3.2 Production of solid dispersions by hot-melt extrusion

Hot-melt extrusion (HME) is the process of transferring a powder blend of drug and carrier by a rotating screw through the heated barrel of an extruder and pressing the melt through a die into a product of uniform shape (McGinity & Zhang 2003). HME was first introduced in the plastics industry in the mid-nineteenth century to apply polymeric insulation coatings to wires (Crowley et al. 2007). First applications of HME as a manufacturing tool in the pharmaceutical industry were realized by Doelker et al. in 1971 (Doelker 1971).

Until now, several research groups have demonstrated HME as a viable method to prepare pharmaceutical drug delivery systems (Breitenbach 2002, McGinity & Zhang 2003, Leuner 2004, Repka et al. 2007), because it offers many advantages over other techniques. HME represents a fast, continuous manufacturing process without requirements of further drying or discontinuous process steps. The high flexibility of the process features enables the production of single- and multi-particulates. The short thermal exposure of the drug allows the processing of heat sensitive actives. Additionally, the process temperature can be reduced by adding plasticizers (McGinity & Zhang 2003, Zhu et al. 2002), compressed gas (Verreck et al. 2006a, Verreck et al. 2006b), or by employing the plasticization effect of actives on the polymer (Repka et al. 1999). Different working principles of extrusion exist, whereas screw extrusion is mainly applied in pharmaceutical processing. A screw extruder provides high shear stress and intense mixing and can therefore handle high drug loads (van Lengerich et al. 2007). These machines exist as single-screw or twin-screw extruders. The single-screw extruder is the most widely used extrusion system in the world and has the advantage of a high pressure build-up and generation of mechanical energy to induce specific modifications of the product. Twin-screw extruders allow different configurations and enable different conditions in all zones of the extruder. In such systems the screws can either rotate in the same (co-rotating) or the opposite (counter-rotating) direction. Counter-rotating designs are utilized where very high shear forces are needed. As the material is squeezed through the gap between the two screws, the material is exposed to high shear forces where the screws come together. Additionally, the layout is beneficial for dispersing particles in a blend. Disadvantages of this design are potential air entrapment, low maximum screw speeds and output. Co-rotating twin-screw extruders, on the other hand, are the most important type of extruders in industry. They can be operated at high screw speeds resulting in high outputs, while maintaining good mixing and conveying characteristics.

3.3 Patent situation

The number of hot-melt extrusion patents issued for pharmaceutical applications has decisively increased since 1983 (Figure 3.1). The greatest part of these patents originates from Germany and the United States, followed by Japan, France, and the UK (Figure 3.2).
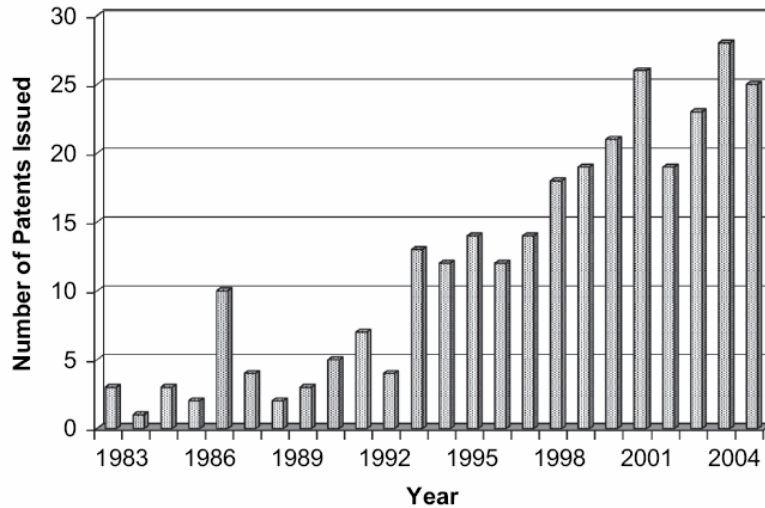
Figure 3.1: The number of hot-melt extrusion patents for pharmaceutical applications from 1983 to 2006 (Crowley 2007)
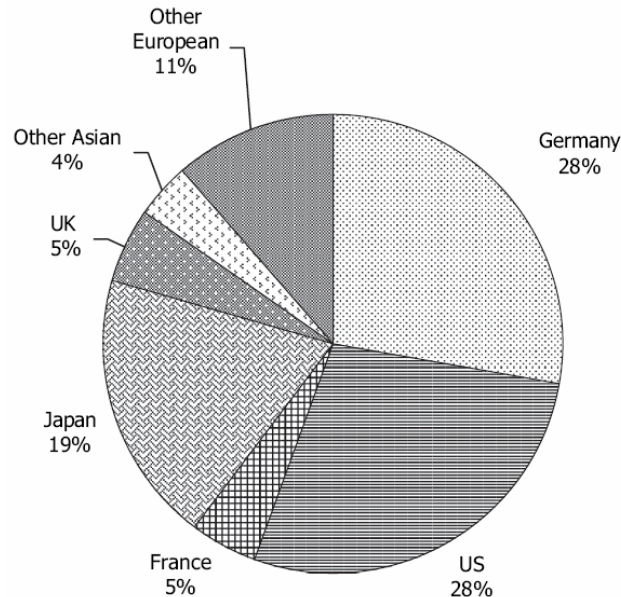
Figure 3.2: The number and percentage of hot-melt extrusion patents issued by country since 1983 for pharmaceutical applications (Crowley 2007)

This high number of patents issued in the last few years reflects the great international interest in the pharmaceutical application of hot-melt extrusion. This fact entails a challenge, namely to develop new approaches in respect of formulations and processing.

4 Results and discussion

4.1 Hot-melt extrusion process

4.1.1 Introduction and objective

In this study, solid dispersions were produced via hot-melt extrusion. During this process a powder blend of active drug substance and carrier is transferred by rotating screws through the heated barrel of the extruder. This process is mainly determined by the configuration of the screw, the heating profile of the barrel, the feeding rate of the powder blend, and the design of the die plate. Depending on the screw configuration, the screw speed can have an effect on the properties of the product also.

Recent studies by Nakamichi et al. (2002) showed that especially the configuration of the screw plays an important role in changing the crystallinity and the dissolution properties of a solid dispersion. In their study they collected extrudate samples from processes with and without kneading elements and investigated the usefulness of these elements for hot-melt extrusion. Furthermore, they examined the influence of the screw revolution speed in combination with the configuration of the screw.

They found that samples prepared with kneading elements with an advance angle of 60° were transparent and exhibited supersaturation on dissolution testing. Detaching the kneading elements from the screw and operating only feed screw elements, the crystallinity could be reduced and the dissolution rate increased in comparison to the physical mixture, but no supersaturation occurred.

In case where kneading elements were used, a transparent mass was produced, irrespective of the screw revolution speed, and an enhanced dissolution profile was obtained. However, in case where the screws consisted of feed screw elements alone, the physicochemical state and the dissolution profiles of the treated samples were different. As the feed screw elements only transport the material, a slower screw speed achieves a longer residence time of the material in the heated barrel which supports a good dispersion of the drug in the polymer matrix. This leads to a lower crystalline state and a higher dissolution rate.

Yoshinaga et al. (2000) also reported that highly efficient kneading is necessary and that the kneading elements have marked effects on the residence time and high shear mixing, and facilitate dispersing the drug in the polymer.

Following the results of these studies, the configuration of the screw for the preparation of solid dispersions was developed. Besides the feed screw elements, kneading elements were installed into the screw.

As only little information can be found about the influence of the die plate design on the hot-melt extrusion process (Scharf 2008), the objective of this study was to optimize the extrusion process by variation of the die plate design.

4.1.2 Extrusion parameters and die plate design

The screw (Chapter 7.2.1.3) has a diameter of 18 mm and consists mainly of conveying and kneading elements (Figure 4.1). The conveying elements at the beginning and at the end take on the feeding of the powder blend into the barrel and the transporting of the melt to the die plate. The kneading elements in the middle, which generate shear forces and therefore a mechanical energy input, support the melting process and provide the homogenization of the melt. The combing mixer element and the smaller kneading unit at the end of the screw maintain the homogeneous melt before it reaches the die plate. In general, kneading elements with a high advance angle have higher mixing and shearing properties than the smaller ones. Therefore, the first kneading unit consists of four elements with three increasing twist angles of 30°, 60°, and 90°, which result in an optimal mixing and shearing of the powder blend.
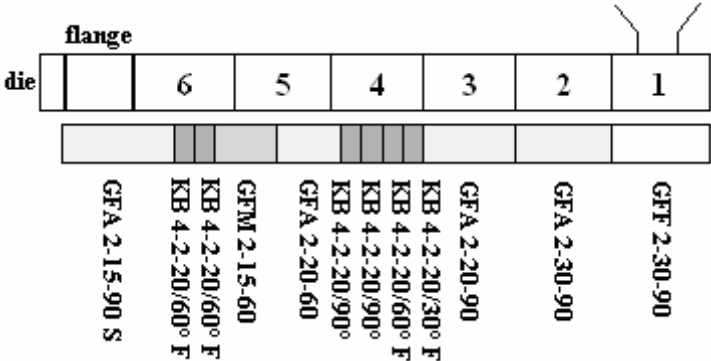
Figure 4.1: Extruder barrel, configuration of the screw, and position of the screw elements; GFF & GFA = conveying elements, GFM = combing mixer element, KB = kneading block

The barrel of the extruder has a length of 30 times the screw diameter (30D) resulting in a barrel length of 54 cm. The barrel consists of six separately heatable zones and a heatable die plate. The first zone of the barrel (Figure 4.1) cannot be heated and therefore, acts as powder intake only. The second and third zone should not be heated to high temperatures, because they are too close to the feeding zone. If the powder blend is molten before it is drawn back into the barrel, the feeding zone blocks. While the feedstock is moved along the barrel, thermal energy is generated by shearing, caused by the rotating screws, as well as by electrical heating bands of the barrel. In the fourth and fifth barrel the maximum temperature is reached. In combination with the shear forces of the kneading elements the powder blend is molten, even if the temperature of the barrel is below the melting point of the powder. The sixth zone

acts as bridge leading to the flange and thus the die plate. With the temperature of this flange the viscosity of the melt at the point of withdrawal from the die can be controlled.

During the hot-melt extrusion process the temperature of barrels four and five is increased until a transparent strand is obtained. As a second step the temperature of the flange is decreased until the transparent strands exhibit the right viscosity to leave the die plate as non-sticking, semisolid products.

The throughput of the material and the pressure at the die plate can be controlled by the feeding rate of the powder blend. In this study the feeding rate varies depending on the carrier used and lies between 0.3 and 1.0 kg/h (chapter 7.2.1.3). Extruding with a pressure of about 20 bar at the die plate leads to strands of sufficient viscosity to obtain semisolid strands.

The customary die plate, which is often used for hot-melt extrusion, consists of the die plate and a cone which serves as a crossing to the flat screw tips (Figure 4.2). This cone is responsible for the even distribution of the melt to the dies. Between the screw and the customary die plate dead storage capacity emerges, which caused the melt to dam up before leaving the die.

Figure 4.2: Comparison of standard and new die plates

Caused by this accumulation the die plate blocked and the collected melt recrystallized. In order to avoid this, special die plates were designed.

The new construction consists of two die plates (Figure 4.3). The first one has only one die in the middle of the plate. It has a diameter of 7 mm and collects the melt from the cylinder in only one strand. Because of the flat design of the die plate no dead storage capacity emerges and the molten product cannot accumulate. Thus, the melt does not recrystallize before leaving the die plate. The large diameter prevents blocking, because resistance given by the die plate is only small.

The second plate possesses a star-shaped depression on its reverse with eight dies sized 1 mm at the ends. The melt fed through the first die plate hits the second plate in the centre and is then distributed through the star-shaped depression to the dies. Through these the melt leaves the plate as semisolid strands. With the help of this design, the dead storage capacity is kept at a minimum (Figure 4.2) and blocking of the dies can be avoided.
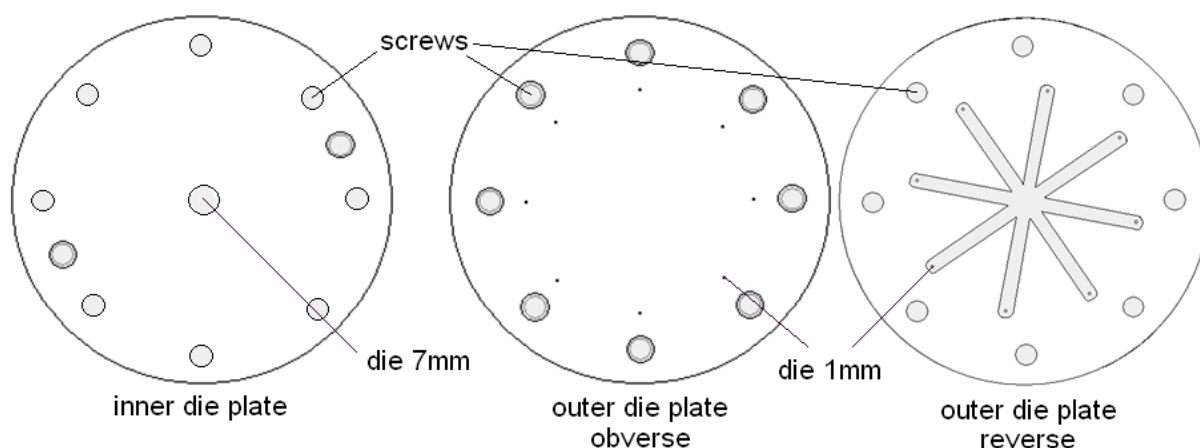
Figure 4.3: Design of new die plate

The shape of the die dictates the physical shape of the strands. Upon leaving the die the cross section of the extrudates increases depending on the viscoelastic properties of the polymers. This phenomenon is known as "die swell" and occurred in all formulations (Crowley et al. 2007). This entropy-driven event can be observed when individual polymer chains recover from deformation caused by the rotating screws.

Strands leaving the die were collected manually, cooled at room temperature and manually broken into smaller fragments. Caused by the die swell phenomenon and the way of collecting the strands, the diameter of the extrudates varied between the formulations and within each batch.

4.1.3   Influence of the die plate design

In order to scrutinize the importance of the extrusion parameters and of the die plate design respectively, the experiments with the customary and the new die plate are compared below.

Blends of basic butylated methacrylate copolymer (aPMMA) and acetaminophen (ACE) with drug loads of 10% and 30% were extruded on a Leistritz extruder (7.2.1.3) with the customary and the new die plate. Both plates had eight dies with a diameter of 1 mm. Transparent glassy solid solutions with a drug load of 10% can be produced with both die plates. In contrast, differences can be observed for the formulation with 30% ACE. With the new die plate a glassy solid solution is obtained. With the customary die plate the strands have an opaque appearance, which indicates a crystalline state. Figure 4.4 shows the XRPD patterns of the two extrudates. The extrudates produced with the new die plate have an amorphous state whereas the extrudates produced with the customary die plate are partially crystalline.
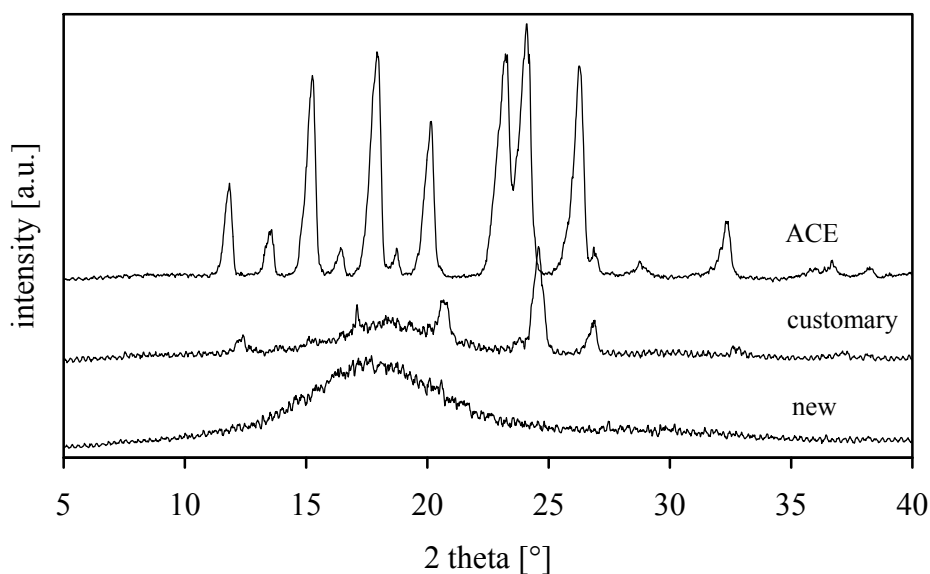
13

Figure 4.4: XRPD patterns of ACE, aPMMA/ACE 30% solid dispersion produced with customary die plate, aPMMA/ACE 30% solid dispersion produced with new die plate

During the process the screw speed was varied in order to test its influence on the solid state of the strands. For none of the formulations a change in solid state could be observed. As described by Nakamichi et al. (2002) the screw speed had no influence on the solid state of the transparent extrudates when kneading blocks were part of the screws.

4.1.4 Summary

These results show that the hot-melt extrusion process is influenced by several parameters, and that the right coordination of these parameters is decisive for the production of solid dispersions.

The solid state and the viscosity of the extrudates can be controlled by the temperature of the barrels. Besides the configuration of the screw and the temperature profile of the barrel, the design of the die plate represents the third important extrusion parameter. By keeping the dead storage capacity at a minimum, an early solidification and thus a blockage of the dies can be prevented. In comparison with these main extrusion parameters the screw speed plays a minor role. The diameter of the extrudates is difficult to adjust as most polymers show viscoelastic properties.

4.2 Solubility enhancement of celecoxib by hot-melt extrusion with basic butylated methacrylate copolymer

4.2.1 Introduction and objective

The goal of these experiments was to produce solid dispersions with a poorly water-soluble drug via hot-melt extrusion in order to improve the drug release. The drug in a solid dispersion can appear as a separate amorphous or crystalline phase or can be dispersed on a molecular basis. Whether molecular dispersion of the drug in the carrier is the best system to enhance dissolution cannot be affirmed generally, as solubility improvements by all systems are known in literature (Urbanetz 1999, Law et al. 2000, Sethia & Squillante 2003). Therefore, the influence of the solid state on the drug release was tested. The drug load was supposed to be as high as possible and the number of excipients was to be kept at a minimum. The temperature had to be as low as possible in order to prevent decomposition processes.

First experiments were performed with the poorly water-soluble BCS Class II (Yazdanian et al. 2004) drug celecoxib (CEL), which has a solubility of 2.6 mg/L in water and 3 mg/L in 0.1 N HCl (Table 8.1. appendix). Besides the poor aqueous solubility, CEL exhibits manufacturing and handling problems due to its cohesive needle-shaped crystals (Banga et al. 2007), having high surface energy and electric charge. CEL forms metastable polymorphs with negligible difference in melting point (Figure 8.1 appendix). These metastable forms are easily revertible to the stable form (Ferro & Miyake 2001). The low aqueous solubility contributes to high variability in absorption after oral administration (Paulson et al. 2001). Thus, it is important to improve the solubility and dissolution rate of CEL to improve its bioavailability.

Carriers for the production of solid dispersions via the melting method have to meet several requirements. In general, carriers should be non-toxic and pharmacologically inert. They should be chemically and physically stable at melting with a low melting point. Further prerequisites are the chemical compatibility with the drug, the miscibility with the drug in the liquid state, and the ability to increase the aqueous solubility of the drug. This can be obtained by assessing water-soluble excipients with a rapid dissolution. Excipients with a high number of functional groups are able to form hydrogen bondings, van der Waals forces, and electrostatic interactions. A low water uptake, a high viscosity, and a high glass transition support a good stability.

In a first step various excipients were examined for suitability as solubility enhancers in melt embedding processes. To find suitable carriers, different tools like solubility parameter calculation, theory of Gordon-Taylor, differential scanning calorimetry, hot stage microscopy, X-ray powder diffraction, and intrinsic dissolution were employed (Table 8.2 to Table 8.5 and

Figure 8.2 to Figure 8.7 appendix). As a result of these preliminary investigations, basic butylated methacrylate copolymer (aPMMA) exhibited the best solubility improvement for CEL. The solubility enhancing effect of aPMMA on CEL could be obtained by the melting (chapter 7.2.1.1) as well as by the solvent method (chapter 7.2.1.2) (Figure 8.8 and Figure 8.9 appendix). The preliminary tests showed that intrinsic dissolution is one of the critical tests to ensure predictability of solubility enhancement.

4.2.2 Extrusion with basic butylated methacrylate copolymer

Basic butylated methacrylate copolymer (aPMMA) is a suitable carrier for hot-melt extrusion (Leuner & Dressman 2000, Six et al. 2004). The glassy substance has a T_g at 44 °C and can therefore be easily processed into non-sticking transparent strands. aPMMA itself is stable at higher temperatures and can be processed up to at least 200 °C without any decomposition problems (Figure 8.2). After cooling at room temperature, the polymer forms hard, brittle strands.

The Gordon-Taylor equation is one means of predicting the T_g of a drug carrier blend in miscible systems based on the T_g, the densities, and the weight fractions of the pure components. Theoretical and experimental T_g of drug carrier blends were compared to evaluate the influence of the drug content on the T_g of the blend.

Often, drugs have a plasticizing effect on the polymers (Repka et al. 1999). They settle between the polymer chains and decrease the interaction between the polymer molecules. The chains become more flexible and the glass transition temperature of the polymer decreases. In the case of celecoxib (CEL) and aPMMA both a plasticizing and an antiplasticizing effect can be observed (Figure 4.5). At a drug content of up to 25%, the drug has a plasticizing effect on the polymer as the T_g of the blend is below the T_g of the pure polymer. At higher drug contents CEL has an antiplasticizing effect on the polymer. From 60% drug content onward, the T_g reaches the T_g of the pure amorphous drug, which indicates that the properties of the drug predominate. A 1:1 (molar fraction with aPMMA monomer) blend of CEL and aPMMA has a drug content of 60%. At drug loads higher than 60% CEL is present in a surplus thus, predominating the properties of the melt.
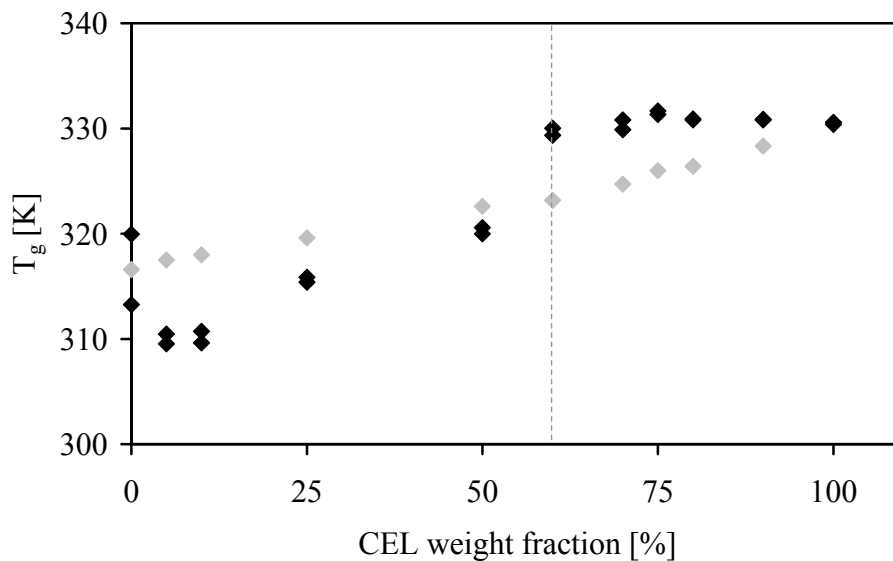
16

Figure 4.5: Influence of CEL drug load on the glass transition temperature of the carrier aPMMA; black symbols = experimental T_g, grey symbols = expected T_g according to Gordon-Taylor (Forster et al. 2001c) (ρ_{CEL} = 1.40 g/cm³, ρ_{aPMMA} = 1.11 g/cm³); broken line indicates 1:1 molar fraction

Besides the drug, water can have a plasticizing impact on the polymer. This impact results from the water uptake of the respective polymer. Especially polymers with hydrophilic functional groups tend to take up a high amount of water. Additionally, water has a negative effect on the stability of amorphous substances. Amorphous forms represent metastable systems which are more stable if the glass transition temperature is high. As water can decrease the T_g, the amorphous system tends to recrystallize earlier.

Therefore, the water uptake of the drug melt, of the carrier melt, and of the molten 1:1 blend of both substances was examined. All samples were stored under two different conditions: at 25 °C over silica gel and at 40 °C, 75% relative humidity. Figure 4.6 shows that the water uptake of all samples is below 2% and therefore quite low. The pure carrier melt and the molten blend take up small amounts of water when stored at 75% relative humidity. The pure drug melt is unbiased as the amount of water is the same under both storage conditions. Amorphous CEL recrystallizes within the first few days after production. Therefore, the data represent rather the water uptake of the crystalline drug and not of the amorphous form.

In this case, the properties of the blend are more strongly influenced by the properties of the carrier as their behaviour towards water uptake is more alike than compared to the pure drug melt. Overall, the effect of water seems to be negligible for systems with aPMMA.
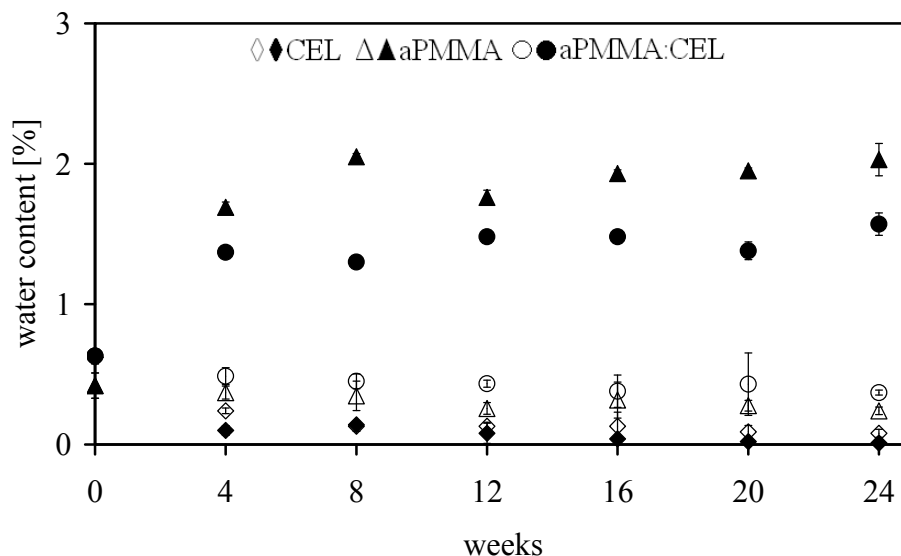
Figure 4.6: Water uptake of CEL melt, aPMMA melt, and molten blend of CEL and aPMMA 1:1 examined by Karl-Fischer titration; open symbols represent storage at 25 °C over silica gel, closed symbols represent storage at 40 °C, 75% relative humidity; ♦ = ● (0 weeks), mean ± SD; n=3

4.2.3 Influence of the solid state characteristics

Transparent extrudates with a drug load of 50% can be produced with the temperature profile described in Figure 4.7. The maximum temperature of 157 °C lies 5 °C below the melting point of CEL. As CEL is soluble in the molten carrier it is not necessary to reach the melting temperature of the drug. The shear forces acting in the two barrels ensure the mixing of CEL and aPMMA, so that the drug is partially molten and additionally dissolved in the molten carrier.
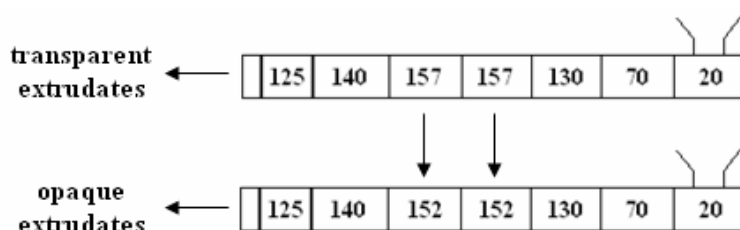
Figure 4.7: Temperature profiles of the extruder barrel for the production of transparent and opaque strands of CEL/aPMMA 1:1 (w/w)

Decreasing the temperature in the centre leads to opaque strands of CEL and aPMMA. Transparent and opaque extrudates are examined by DSC, in order to determine whether the drug is completely molten or dissolved in the carrier or whether crystalline amounts are still detectable. Figure 4.8 shows the DSC patterns of the transparent and opaque extrudates. For

the transparent extrudate a single glass transition temperature at 53 °C only is observed while for the opaque sample a T_g at 53 °C and, additionally, an endothermic melting peak at the melting point of CEL is detected. The melting point of the pure drug is 25 °C above this peak which indicates an interaction of the drug with the molten carrier. These results point to an amorphous one-phase system for the transparent and an amorphous and crystalline two-phase system for the opaque extrudates.

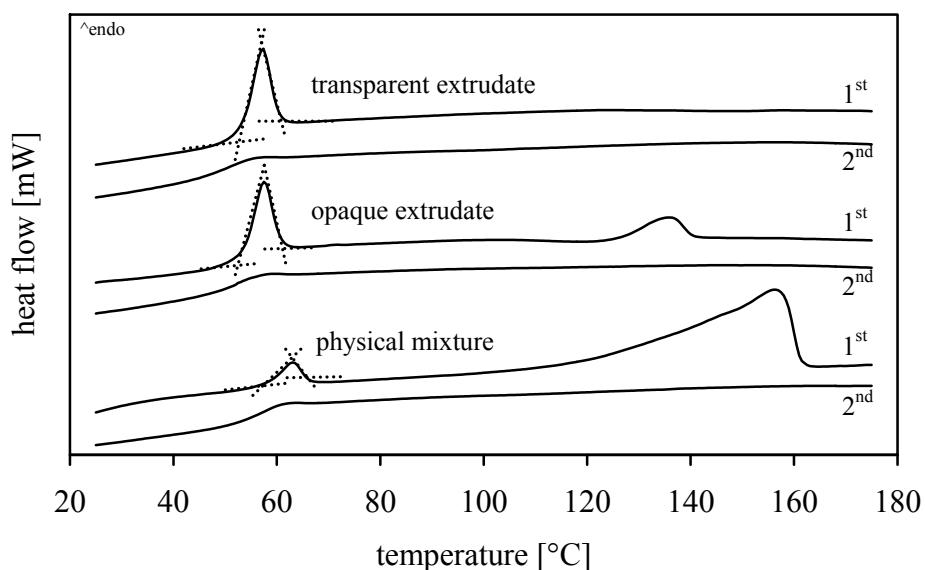Figure 4.8: DSC patterns of transparent and opaque CEL/aPMMA 1:1 (w/w) extrudates and CEL/aPMMA 1:1 (w/w) physical mixture; 1st indicates first heat scan, 2nd second heat scan; heating rate 10 K/min

Extrudates were characterized regarding their dissolution behaviour in 0.1 N HCl under non-sink conditions employing the paddle method according to Ph.Eur. for 30 minutes. The drug release from the opaque extrudate results in a low supersaturation within the first 10 minutes whereas the transparent extrudate reaches a high supersaturation (Figure 4.9). Subsequently, both extrudates show similar profiles. As the dissolution of both extrudates ends up with the same dissolved drug amount after 10-15 minutes the physical state of the drug in the carrier has a subordinate influence on the second part of the dissolution profile.

Amorphous substances have a higher solubility than the corresponding thermodynamically stable crystalline forms, because their internal bonding forces are weaker. Solutions derived from amorphous forms are supersaturated, and crystallization begins as soon as a crystal of the stable form develops. This process is triggered off when the amorphous drug gets into contact with the dissolution medium.
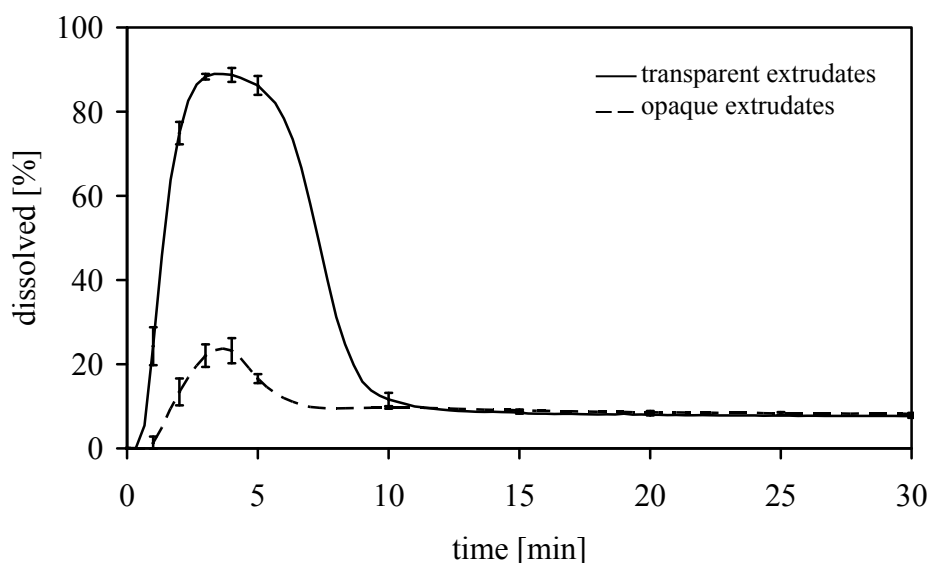
Figure 4.9: Dissolution profiles of transparent and opaque extrudates; 200 mg drug; 0.1 N HCl, non-sink conditions, 37 °C, paddle, 50 rpm, 250 nm; mean ± SD, n=3

4.2.4 Testing of drug load

Poorly water-soluble drugs often have to be administered in a high dose. Therefore, only a small amount of excipients can be added to the formulation in order to preclude difficulties relating to patient compliance. Thus, it is important to be able to produce solid dispersions containing as much of the active substance as possible. The maximum load with CEL for aPMMA was tested by intrinsic dissolution studies. Compacts with drug loads of 5, 10, 25, 50, 62.5, 75, and 100% (w/w) were dissolved in 0.1 N HCl + 0.15% cetrimid, and the dissolution rate was deduced from the slope of the particular dissolution profiles.

As shown in Figure 4.10 the dissolution rate is controlled by the drug/carrier ratio of the formulation. The dissolution rate increases with increasing the drug amount in the blend up to a drug load of 50% and decreases markedly from amounts higher than 50%. This examination shows that the maximum drug load for the CEL/aPMMA blend lies between 50 and 62.5%. This observation leads to the assumption that the improvement of drug release is based on a chemical interaction between drug and carrier. As a stoichiometric 1:1 proportion of CEL and the aPMMA monomer is realized at a drug load of 60%, the results indicate that above this drug load a surplus of crystalline drug is present in the formulation which sets off recrystallization and, therefore, dominates the dissolution properties of the solid dispersion.
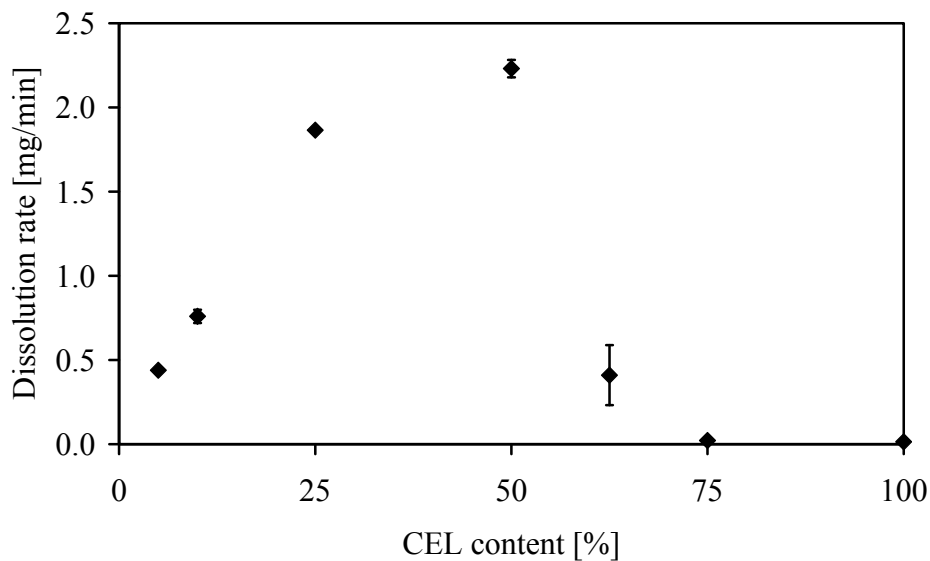
Figure 4.10: Preliminary testing of the influence of the drug content on the dissolution rate of the solid dispersion; mean ± SD, n=3

As additional shear and mixing forces in the extruder might enable a higher drug load, this assumption was verified in an extrusion process. Therefore, a blend with a drug content of 62.5% was extruded. The resulting strands were opaque and showed a partially crystalline structure in the XRPD pattern (Figure 4.11).
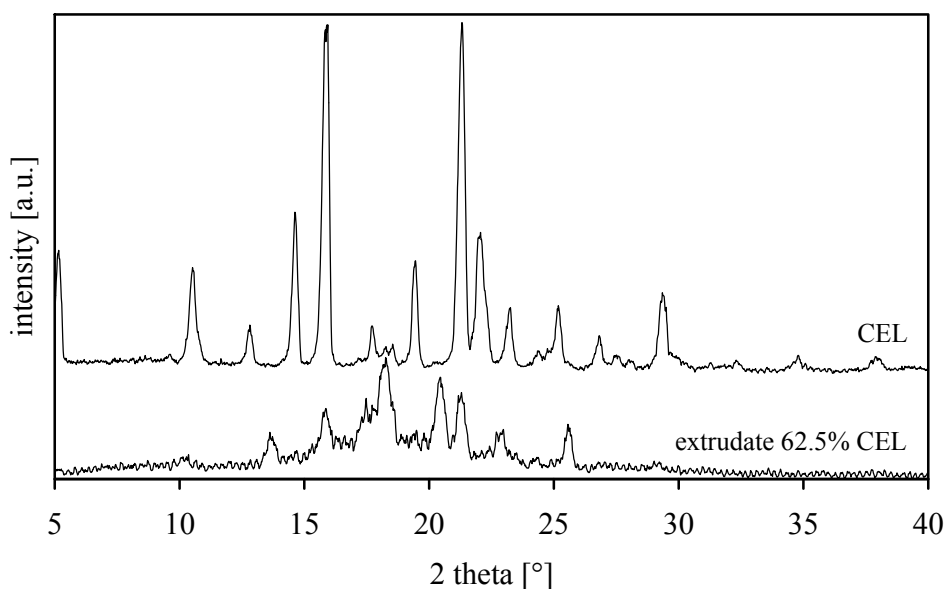
Figure 4.11: XRPD patterns of pure CEL and aPMMA/CEL 62.5% (w/w) extrudate

Drug release from the extrudates with a drug load of 62.5% resulted in a much lower supersaturated solution than drug release from the transparent strands with a drug load of 50% (Figure 4.12). This result is similar to the dissolution profile of the opaque strands shown in

Figure 4.9. Thus, preliminary testing of the drug load by intrinsic dissolution studies is a helpful tool to predict the maximum drug load of a formulation.
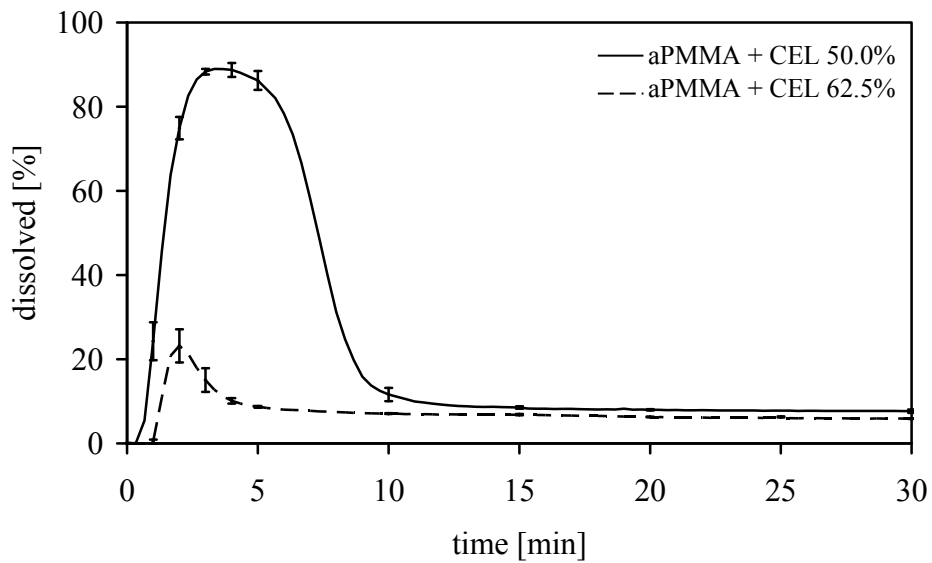
Figure 4.12: Drug release from extrudates with 50% (w/w) and 62.5% (w/w) drug load; 200 mg drug; 0.1 N HCl, non-sink conditions, 37 °C, paddle, 50 rpm, 250 nm; mean ± SD, n=3

4.2.5   Physical and chemical characterization of extrudates

Figure 4.13 shows the DSC patterns of aPMMA, CEL, the physical mixture, and the extrudate. The type and position of the thermal signal explain the solid state characteristics of the solid dispersion.
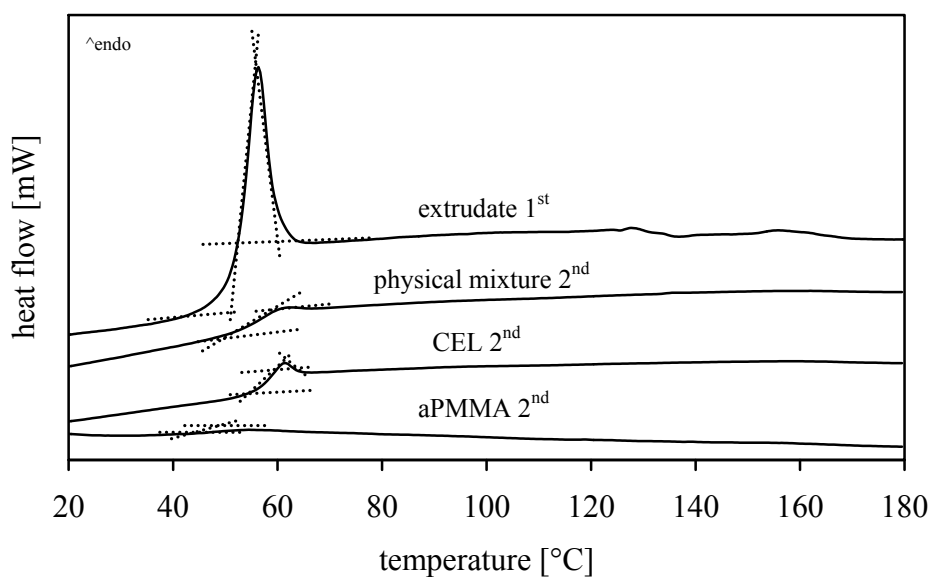
Figure 4.13: DSC patterns of pure carrier, pure drug, CEL/aPMMA 1:1 (w/w) physical mixture, and CEL/aPMMA 1:1 (w/w) extrudate; 1st indicates first heat scan, 2nd second heat scan; heating rate 10 K/min

CEL and aPMMA can both have an amorphous form. A single glass transition can be detected for the physical mixture and the extrudate, the latter in form of a relaxation peak. The glass transition of the physical mixture and the extrudate lies between the glass transitions of the pure substances. This indicates that the solid dispersion consists of only one amorphous phase so that the drug is molecularly dispersed in the carrier resulting in a glassy solid solution.

The preliminary experiments on the influence of CEL load on the T_g of the carrier (Figure 4.5) and on the dissolution rate of the solid dispersions (Figure 4.10) show that the maximum drug load for the production of glassy solid solutions lies between 50 and 75% (w/w) and between 50 and 62.5% (w/w) respectively. CEL has a molecular weight of 381 and the aPMMA monomer of 257. Assuming a chemical interaction between the acidic sulfonamide of CEL and the basic dimethylamine of aPMMA, a stoichiometric 1:1 mixture with 60% CEL load would still result in the formation of a glassy solid solution. In order to evaluate the existence of chemical interactions between drug and carrier, FT-IR spectra of the pure substances and the melt were examined.

The parts of the FT-IR spectra highlighted in Figure 4.14 show the stretching vibrations in the area between 3600 and 2600 cm^{-1}. As in the 1:1 (w/w) extrudate the amount of aPMMA monomer molecules is higher than the amount of CEL molecules, specifically the changes in the CEL signals were compared. The signals of aPMMA are less expressive because a surplus of the carrier is given.
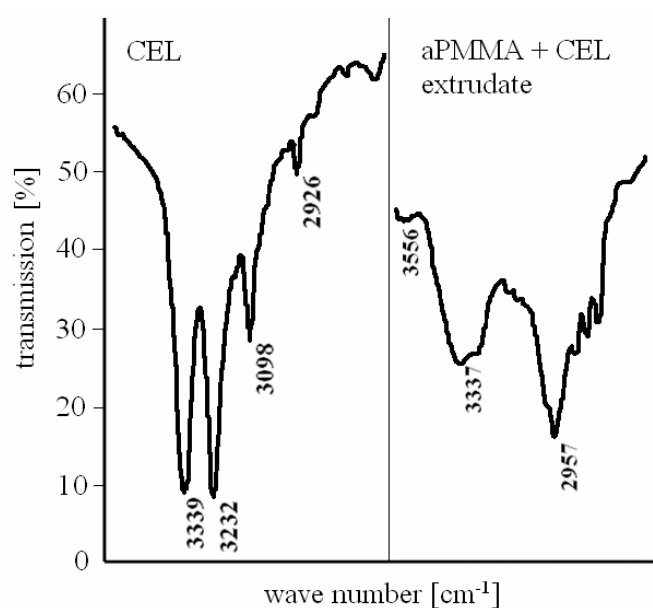

Figure 4.14: FT-IR spectra of CEL and CEL/aPMMA 1:1 (w/w) extrudate

The bands at 3339 and 3232 cm^{-1} are seen as doublet, which are attributed to the N-H stretching vibration of the –SO$_2$NH$_2$ group. In the spectrum of the extrudate the bands corresponding to N-H stretching of the -NH$_2$ group become diffused and broaden indicating the formation of an amorphous form (Chawla et al. 2003). Whether the change of the solid state from crystalline to amorphous is based on a transformation or a molecular dispersion of the drug in the carrier, accompanied by a chemical interaction, is not completely detectable at this drug load. The chemical interaction of CEL and aPMMA is investigated in more detail in chapter 4.5.

4.2.6 Dissolution experiments

The dissolution of each sample was determined under sink and non-sink conditions. Sink conditions were created by adding small amounts of the surfactant cetrimid. In the hot-melt extrusion process drugs are exposed to high temperatures. Therefore, decomposition is likely to occur in such processes. In order to have a clue to whether the drug is still present in its original form after extrusion, ultraviolet spectra of the drug before and after extrusion were evaluated. Figure 4.15 shows the same spectra for all formulations indicating a chemically unchanged drug. The small shift in the cetrimid spectra probably results from interactions of the sulfonamide group with the cetrimid molecule (Neil 1984).
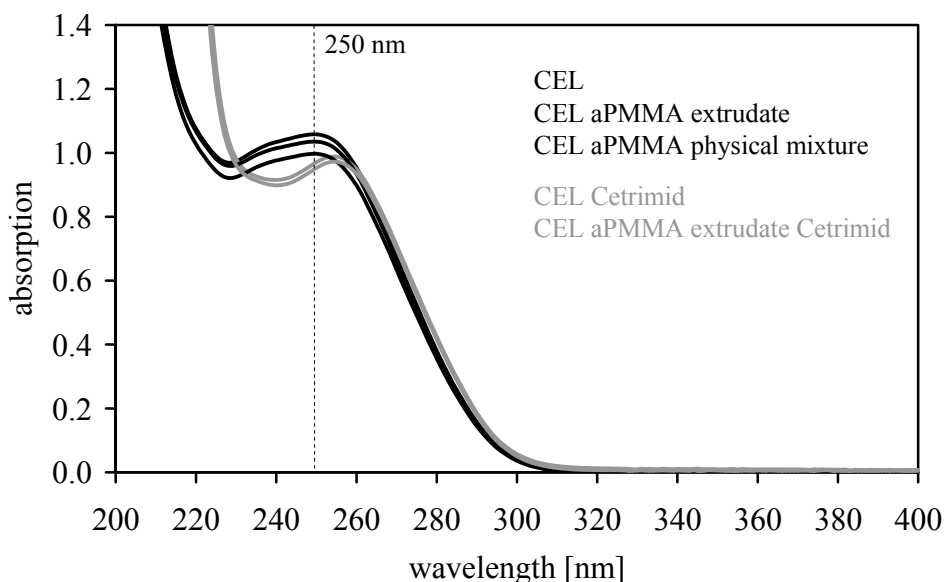
Figure 4.15: Ultraviolet spectra of CEL, CEL/aPMMA 1:1 (w/w) physical mixture, and CEL/aPMMA 1:1 (w/w) extrudate in 0.1 N HCl + 10% ethanol (black lines) and 0.1 N HCl + 0.3% cetrimid (grey lines); concentration 10 mg CEL / 500 mL; broken line expresses wavelength, at which measurements were taken

Under sink conditions differences in the dissolution rate were observed between the pure drug, the physical mixture, and the extrudate (Figure 4.16).

Figure 4.16: Drug release of CEL, CEL/aPMMA 1:1 (w/w) physical mixture, and CEL/aPMMA 1:1 (w/w) milled extrudate; 100 mg drug; 0.1 N HCl + 0.3% cetrimid, sink conditions, 37 °C, paddle, 50 rpm, 250 nm; mean ± SD, n=3

80% of CEL are dissolved after 11 min, but already released from the physical mixture after 7 min, and from the extrudate even after 1 min. As CEL and aPMMA are employed in a micronized form with a particle size of 6 μm and 9 μm respectively, and the milled extrudate with a particle size of <125 μm, the improvement of the dissolution rate is not based on any size effects, but due to glassy solid solution formation. Complete wettability is ensured by the addition of the surfactant cetrimid.
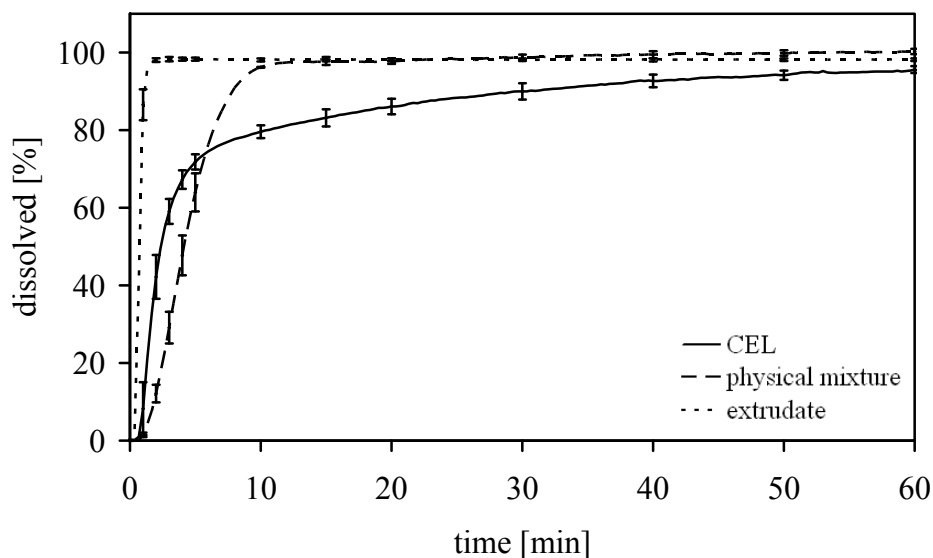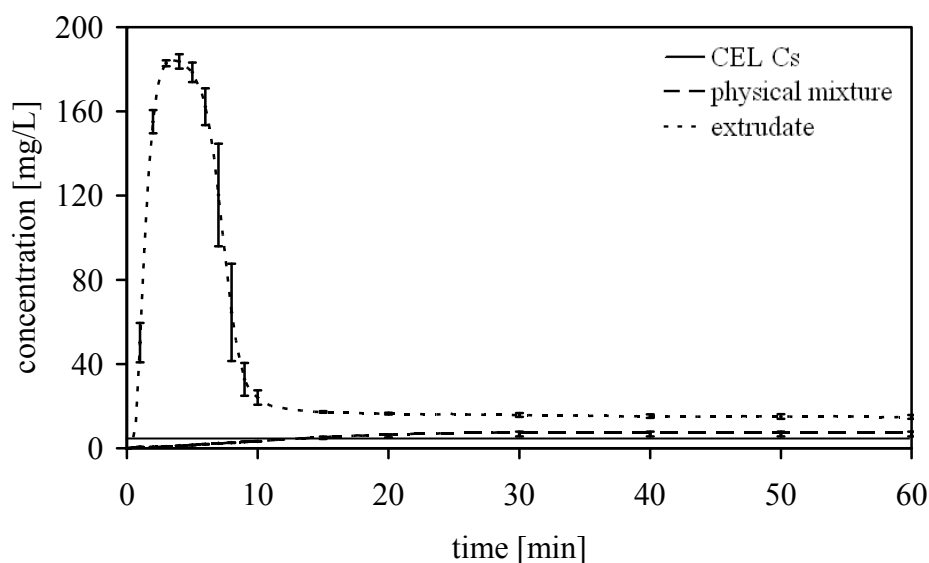

Figure 4.17: Drug release of CEL, CEL/aPMMA 1:1 physical mixture, and CEL/aPMMA 1:1 milled extrudate; 200 mg drug; 0.1 N HCl, non-sink conditions, 37 °C, paddle, 50 rpm, 250 nm; mean ± SD, n=3

25

Under non-sink conditions (Figure 4.17) a considerable difference can be observed between CEL, the physical mixture, and the extrudate. The c_s of CEL in 0.1 N HCl amounts to 3 mg/L and can be improved to a small extent only by simple physical mixing with aPMMA. The drug release from hot-melt extruded glassy solid solutions is very fast and results in a 58 fold supersaturated solution.

Within the first three minutes CEL is almost completely dissolved from the extrudate. 100% cannot be reached because the drug already starts to form crystals in the supersaturated solution. The residue was collected, dried, and evaluated via XRPD. The pattern shows crystalline peaks which are similar to those of CEL before dissolution (Figure 4.18). Whether the drug has the same modification after dissolution and precipitation cannot be established finally, as the peaks are not very distinct.
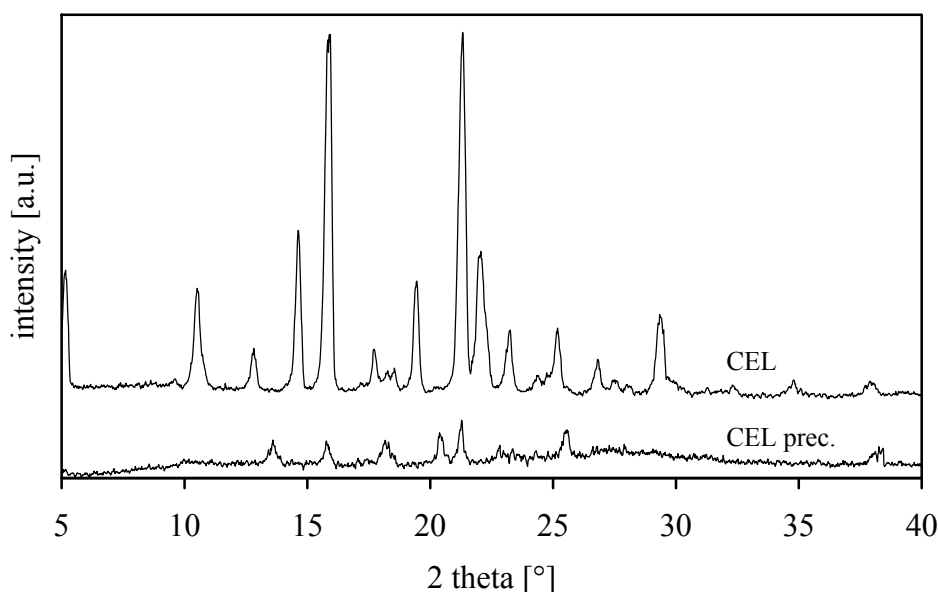
Figure 4.18: XRPD patterns of CEL as basic material before dissolution and as precipitated residue after dissolution

4.2.7 Dissolution mechanism

Knowledge of the mechanism of drug release from solid dispersions is essential for understanding the enhancement in the dissolution rate of a poorly soluble drug. Two mechanisms of drug release from solid dispersions are known from literature (Corrigan 1985, Craig 2002). Carrier-controlled dissolution occurs in case the drug release is dependent on the properties of the carrier. Drug-controlled dissolution predominates in case the drug release is dependent on the properties of the drug. In order to reveal the mechanism of drug release from

CEL/aPMMA solid dispersions, the glassy solid solution (transparent) and the crystalline glass suspension (opaque) were dissolved in 0.1 N HCl for 2 min and then examined in more detail via SEM analysis. Figure 4.19 shows the images of the strands before and after dissolution. Two processes take place. The first one is recrystallization of the opaque strands when getting into contact with the dissolution medium. The second one is dissolution from the surface which becomes obvious when comparing the thickness of the strands before and after dissolution. After 2 min dissolution the thickness of the transparent strand has decreased to a higher extent than the thickness of the opaque strand, which corresponds with the dissolution profile in Figure 4.9.

Thus, two different mechanisms can be defined. The crystalline glass suspension follows a drug-controlled dissolution, because the rate-determining step is the dissolving of the poorly water-soluble drug. Consequently, the dissolution is not associated with the polymer but is, instead, dominated by the poor solubility properties of the drug. The glassy solid solution follows a carrier-controlled dissolution, because the particles are molecularly dispersed in the carrier and are, therefore, dissolved into the polymer-rich diffusion layer together with the carrier.
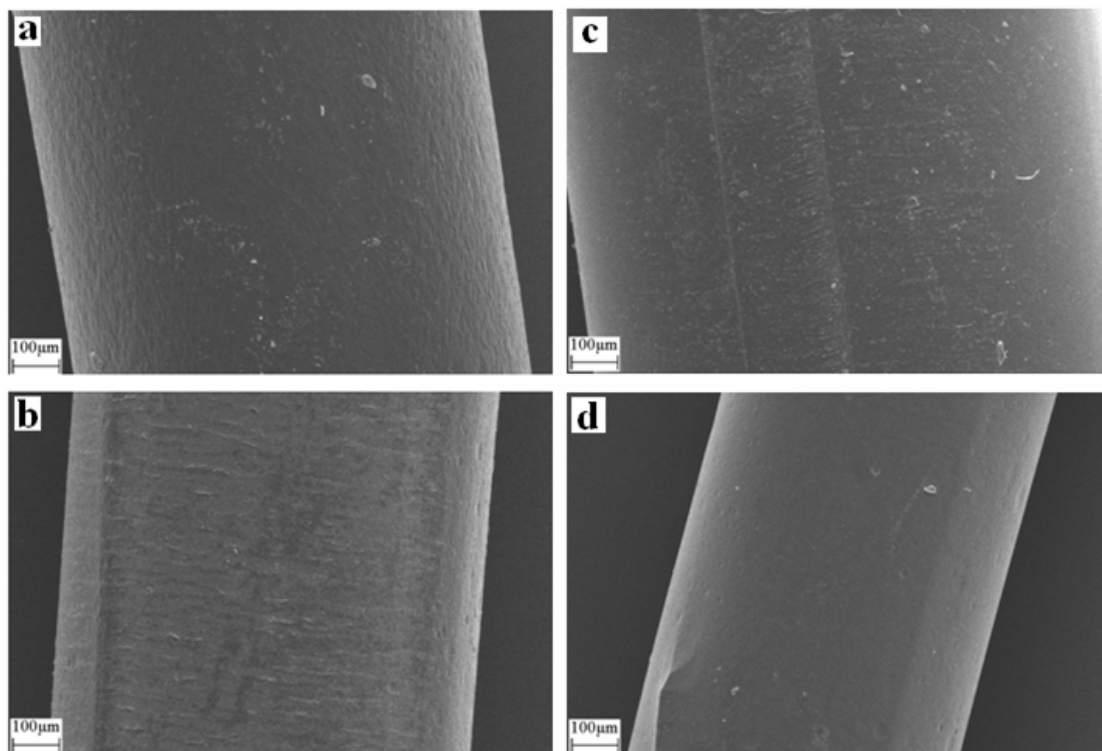

Figure 4.19: SEM images of opaque (a&b) and transparent (c&d) aPMMA/CEL 1:1 (w/w) extrudates before (a&c) and after (b&d) 2 min dissolution; high voltage 20 kV

4.2.8 Wettability

The low dissolution rate of drug particles is mainly caused by poor solubility of the drug and poor wettability of the powder. The low dissolution rate of poorly wettable particles is related to the formation of powder aggregates, which behave as larger particles with a corresponding smaller surface. Thus, the effective surface area that is exposed to the dissolution medium decreases. Depending on the wettability, the effective surface area is much smaller than the true surface area of the particles. The wettability can be increased by adding surfactants, by modifying the surface area, or by processing with water-soluble excipients.

Contact angles of crystalline CEL and its amorphous melt were examined in order to reveal wettability changes through surface modification. The contact angle of the physical mixture with aPMMA was measured to find out whether simple mixing of an excipient with more favourable properties is sufficient to increase the wettability of the drug or whether the drug has to be processed with the excipient. Figure 4.20 shows that CEL has poor wettability properties as shown by a high contact angle. Changing the solid state by transferring the drug into its amorphous form leads to a lower contact angle. In such systems CEL is present in a disordered molecular arrangement leading to interactions of moderate strength (Gupta et al. 2005). In conclusion, it is easier for the water molecules to get into contact with the drug molecules. As expected, the contact angle of the physical mixture lies between the ones of the pure components. The best wettability can be obtained by processing the drug with aPMMA, as in this case the improvement of the wettability by both the addition of a better wettable excipient and the change in surface modification coincide.
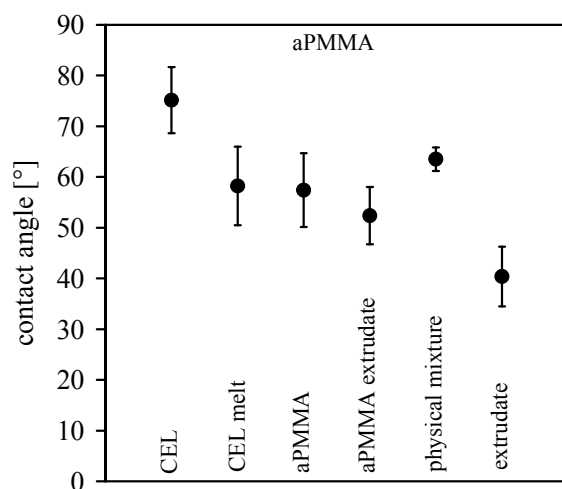

Figure 4.20: Contact angles of crystalline and amorphous drug and carrier, their physical mixture 1:1 (w/w), and the extrudate 1:1 (w/w); liquid: water; mean ± SD, n=5

4.2.9 Physical stability of extrudates

An important issue in the formulation of glassy solid solutions is the physical stability of the amorphous system. As these metastable systems have a higher free energy they favour the conversion to lower energy and thus, more stable crystalline forms upon storage (Hancock et al. 1995, Kakumanu & Bansal 2002). The rate of crystallization increases significantly above T_g because of the enhanced molecular mobility in the supercooled liquid state above T_g relative to that in the glassy state below T_g (Debenedetti & Stillinger 2001). The stabilization of the amorphous form can be achieved by limiting the molecular mobility via storage of the amorphous materials at temperatures as low as 50 K below T_g (Hancock et al. 1998, Zhou et al. 2002). Furthermore, stabilization can be obtained by increasing the T_g of the drug system by addition of a high T_g additive or by specific reversible chemical drug-carrier interactions.

Temperature and humidity are the key parameters for most stability issues. Therefore, long-term and accelerated stability was tested according to ICH guideline. Samples were stored at 25 °C over silica gel, at 25 °C, 60% RH (long-term stability) and at 40 °C, 75% RH (accelerated stability) for at least six months. The stability of the samples was evaluated via XRPD analysis (Figure 4.21, Figure 4.22, and Figure 4.23).

As the glassy solid solution with CEL and aPMMA has a quite low T_g, stability was first tested upon storage without any temperature or humidity impact. Under these conditions the system was stable for at least six months which was proven by the formation of halos in the XRPD patterns indicating the amorphous state of the system (Figure 4.21).
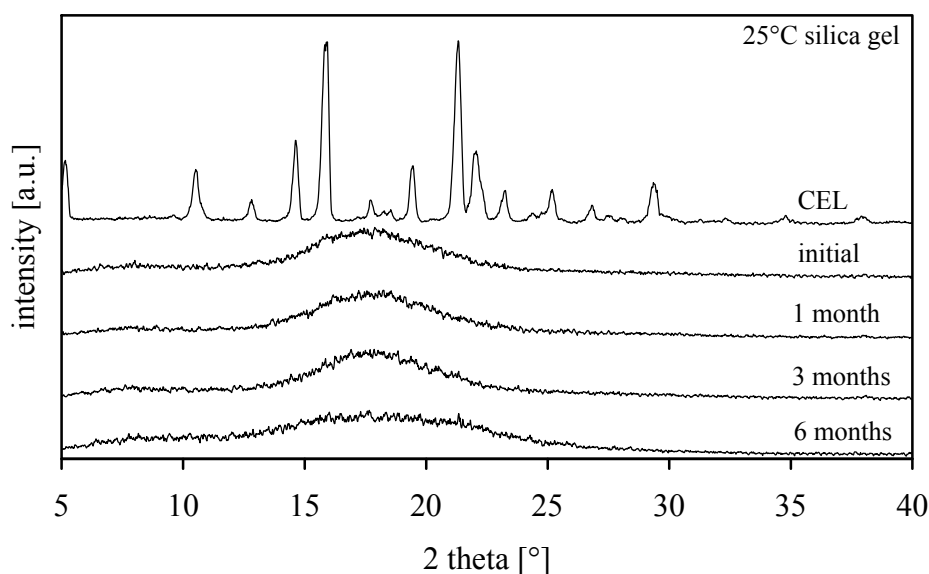
Figure 4.21: XRPD patterns of CEL and aPMMA/CEL 1:1 (w/w) milled extrudates after storage at 25 °C over silica gel up to 6 months

Long-term stability tests at 60% RH showed the same amorphous XRPD patterns as the samples that were not stored under specific humidity conditions (Figure 4.22).

Figure 4.22: XRPD patterns of CEL and aPMMA/CEL 1:1 (w/w) milled extrudates after open storage at 25 °C, 60% relative humidity up to 6 months

Samples stored in aluminum foil at accelerated conditions (40 °C, 75% RH) were also stable for at least six months (Figure 4.23). The significance of the small peak at 38° has to be examined after further storage. These results indicate that neither temperature up to 40 °C nor humidity up to 60% RH have a negative effect on the stability of the glassy solid solution.
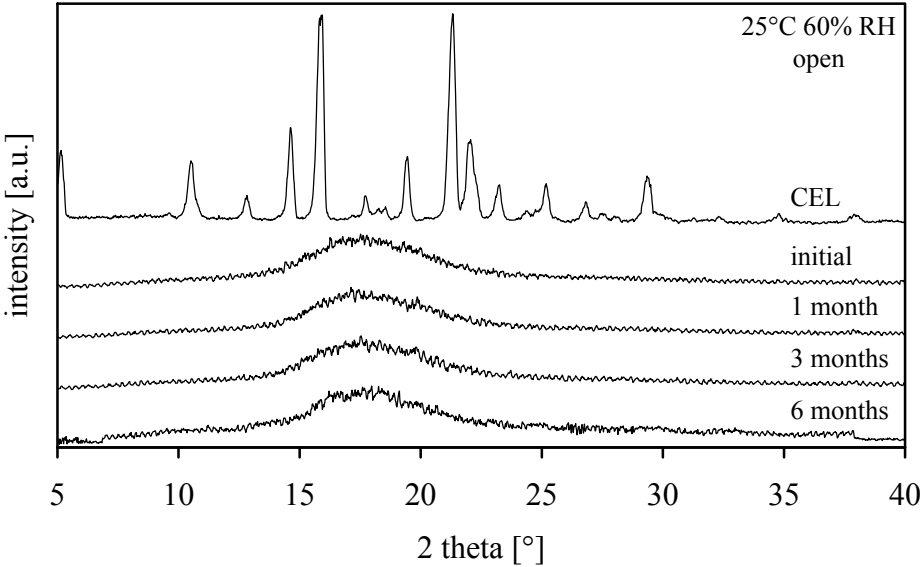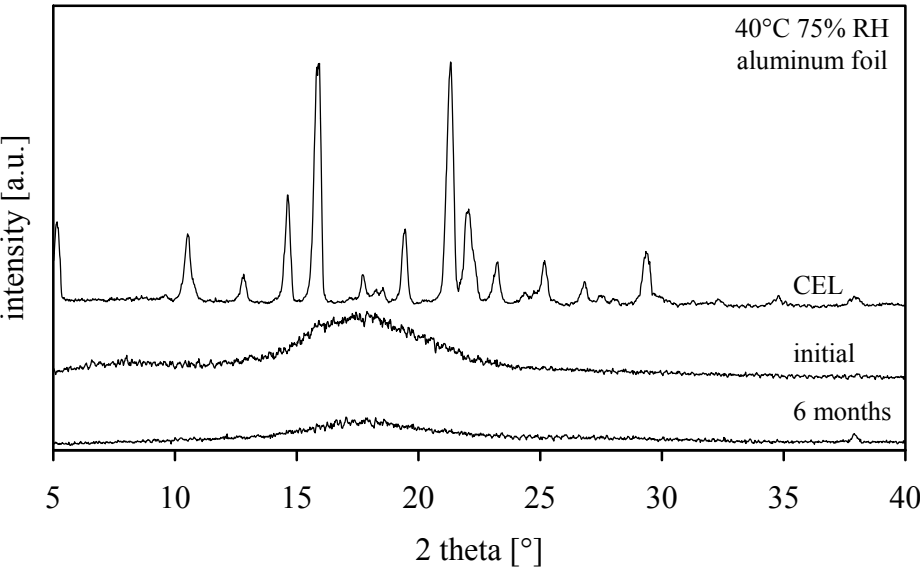

Figure 4.23: XRPD patterns of CEL and aPMMA/CEL 1:1 (w/w) milled extrudates after closed storage at 40 °C, 75% relative humidity in aluminum foil up to 6 months

Often stability problems become apparent in the dissolution profile, since the stable crystalline form possesses poorer solubility properties than the metastable amorphous form. Therefore, the drug release from glassy solid solutions was additionally examined after six months following storage at 25 °C over silica gel, at 25 °C, 60% RH, and at 40 °C, 75% RH. Figure 4.24 shows the dissolution profiles of CEL/aPMMA extrudates after storage under three different storage conditions. The results indicate that the dissolution rate is not affected at increased temperature or humidity, thus, supporting the results of the XRPD analysis. The small deviation of the sample stored at accelerated conditions should not be overrated as recrystallization from supersaturated solutions is purely coincidental. Therefore, the time of dissolution and the amount of maximum drug dissolved can vary slightly within each sample.
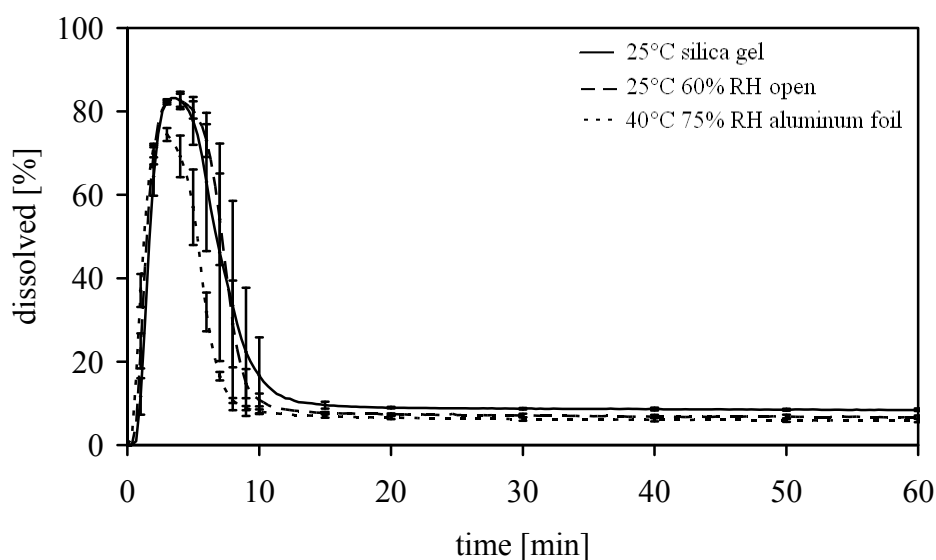
Figure 4.24: Drug release of CEL/aPMMA 1:1 (w/w) milled extrudate after 6 months storage under different conditions; 200 mg drug; 0.1 N HCl, non-sink conditions, 37 °C, paddle, 50 rpm, 250 nm; mean ± SD, n=3

4.2.10 Summary

aPMMA is a suitable carrier to enhance the solubility of CEL. Glassy solid solutions of the two components can be produced by hot-melt extrusion at a temperature 5 °C below the melting point of the drug without incurring decomposition. The maximum drug load is at least 50% and might be increased up to 60%. The maximum drug load can be predicted by intrinsic dissolution experiments. Such systems are stable at increased temperature and humidity for at least six months which is due to the very low water uptake of the components. Glassy solid solutions of CEL and aPMMA have a fast dissolution rate and result in a 58 fold supersaturated solution. The mechanism of drug release from these glassy solid solutions is

carrier-controlled and governed by dissolution. The enhancement of the dissolution rate is based on improved solubility and wettability. aPMMA seems to interact chemically with CEL which is investigated in more detail in chapter 4.5.

4.3 Solubility enhancement of celecoxib by hot-melt extrusion with other carriers

4.3.1 Introduction and objective

aPMMA is a useful carrier to enhance the solubility of the poorly water-soluble drug CEL. In order to investigate, whether the procedure of forming glassy solid solutions by hot-melt extrusion can be transferred to other excipients, two further carriers were tested on their solubility enhancing ability for CEL.

Copovidone (COP) is a water-soluble carrier and is often used in hot-melt extrusion to form glassy solid solutions (Leuner & Dressman 2000). Forster et al. (2001) extruded 1:1 blends of indomethacin and lacidipine with COP and obtained glassy solid solutions. Verreck et al. (2005) investigated the solubility enhancement of itraconazole by processing this poorly water-soluble drug with COP in combination with pressurized carbon dioxide as a temporary platicizer. For blends with 10% drug they obtained a solubility enhancement. Kaletra[®] (combination of lopinavir and ritonavir) is the most famous hot-melt extruded product on the market, which also contains COP as carrier.

Besides these traditional carriers, in literature also the use of new polymers can be found. Polyethylene glycol-polyvinyl alcohol copolymer (PEG-PVA), for instance, is a semi-crystalline hydrophilic polymer, which was first used in the formulation of solid dispersions by Janssens et al. (2007). They produced solid dispersions of PEG-PVA and itraconazole by hot-melt extrusion at a temperature of 180 °C, and could improve the solubility and the dissolution rate of the drug up to a drug load of 20%.

The ability of the traditional carrier COP and the new carrier PEG-PVA to produce glassy solid solutions with CEL and to improve its solubility were tested.

4.3.2 Extrusion with copovidone

Copovidone has a glass transition temperature at 107 °C and can be processed easily into transparent strands by hot-melt extrusion. CEL/COP 1:1 (w/w) blends were produced with the temperature profile shown in Figure 4.25. The melt leaves the die plate as colourless transparent semisolid strands, which are cooled at room temperature. The extrusion process is very stable and insensitive, since COP has good thermoplastic properties.

| 130 | 140 | 157 | 157 | 130 | 70 | 20 |
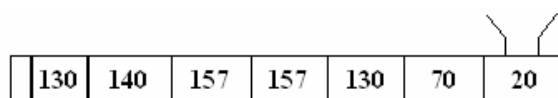
Figure 4.25: Temperature profile of the extruder barrel for CEL/COP 1:1 (w/w); temperatures in °C

Figure 4.26 shows the DSC patterns of COP, CEL, the physical mixture, and the extrudate. CEL and COP seem to be able to form a glassy solid solution, which is reflected by the T_g of the physical mixture lying between the T_g of drug and carrier. Unlike this, separate thermal signals for CEL and COP, both in an amorphous state, were detected for the extrudate. This indicates that a glass suspension with two amorphous phases is formed with CEL and COP.
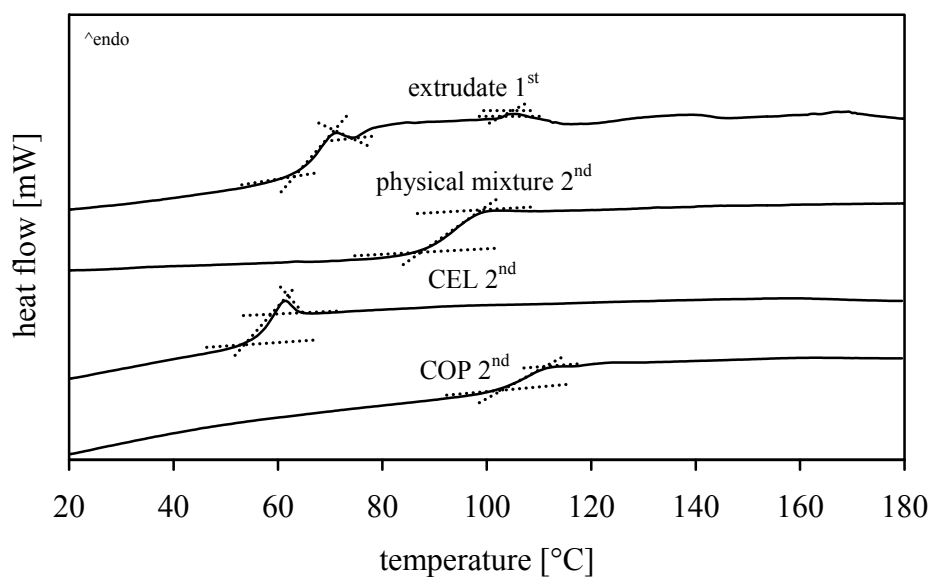
Figure 4.26: DSC patterns of pure carrier, pure drug, CEL/COP 1:1 (w/w) physical mixture, and CEL/COP 1:1 (w/w) extrudate; 1st indicates first heat scan, 2nd second heat scan; heating rate 10 K/min
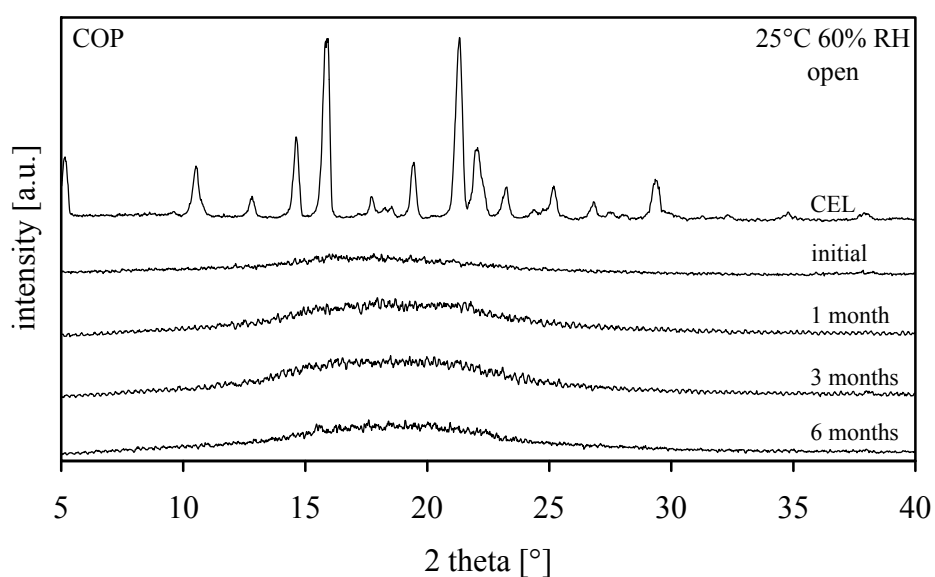
Figure 4.27: XRPD patterns of CEL and CEL/COP 1:1 (w/w) milled extrudates after open storage at 25 °C, 60 % relative humidity up to 6 months

CEL/COP extrudates were stored under long-term and accelerated conditions. All samples were stable for at least six months which is demonstrated in Figure 4.27 and Figure 4.28. Compared to povidone, the influence of moisture on copovidone is reduced. Nonetheless, the water content of 2.8% for COP stored under dry conditions, located on top of silica gel, is markedly increased under accelerated storage conditions to 14.9%. As the moisture uptake is strongly dependent on the drug that is incorporated, in this case, water has no negative influence on solid-state stability.
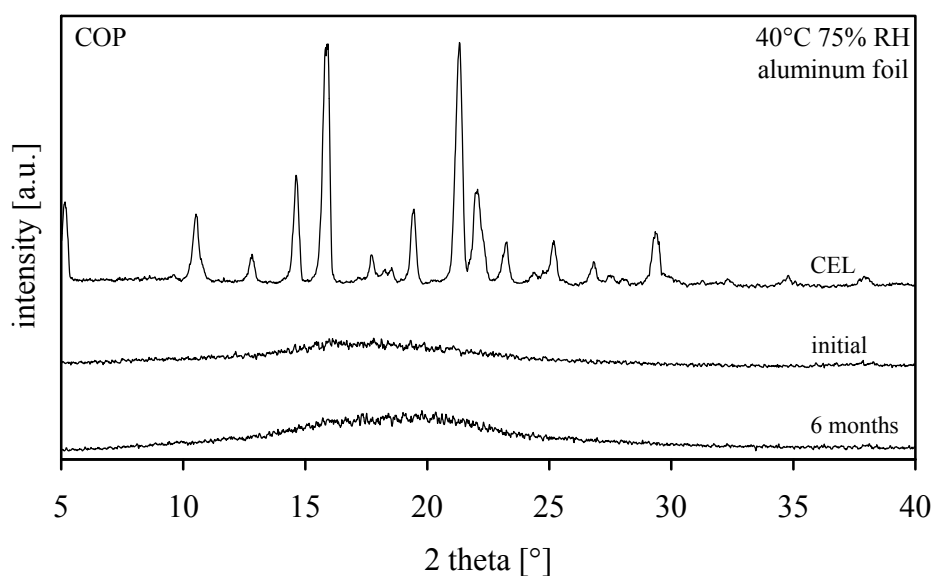
Figure 4.28: XRPD patterns of CEL and CEL/COP 1:1 (w/w) milled extrudates after storage at 40 °C, 75% relative humidity up to 6 months

The dissolution of each sample was determined under sink and non-sink conditions. Figure 4.29 shows the ultraviolet spectra of CEL and CEL/COP extrudates in 0.1 N HCl and 0.1 N HCl with surfactant. As the absorption and the position of the absorption maximum of the pure drug and the extrudate are similar, it can be assumed that the drug has not decomposed during the hot-melt extrusion process.

The small shift in the cetrimid spectrum is likely to result from interactions of the sulfonamide group with the cetrimid molecule (Neil et al. 1984).
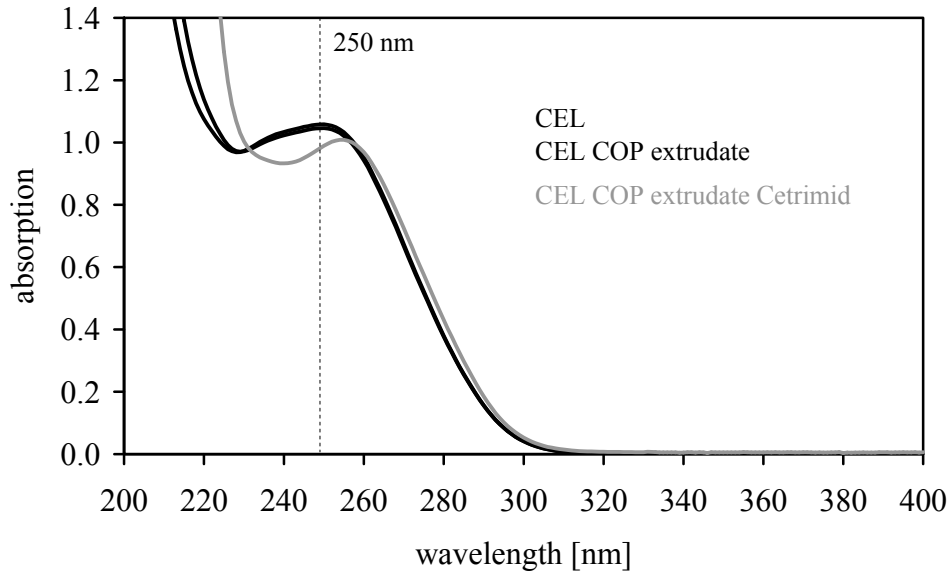
Figure 4.29: Ultraviolet spectra of CEL and CEL/COP 1:1 (w/w) extrudate in 0.1 N HCl (black lines) and 0.1 N HCl + 0.3 % cetrimid (grey line); concentration 10 mg CEL / 500 mL; broken line expresses wavelength, at which measurements were performed

Only slight differences in the dissolution rate can be observed between the pure crystalline drug, the physical mixture, and the extrudate under sink conditions (Figure 4.30). 80% of the pure drug are dissolved after 10 min, and 80% of the drug are released from the physical mixture and the extrudate after 7 min.
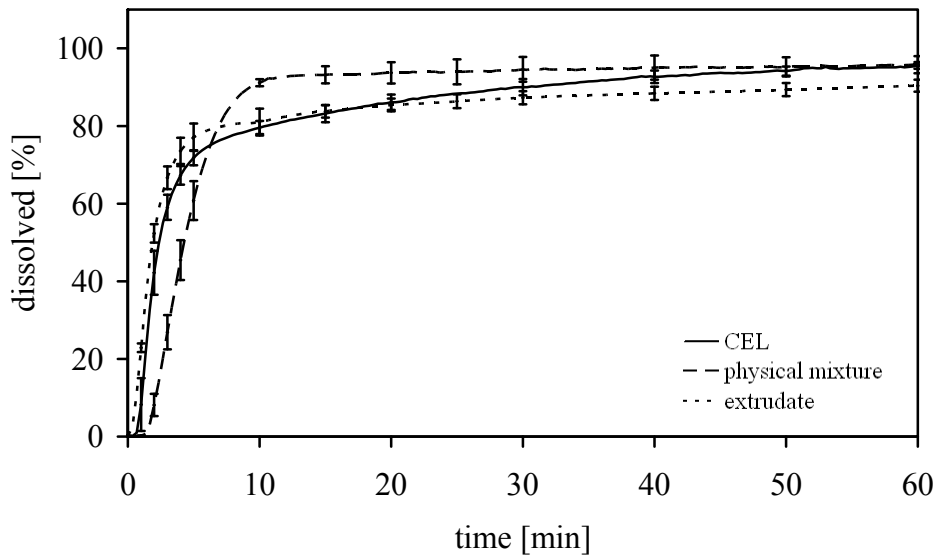
Figure 4.30: Drug release of CEL, CEL/COP 1:1 (w/w) physical mixture, and CEL/COP 1:1 (w/w) extrudate; 100 mg drug; 0.1 N HCl + 0.3 % cetrimid, sink conditions, 37 °C, paddle, 50 rpm, 250 nm; mean ± SD, n=3
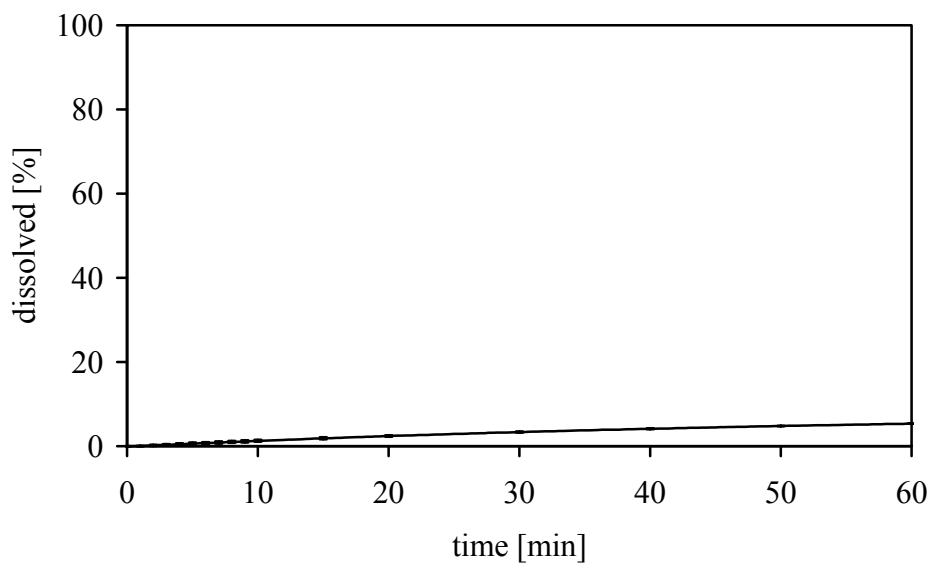
Figure 4.31: Drug release of CEL/COP 1:1 (w/w) extrudate; 200 mg drug; 0.1 N HCl, non-sink conditions, 37 °C, paddle, 50 rpm, 250 nm; mean ± SD, n=3

Under non-sink conditions (Figure 4.31) a poor solubility of the drug can be observed. This indicates that COP in a 1:1 blend with CEL is not suitable to enhance the solubility. The poor solubility might be caused by the solid state of the drug, as the drug is not molecularly dispersed in the carrier and coexists as a separate amorphous phase. Moneghini et al. (1998) and Zingone et al. (1994) reported that a high copovidone content could lead to a decrease in the release rate of a drug. This observation was attributed to a high viscosity in the diffusion boundary layer adjacent to the dissolving surface and to gel formation.

To examine whether the dissolution behaviour can be attributed to the solid state characteristics, the extrudates are evaluated before and after 2 min dissolution (Figure 4.32). COP forms strands with a very smooth surface (a&b). During dissolution the external layer of the strand flakes off (c).
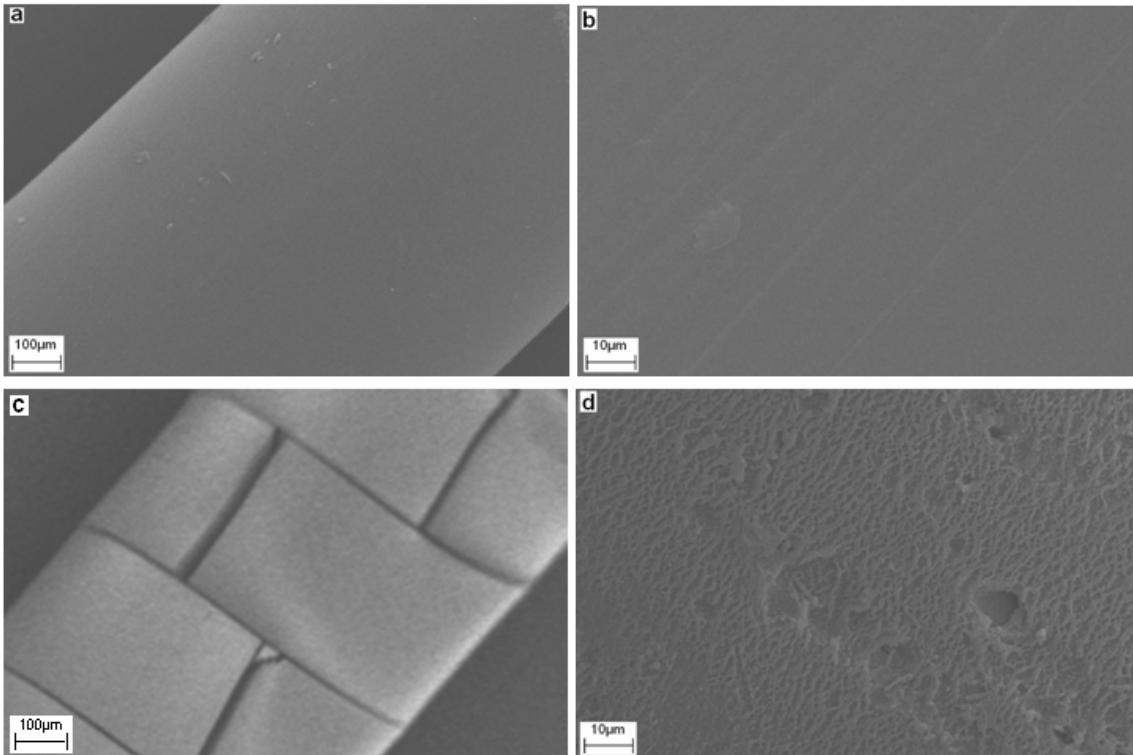
Figure 4.32: SEM images of CEL/COP 1:1 (w/w) extrudates before (a&b) and after (c&d) 2 min dissolution; overview (a&c) and detailed images (b&d); high voltage 20 kV

The poor solubility of a drug can often be attributed to the poor wettability of the drug and its formulation. Therefore, the contact angles of the crystalline and amorphous drug, the physical mixture, and the melt were determined. Figure 4.33 shows that COP has a smaller contact angle than CEL, and that the contact angle of the drug can be decreased to the contact angle of COP by hot-melt extruding it with the carrier.
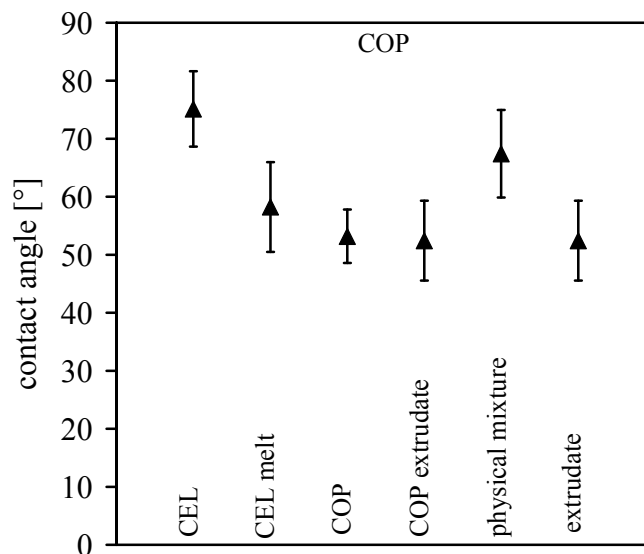
Figure 4.33: Contact angles of crystalline and amorphous drug and carrier, their physical mixture 1:1 (w/w), and the extrudate 1:1 (w/w); liquid: water; mean ± SD, n=5

4.3.3 Extrusion with polyethylene glycol-polyvinyl alcohol copolymer

The polyethylene glycol-polyvinyl alcohol copolymer (PEG-PVA) has two glass transitions at about -60 °C relating to the PEG phase and at about 50 °C relating to the PVA phase of the copolymer. PEG-PVA does not contain any free PEG, which could be detected by liquid and size exclusion chromatography (Mittwollen 2008). PEG-PVA cannot be extruded as pure carrier. At low temperatures the powder cannot be molten and dams up before the die plate. At higher temperatures the powder can be molten, but discolours. Therefore, PEG-PVA was only processed in a blend with CEL. The CEL/PEG-PVA 1:1 (w/w) blend was extruded with the temperature profile described below (Figure 4.34). The melt leaves the die plate as pale yellow, at the edges slightly opaque, semisolid strands, which are cooled at room temperature. From literature it is known, that at temperatures > 160 °C the polymer gets partially insoluble (Mittwollen 2008). This might be caused by the orientation of the PEG and PVA chains in the heat and under shear forces (Janssens et al. 2007). Nevertheless, Janssens et al. could improve the solubility of itraconazole by processing the drug with PEG-PVA at 180 °C. As at lower temperatures the CEL/PEG-PVA extrudates had a completely opaque appearance, the temperature profile was set as described in Figure 4.34.
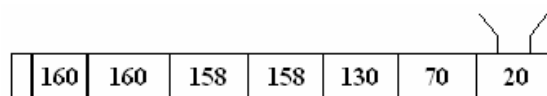
Figure 4.34: Temperature profile of the extruder barrel for CEL/PEG-PVA 1:1 (w/w); temperatures in °C

In order to evaluate the influence of water on the polymer properties, the water uptake of the drug melt, the carrier melt, and the molten 1:1 blend of both substances was examined. All samples were stored under two different conditions: 25 °C over silica gel and 40 °C, 75 % relative humidity. Figure 4.35 shows that the water uptake of PEG-PVA at 75 % relative humidity is much higher than of the drug. The water uptake of the blend is decreased compared to the water uptake of the pure carrier. The results indicate that water might have an influence on the properties and the stability of the resulting solid dispersions.
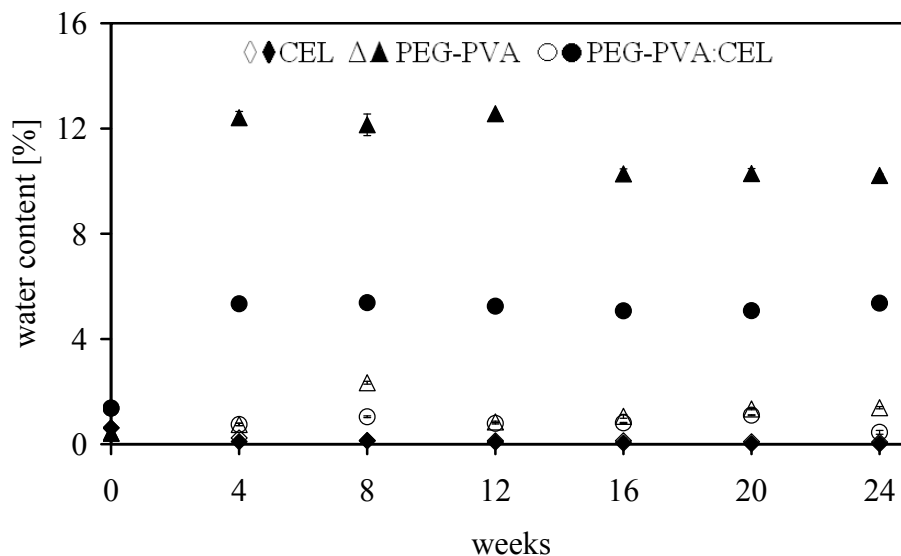
Figure 4.35: Water uptake of CEL melt, PEG-PVA melt, and molten blend of CEL/PEG-PVA 1:1 examined by Karl-Fischer titration; open symbols represent storage at 25 °C over silica gel, closed symbols represent storage at 40 °C, 75 % relative humidity; mean ± SD, n=3

The solid-state characteristics of the extrudates were evaluated by DSC analysis. CEL and PEG-PVA seem to be able to build a glassy solid solution, which is reflected by the T_g of the physical mixture lying between the T_g of drug and carrier.
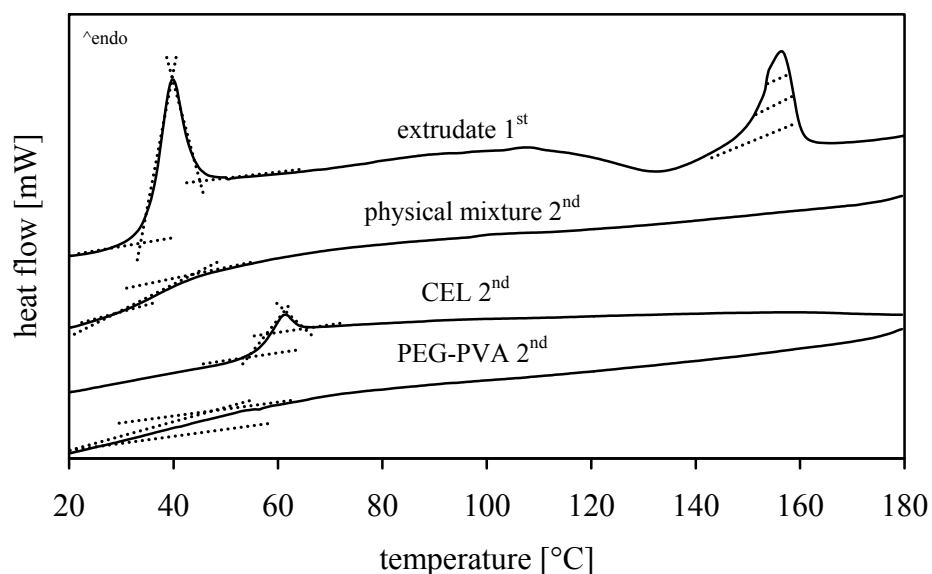
Figure 4.36: DSC patterns of pure carrier, pure drug, CEL/PEG-PVA 1:1 (w/w) physical mixture, and CEL/PEG-PVA 1:1 (w/w) extrudate; 1st indicates first heat scan, 2nd second heat scan; heating rate 10 K/min

Contrary to this, one amorphous and one crystalline phase are detected in the extrudate. The endothermic peak is located slightly below the melting point of the pure drug at 160 °C.

Therefore, in the hot-melt extrusion process a crystalline glass suspension was built. As against the pure drug, the melting enthalpy is decreased, which indicates, that the drug is partly dissolved in the carrier.

The crystalline parts in the XRPD patterns of the melts mostly derive from the pure carrier, which itself has a partly crystalline structure (Figure 4.37). The peak at about 20° can be attributed to the PEG chain of the copolymer.
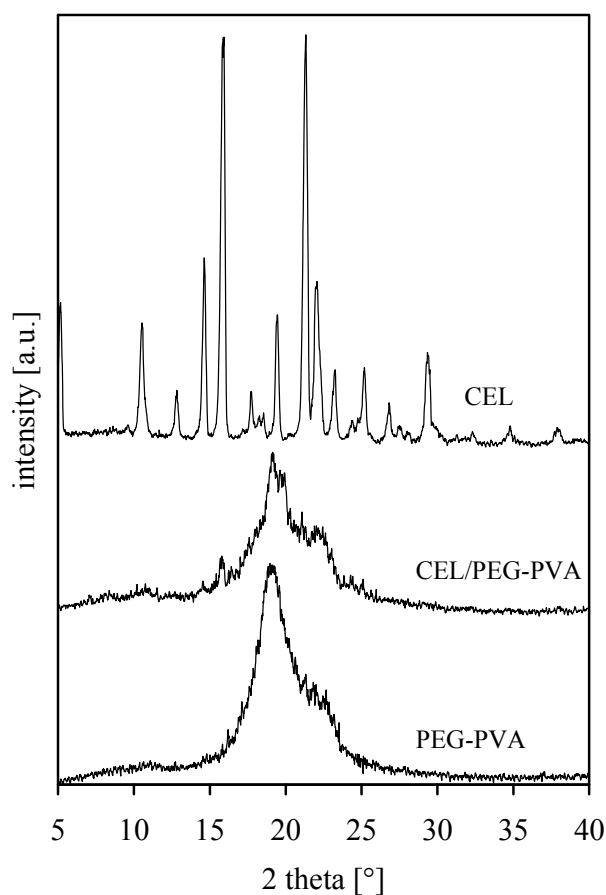
Figure 4.37: XRPD patterns of CEL, CEL/PEG-PVA 1:1 (w/w) milled extrudates, and PEG-PVA

The solid-state stability of the extrudates was evaluated under long-term (Figure 4.38) and accelerated conditions (Figure 4.39).

The initial XRPD patterns reflect the semi-crystalline structure of PEG-PVA, but not the crystalline peaks of the drug. After one month, small peaks, which might be related to the crystalline drug, emerge. The peaks grow during storage, which indicates that the drug cannot be kept in its amorphous form by embedding it in PEG-PVA.
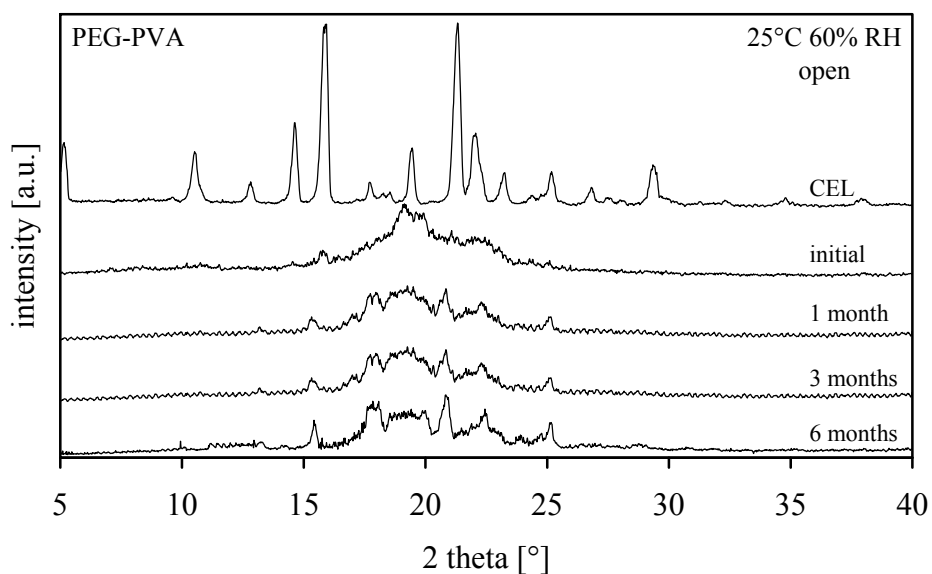
Figure 4.38: XRPD patterns of CEL and CEL/PEG-PVA 1:1 (w/w) milled extrudates after open storage at 25 °C, 60% relative humidity up to 6 months
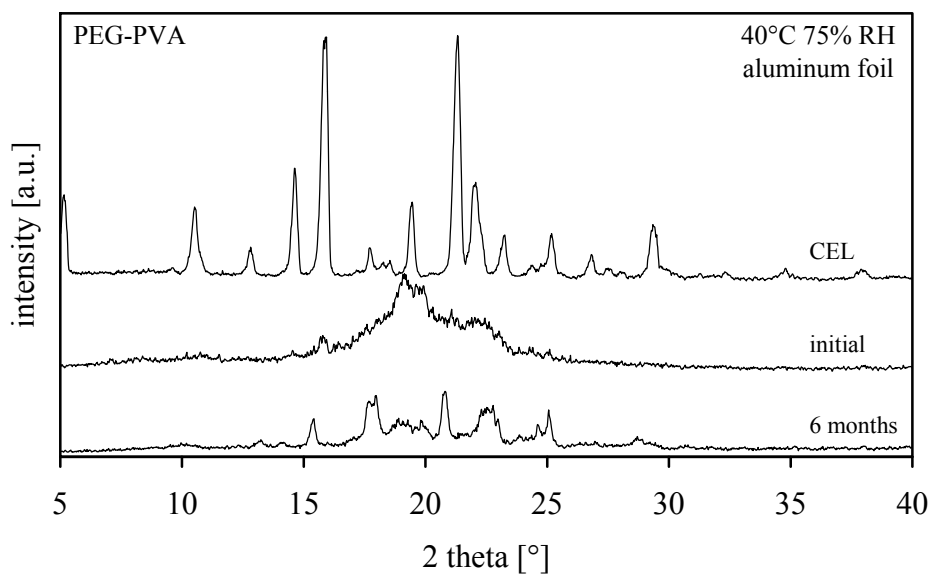
Figure 4.39: XRPD patterns of CEL and CEL/PEG-PVA 1:1 (w/w) milled extrudates after storage at 40 °C, 75% relative humidity in aluminum foil up to 6 months

The dissolution of each sample was determined under sink and non-sink conditions. Figure 4.40 shows the ultraviolet spectra of CEL and CEL/PEG-PVA extrudates in 0.1 N HCl and 0.1 N HCl with surfactant. As the spectra of the pure drug and the extrudate are similar, the drug seems to be present in an unchanged state in the extrudate.
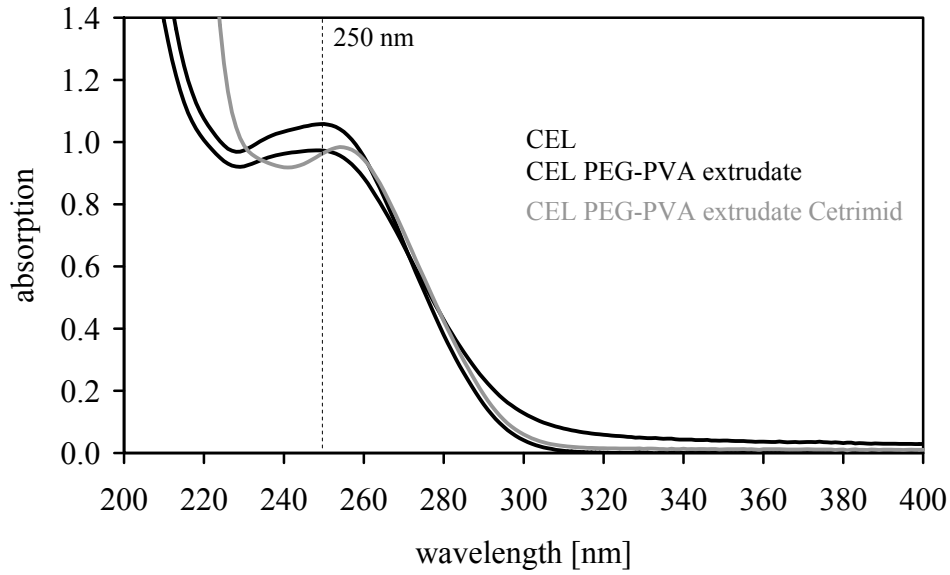
Figure 4.40: Ultraviolet spectra of CEL and CEL/PEG-PVA 1:1 (w/w) extrudate in 0.1 N HCl (black lines) and 0.1 N HCl + 0.3 % cetrimid (grey line); concentration 10 mg CEL / 500 mL; broken line expresses wavelength, at which measurements were performed

Only slight differences in the dissolution rate can be observed between the pure drug, the physical mixture, and the extrudate under sink conditions. 80% of the drug are dissolved after 11 min and released from the physical mixture after 7 min, and from the extrudate after 11 min.
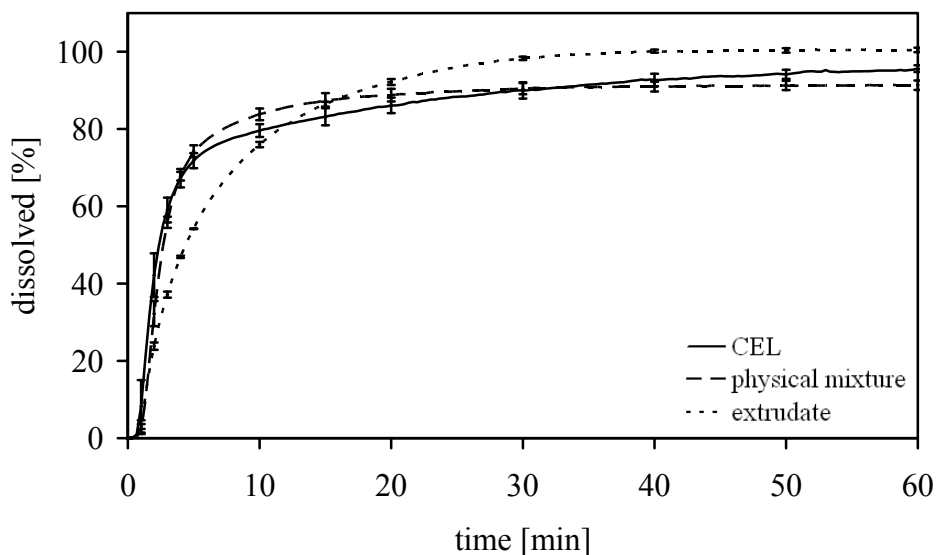
Figure 4.41: Drug release of CEL, CEL/PEG-PVA 1:1 (w/w) physical mixture, and CEL/PEG-PVA 1:1 (w/w) extrudate; 100 mg drug; 0.1 N HCl + 0.3 % cetrimid, sink conditions, 37 °C, paddle, 50 rpm, 250 nm; mean ± SD, n=3

43

Under non-sink conditions (Figure 4.42) a poor solubility of the drug can be observed. This indicates that PEG-PVA in a 1:1 blend with CEL is not suitable for enhancing the solubility. The poor solubility might be caused by the solid state of the drug, as the drug is not completely dispersed in the carrier on a molecular basis and partly coexists as a separate crystalline phase. Additionally, the poor solubility might be caused by the poor aqueous solubility of the carrier after processing at high temperatures and high shear forces (Janssens et al. 2007).
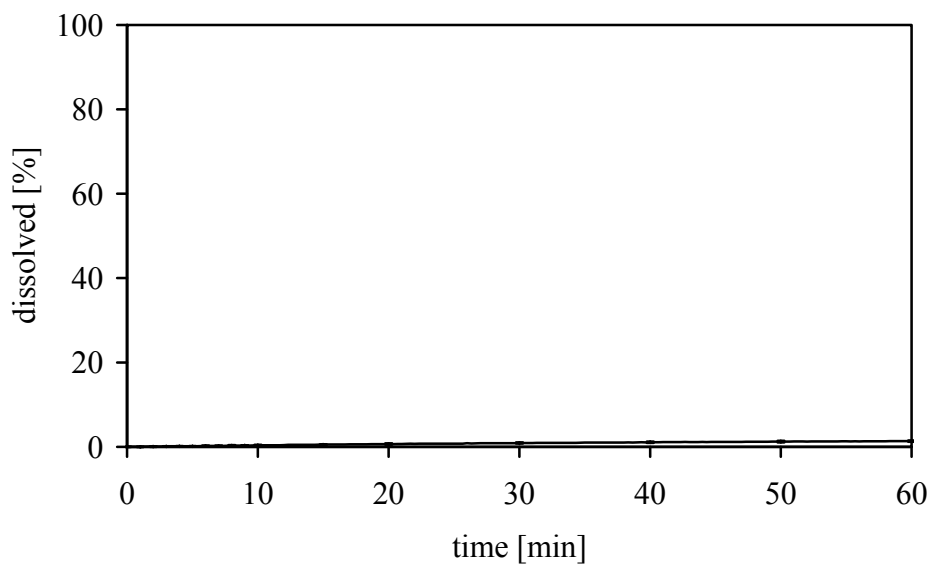
Figure 4.42: Drug release of CEL/PEG-PVA 1:1 (w/w) extrudate; 200 mg drug; 0.1 N HCl, non-sink conditions, 37 °C, paddle, 50 rpm, 250 nm; mean ± SD, n=3

To examine, whether the dissolution behaviour can be attributed to the solid state characteristics, the extrudates are evaluated before and after 2 min dissolution (Figure 4.43). CEL/PEG-PVA extrudates have a quite rough surface.
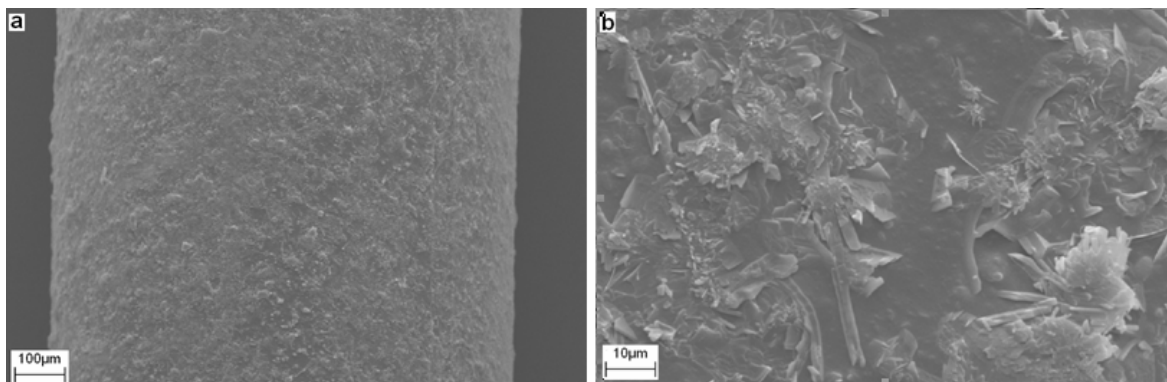
Figure 4.43: SEM images of CEL/PEG-PVA 1:1 (w/w) extrudates before 2 min dissolution; overview (a) and detailed image (b); high voltage 20 kV

During dissolution the outer layer of the strand dissolves to a certain extent (Figure 4.44). The outer layer peels off and leaves small sheds on the surface of the core strand (c). The detailed images of the sheds (d) and the core (e) show that the sheds themselves have a rough surface whereas the core is smooth with small wholes that are derived from dissolution.
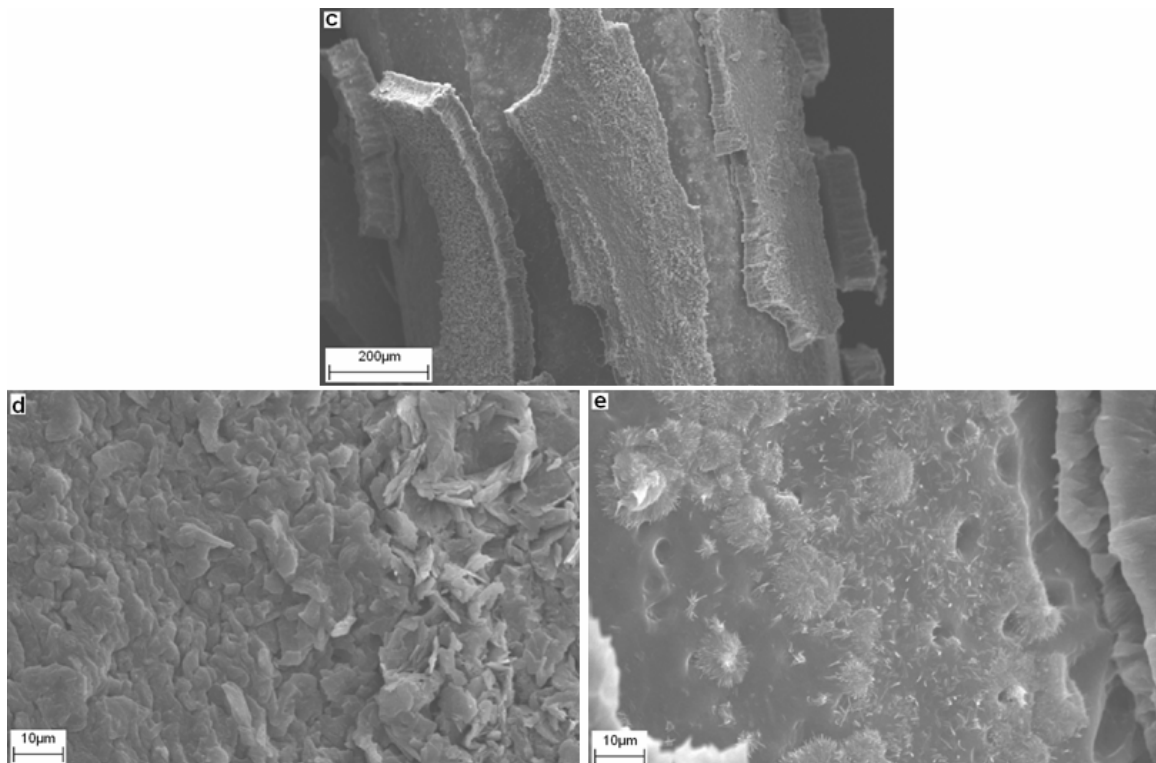
Figure 4.44: SEM images of CEL/PEG-PVA 1:1 (w/w) extrudates after (c&d) 2 min dissolution; overview (c) and detailed images of sheds (d) and core (e); high voltage 20 kV
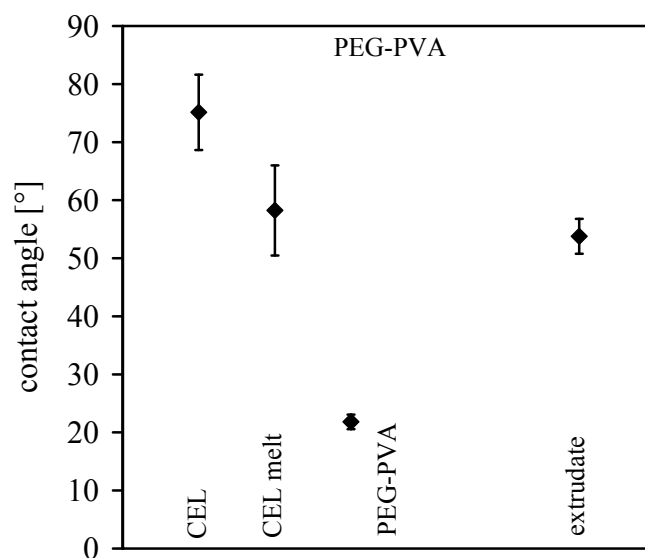
Figure 4.45: Contact angles of crystalline and amorphous drug and carrier, their physical mixture 1:1 (w/w), and the extrudate 1:1 (w/w); liquid: water; mean ± SD, n=5

In order to investigate, whether the outer layer of the extrudates mainly consists of hydrophilic carrier or poorly soluble drug, the contact angles of the drug, the carrier, and the extrudate were measured (Figure 4.45). Caused by its high hydrophilicity, PEG-PVA has a very small contact angle. The contact angle of the extrudate is similar to the contact angle of the CEL melt. Therefore, the outer layer rather consists of drug or a drug/carrier blend than of the pure hydrophilic carrier.

4.3.4 Summary

Besides aPMMA, also COP and PEG-PVA serve as carriers for solid dispersion production by hot-melt extrusion. aPMMA and COP have an appropriate thermoplastic behaviour and can be easily processed to semisolid strands whereas PEG-PVA needs to be processed in blends with drugs or other excipients.

Extrudates with a transparent appearance do not always represent glassy solid solutions, but can also depict amorphous suspensions with two phases. In such amorphous suspensions the drug is not molecularly dispersed in the carrier. This has a negative effect on the dissolution rate of the drug. Although the carriers cause an increase of wettability of the extrudates, the solubility cannot be improved. Thus, a remarkable improvement of the dissolution can only be realized by a system, wherein the drug is molecularly dispersed. Otherwise, drug release is predominantly influenced by the poor dissolution properties of the drug.

In general, the formation of glassy solid solutions, and thereby a molecular dispersion of the drug, seems to be possible with COP and PEG-PVA, as can be derived from the DSC analysis of the physical mixtures. As the amount of the carrier and the processing temperature has an influence on the solid state and the solubility of the system, further studies are needed to find a suitable process to produce glassy solid solutions with COP and PEG-PVA.

4.4 Solubility enhancement of different drugs by hot-melt extrusion with basic butylated methacrylate copolymer

4.4.1 Introduction and objective

The solubility of the poorly water-soluble drug CEL can be enhanced through the formation of glassy solid solutions with aPMMA via hot-melt extrusion. In order to explore, whether the formation of a glassy solid solution with aPMMA is substance-specific for CEL, or whether this process can also be transferred to other poorly water-soluble drugs, two other drugs were hot-melt extruded with aPMMA. The behaviour during hot-melt extrusion and the properties of the resulting extrudates were compared to CEL.

As against CEL, naproxen (NAP, chapter 7.1.1) is a smaller molecule, which has approximately the same melting point, but which cannot be transferred to its amorphous form by melting and cooling the melt (Table 4.1). Due to the carbonic acid, NAP has a smaller pK_a than CEL, and therefore, a more acidic character. Oxcarbazepine (OXC, chapter 7.1.1) has a considerably higher T_m than CEL and NAP and decomposes at temperatures above T_m. OXC is less lipophilic and less acidic than NAP and CEL.

Table 4.1: Chemical properties of CEL, NAP, and OXC

	celecoxib	naproxen	oxcarbazepine
MW	381	230	252
MP [°C]	162	157	231
T_g 2nd heating [°C]	57	-	62 / 167
logP	4.2	3.0	1.2
pKa	9.68a	4.84a	13.73a / -0.53b
Hbond acceptors	5	3	4
Hbond donors	2	1	2
Solubility in water at 25 °C	3 mg/L	16 mg/L	83 mg/L

4.4.2 Extrusion with naproxen

The blend of aPMMA and NAP with a drug load of 50% was hot-melt extruded employing the temperature profile described in Figure 4.46.
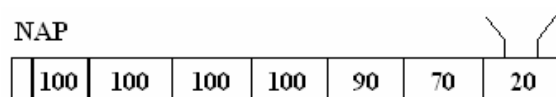
Figure 4.46: Temperature profile of the extruder barrel for NAP/aPMMA 1:1 (w/w); temperatures in °C

Transparent strands could be produced at a wide temperature range. Although NAP has a T_m of 157 °C, a temperature of 100 °C in barrel four and five was sufficient to obtain transparent

strands. The temperature at the die plate could not be further decreased because of the viscosity of the melt. If the viscosity is too high, the melt cannot pass the dies and causes a high pressure at the die plate. The low processing temperature indicates that NAP is highly soluble in aPMMA, and that interactions between the two components take place in the melt (Govindarajan & Suryanarayanan 2006, Quinteros et al. 2008). In order to elucidate the interactions between NAP and aPMMA, FT-IR analysis was performed with the pure carrier, the pure drug, and the aPMMA/NAP 1:1 (w/w) melt (Figure 4.47). In the 1:1 (w/w) blend, NAP molecules are present in surplus. Therefore, especially indicative bands of the carrier were analyzed to discover the interaction between drug and carrier.
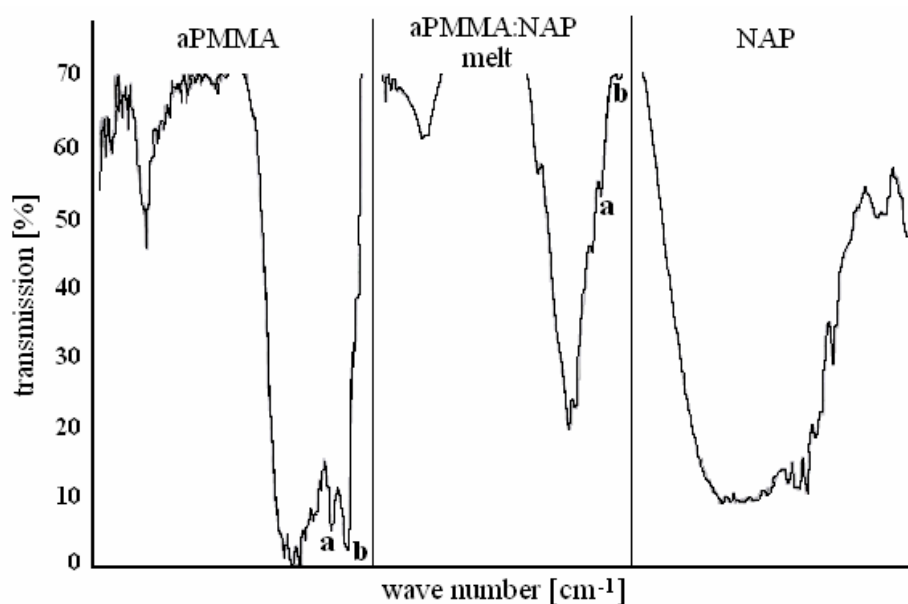
Figure 4.47: FT-IR analysis of aPMMA, aPMMA/NAP extrudate 1:1 (w/w), and NAP; a and b = bands of the non-protonated dimethylamino groups at 2770 (b) and 2816 (a) cm^{-1}

The absorption bands of the non-protonated dimethylamino groups appear at 2770 and 2816 cm^{-1} in the IR spectrum of the pure carrier. In the IR spectrum of the melt, these bands disappeared, indicating a complete protonation of the dimethylamino groups. Thus, an acid-base reaction between the dimethylamino group of aPMMA and the carboxylate group of NAP is taking place. Further investigations on the interactions between NAP and aPMMA are described in chapter 4.5.

NAP/aPMMA 1:1 (w/w) extrudates were characterized by DSC and XRPD analysis to reveal the physical state of the extrudates. Figure 4.48 shows the DSC patterns of the pure drug, the pure carrier, the physical mixture, and the extrudate. A single T_g, indicating the formation of a glassy solid solution, was proven for the physical mixture and the extrudates. For the

extrude a small endothermic signal was determined at about 140 °C, which is not conform to the results of the XRPD analysis, the extrusion behaviour, and the macroscopic appearance and is therefore neglected.
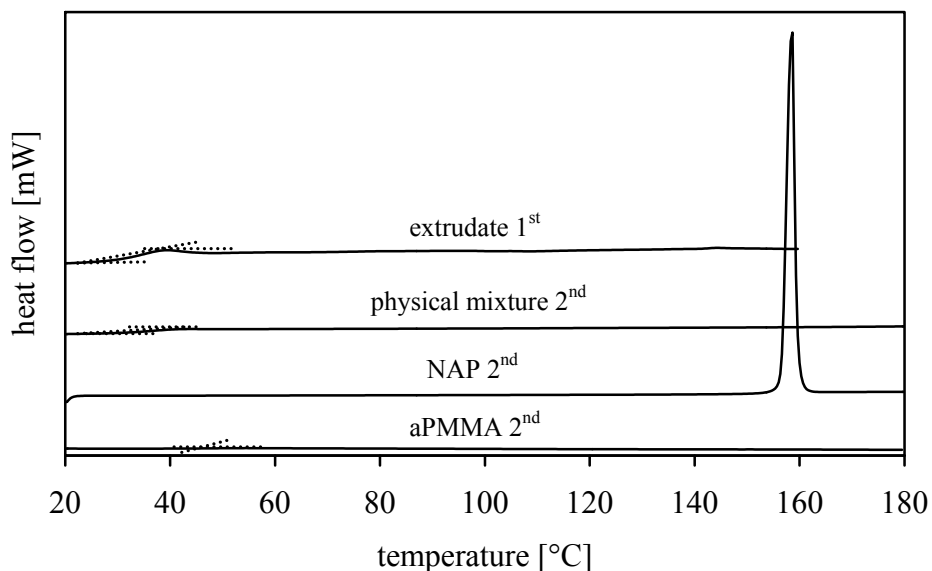
Figure 4.48: DSC patterns of pure carrier, pure drug, NAP/aPMMA 1:1 (w/w) physical mixture, and NAP/aPMMA 1:1 (w/w) extrudate; 1st indicates first heat scan, 2nd second heat scan; heating rate 10 K/min

Long-term and accelerated stability tests were performed according to the ICH guidelines (chapter 7.2.3). NAP/aPMMA extrudates were stable at 25 °C over silica gel (Figure 4.49) and at 60 % RH (Figure 4.50) for at least six months.

Figure 4.49: XRPD patterns of NAP and NAP/aPMMA 1:1 (w/w) milled extrudates after storage at 25 °C over silica gel up to 6 months

49
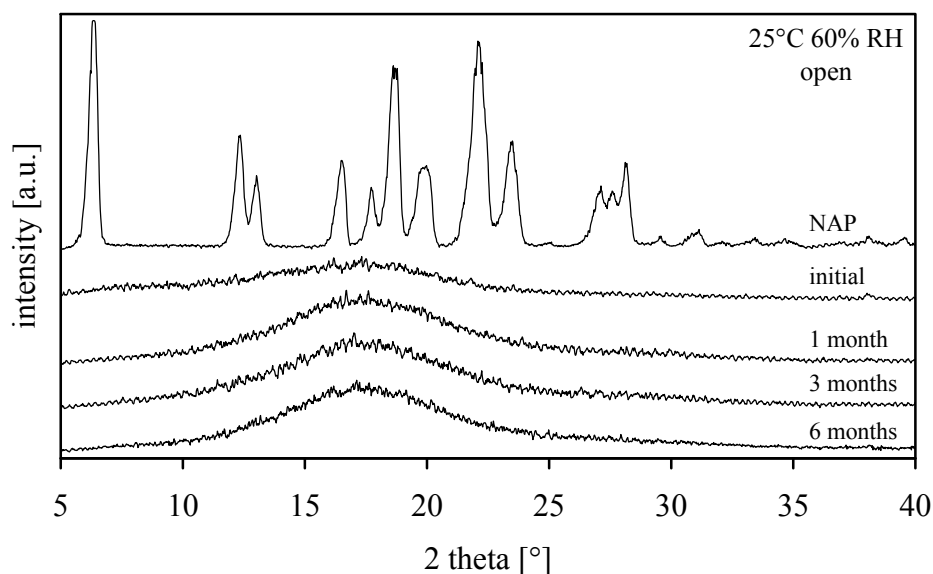
Figure 4.50: XRPD patterns of NAP and NAP/aPMMA 1:1 (w/w) milled extrudates after open storage at 25 °C, 60 % relative humidity up to 6 months

The extrudates did not withstand the accelerated stability test at 40 °C, 75% RH. The extrudates did not recrystallize, but were molten to a single lump, because the storage temperature was higher than the T_g of the glassy solid solution.

The dissolution behaviour of each sample was determined under sink and non-sink conditions. In order to have a clue to whether the drug is still present in its original form after hot-melt extrusion, ultraviolet spectra of the drug before and after extrusion were evaluated.
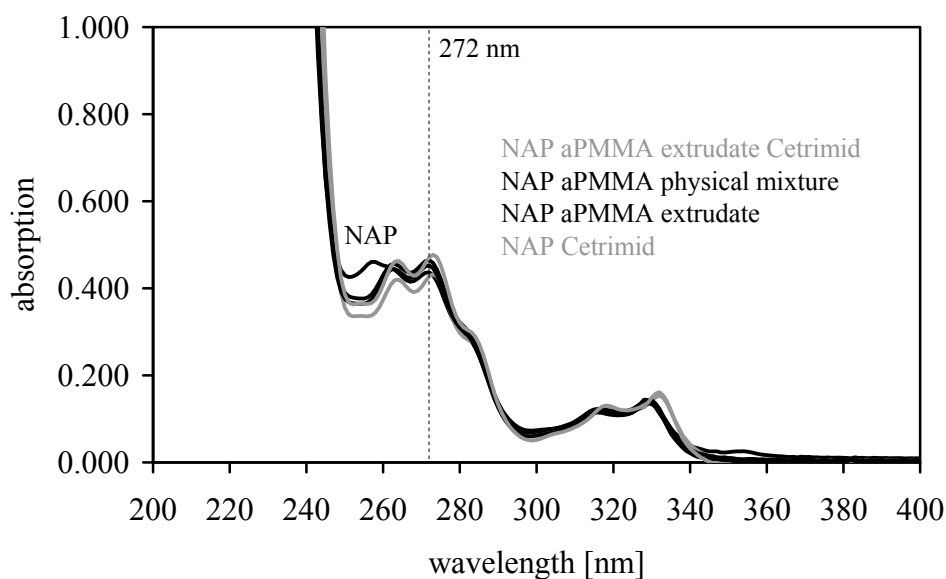
Figure 4.51: Ultraviolet spectra of NAP, NAP/aPMMA 1:1 (w/w) physical mixture, and NAP/aPMMA 1:1 (w/w) extrudate in 0.1 N HCl (black lines) and 0.1 N HCl + 0.3 % cetrimid (grey lines); concentration 10 mg NAP / 500 mL; broken line expresses wavelength, where measurements were performed at

Figure 4.51 shows the same spectra for all formulations, indicating a chemically unchanged drug.

Under sink conditions differences in the dissolution rate can be observed between the pure drug, the physical mixture, and the extrudate (Figure 4.52). The drug is completely dissolved within 20 min. By physical mixing with aPMMA the drug is already released after 6 min. An unexpected slower dissolution is obtained by drug release from the glassy solid solution.

Figure 4.52: Drug release of NAP, NAP/aPMMA 1:1 (w/w) physical mixture, and NAP/aPMMA 1:1 (w/w) extrudate; 50 mg drug; 0.1 N HCl + 0.3 % cetrimid, sink conditions, 37 °C, paddle, 50 rpm, 272 nm; mean ± SD, n=3
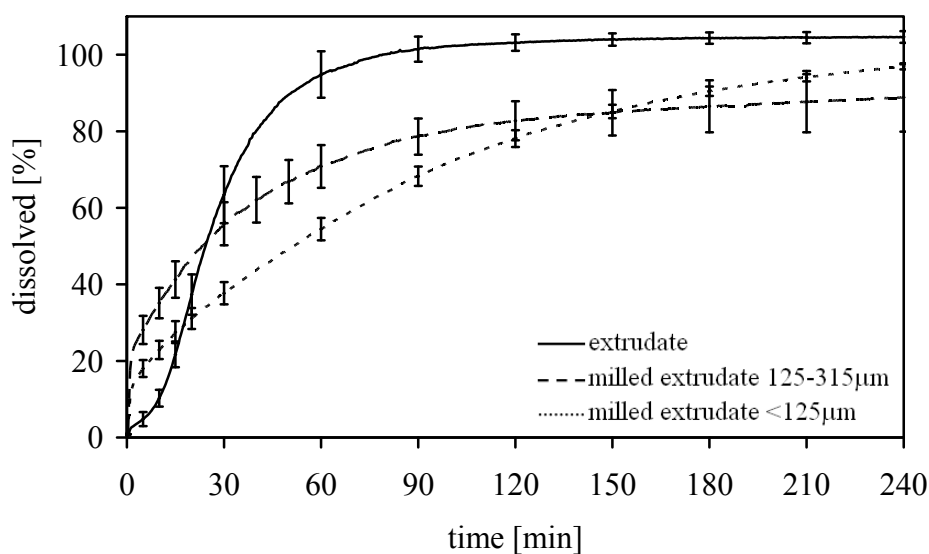
Figure 4.53: Drug release of NAP/aPMMA 1:1 (w/w) extrudate, NAP/aPMMA 1:1 (w/w) milled extrudate 125-315 μm, and NAP/aPMMA 1:1 (w/w) milled extrudate <125 μm; 50 mg drug; 0.1 N HCl + 0.3 % cetrimid, sink conditions, 37 °C, paddle, 50 rpm, 272 nm; mean ± SD, n=3

In Figure 4.53 the dissolution profiles of the entire extrudates and the milled extrudates of two particle sizes are compared.

Within the first minutes, a small particle size is preferential for the drug release, afterwards, drug release from the entire extrudates is faster. NAP/aPMMA melts have poor wettability properties and float on the surface of the dissolution medium. At the beginning, some particles of the milled extrudates are completely wetted by the dissolution medium and are dissolved. The other particles, which float on the surface, form agglomerates that stick together. Therefore, drug release is slower.

Under non-sink conditions no supersaturation is obtained (data not shown). The results of the dissolution experiments under sink and non-sink conditions show, that the formation of a glassy solid solution with aPMMA is not useful to enhance the solubility and the dissolution rate of the poorly water-soluble drug NAP. This might be caused by the high interaction of the drug and the carrier.

4.4.3 Extrusion with oxcarbazepine

Blends of aPMMA and OXC with a drug load of 10% and 50% were hot-melt extruded with the following temperature profiles (Figure 4.54). Transparent, pale yellow extrudates with a drug load of 10% were obtained at a maximum temperature of 210 °C in barrel four and five. To obtain transparent strands with 50% drug load, the temperature of the barrels four and five had to be increased to at least 215 °C. Caused by the high temperature, extrudates had a brown colour, indicating a decomposition of the drug.
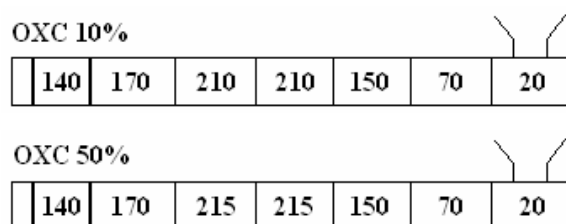
Figure 4.54: Temperature profile of the extruder barrel for OXC/aPMMA 1:9 and 1:1 (w/w); temperatures in °C

OXC/aPMMA 1:9 (w/w) and 1:1 (w/w) extrudates were characterized employing DSC and XRPD analysis to reveal the physical state of the extrudates. Figure 4.55 shows the DCS patterns of the pure drug, the pure carrier, the physical mixture, and the extrudates. A single

T_g, indicating the formation of a glassy solid solution, can be detected for the extrudates. A glass transition for the physical mixture cannot be detected.
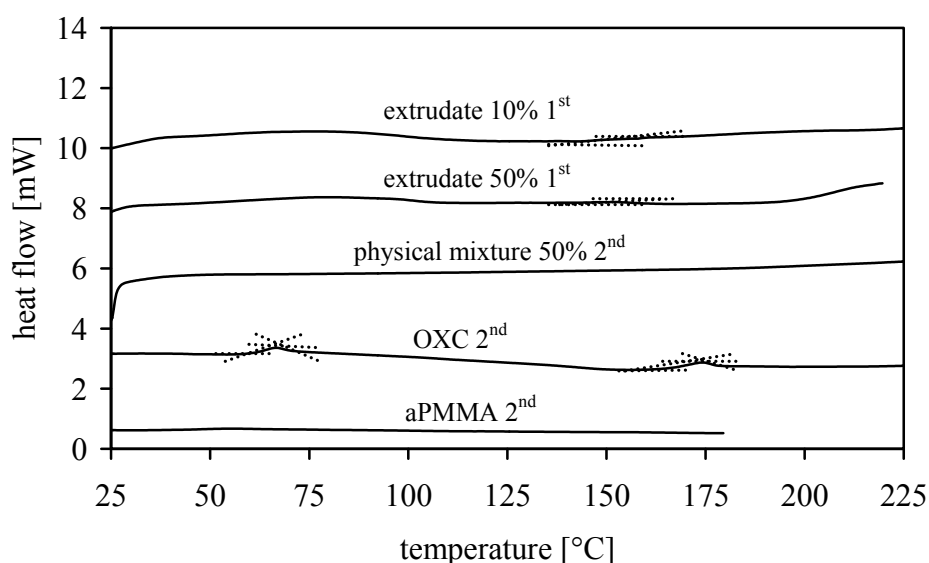
Figure 4.55: DSC patterns of pure carrier, pure drug, OXC/aPMMA 1:1 (w/w) physical mixture, OXC/aPMMA 1:1 (w/w) extrudate, and OXC/aPMMA 1:9 (w/w) extrudate; 1st indicates first heat scan, 2nd second heat scan; heating rate 10 K/min

Long-term and accelerated stability tests were performed according to the ICH guidelines (chapter 7.2.3). OXC/aPMMA 1:9 (w/w) and 1:1 (w/w) extrudates were stable at 25 °C over silica gel (Figure 4.56 and Figure 4.57) and at 60% RH (Figure 4.58 and Figure 4.59) for at least six months.
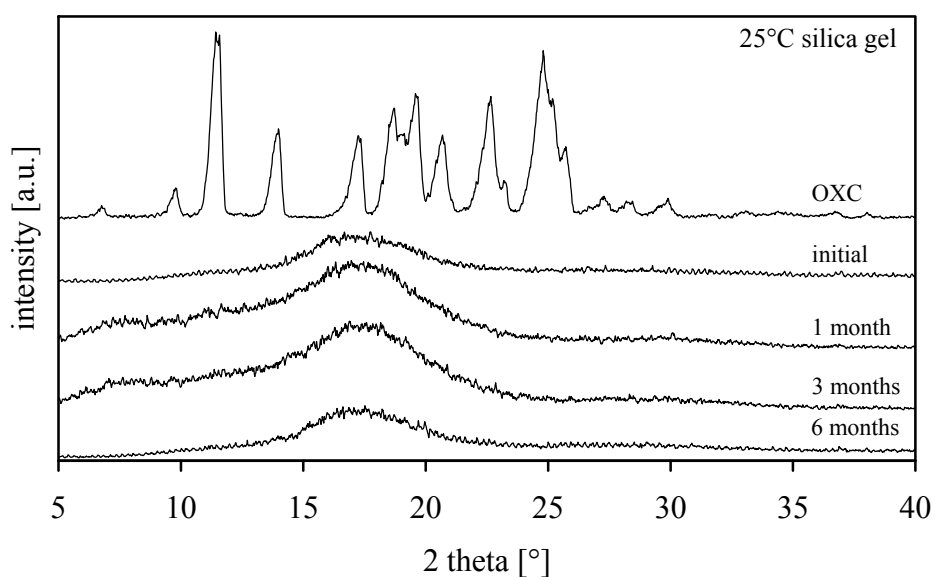
Figure 4.56: XRPD patterns of OXC and OXC/aPMMA 1:9 (w/w) milled extrudates after storage at 25 °C over silica gel up to 6 months
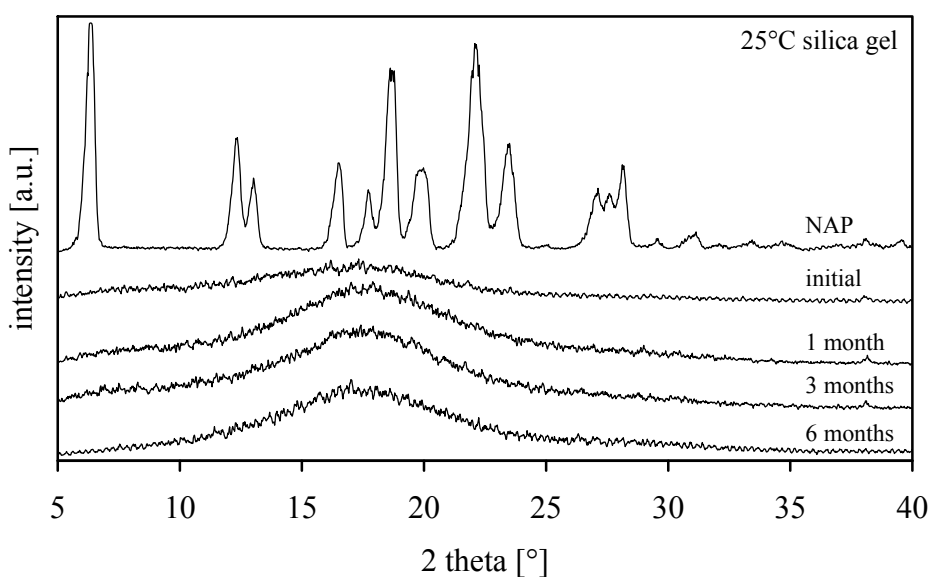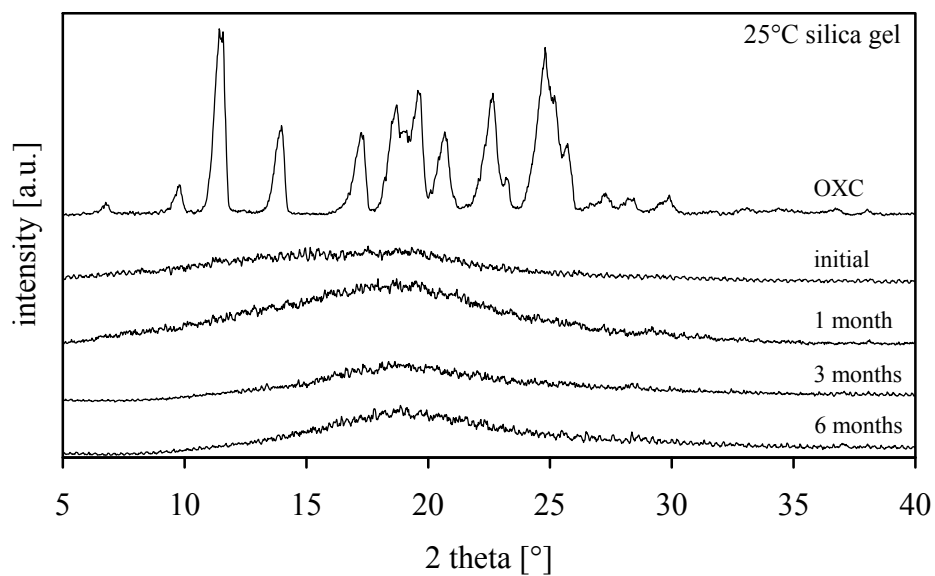
Figure 4.57: XRPD patterns of OXC and OXC/aPMMA 1:1 (w/w) milled extrudates after storage at 25 °C over silica gel up to 6 months
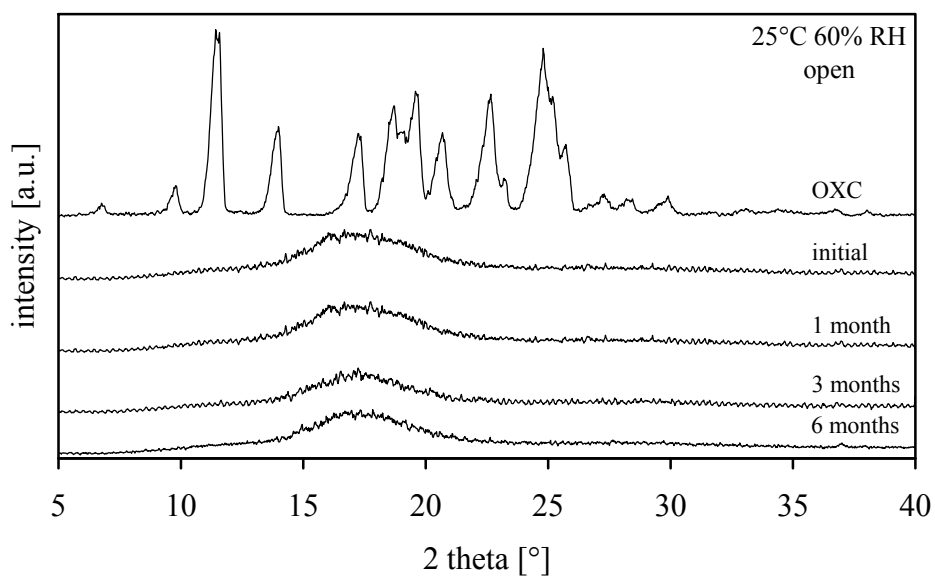
Figure 4.58: XRPD patterns of OXC and OXC/aPMMA 1:9 (w/w) milled extrudates after open storage at 25 °C, 60% relative humidity up to 6 months
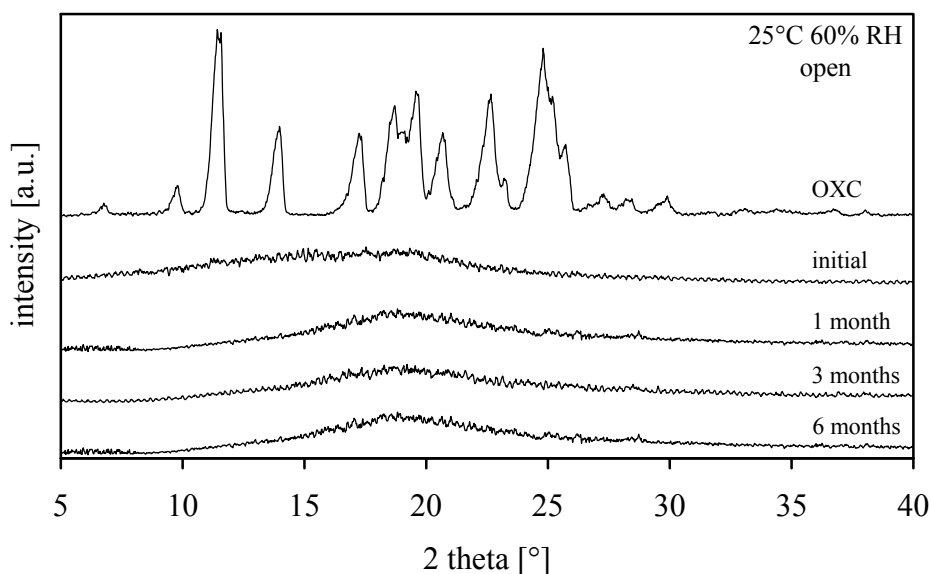
Figure 4.59: XRPD patterns of OXC and OXC/aPMMA 1:1 (w/w) milled extrudates after open storage at 25 °C, 60% relative humidity up to 6 months

OXC/aPMMA 1:9 (w/w) extrudates were stable under accelerated conditions in aluminum foil for at least six months (Figure 4.60). The storage stability of extrudates with a drug load of 50% was not tested under accelerated conditions.
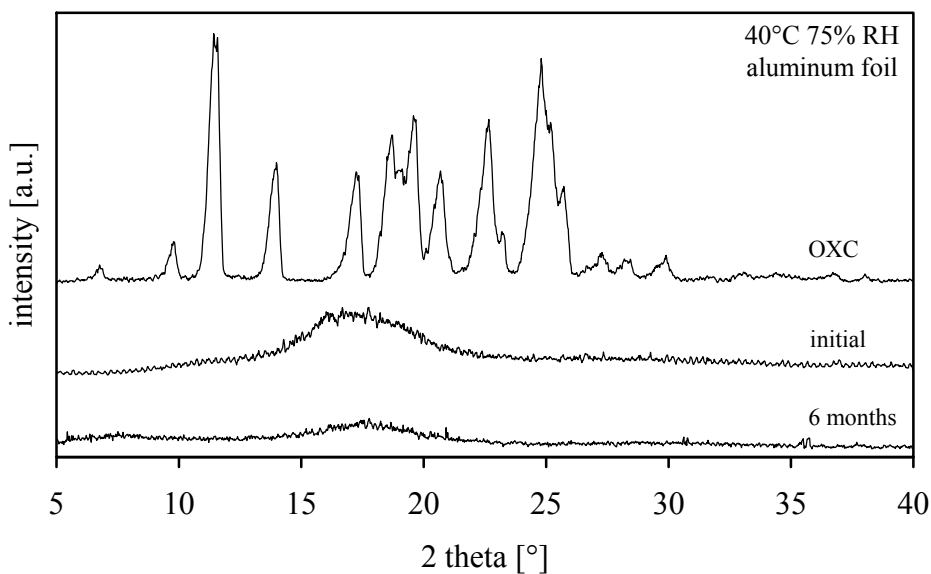
Figure 4.60: XRPD patterns of OXC and OXC/aPMMA 1:9 (w/w) milled extrudates after closed storage at 40 °C, 75% relative humidity in aluminum foil up to 6 months

The dissolution of each sample was determined under sink and non-sink conditions. In order to have a clue to whether the drug is still present in its original form after hot-melt extrusion, ultraviolet spectra of the drug before and after extrusion were evaluated. Figure 4.61 shows the

absorption spectra of OXC, the OXC/aPMMA 1:1 (w/w) physical mixture, and extrudate in 0.1 N HCl with and without surfactant. After hot-melt extrusion, the absorption spectrum of OXC has changed distinctly. The first absorption maximum is shifted from 254 nm to 268 nm without surfactant and to 274 nm with surfactant. The absorption at the second maximum has increased and is shifted from 304 nm to 370 nm. The change of the absorption and the shift of the absorption maxima may be caused by decomposition of the chromophoric system.
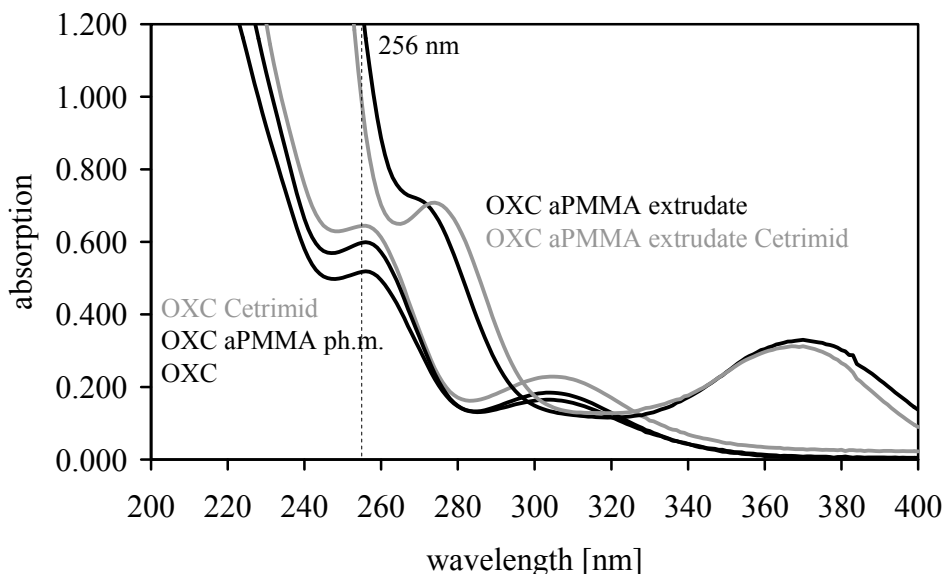
Figure 4.61: Ultraviolet spectra of OXC, OXC/aPMMA 1:1 (w/w) physical mixture, and OXC/aPMMA 1:1 (w/w) extrudate in 0.1 N HCl (black lines) and 0.1 N HCl + 0.3% cetrimid (grey lines); concentration 10 mg OXC / 500 mL; broken line expresses wavelength, at which measurements were performed

Therefore, the absorption values of the extrudates were converted to the absorption values of the pure drug. Under sink conditions differences in the dissolution rate are observed between OXC, the physical mixture OXC/aPMMA 1:1 (w/w), and the extrudate (Figure 4.62). 80 % of OXC are dissolved after 11 min, but already released from the physical mixture after 5 min and from the extrudate even after 1 min. These results are similar to those found for CEL. Since OXC and aPMMA are employed in a micronized form with a particle size of 1.5 μm and 9 μm (Table 8.7 appendix) respectively, and the extrudate as entire strands, the improvement of the dissolution rate is not based on any size effects, but due to glassy solid solution formation.
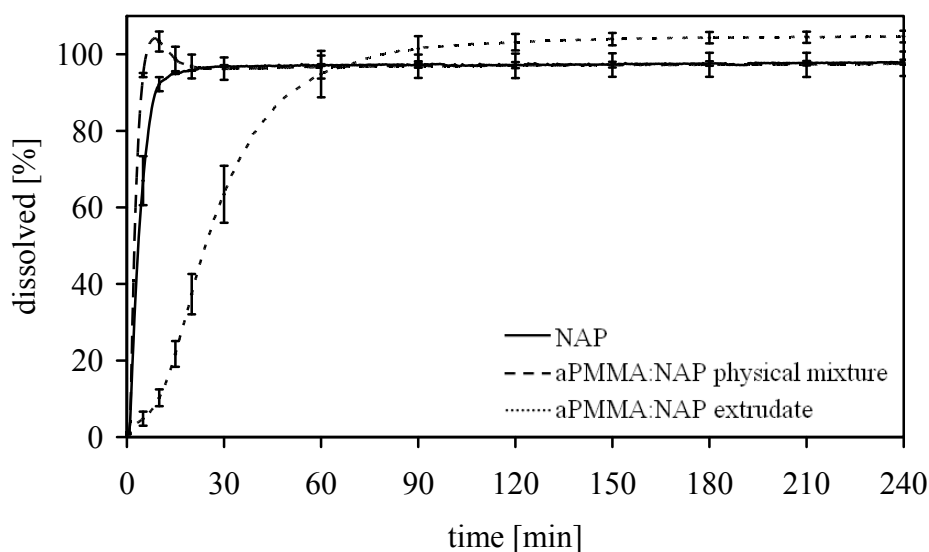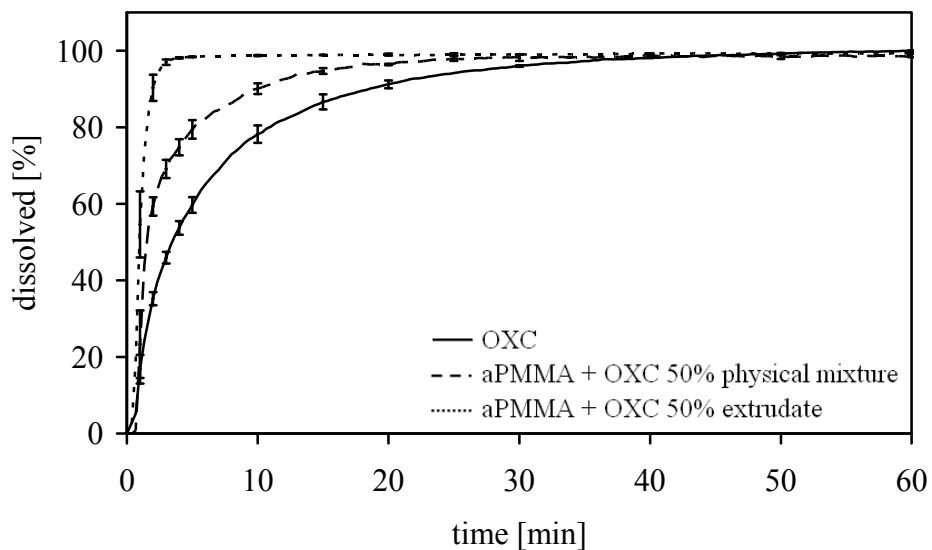
Figure 4.62: Drug release of OXC, OXC/aPMMA 1:1 (w/w) physical mixture, and OXC/aPMMA 1:1 (w/w) extrudate; 20 mg drug; 0.1 N HCl + 0.3 % cetrimid, sink conditions, 37 °C, paddle, 50 rpm, 256 nm; mean ± SD, n=3

The drug load has no effect on the dissolution rate as can be observed in Figure 4.63. In this case 80% of the drug are released after 2 min instead of 1 min like in the formulation with 50% drug load.
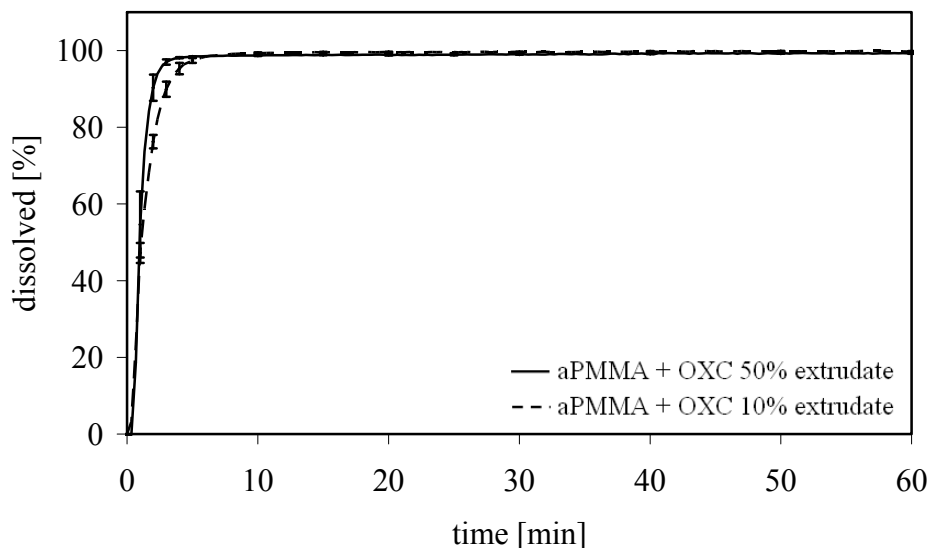
Figure 4.63: Drug release of OXC/aPMMA 1:1 (w/w) extrudate and OXC/aPMMA 1:9 (w/w) extrudate; 20 mg drug; 0.1 N HCl + 0.3 % cetrimid, sink conditions, 37 °C, paddle, 50 rpm, 256 nm; mean ± SD, n=3

Under non-sink conditions (Figure 4.64) a considerable difference can be observed between OXC, the physical mixture, and the extrudate. Already by physical mixing of drug and carrier with mortar and pestle the dissolution rate of the drug is increased. However, a complete dissolution of the drug can only be obtained by transferring the drug to its amorphous state and dispersing it on a molecular base. Thus, drug release from hot-melt extruded glassy solid solutions of OXC/aPMMA is very fast and results in a supersaturated solution. The supersaturated solution is stable for at least four hours. After 24 hours the supersaturation of the solution was examined again. The drug recrystallized and the saturation of the solution decreased in relation to the concentration of the pure drug.
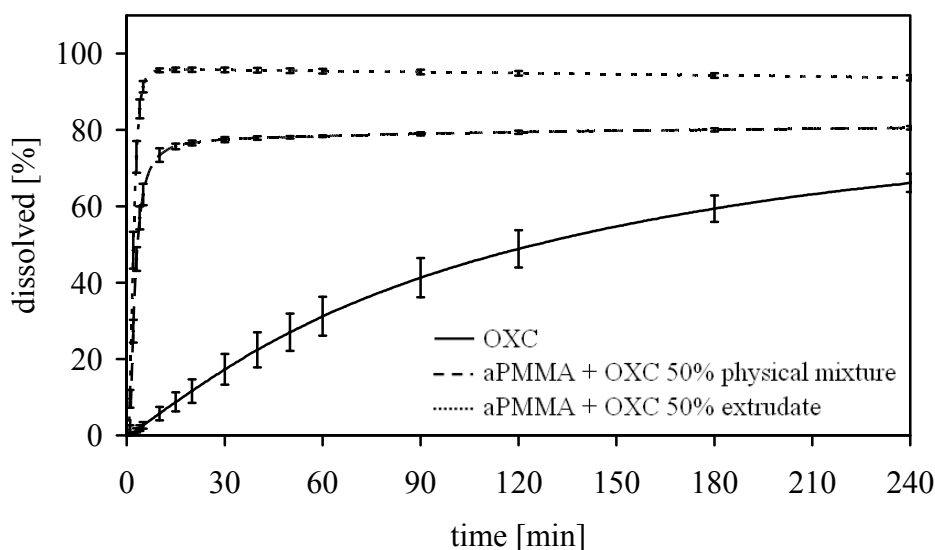
Figure 4.64: Drug release of OXC, OXC/aPMMA 1:1 (w/w) physical mixture, and OXC/aPMMA 1:1 (w/w) extrudate; 150 mg drug; 0.1 N HCl, non-sink conditions, 37 °C, paddle, 50 rpm, 256 nm; mean ± SD, n=3

Similar results were observed for the drug release from extrudates with a drug load of 10% (Figure 4.65). As against the formulation with a drug load of 50%, drug release from the extrudates with 10% drug resulted in a more stable supersaturated solution. Even after 24 hours the drug was kept in solution. This indicates that the carrier has an influence on the solution-state stability of the drug. In this case, not only the physical stability during storage, but also the stability during dissolution can be controlled by aPMMA.
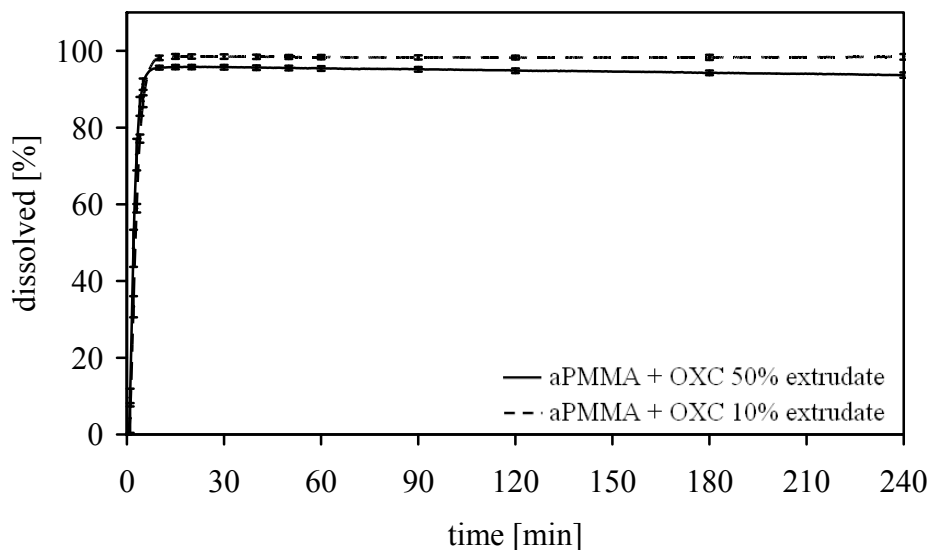
Figure 4.65: Drug release of OXC/aPMMA 1:1 (w/w) extrudate and OXC/aPMMA 1:9 (w/w) extrudate; 150 mg drug; 0.1 N HCl, non-sink conditions, 37 °C, paddle, 50 rpm, 256 nm; mean ± SD, n=3

In order to elucidate the interactions between OXC and aPMMA, FT-IR analysis was performed with the pure carrier and the aPMMA/OXC 1:1 (w/w) melt (Figure 4.66). In the 1:1 (w/w) blend, OXC molecules are present in surplus. Therefore, specifically indicative bands of the carrier were analyzed to discover the interaction between drug and carrier.
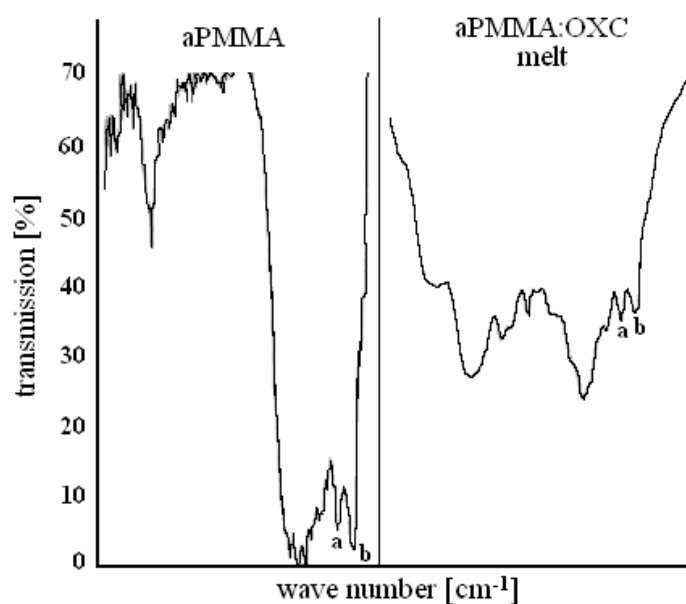
Figure 4.66: FT-IR analysis of aPMMA and aPMMA/OXC extrudate 1:1 (w/w); a and b = bands of the non-protonated dimethylamino groups at 2770 (b) and 2816 (a) cm^{-1}

The absorption bands of the non-protonated dimethylamino groups appear at 2770 and 2816 cm^{-1} in the IR spectrum of the pure carrier. In the IR spectrum of the melt these bands are much smaller, indicating a protonation of the dimethylamino groups. Thus, a reaction between the dimethylamino group of aPMMA and the CH-acidic group of OXC may take place. Further investigations on the interactions between OXC and aPMMA are described in chapter 4.5.

4.4.4 Summary

The use of aPMMA as solubility enhancing carrier in hot-melt extrusion can not be transferred easily to all drugs. Depending on the properties of the drug, specifically the melting point and the pK$_a$, aPMMA can be a useful carrier in glassy solid solution formation, but might be insufficient for solubility improvement.

The formation of a glassy solid solution evolves from interactions between the drug and the carrier. Bonds can differ in their strength and can be advantageous or disadvantageous for a fast dissolution. All three drugs can build amorphous glassy solid solutions with aPMMA, but only the dissolution rate of CEL and OXC could be improved.

Furthermore, decomposition processes can occur, when processing the drug at high temperatures. Since OXC does not seem to be soluble sufficiently in the molten carrier, the process temperature cannot be decreased to lower temperatures.

The amount of carrier can have an influence on the solution-state stability of the drug, as could be observed for OXC.

In conclusion, hot-melt extrusion with aPMMA is a suitable method to increase the solubility of poorly soluble drugs, but each formulation has to be analyzed separately. As every drug shows a different behaviour, no general prediction can be made so far.

4.5 Prediction of solid dispersion production

4.5.1 Introduction and objective

A prerequisite for the formation of a glassy solid solution is the miscibility of drug and carrier in the molten state. Two substances are miscible when their melt appears in a transparent single-phase state. In order to be able to form such systems, drugs and carriers have to comply with several requirements.

Pharmaceutical drugs and excipients can be characterized by means of their structure and functional groups. A good miscibility between substances is obtained if they have similar hydrophilic or lipophilic properties, or if they possess functional groups that are able to interact. Whether a drug is miscible with a carrier is difficult to predict, but very important for the formulation of glassy solid solutions. Laboratory-scale hot-melt extruders require considerable quantities of drug substance, which are not always available at the early developmental stage when pilot formulation studies are undertaken.

In literature several tools for the prediction of miscibility are described. The calculation of solubility parameters have been used with some success in studies by Suzuki and Sunada (1997), Greenhalgh et al. (1999), Hancock et al. (1997), and Forster et al. (2001b). Hot stage microscopy can be a useful tool to predict the miscibility of drug and carrier, if both substances can be molten (Forster 2001b). As most polymers have a high T_g and occur as highly viscous melts at high temperatures, the miscibility of these substances with molten drugs is sometimes not detectable. The analysis of the melting endotherm onset temperature and heat of fusion can be used to investigate miscibility (Theeuwes 1974, Forster 2001b, Oladiran 2007). In order to investigate the interactions between drug and carrier on a molecular level, molecular dynamics simulations can be performed. By comparing electrostatic forces, hydrogen bonds and van der Waals dispersion forces between drug and carrier, the miscibility can be predicted (Langer 2003a, Langer 2003b).

In spite of several tools existing to predict the miscibility of drug and carrier the process of glassy solid solution formation is still not clarified. Therefore, the miscibility of several drugs with different chemical structures and four different carriers was examined. Their miscibility was investigated by means of solubility parameters, DSC measurements, and molecular dynamics simulations. Several drug/carrier blends were hot-melt extruded and characterized by DSC and XRPD analysis, in order to obtain information about the solid state of the molten systems.

4.5.2 Chemical structure and properties of drugs and carriers

4.5.2.1 Drugs

The following drugs (chapter 7.1.1) were investigated for miscibility studies (Figure 4.67).
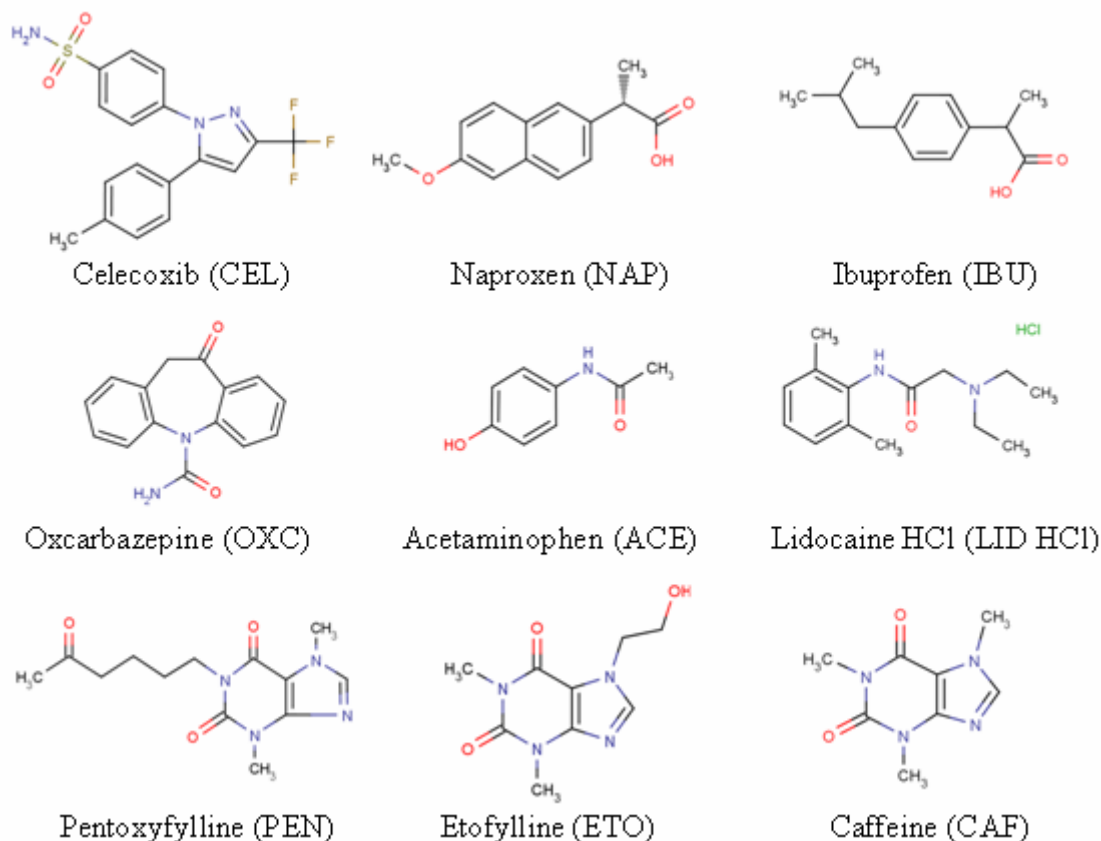
Figure 4.67: Drugs investigated for miscibility studies

NAP and IBU are compounds containing a carboxyl group. Each oxygen atom carries two pairs of unshared valence electrons. These oxygen atoms are electronegative with respect to the carbonyl carbon and the hydroxyl hydrogen. Thus, the carboxyl group is polar and can lose a proton to a strong or moderately strong base. Caused by the carboxyl group these compounds have an acidic character. The water-solubility is decreased to a high extent by the lipophilic part of the molecule which is expressed by the logP value of 3 for NAP and 3.7 for IBU (Table 4.2).

The properties of CEL are mainly influenced by the sulfonamide group which has a weak acidic character. CEL is a high lipophilic compound as it has a high logP value of 4.2.

OXC also has a weak acidic character as the methylene group in the two-carbon bridge between an aromatic ring and a carbonyl group has C-H acidity. The entire molecule has a less lipophilic character than NAP, IBU, and CEL as the logP value (1.2) is smaller. The poor solubility of this compound is mainly due to its high lattice energy.

drug	MW	T_m [°C]	H_f [J/g]	T 2nd [°C]	pK_a	logP	δ_t [MPa$^{0.5}$]	HB_{acc}	HB_{don}	c_s H_2O [mg/L]
CEL	381	162	102	57 T_g	9.68a -6.12b	4.213	25.10	5	2	3
NAP	230	157	143	157 T_m	4.84a	2.998	22.47	3	1	15.9
IBU	206	76	134	-45 T_g	4.41a	3.722	19.36	2	1	21
LID HCl	271	72	266	36 T_g			(13.57)*			
ACE	151	169	185	23 T_g 158 T_m	9.86a 1.72b	0.339	24.61	3	2	14000
OXC	252	231	158	62 T_g 167 T_g	13.73a -0.53b	1.246	26.91	4	2	83
PEN	278	105	127	-16 T_g	0.76b	0.322	25.10	7	0	77000
ETO	224	163	153	147 T_m 164 T_m	14.41a	-0.551	33.86	7	1	
CAF	194	236	103	238 T_m	0.73b	-0.131	29.13	6	0	21600

Acetaminophen is a weak acid relating to the phenol group, whereas the deprotonated phenolate represents a comparatively strong base. The amide is less basic than an amine, so that the weak acidic character prevails. ACE was chosen as model drug because it has a similar melting point as the extremely poorly water-soluble drug CEL. Furthermore, LID HCL was extruded in order to examine the behaviour of salts with respect to glassy solid solution formulation with aPMMA. Finally the three water-soluble xanthines PEN, ETO and CAF were chosen to investigate the influence of the melting temperature of the drug on the behaviour in solid dispersion formulation. The xanthine derivates do not possess any basic qualities as they form cyclic acid amides. PEN, ETO, and CAF as tertiary amines have a neutral character. The 7-hydroxyalkyl derivative ETO possesses a polar substituent.

4.5.2.2 Basic butylated methacrylate copolymer

aPMMA is an alternating copolymer consisting of 50% dimethylaminoethylmethacrylate, 25% methylmethacrylate and 25% butylmethacrylate (Figure 4.68).
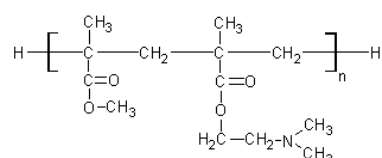
Figure 4.68: Chemical structure of basic butylated methacrylate copolymer

The monomer contains two carbonyl groups and a dimethylamino group as functional groups. As the carbonyl groups are located quite close to the carbon chain, merely a few interactions

can be undergone with these polar groups. Therefore, the most reactive part is the amine. It is a weak base, which can donate a pair of unshared valence electrons from the nitrogen and form a bond with a proton. Caused by its basicity the amine can interact with acids in an acid-base reaction (Quinteros 2008).

Especially drugs with an acidic functional group, like NAP, IBU, CEL or OXC are readily soluble in the aPMMA melt. The deciding factor for the amount of drug dissolving in the molten carrier is its pK_a, whereby acidic drugs with a small pK_a have a higher solubility in aPMMA.

4.5.2.3 Copovidone
COP is a statistic copolymer consisting of vinylpyrrolidone and vinylacetate (Figure 4.69).
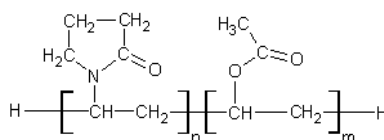
Figure 4.69: Chemical structure of copovidone

As the polymer comprises hydrophilic carbonyl groups as well as lipophilic carbon chains, both hydrophilic and lipophilic substances dissolve in the molten carrier. The included carbonyl groups are the functional units, which can form hydrogen bondings to polyphenols and yield interactions with phenolic OH-groups. Therefore, specifically the phenolic group of ACE, the acidic groups of NAP and CEL, and to a lesser extent the alcoholic group of ETO can interact with the carbonyl groups of copovidone. Besides the hydrophilic interactions additionally van der Waals forces support the dissolving of the drugs in the molten carrier to a greater extent.

4.5.2.4 Polyethylene glycol – polyvinyl alcohol copolymer
The polyethylene glycol - polyvinyl alcohol graft copolymer (Figure 4.70) is a hydrophilic molecule that is readily soluble in water.
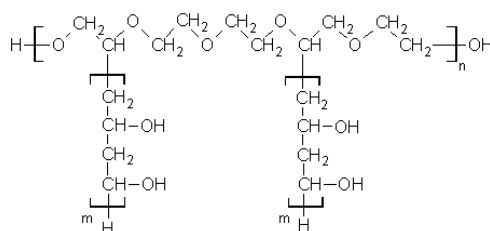
Figure 4.70: Chemical structure of polyethylene glycol – polyvinyl alcohol copolymer

The polyvinyl alcohol moiety has good melt extrusion properties and the polyethylene glycol part acts as an internal plasticizer. The PEG moiety of the polymer enables the high aqueous solubility caused by the hydration of the ether oxygen whereas PVA's aqueous solubility is only slight.

4.5.2.5 Isomalt

Isomalt (Figure 4.71) is a sugar alcohol that possesses considerable hydrophilic qualities because of the high amount of OH groups. Thus, drugs that can easily form hydrogen bonds dissolve in this carrier.
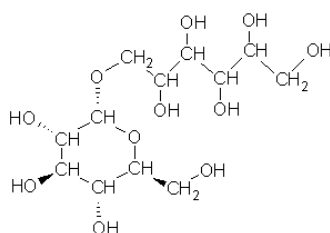
Figure 4.71: Chemical structure of isomalt

4.5.3 Solubility parameters

As a first tool, the estimates of the solubility parameter were used to predict the miscibility. Compounds with similar values for δ are likely to be miscible. This miscibility is caused by the balancing of the energy of mixing released by interactions within the components by the energy released by interactions between the components (Greenhalgh 1999). Three-dimensional solubility parameters by Hansen (1969) can be calculated by group contributions for dispersion forces, polar forces and hydrogen bonding forces provided by Van Krevelen/Hoftyzer (1976) and Fedors (1974). To represent the three-dimensional solubility parameters in a graphical form, the data are transferred into a two-dimensional plot. By means of thermodynamic considerations Bagley et al. concluded that the effects of δ_d and δ_p show close similarity and so introduced the combined solubility parameter δ_v (Bagley et al. 1971). The parameter for components of intermolecular hydrogen bonding δ_h and the combined parameter δ_v are plotted in a diagram (chapter 7.2.2.1) to project the three-dimensional solubility parameter space into a two-dimensional plot which is called Bagley diagram (Figure 4.72). The Bagley diagram shows that the carriers differ more in their hydrogen bond properties than in the dispersion and polar forces represented by the combined solubility parameter δ_v. Small differences between the corresponding solubility parameters (Δδ) can be observed for aPMMA and IBU and NAP. Δδ values of aPMMA and PEN, CEL, OXC, and ACE are only marginally higher, whereas CAF and ETO show Δδ values $>10 MPa^{0.5}$. Since

COP and aPMMA have similar hydrogen bond as well as polar and dispersion forces, they should be miscible with the same drugs. PEG-PVA is a carrier with significantly higher hydrogen bond forces due to the PEG moiety of the copolymer. Therefore, only ETO has a $\Delta\delta<10\text{MPa}^{0.5}$. ISO has even higher hydrogen bond forces than PEG-PVA and shows therefore $\Delta\delta$ values $>10\text{MPa}^{0.5}$ with all drugs.
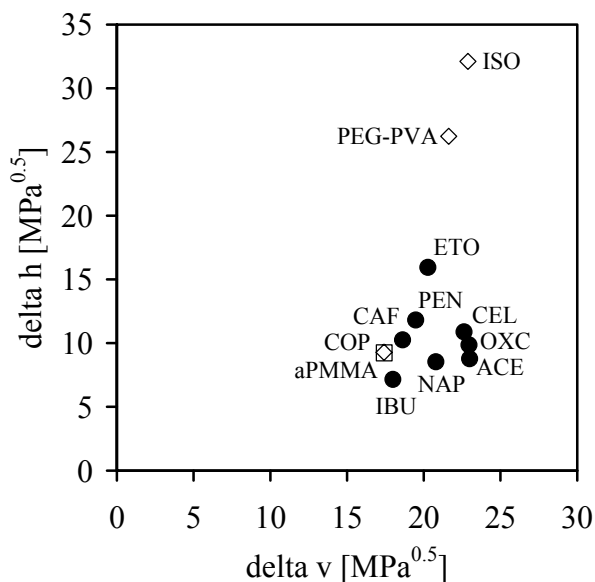
Figure 4.72: Location of carriers (open symbols) and drugs (closed symbols) within the Bagley plot

Greenhalgh et al. (1999) classified compounds according to their difference in solubility parameters. The authors found out that compounds with a $\Delta\delta<7.0\text{MPa}^{0.5}$ were likely to be miscible, but likely to be immiscible with a $\Delta\delta>10\text{MPa}^{0.5}$. Forster et al. (2001b) investigated the selection of excipients for melt extrusion by solubility parameter calculation. They demonstrated that compounds with a $\Delta\delta<2\text{MPa}^{0.5}$ were likely to be miscible and were able to form glassy solid solutions when melt extruded. Like Greenhalgh et al. they observed that compounds with a $\Delta\delta>10\text{MPa}^{0.5}$ were likely to be immiscible and could not be expected to form glassy solid solutions.

According to the results of Greenhalgh et al. and Forster et al., the total solubility parameters (chapter 7.2.2.2) of all drug carrier blends, which were subject to the hot-melt extrusion process in the further investigation, were compared and the corresponding $\Delta\delta$ values were calculated. Table 4.3 shows the $\Delta\delta$ values of the total solubility parameters and the distance of the respective compounds within the Bagley diagram (chapter 7.2.2.3). The data demonstrate that the $\Delta\delta$ values of the total solubility parameters are not always consistent with the distance of the respective compounds within the Bagley diagram as can be observed for the PEG-

PVA/ETO blend. In such cases, a more detailed interpretation of the three-dimensional parameters is mandatory. Overall, a high $\Delta\delta_h$ leads to a high distance in the Bagley diagram.

Table 4.3: Differences in solubility parameters between several carriers and drugs and their distance, calculated by the Pythagorean Theorem (chapter 7.2.2.3), within the Bagley diagram; glassy solid solutions are printed in bold

carrier	drug	$\Delta\delta_h$ [MPa$^{0.5}$]	$\Delta\delta_v$ [MPa$^{0.5}$]	$\Delta\delta_{total}$ [MPa$^{0.5}$]	distance [MPa$^{0.5}$]
aPMMA	PEN	1.0	1.2	1.5	1.56
aPMMA	IBU	2.1	0.6	**0.4**	**2.21**
aPMMA	CAF	2.5	2.1	3.1	3.27
COP	NAP	0.7	3.4	**2.7**	**3.43**
aPMMA	NAP	0.7	3.4	**2.7**	**3.46**
COP	CEL	1.7	5.2	**5.4**	**5.45**
aPMMA	CEL	1.6	5.2	**5.4**	**5.45**
aPMMA	OXC	0.6	5.5	**5.3**	**5.57**
COP	ACE	0.5	5.6	**4.9**	**5.58**
aPMMA	ACE	0.5	5.6	**4.9**	**5.60**
aPMMA	ETO	6.7	2.9	6.1	7.26
COP	ETO	6.7	2.8	**6.1**	**7.30**
PEG-PVA	ETO	10.3	1.4	8.2	10.37
PEG-PVA	CEL	15.4	1.0	8.9	15.38
ISO	ETO	16.2	2.6	**13.6**	**16.38**
PEG-PVA	NAP	17.7	0.8	11.5	17.71
ISO	CEL	21.2	0.3	14.3	21.24
ISO	ACE	23.3	0.1	14.8	23.34
ISO	NAP	23.6	2.1	17.0	23.67

As already expected from the chemical structure of the carriers and drugs, aPMMA is predicted to be miscible with IBU and NAP, and COP with NAP, CEL, and ACE. ISO seems to be immiscible with all drugs as inferred by the high differences, because ISO has extremely hydrophilic properties. Deriving from the table it can be deduced with few exceptions only that two substances are miscible if their distance in the Bagley plot is ≤5.60 or if the difference in their total solubility parameters is ≤5.4.

4.5.4 Production and characterization of extrudates

Extrusion experiments (chapter 7.2.1.3) were performed in order to examine the miscibility of drugs and carriers predicted by solubility parameter calculation and characterization of the chemical structure. All blends showed a different behaviour during the melt extrusion process and during cooling of the strands. For the formation of transparent semisolid strands the glass transition temperature, the physical state and the stickiness (Palzer 2005) of the extrudates play a decisive role. In case of glassy solid solutions the extrudates appear as a transparent colourless strand with a single T_g. Sticking effects occur when the T_g of the extrudate is

located below room temperature. Significant discolouration points to decomposition effects, which are likely to occur at high temperatures. The miscibility of two compounds is independent of the stability of the glassy solid solution. The extrusion of different drug carrier blends led to the following results (Table 4.4).

Table 4.4: Extrudates with aPMMA, COP, and PEG-PVA; T_g = mean [°C], T_m = peak [°C], * = second heat scan of physical mixture

drug	carrier	drug content [%]	T_g or T_m [°C] 1st heat scan extrudate	colour of extrudate	formation of strands	sticki-ness	crystalline
CEL	aPMMA	50	48 T_g	colourless to pale yellow	+	-	-
CEL	COP	50	63 T_g 104 T_g	colourless	+	-	-
CEL	PEG-PVA	50	35 T_g 157 T_m	pale yellow	+	-	+ partly
NAP	aPMMA	50	31 T_g (147 T_m)	colourless	+	-	-
NAP	COP	50	blend could not be dispensed into the extruder				
NAP	PEG-PVA	50	35 T_g 106 T_m 148 T_m	white	+	-	+ when cooling
IBU	aPMMA	50	-4 T_g	colourless	+	+	-
ACE	aPMMA	10	not investigated	pale yellow	+	-	-
ACE	aPMMA	30	27 T_g	brown	+	-	-
ACE	COP	50	30 T_g 134 T_m 160 T_m	colourless	+	-	+ after months
OXC	aPMMA	10	neither T_m nor T_g detected	pale yellow	+	-	-
OXC	aPMMA	50	22 T_g	brown	+	-	-
LID HCl	aPMMA	50	24 T_g*	colourless	+	+	+ after 24 hours
PEN	aPMMA	50	-16 T_g*	white	-	-	+ when cooling
ETO	aPMMA	50	17 T_g* 135/140/147/163 T_m*	white	+	-	+ partly
ETO	COP	50	41 T_g*	white	+	-	+
ETO	PEG-PVA	50	38 T_g 157 T_m 192 T_m	white	+	-	+ when cooling
CAF	aPMMA	50	232 T_m*	white-yellow	+	-	+

Systems with a single T_g could be obtained with CEL/aPMMA, NAP/aPMMA, IBU/aPMMA, ACE/aPMMA, OXC/aPMMA, LIDHCl/aPMMA, PEN/aPMMA, and ETO/COP. A small

endothermic peak could be detected in the DSC for the NAP/aPMMA blend, which is not concordant with the appearance of the extrudates and the results of XRPD analysis. The T_g of IBU/aPMMA lies below room temperature which generates the sticking properties of the strands. The extrudates of LIDHCl/aPMMA show the same sticking behaviour and, additionally, recrystallization after 24 h. The viscosity of the transparent ETO/COP melts is too low to build semisolid strands. Decreasing the temperature, leads to a sudden increase of the viscosity, resulting in crystalline strands. Thus, the production of a glassy solid solution in this case rather presents a problem of process design. CEL/COP extrudates depict a two-phase system with two separate amorphous parts. Systems with an amorphous and crystalline structure are formed by all the other blends. The CEL/PEG-PVA and the ETO/aPMMA extrudates are only partially crystalline and maintain this solid state during storage at least for six months. In these systems the drug is mainly stabilized in its amorphous form by interactions with the carrier. Full details on the XRPD analysis and the stability tests are given on the appendix (Figure 8.10 to Figure 8.19).

The appearance of the extrudates and the results from DSC and XRPD analysis are good tools to determine the solid state properties of the strands and to identify the type of solid dispersion. Table 4.5 reviews the results of all hot-melt extruded samples. With the help of DSC data it is possible to distinguish between a one-phase glassy solid solution, where the drug is dispersed in the amorphous carrier on a molecular base, and a two-phase amorphous suspension with either two amorphous or one amorphous and one crystalline phase. The XRPD pattern also informs about the solid state of the extrudates telling the difference between amorphous or crystalline forms. Even the visual appearance of the strands can disclose the solid state characteristics because amorphous one-phase systems have a transparent appearance whereas two-phase systems are usually opaque.
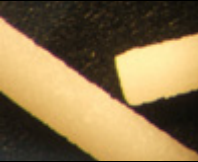
Single-phase glassy solid solutions could be obtained for the blends CEL/aPMMA, NAP/aPMMA, IBU/aPMMA, ACE/aPMMA, OXC/aPMMA, and ETO/COP. In CEL/COP extrudates two separate amorphous phases can be detected which point to an amorphous suspension with two amorphous phases, although CEL/COP strands show a transparent appearance. The viscosity of the melt composed of PEN/aPMMA is too low to build semisolid strands. The melt has an opaque appearance. This points to an immiscible system, even if an amorphous one-phase system was detected by DSC and XRPD analysis. PEN itself can be changed to the amorphous state in a melt extrusion process and can therefore form a separate stable amorphous phase. The issue of the solid state properties of the PEN/aPMMA solid dispersion are not completely solved. As the signal for the T_g of aPMMA was missing in

the DSC analysis, it is not clear if the melt is composed of one or two phases. All other formulations result in amorphous suspensions wherein the excipient is present in an amorphous and the drug in a partially or completely crystalline state.

Table 4.5: Identification of hot-melt extruded solid dispersions regarding solid state properties

compounds		DSC: phases & physical state		XRPD: physical state & stability 25°C silica gel		macroscopic appearance	result amorphous (A) crystalline (C)
CEL 50%	aPMMA	one	amorphous	amorphous	6 months		glassy solid solution (A)
CEL 50%	COP	two	amorphous, amorphous	amorphous	6 months		glass suspension (A/A)
CEL 50%	PEG-PVA	two	amorphous, crystalline	partly crystalline	initial 6 months		glass suspension (A/C)
NAP 50%	aPMMA	one	amorphous	amorphous	6 months		glassy solid solution (A)
NAP 50%	PEG-PVA	two	amorphous, crystalline 2x	crystalline	when cooling		glass suspension (A/C)
IBU 50%	aPMMA	one	amorphous	amorphous	6 months		glassy solid solution (A)
ACE 30%	aPMMA	one	amorphous	amorphous	6 months		glassy solid solution (A) / (glass suspension)
ACE 50%	COP	two	amorphous, crystalline 2x	amorphous	6 months		glass suspension (A/C)
OXC 10%	aPMMA	one	amorphous	amorphous	6 months		glassy solid solution (A)

Table 4.6: Identification of hot-melt extruded solid dispersions regarding solid state properties, continued

compounds		DSC: phases & physical state		XRPD: physical state & stability 25°C silica gel		macroscopic appearance	result amorphous (A) crystalline (C)
OXC 50%	aPMMA	one	amorphous	amorphous	6 months		glassy solid solution (A)
LID HCl 50%	aPMMA	one	amorphous	-	24 hours		glass suspension (A/C) ?
PEN 50%	aPMMA	one	amorphous	amorphous	6 months		glass suspension (A/A) ?
ETO 50%	aPMMA	two	amorphous, crystalline 4x	partly crystalline	initial 6 months		glass suspension (A/C)
ETO 50%	COP	one	amorphous	amorphous	6 months		glassy solid solution (A)
ETO 50%	PEG-PVA	two	amorphous, crystalline 2x	crystalline	when cooling		glass suspension (A/C)
CAF 50%	aPMMA	one	crystalline	crystalline	initial		glass suspension (A/C)

ACE/aPMMA extrudates had a transparent appearance and showed an amorphous state in the XRPD pattern (Figure 8.10 and Figure 8.11 appendix). However, in the DSC pattern a small crystalline peak was revealed (data not shown) indicating that the drug is present in two physical forms simultaneously. Qui et al. (2008) found that the drug crystals were preferentially located in the centre, rather than on the surface of the extrudate.

4.5.5 Thermoanalytical investigations

Whether and to what extent a drug is soluble in a carrier is determined by means of melting enthalpy and onset melting temperature measurements of drug/carrier blends. The following

results arise from DSC measurements. The values for the enthalpy and the melting temperature are derived from the first heating step. All blends are prepared in advance with mortar and pestle. As the carriers applied in this study concern polymers possessing a high viscosity in the molten state, the samples mix insufficiently in the DSC-pan. Thus a complete interaction between drug and carrier molecules is not possible, and only directly adjacent molecules are able to interact. Therefore the determination of the enthalpy and melting temperature ratios merely allow a rough estimation of convenient combinations of drug and carrier and not an exact determination of the saturation solubility of a drug in a molten carrier as described by Theeuwes (1974) and Oladiran et al. (2007). For the DSC measurements a heating rate of 10 K/min is chosen, as it is suitable for the determination of melting points as well as of glass transition temperatures. With a slower heating rate the drug has more time to dissolve in the molten carrier and the solubility might increase. The exact values given in the following tables are thus dependent on the test conditions.

The ratio "enthalpy drug in carrier / enthalpy drug" is a parameter that specifies to what extent the drug is soluble in the molten carrier under the chosen test conditions. Thereby a value of one signifies a complete insolubility of the drug in the molten carrier as the enthalpy of the drug in the blend with the carrier has not decreased.

Table 4.7: Melting enthalpies of the pure drug and the drug in a 1:1 (w/w) blend with a carrier

drug	carrier	melting enthalpy of pure drug [J/g]	melting enthalpy of drug in 1:1 (w/w) blend with carrier [J/g]	ratio (enthalpy drug in carrier) / (enthalpy drug)
IBU	aPMMA	134	45	0.34
NAP	aPMMA	143	50	0.35
OXC	aPMMA	158	93	0.59
CEL	aPMMA	102	75	0.74
LID HCl	aPMMA	266	231	0.87
ETO	aPMMA	153	134	0.88
CAF	aPMMA	103	100	0.97
ACE	aPMMA	185	186	1.01
PEN	aPMMA	127	136	1.07
ACE	COP	185	89	0.48
NAP	COP	143	73	0.51
CEL	COP	102	61	0.60
ETO	COP	153	127	0.83
CEL	PEG-PVA	102	49	0.48
NAP	PEG-PVA	143	109	0.76
ETO	PEG-PVA	153	154+13	1.09
ETO	ISO	153	103	0.67
ACE	ISO	185	170	0.92
NAP	ISO	143	138	0.97
CEL	ISO	102	100	0.98

Hence, CAF, ACE, and PEN are not soluble in aPMMA, and NAP and CEL are not soluble in ISO at 1:1 (w/w) drug/carrier blends (Table 4.7). Good solubilities were found for the blends IBU, NAP, and OXC with aPMMA, ACE, NAP, and CEL with COP, CEL with PEG-PVA and ETO with ISO.

The melting temperature of the drug can also be affected if the drug is soluble in the molten carrier. With increasing solubility the melting temperature of the drug decreases, which is accompanied by a widening of the melting peak. The ratio "T_m drug in carrier / T_m drug" signifies the extent of solubility with a ratio of one indicating no melting point shift. A decisive melting temperature decrease can be observed for CEL and NAP in a 1:1 blend with aPMMA and for ACE and NAP in combination with COP (Table 4.8). The interpretation of the melting point decrease is less exact, because the onset temperature is difficult to determine for broad peaks. The onset melting temperature is less dependent on the heating rate than the peak of the melting endotherm, but can vary slightly by changing the test conditions.

Table 4.8: Onset melting temperatures of the pure drug and the drug in a 1:1 (w/w) blend with a carrier

drug	carrier	onset T_m of pure drug [°C] and [K]	onset T_m of drug in 1:1 blend with carrier [°C] and [K]	ratio (T_m drug in carrier) / (T_m drug)
CEL	aPMMA	162 / 435	97 / 370	0.85
NAP	aPMMA	157 / 430	96 / 369	0.86
OXC	aPMMA	231 / 504	201 / 474	0.94
ACE	aPMMA	169 / 442	155 / 428	0.97
IBU	aPMMA	76 / 349	70 / 343	0.98
LID HCl	aPMMA	72 / 345	68 / 341	0.99
CAF	aPMMA	236 / 509	230 / 503	0.99
ETO	aPMMA	163 / 436	162 / 435	1.00
PEN	aPMMA	105 / 378	104 / 377	1.00
ACE	COP	169 / 442	122 / 395	0.89
NAP	COP	157 / 430	113 / 386	0.90
ETO	COP	163 / 436	133 / 406	0.93
CEL	COP	162 / 435	136 / 409	0.94
CEL	PEG-PVA	162 / 435	151 / 424	0.97
NAP	PEG-PVA	157 / 430	151 / 424	0.97
ETO	PEG-PVA	163 / 436	161 / 434	1.00
ETO	ISO	163 / 436	145 / 418	0.96
ACE	ISO	169 / 442	164 / 437	0.99
CEL	ISO	162 / 435	161 / 434	1.00
NAP	ISO	157 / 430	156 / 429	1.00

For a better understanding of the examination of the onset melting temperature and the melting enthalpy Figure 4.73 gives an overview over the DSC patterns of the pure drugs, the pure carriers, and the physical mixtures. Values were taken from the first heat scan of the drugs and the physical mixtures at 10 K/min.

(a)

(b)

(c)

(d)

(i)

(j)

(k)

(l)
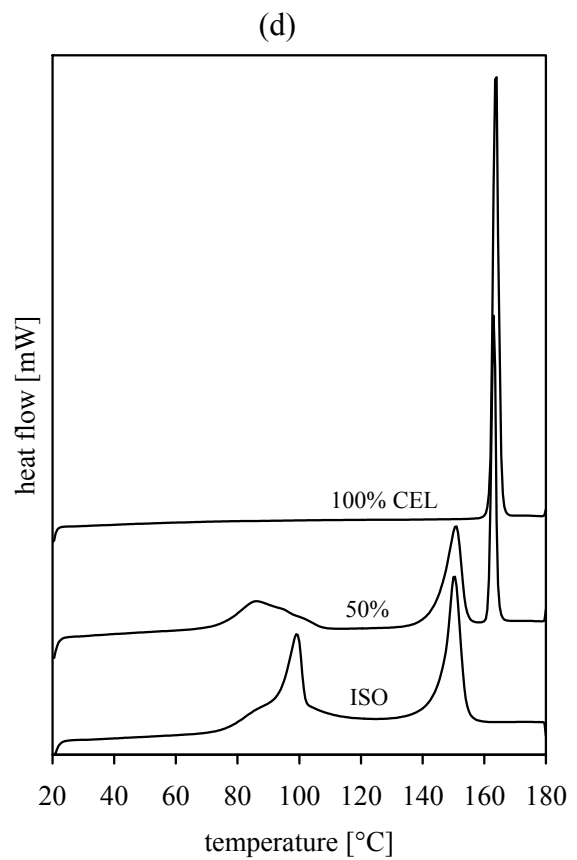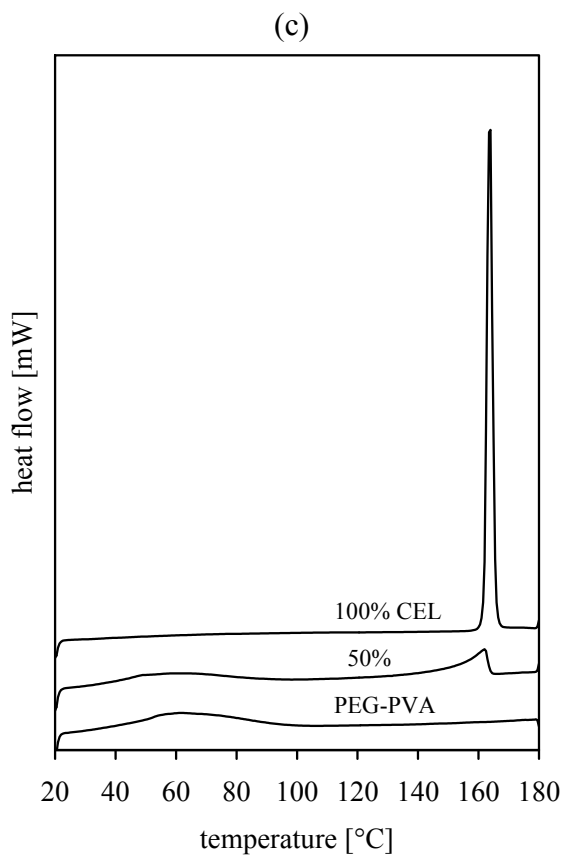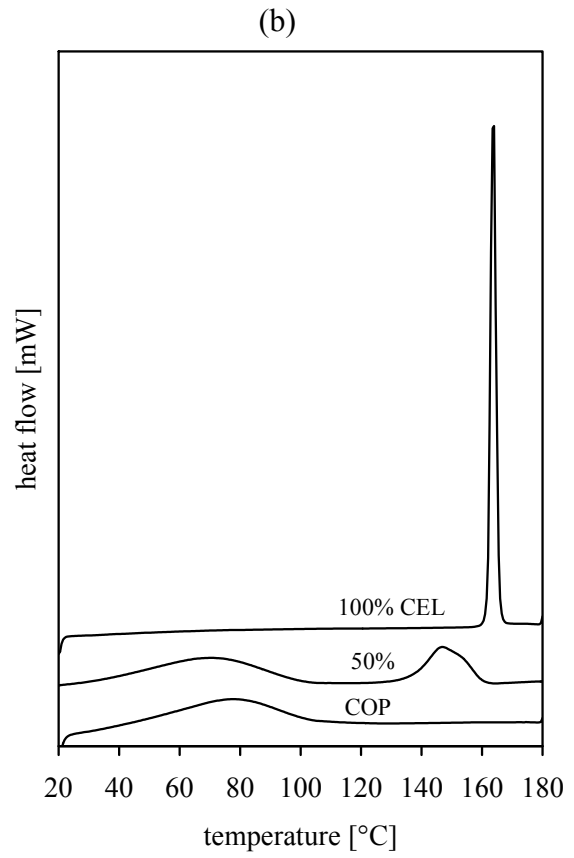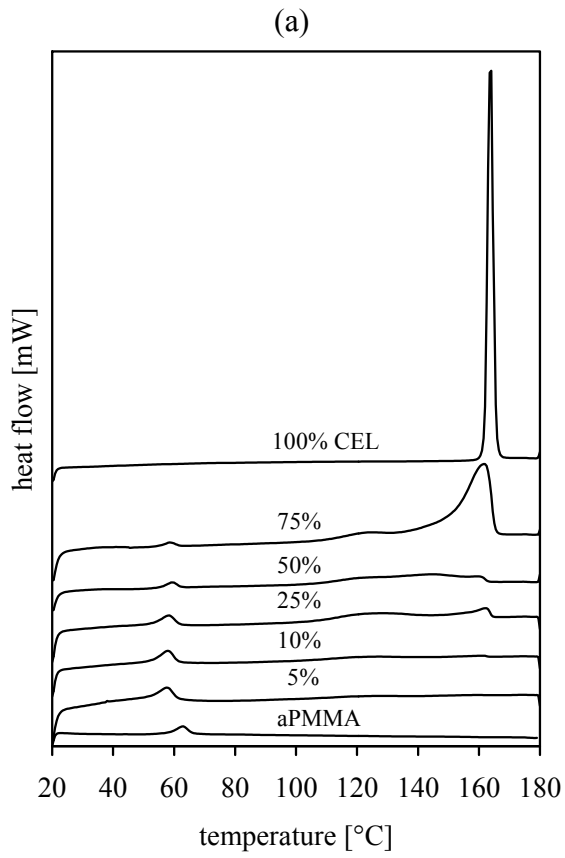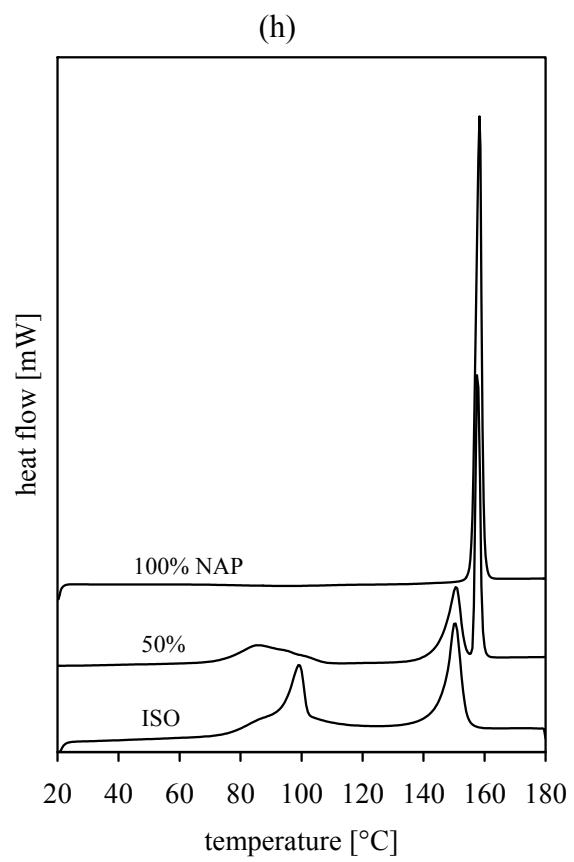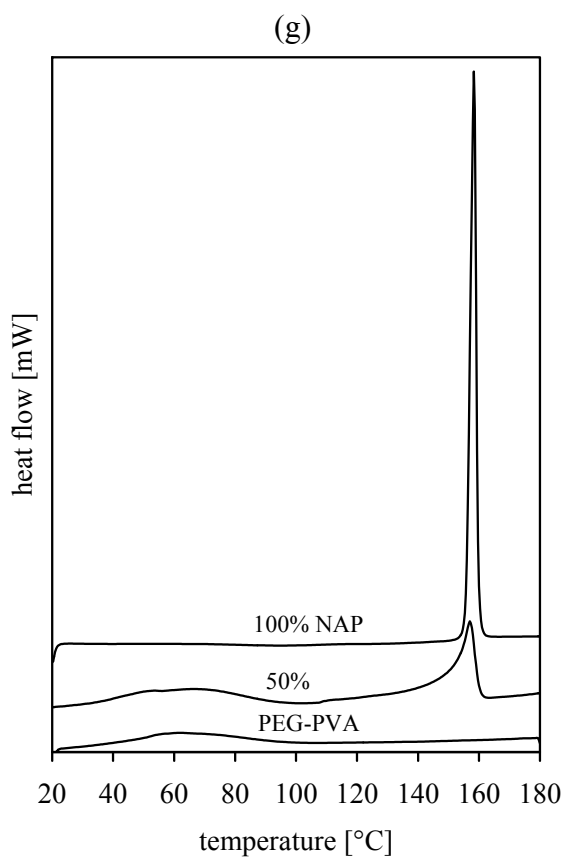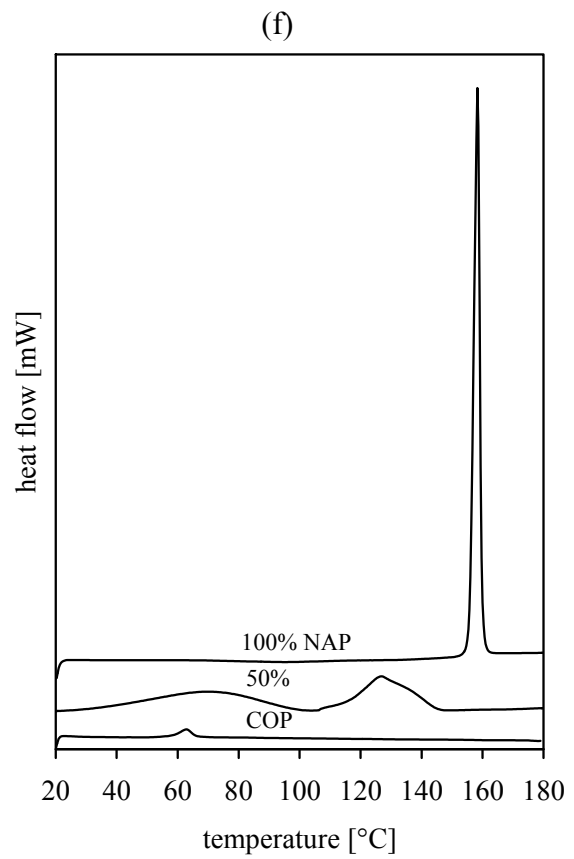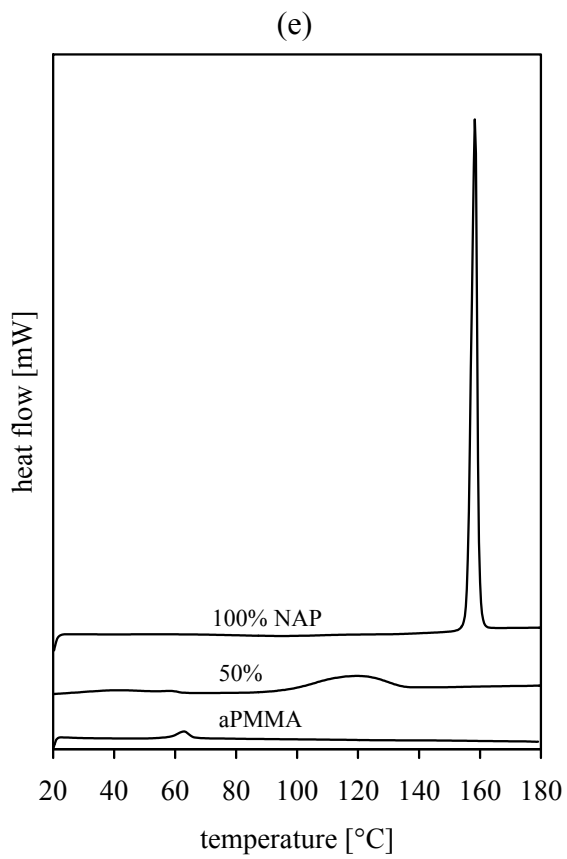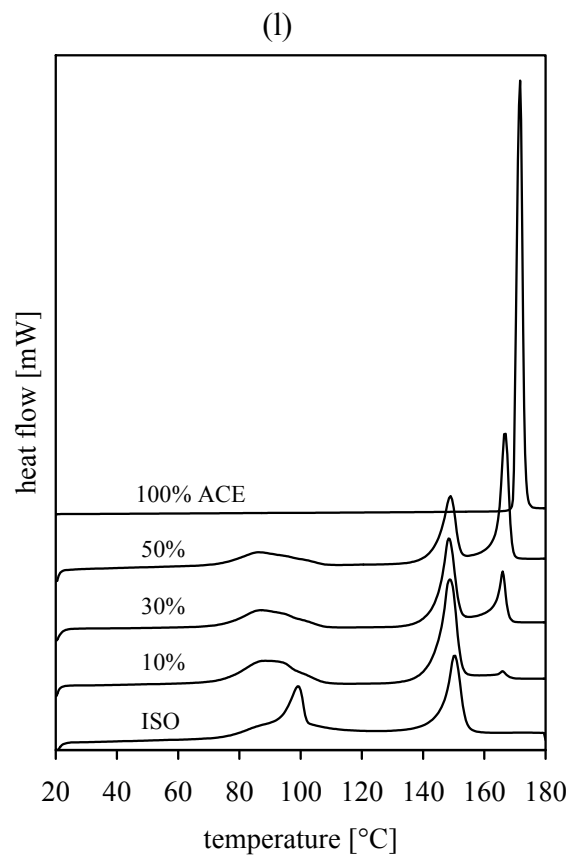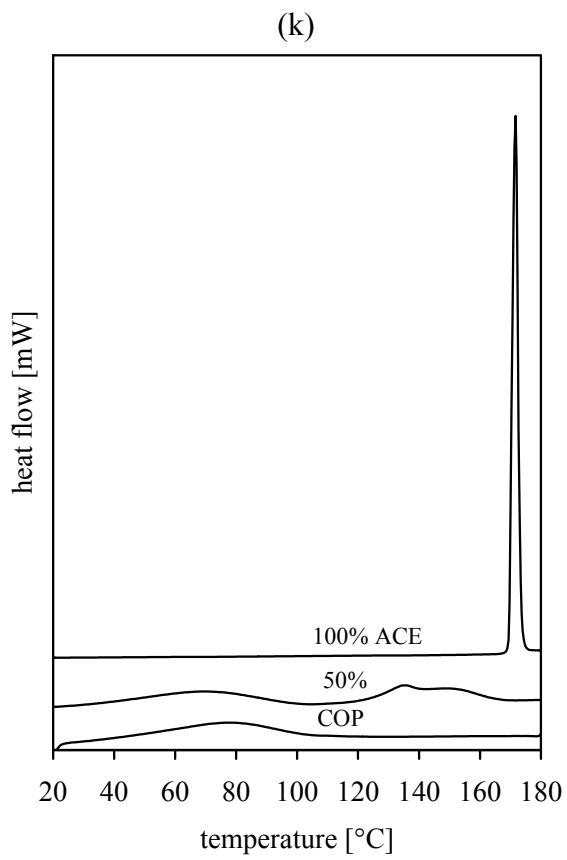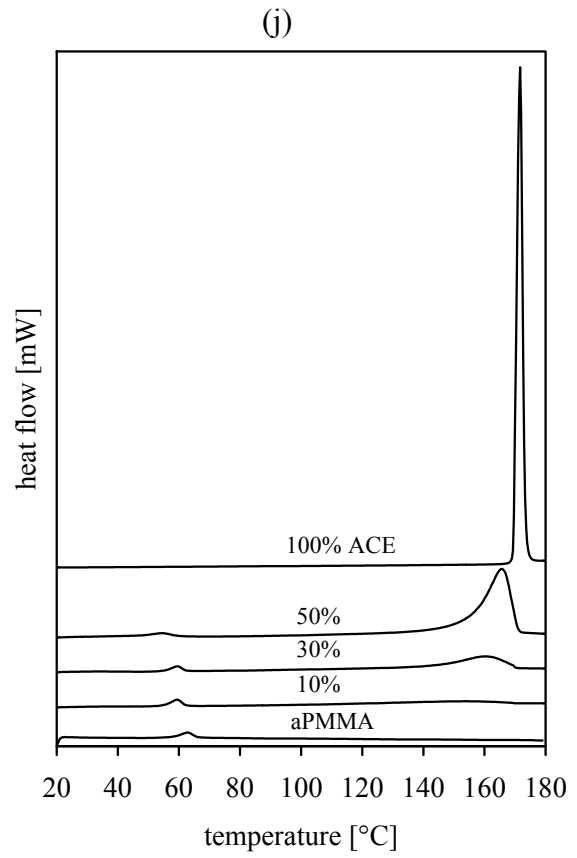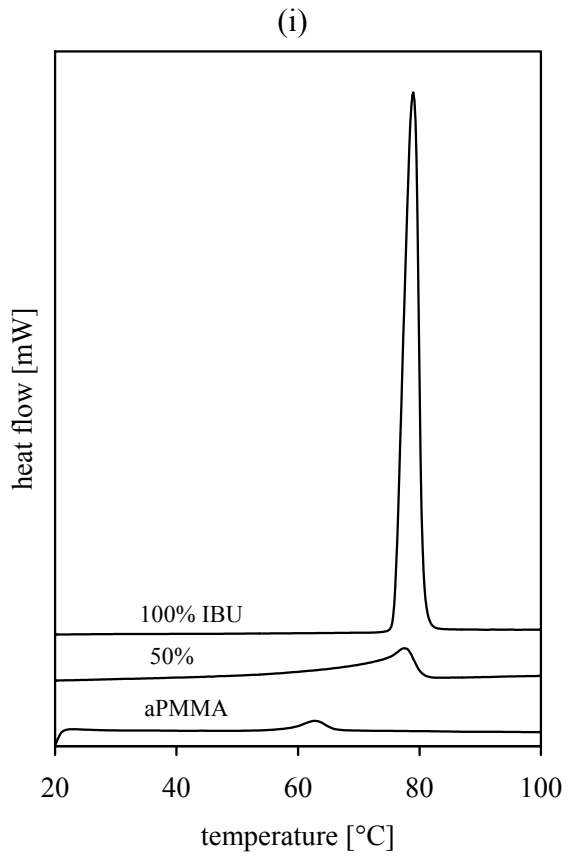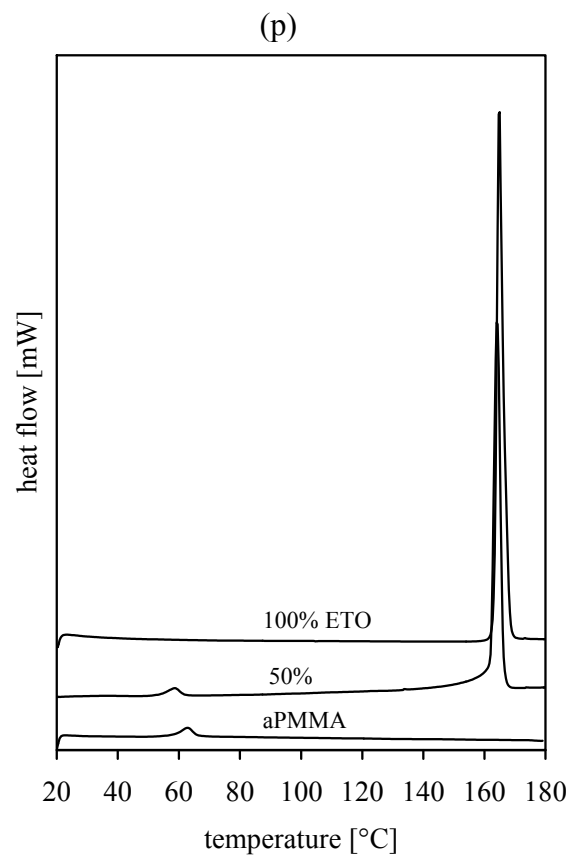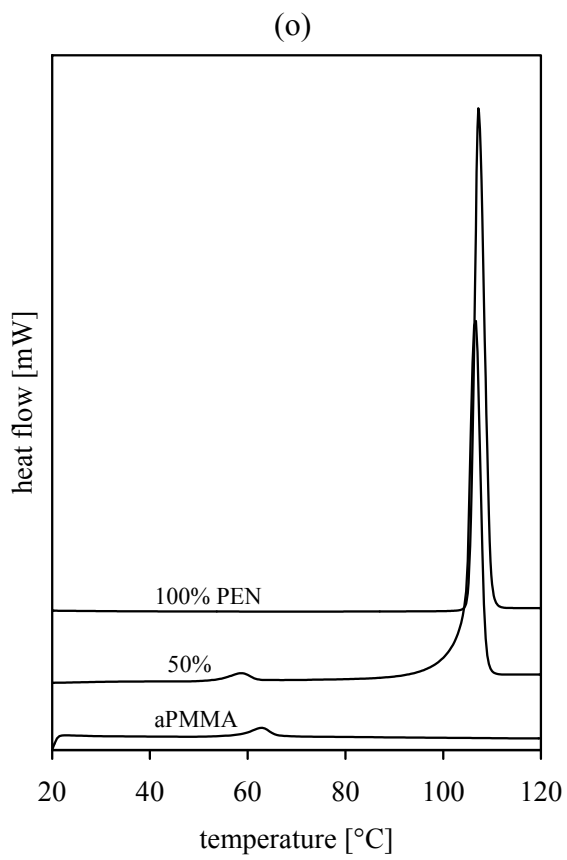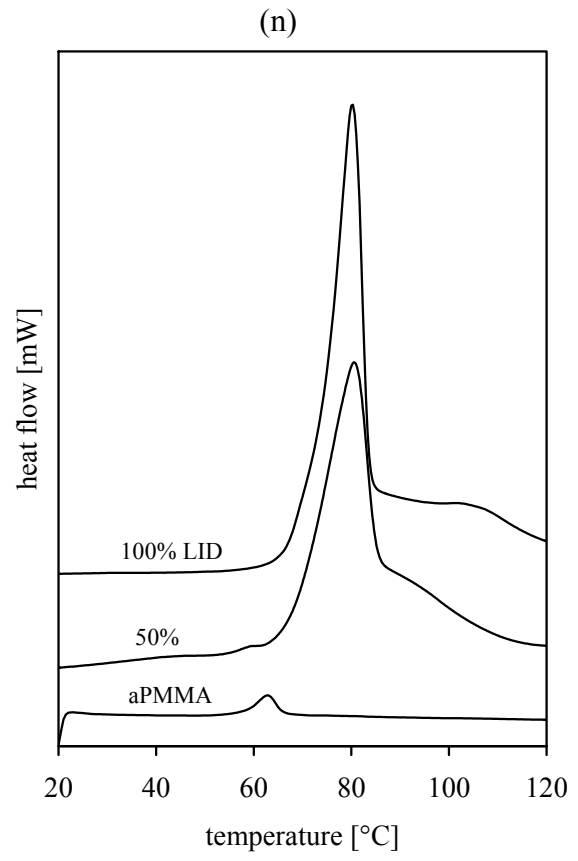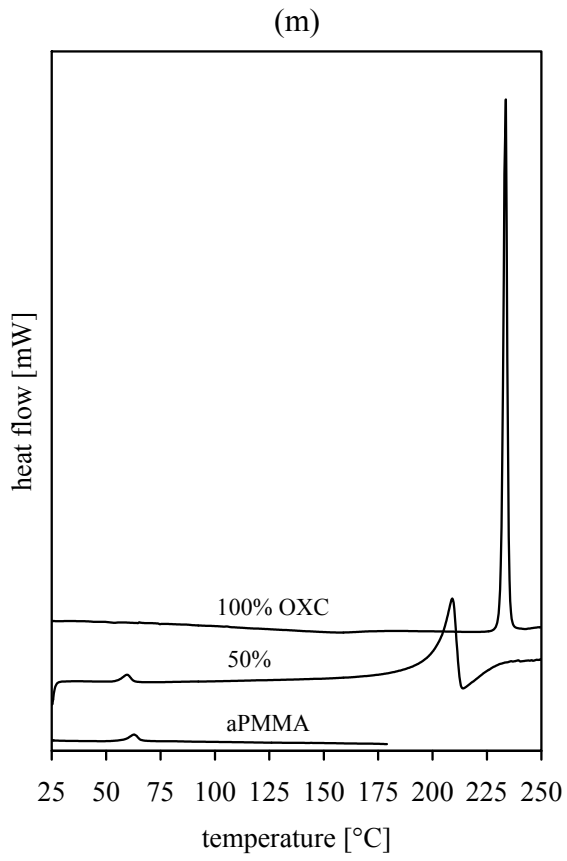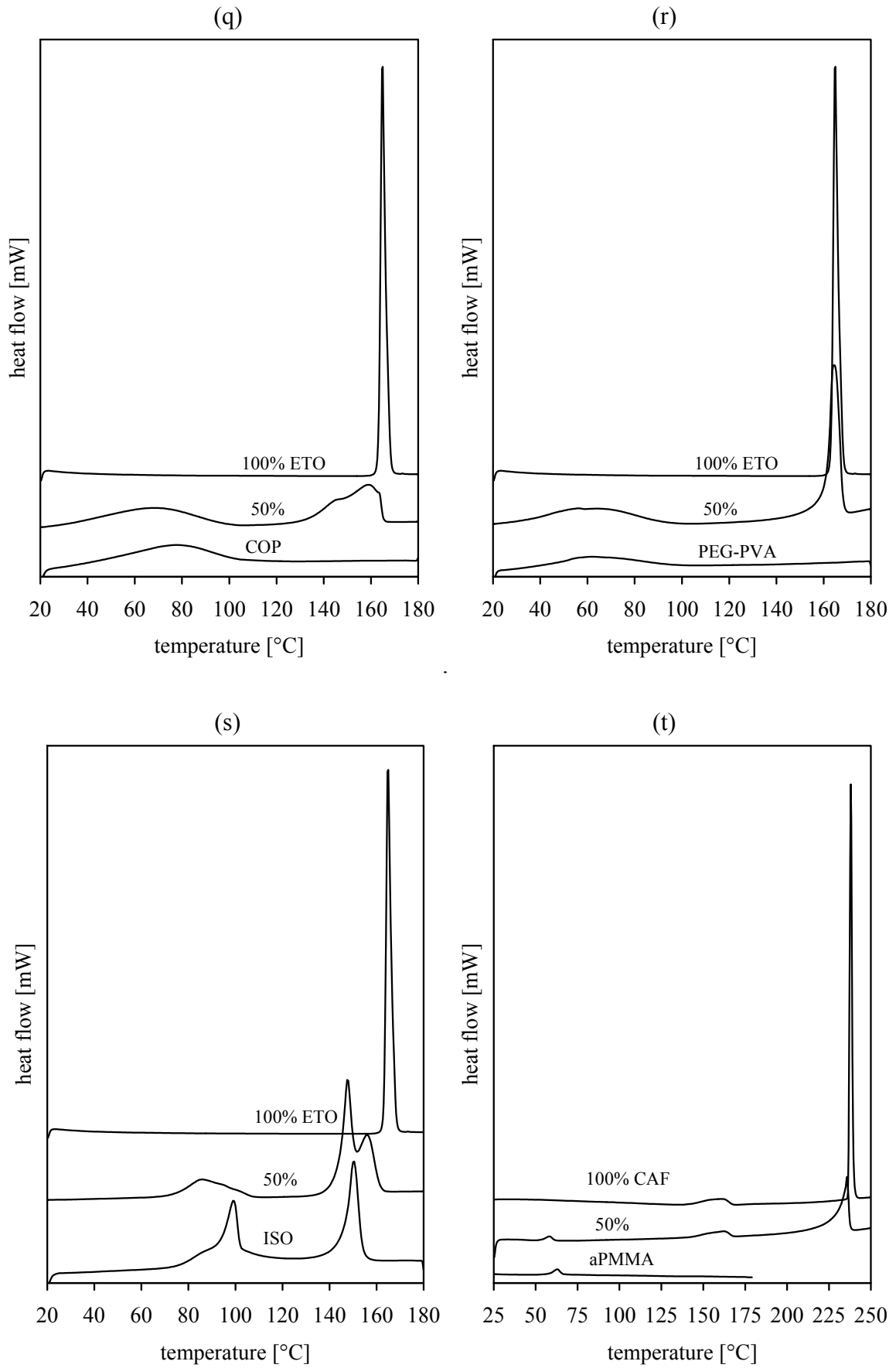
Figure 4.73: DSC patterns of pure drugs, pure carriers, and physical mixtures; curves represent first heat scan; abscissas with different scale

In Figure 4.74 the ratio of the enthalpy decrease is plotted against the ratio of the melting temperature reduction. The distance of each drug/carrier blend from the point of complete insolubility (1/1) is calculated with the Pythagorean Theorem (chapter 7.2.2.3). If the blends have a large distance from point 1/1 (Table 4.9) the drug is well soluble in the carrier. If the ratios "enthalpy drug in carrier / enthalpy drug" and "T_m drug in carrier / T_m drug" respectively, assume the value one, neither a melting temperature shift nor an enthalpy decrease are obvious. A large distance is seen for the blends NAP, IBU, OXC, and CEL with aPMMA, ACE, NAP, and CEL with COP, PEG-PVA with CEL, and ETO with ISO. In contrast, CEL is completely insoluble in ISO.

Figure 4.74: Prediction of drug/carrier miscibility by DSC analysis;
○ indicates zero miscibility ($E_{udragit\ E}$ = aPMMA, $P_{VP\ VA64}$ = COP, $K_{ollicoat\ IR}$ = PEG-PVA, I_{somalt} = ISO)
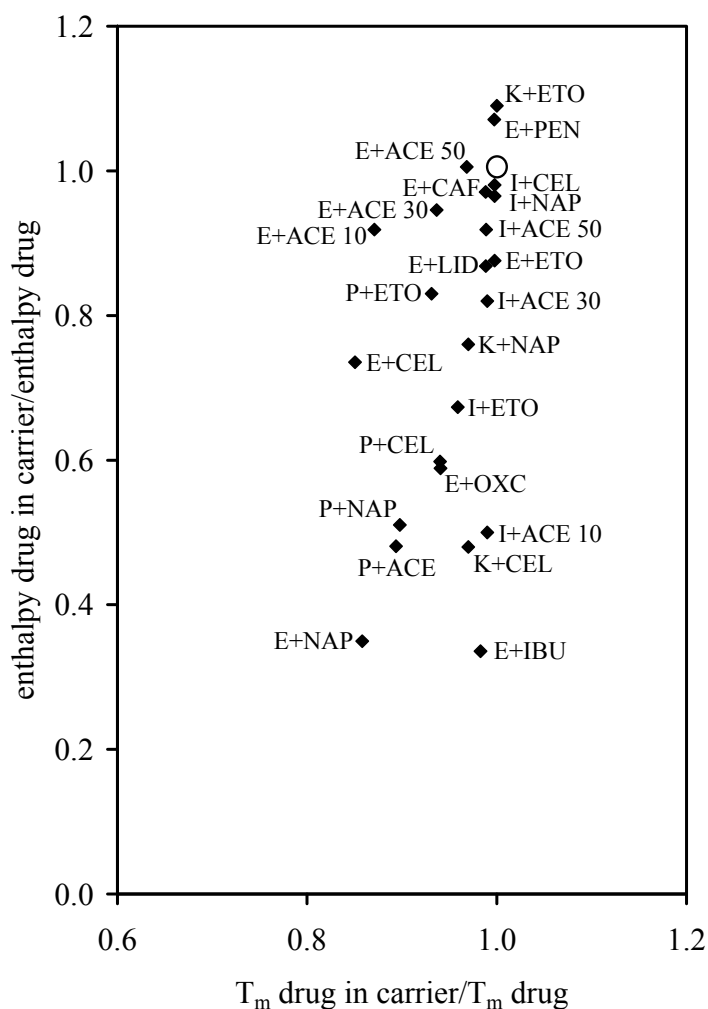
Table 4.9: Distances from point 1/1 (open circle) in Figure **4.74**, glassy solid solutions are printed in bold

sample	distance
aPMMA+NAP	**0.67**
aPMMA+IBU	**0.66**
COP+ACE	**0.53**
PEG-PVA+CEL	0.52
COP+NAP	**0.50**
ISO+ACE 10%	**0.50**
aPMMA+OXC	**0.42**
COP+CEL	**0.41**
ISO+ETO	**0.33**
aPMMA+CEL	**0.30**
PEG-PVA+NAP	0.24
COP+ETO	**0.18**
ISO+ACE 30%	0.18
aPMMA+ACE 10%	**0.15**
aPMMA+LID HCl	0.13
aPMMA+ETO	0.12
PEG-PVA+ETO	0.09
ISO+ACE 50%	0.08
aPMMA+ACE 30%	**0.08**
aPMMA+PEN	0.07
ISO+NAP	0.04
aPMMA+ACE 50%	0.03
aPMMA+CAF	0.03
ISO+CEL	0.02

Deriving from the table it can be deduced with few exceptions only that two substances are miscible if their distance in the DSC plot is >0.18, specifically ≥0.30. Since PEG-PVA has a partly crystalline structure itself, it is difficult to predict miscibility with this carrier.

ACE is soluble in the carriers aPMMA and ISO to a lower extent, so that in this graph the 1:1 blends of ACE with aPMMA and ISO are included in the systems of insolubility. Therefore, the ratios of melting enthalpy and onset melting temperature are investigated for blends of ACE with aPMMA and ISO in different proportions. The values in Table 4.10 and in Table 4.11 demonstrate that the distance in Figure 4.74 and the solubility of the drug in the carrier respectively, increases with decreasing drug amount in the blend. For blends of ACE with ISO the melting enthalpy decreases decisively with decreasing drug content whereas for blends with aPMMA only slight differences are detected.

Table 4.10: Melting enthalpies and onset melting temperatures of the pure drug and the drug in a blend with aPMMA and ISO in different proportions

sample	melting enthalpy of pure drug [J/g]	melting enthalpy of drug in carrier [J/g]	enthalpy ratio	onset T_m of pure drug [°C] and [K]	onset T_m of drug in carrier [°C] and [K]	T_m ratio
aPMMA+ACE 10%	185	170	0.92	169 / 442	112 / 385	0.87
aPMMA+ACE 30%	185	175	0.95	169 / 442	141 / 414	0.94
aPMMA+ACE 50%	185	186	1.01	169 / 442	155 / 428	0.97
ISO+ACE 10%	185	93	0.50	169 / 442	163 / 436	0.99
ISO+ACE 30%	185	152	0.82	169 / 442	163 / 436	0.99
ISO+ACE 50%	185	170	0.92	169 / 442	164 / 437	0.99

In spite of the high enthalpy decrease of ACE in ISO, the onset melting temperature is unchanged. This shows that the crystal lattice of the surplus drug remains untouched by the molecules of the molten carrier.

The same experiments were performed with blends of CEL and aPMMA in different proportions. In comparison with ACE, the solubility of CEL in aPMMA is independent of the amount of CEL in the blend, as can be concluded from the calculated distances (Table 4.11). The values for the blend with 5% drug load have a high standard deviation and might therefore be too high.

Table 4.11: Melting enthalpies and onset melting temperatures of pure CEL and CEL in a blend with aPMMA in different proportions; distance of each blend from point 1/1 in Figure 4.74 is calculated with the Pythagorean Theorem (chapter 7.2.2.3).

| drug load [%]	melting enthalpy of pure drug [J/g]	melting enthalpy of drug in carrier [J/g]	enthalpy ratio	onset T_m of pure drug [°C] and [K]	onset T_m of drug in carrier [°C] and [K]	T_m ratio	distance
5	102	81	0.79	162 / 435	61 / 334	0.77	0.31
10	102	59	0.58	162 / 435	102 / 375	0.86	0.44
25	102	74	0.73	162 / 435	119 / 392	0.90	0.29
50	102	75	0.74	162 / 435	97 / 370	0.85	0.30
75	102	77	0.75	162 / 435	149 / 422	0.97	0.25

The results of these investigations show that the determination of the thermal behaviour by DSC analysis is a very useful tool to predict the miscibility of drugs and carriers in a hot-melt extrusion process, and thus, the formation of glassy solid solutions. This method represents a simple screening test, which is beneficial for early small-scale investigations of new chemical entities.

4.5.6 Molecular modelling

Macromolecular molecules like pharmaceutical drugs and excipients, especially polymers, cannot be described by a single conformation but must be thought of as a combination of individual conformations, which give rise to flexible molecules with characteristic average molecular properties. Fluctuating and conformational changes of the flexible molecules play a decisive role for the characteristic average molecular properties. In order to determine the accurate structure and properties of these flexible molecules and to examine the interactions between a given carrier and a drug in the molten state, the molecules can be modelled by computational techniques.

Molecular dynamics is a form of molecular modelling allowing molecules to interact for a period of time showing the motion of the molecules in the liquid state. With the help of this simulation the miscibility of substances can be examined on a molecular level (Langer 2003).

The interaction energy between drug and carrier molecules can be subdivided into electrostatic forces, hydrogen bonds, and van der Waals dispersion forces.

The interactions between neutral neighbouring atoms are described by van der Waals forces which include attractive long-range forces generated by interactions due to momentary polarization and repulsive short-range forces which are the result of overlapping electron orbitals. The Lennard-Jones potential (LJ) is a method to calculate the van der Waals

interaction energy in molecular dynamics and is a relatively good approximation to the attractive dispersion forces and repulsive components of the system.

Hydrogen bond and electrostatic interactions are computed, based on Coulomb's law, which indicates that the magnitude of the electrostatic force between two-point electric charges is directly proportional to the product of the magnitudes of each charge and inversely proportional to the square of the distance between the charges. These interactions are summarized in the Coulomb short-range interaction term C.

The Lennard-Jones potential between drug and carrier increases with an increasing molecular weight of the drug. Therefore, the values of the Lennard-Jones potential are used to relate the Coulomb interaction energy to the molecular weight of the drug by the ratio

$$P = \frac{C}{LJ}$$

Equation 3.

Molecular dynamics (MD) simulations (chapter 7.2.2.17) were computed for the carriers ISO and aPMMA. ISO was chosen as hydrophilic carrier. Additionally, first experiences had already been gained in a previous study by Langer et al. (2003). For the calculations with aPMMA the structure of the polymer had to be simplified. The aminoalkyl-methacrylate copolymer has two carbonyl groups and one ethyldimethylamino group as functional groups. As the carbonyl groups are located quite close to the carbon chain, the ethyldimethylamino group seems to be the main reaction partner for the drugs. Therefore, the ethyldimethylamino component (aPMMA*) was chosen for further MD simulations.

To investigate the interactions of drugs with the carrier ISO, small carrier models made up of 34 molecules were constructed with the computer (Figure 4.75). These carrier entities were heated to 373 K (onset melting temperature of ISO 365 K) and conveyed to the liquid state. An adequate number of carrier molecules was removed from the centre of the entity and replaced by a drug molecule. Drug-carrier interactions could then be calculated whereas drug-drug interactions were not taken into account.
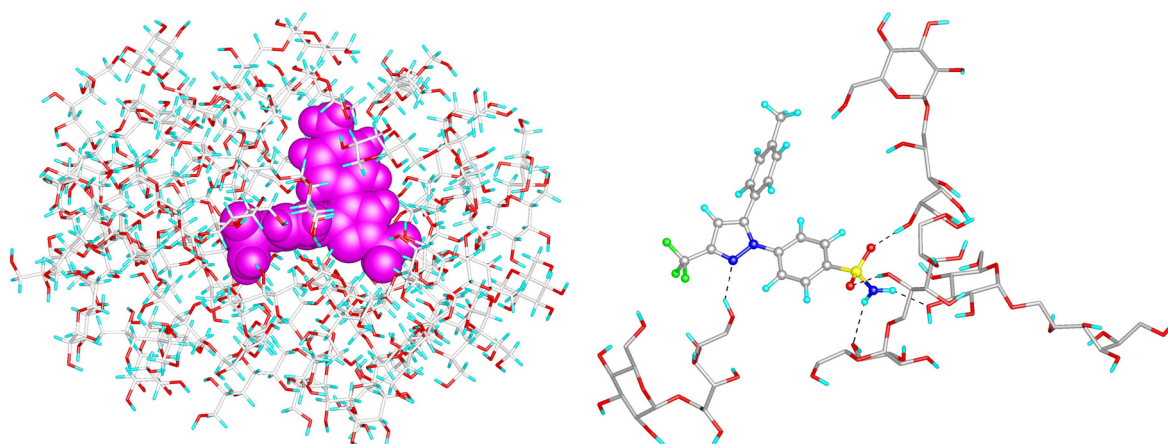
Figure 4.75: CEL in an environment composed of 34 ISO molecules; *left*: CEL is displayed in its spacefill form in magenta, ISO molecules in stick; *right*: Detailed view of CEL with adjacent ISO molecules, CEL is displayed in ball&stick, ISO molecules in stick (carbon: grey, oxygen: red, hydrogen: cyan, fluorine: green, nitrogen: blue, sulphur: yellow); five hydrogen bonds are displayed as grey dotted lines

For each drug/ISO mixture a simulation for 2 ns was performed. Table 4.12 shows the Coulomb and Lennard-Jones contributions to the interaction energies and the P ratios of the two parameters. The high Coulomb value of ISO (-333.5 kJ/mol) is due to the high number of hydroxyl groups which are able to form molecular hydrogen bondings. Interaction energies contributed by the Coulomb term for all drug/ISO models are decisively smaller than for the pure ISO entity. According to Langer (2003) drugs ae miscible with ISO if P is >0.5.

Table 4.12: Interaction energies of drugs with ISO; transparent melts are printed in bold

sample	T [K]	C [kJ/mol]	LJ [kJ/mol]	P
ISO	373	-333.5	-274.4	1.20
ACE	373	-101.0	-138.7	**0.73**
ETO	373	-131.4	-201.3	**0.65**
CAF	373	- 77.4	-177.3	0.44
PEN	373	-103.5	-249.5	0.41
OXC	373	- 93.4	-237.1	0.39
NAP	373	- 73.8	-215.8	0.34
CEL	373	- 86.4	-320.5	0.27
IBU	373	- 39.6	-213.8	0.19

The highest Coulomb terms are achieved by molecules with a high number of H bond acceptors (ETO and PEN) or by ACE, which has fewer H bond acceptors but has a sterically advantageous structure because of its low molecular volume (Table 4.13). CEL has more H bond acceptors, but less potential interaction points because of the higher molecular volume

83

and Lennard-Jones contributions. Small Coulomb energy contributions can be determined for molecules with few H bond acceptors like ibuprofen.

Table 4.13: Molecular volume and number of H bond acceptors / donors of drug molecules; V_m calculated on the basis of SPWin

drug	C [kJ/mol]	V_m [cm³/mol]	H bond acceptor	H bond donor
ETO	-131.4	180.9	7	1
PEN	-103.5	247.4	7	0
ACE	-101.0	111.2	3	2
OXC	- 93.4	181.0	4	2
CEL	- 86.4	265.7	5	2
CAF	- 77.4	172.2	6	0
NAP	- 73.8	178.3	3	1
IBU	- 39.6	195.5	2	1

Transparent melts of ACE and ETO with isomalt can be produced by heating their physical mixture above their melting points, thus proving the good predictability by employing molecular dynamics simulations. The poor miscibility of all other drugs with isomalt corresponds also with the calculations.

For molecular dynamics investigations with aPMMA the polymer was simplified to ethyldimethylamine (aPMMA*) molecules. The molecule aPMMA* has completely different properties than ISO as it mainly consists of alkyl groups. Hence, the self-association of the molten carrier is not governed by hydrogen bonding but rather by van der Waals forces as shown in higher Lennard-Jones potentials. Therefore, the Coulomb terms of the pure ethyldimethylamines and also of the drug/ethyldimethylamine samples are exceedingly small. Figure 4.76 shows the survey of CEL in an entity composed of 287 aPMMA* molecules and a detailed view of a CEL molecule with adjacent aPMMA* molecules. The nitrogen of the aPMMA* molecules possesses an unshared pair of valence electrons which can form hydrogen bonds with protons of other molecules. The formation of such hydrogen bonds is demonstrated in Figure 4.76 by the dotted line in the detailed view. The nitrogen-proton bond is much weaker than the oxygen-proton bond, as the nitrogen is less electronegative than the oxygen and thus less polar. From literature it is known that aPMMA enhances the solubility of neutral drugs, i.e. felodipine (Nollenberger 2007).
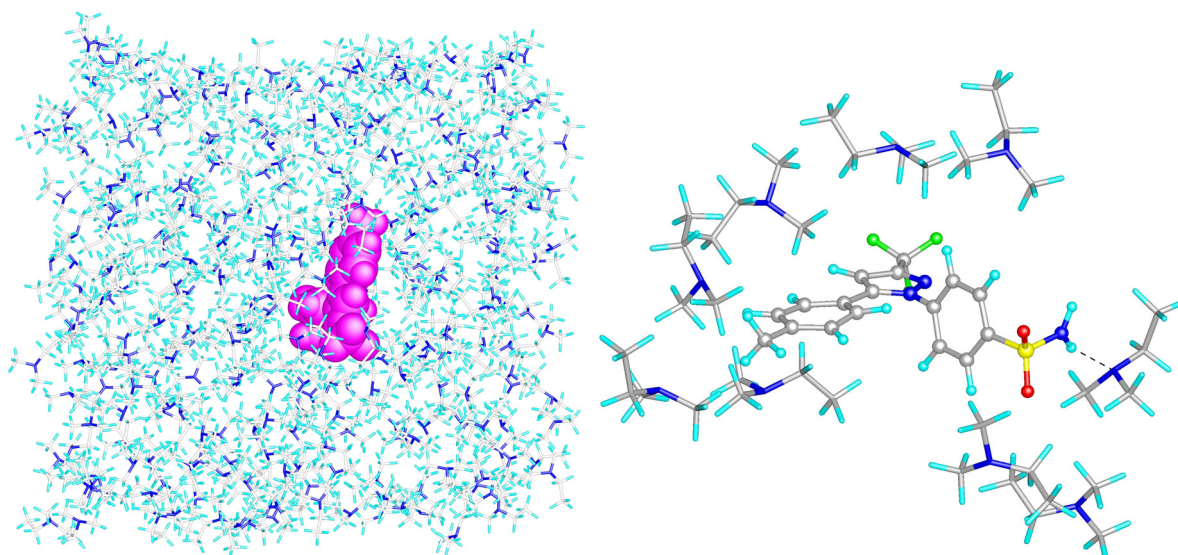
Figure 4.76: CEL in an environment composed of 287 aPMMA* molecules; *left*: CEL is displayed in its spacefill form in magenta, aPMMA* molecules in stick; *right*: Detailed view of CEL with adjacent aPMMA* molecules, CEL is displayed in ball&stick, aPMMA* molecules in stick (carbon: grey, oxygen: red, hydrogen: cyan, fluorine: green, nitrogen: blue, sulphur: yellow); hydrogen bond is displayed as grey dotted line.

In the case of aPMMA* the Lennard-Jones potential is more prominent than the Coulomb forces. Interaction energies were determined at two different temperature settings.

Table 4.14: Interaction energies of drugs with ethyldimethylamine (aPMMA*) at the same temperature; glassy solid solutions are printed in bold

sample	T [K]	C [kJ/mol]	LJ [kJ/mol]	P
LID HCl	336	-9.27	- 98.85	0.094
ACE	336	-4.05	- 77.69	**0.052**
CEL	336	-7.35	-160.92	**0.046**
ETO	336	-3.89	- 99.92	0.039
CAF	336	-2.95	- 89.07	0.033
OXC	336	-3.96	-121.46	**0.033**
PEN	336	-3.54	-127.85	0.028
NAP	336	-1.98	-113.05	**0.018**
IBU	336	-1.45	-103.27	**0.014**
ethyldimethylamine	336	-0.06	- 36.48	0.002

First simulations were performed at a temperature above the glass transition temperature of the carrier but below the melting points of the drugs (Table 4.14). This temperature was kept constant for each drug/aPMMA* simulation. Further, simulations were performed at different temperatures regarding the respective maximum temperature of the hot-melt extrusion process of each drug (Table 4.15).

Table 4.15: Interaction energies of drugs with ethyldimethylamine (aPMMA*) at different temperatures; glassy solid solutions are printed in bold

sample	T [K]	C [kJ/mol]	LJ [kJ/mol]	P
LID HCl	333	-8.90	-100.45	0.089
ACE	443	-3.00	- 72.90	**0.041**
ETO	426	-2.95	- 94.29	0.031
CEL	430	-4.49	-153.99	**0.029**
PEN	373	-3.27	-124.98	0.026
CAF	506	-1.97	- 79.74	0.025
OXC	488	-2.35	-108.72	**0.022**
NAP	373	-1.63	-109.97	**0.015**
IBU	343	-1.48	-103.22	**0.014**
ethyldimethylamine	336	-0.06	- 36.48	0.002

Concerning the Lennard-Jones potential only slight changes in the order of precedence were observed between the two temperature settings (Table 4.16). The highest Lennard-Jones interactions were obtained for CEL, PEN and OXC. NAP and IBU present the lowest P values as the Coulomb interaction forces are smaller than for CEL, PEN and OXC.

Table 4.16: Lennard-Jones potential and molecular volume of drug molecules

drug	LJ [kJ/mol] $T_{m\ const}$	LJ [kJ/mol] $T_{m\ var}$	V_m [cm³/mol]
CEL	-160.92	-153.99	265.7
PEN	-127.85	-124.98	247.4
OXC	-121.46	-108.72	181.0
NAP	-113.05	-109.97	178.3
IBU	-103.27	-103.22	195.5
ETO	- 99.92	- 94.29	180.9
CAF	- 89.07	- 79.74	172.2
ACE	- 77.69	- 72.90	111.2

Figure 4.77 demonstrates that CEL is located in a cavity. Therefore, the molecular volume is important for the formation of Coulomb and Lennard-Jones interactions and has to be taken into consideration when ranking the miscibility of the drugs with aPMMA*. As CAF and especially ACE possess small molecular volumes, the hydrophilic properties have a greater part in the properties of the whole molecule.
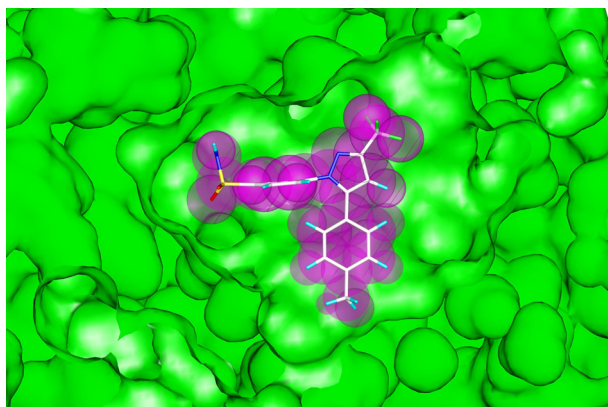
Figure 4.77: Detailed view of CEL with adjacent aPMMA* molecules; CEL is displayed in its spacefill form in magenta, adjacent aPMMA* molecules in green; surface is cut open from above, in order to see, that CEL is located in a cavity

Besides the lipophilic alkyl groups the aPMMA* molecules possess a tertiary amine which can interact with functional groups of the drugs. The unshared valence electron can form hydrogen bonds with protons. Furthermore, alkyl amines undergo complete reaction with strong acids to yield stable amine salts. In conclusion, the prediction of miscibility of aPMMA with drugs is much more complicated than with ISO, because different processes have a share in the interactions between carrier and drug.

As can be concluded from the P values in Table 4.14 and Table 4.15, the predictability of the miscibility with aPMMA* is poor compared to the predictability of the miscibility with ISO. aPMMA* can undergo acid-base reactions in the melt. Therefore, a formation of a salt was assumed for calculations with CEL, NAP, IBU, and OXC (Table 4.17).

Assuming that salts of aPMMA* and acidic drugs are formed within the hot-melt extrusion process, Coulomb and Lennard-Jones interactions are calculated for the acidic drugs accordingly. Table 4.17 shows that in this case the Coulomb interaction terms have another order of magnitude and cannot be directly compared to the results of the previous simulations.

Table 4.17: Interaction energies of drugs calculated as acids with ethyldimethylamine (aPMMA*) at different temperatures; glassy solid solutions are printed in bold

sample	T [K]	C [kJ/mol]	LJ [kJ/mol]	P
CEL	430 K	-583.15	-109.21	**5.34**
NAP	373 K	-547.25	- 74.58	**7.34**
IBU	343 K	-549.04	- 66.43	**8.27**
OXC	488 K	-817.20	- 13.62	**59.99**

The results of the FT-IR analysis in chapter 4.2 and 4.4 indicated the formation of salts of aPMMA with CEL, NAP, IBU, and OXC. Thus, the values calculated from the simulations with the acidic drugs have to be considered when predicting the miscibility with aPMMA. Additionally, the smaller size of the aPMMA* molecules towards the complete polymer aPMMA in the simulations can lead to a slightly changed behaviour of the carrier towards the drugs.

In conclusion, molecular dynamics simulations with polymers are quite complex and need some expertise to serve as useful tool for miscibility prediction. Up to now there is neither definite algorithm nor a predictive parameter in molecular modelling available that gives clear evidence for the predictability of mixing properties of solid state materials.

4.5.7 Summary

The interpretation of the chemical structure, the calculation of solubility parameters, the determination of melting temperatures and enthalpies, and the performance of molecular dynamics simulations are tools to predict the miscibility of drugs and carriers for the formulation of solid dispersions. By employing these tools to different drug/carrier blends (Table 4.18) the following conclusions can be drawn:

Hydrophilicity and lipophilicity of the components can be assessed from the chemical structure. Furthermore, the functional groups indicate the possibility of interacting via hydrogen bonding (e.g. COP/NAP), van der Waals forces, or via salt formation (e.g. aPMMA/IBU). In all, three-dimensional solubility parameters are more expressive than the total solubility parameters, as they differentiate between dispersion, polar and hydrogen bonding components. At $\Delta\delta<5MPa^{0.5}$ good miscibility predictions can be deduced from solubility parameters (COP/NAP, aPMMA/IBU, aPMMA/NAP, COP/CEL, and COP/ACE). The evaluation of the melting behaviour via DSC is a very useful tool. Through the determination of the melting enthalpy decrease of the drug in drug/carrier blends, the miscibility can be predicted on an experimental basis (e.g. aPMMA/CEL). The application of molecular dynamics simulations to simple molecules (e.g. ISO) elucidates well the interaction energies acting between drug and carrier. For more complex polymers (e.g. aPMMA) the use of molecular dynamics simulations is more difficult and needs to be improved further.

The macroscopic appearance of the extrudates and the evaluation of the characteristics via DSC and XRPD point to the physical state of the extrudates. It has to be distinguished between miscibility and stability of the extrudates, as sometimes the extrudates leave the die plate as transparent strands in the hot stage and recrystallize to opaque strands when cooling

down to room temperature. In this case it is quite difficult to determine whether the components are miscible or immiscible (PEG-PVA/NAP, PEG-PVA/ETO). Sometimes, the macroscopic appearance is needed to differentiate between two systems, as amorphous blends, which have an opaque appearance, form rather glass suspensions and not glassy solid solutions (e.g. aPMMA/PEN).

Finally, only the combination of different tools results in a good prediction of miscibility. Among these tools, the evaluation of the melting behaviour via DSC has the highest impact.

Table 4.18: Survey of miscibility for 1:1 (w/w) ratios, HB = hydrogen bond, vdW = van der Waals

sample	structure	δ distance	DSC distance	molecular dynamics	extrusion	macroscopic appearance of cooled extrudates	result
COP:NAP	+ HB	+ 1.97	+ 0.50	?	? feeding problems	transparent	miscible
aPMMA:IBU	+ salt	+ 2.21	+ 0.66	+ Coulomb (salt) / vdW	+	transparent	miscible
aPMMA:NAP	+ salt	+ 3.46	+ 0.67	+ Coulomb (salt) / vdW	+	transparent	miscible
COP:CEL	+ HB	+ 3.63	+ 0.41	?	+	transparent	miscible
COP:ACE	+ HB	+ 3.91	+ 0.53	?	+	transparent	miscible
aPMMA:PEN	-	± 5.39	- 0.07	+ vdW	-	opaque	immiscible
aPMMA:CEL	+ salt	± 5.45	+ 0.30	+ Coulomb (salt) / vdW	+	transparent	miscible
aPMMA:ACE	+ HB	± 5.60	± 0.03-0.15	±	±	transparent	partly miscible
aPMMA:OXC	+ salt	± 7.53	+ 0.42	+ Coulomb (salt)	+	transparent	miscible
aPMMA:CAF	-	± 9.40	- 0.03	±	-	opaque	immiscible
PEG-PVA:ETO	+ HB	± 9.48	- 0.09	?	± recrystallizes	opaque	?
COP:ETO	+ HB	- 12.87	± 0.18	?	+	transparent	partly miscible
ISO:ETO	+ HB	- 13.91	+ 0.33	+ Coulomb	+ preliminary test	transparent	miscible
aPMMA:ETO	?	- 14.42	± 0.12	±	-	opaque	?
PEG-PVA:CEL	+ HB	- 15.38	+ 0.52	?	+	(transparent)	partly miscible
PEG-PVA:NAP	+ HB	- 17.71	± 0.24	?	± recrystallizes	opaque	?
ISO:CEL		- 21.24	- 0.02	-	- preliminary test	opaque	immiscible
ISO:ACE		- 23.34	± 0.08-0.50	+ Coulomb	- preliminary test	opaque	partly miscible
ISO:NAP		- 23.67	- 0.04	-	- preliminary test	opaque	immiscible

4.6 Formulation of solid dosage forms

4.6.1 Introduction and objective

For the formulation of solid dosage forms the extrudates must be processed further. This can be realized by cutting or milling the strands into granules, pellets or fine powder and then processing them into tablets. These processing steps are accompanied by a mechanical energy input which might be harmful to the glassy solid solution formulations. As glassy solid solutions represent metastable systems, they often tend to recrystallize during milling and tabletting. In order to evaluate the susceptibility to precipitation under mechanical energy input, the extrudates were processed into solid dosage forms and tested for solid state transformations by XRPD analysis.

To date, only a few studies (Gryczke 2007) have dealt with the processing of solid dispersions to obtain solid dosage forms. Besides the solid state of the drug, the particle size has a strong influence on the dissolution rate. As postulated by the equation of Noyes and Whitney and Nernst and Brunner respectively, a fast dissolution can be achieved by a high particle surface in combination with a small particle size. Depending on the technique applied, extrudates can be processed into products of different particle size. Whether the particle size has the same influence in amorphous formulations as in crystalline systems still needs to be investigated. Therefore, a second focus will be on the influence of the particle size on the dissolution rate.

A third subject in solid dosage form production is the stability of the glassy solid solution in solution-state. Even if the amorphous system is stable during storage, it often recrystallizes when getting into contact with the dissolution medium as water has a plasticizing effect. Because of that, the positive effect of bioavailability enhancement is counteracted. If solubility of the drug in the dissolution medium to a sufficient extent can only be maintained for some minutes, the period might be too short for drug absorption. Therefore, methods to prevent recrystallization in the dissolution medium were evaluated to prolong the period of supersaturation.

4.6.2 Milling

Extrudates were grinded (chapter 7.2.1.4) into fine particles with a centrifugal mill through a sieve of size 1 mm. The size distribution (chapter 7.2.2.16) of the resulting powder is shown in Figure 4.78.
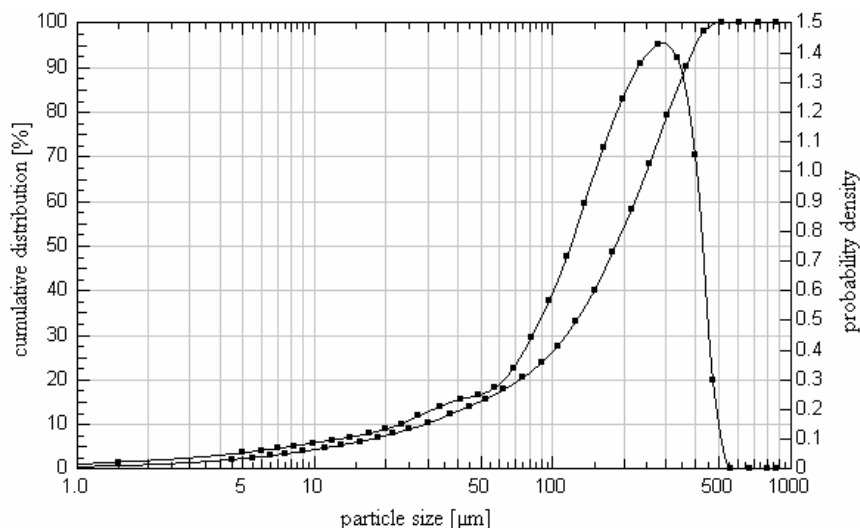
Figure 4.78: Particle size distribution of milled extrudates

Through centrifugal forces, generated by the milling process, mechanical energy is supplied and acts on the amorphous system. The XRPD patterns of the extrudates and the milled extrudates in Figure 4.79 show that the mechanical energy input does not have any negative effect on the solid state of the amorphous system.
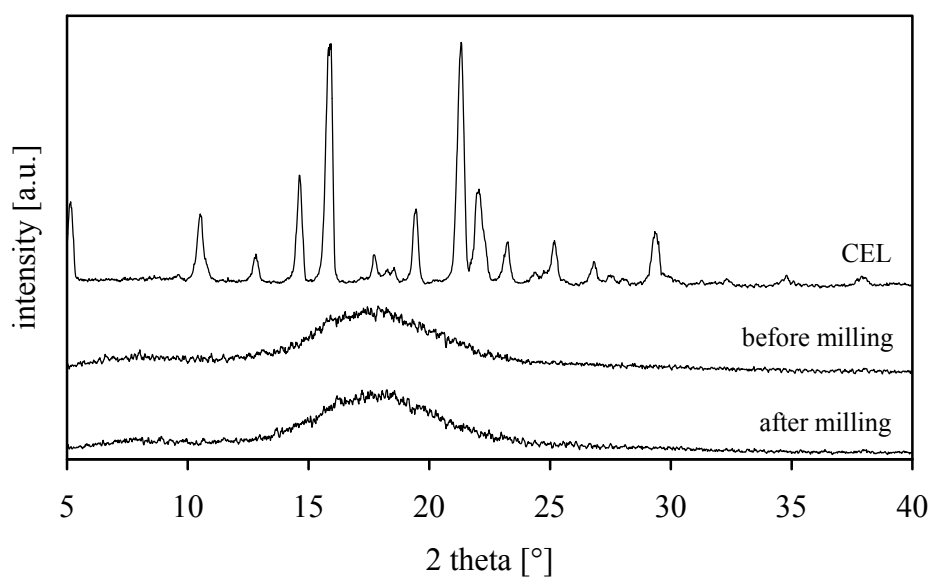
Figure 4.79: XRPD patterns of pure CEL, CEL/aPMMA extrudates (before milling) and milled CEL/aPMMA extrudates (after milling)

The powder was separated into the three fractions 0-125 μm, 125-315 μm, and 315-500 μm by sieving. Dissolution studies with these three fractions were conducted in order to examine the influence of the particle size on the dissolution rate. All tests were performed under sink conditions. Figure 4.80 shows the dissolution profiles of the three fractions. Due to the poor

wetting properties of the powder, samples first floated on the surface and sank after a few seconds. As expected, drug release from the small particles is faster than from the larger particles. This is in accordance with the theory that the faster drug release from small particles is caused by the higher specific surface area and thus leading to a higher contact surface for the dissolution medium.
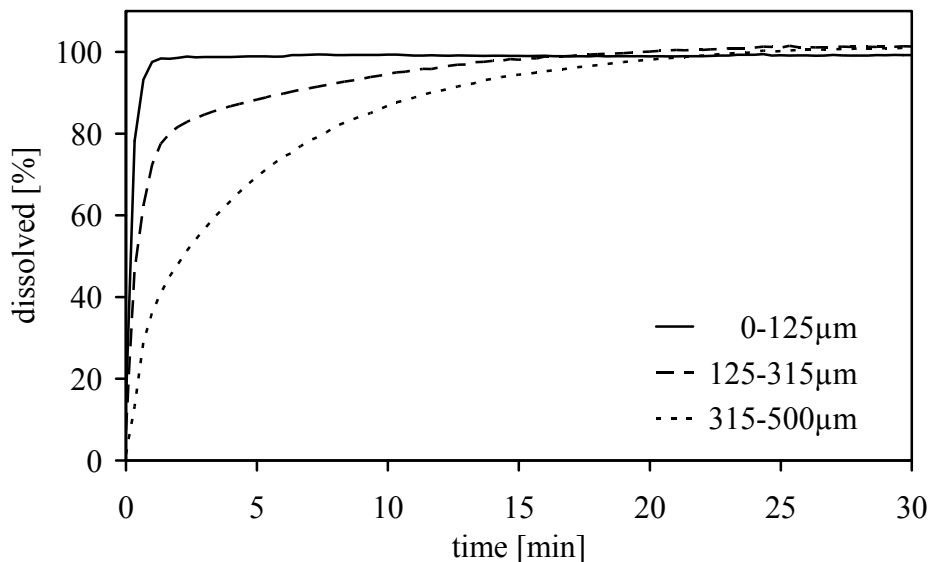
Figure 4.80: Dissolution profiles of milled extrudates; 200 mg drug; 0.1 N HCl + 0.3% cetrimid, sink conditions, 37 °C, paddle, 50 rpm, 250 nm; mean ± SD, n=3

The results explain how a solid dosage form should be designed if fast dissolution is aimed at. In case of processing the extrudates to pellets, it would be advantageous to use a die plate with small dies. Thus, extrudates with a small diameter are produced which can be further processed to pellets of small size.

4.6.3 Solution-state recrystallization inhibition

Glassy solid solutions are faced with physical stability problems, not only during storage but also during the dissolution process. Since water acts as plasticizer, the amorphous system tends to recrystallize when getting into contact with the dissolution medium. In general, recrystallization can be prevented by reducing the molecular mobility of the drug, or by protecting the system against water. To stabilize glassy solid solutions during storage, polymers are often processed, which increase the glass transition of the system or form bonds decreasing the molecular mobility of the amorphous drug.

Recrystallization of the amorphous drug during dissolution is prevented by the addition of polymers, which form a hydrodynamic boundary layer around the drug molecules being

released from the glassy solid solution (Kaushal et al. 2004). A relative increase in the viscosity of the dissolution medium around the drug molecules reduces their diffusion and prevents, therefore, crystal lattice formation. A second mechanism is called water substitution and is mostly known from freeze drying processes. In this process, the stabilizer substitutes water, which is withdrawn from the system during drying, and instead of water, the stabilizer interacts with the amorphous drug and prevents it from recrystallization (Craig 1999). Desiccants in solid dispersion formulations are called moisture scavenger (Phuapradit 2007).

aPMMA was used to stabilize the glassy solid solution of CEL in solid-state. The molecular mobility of the amorphous drug was decreased by interaction of drug and carrier. However, aPMMA has no stabilizing effect on the amorphous form in solution-state. Therefore, a further excipient had to be added to the formulation. This can be realized, for example, by processing a second water-insoluble polymer like Eudragit® NE with the melt (Nollenberger 2007). For solid-state stability it might be preferable to process only a few excipients to form glassy solid solutions, as additional interactions might occur between these components which could lead to recrystallization problems. Thus, the stabilizer was not included in the glassy solid solution but was added to the external phase.

In this study, HPMC, a polymer known to be suitable as carrier for solid dispersion formation (Leuner & Dressman 2000, Verreck et al. 2003, Six et al. 2003) was added to the external phase of the formulation.
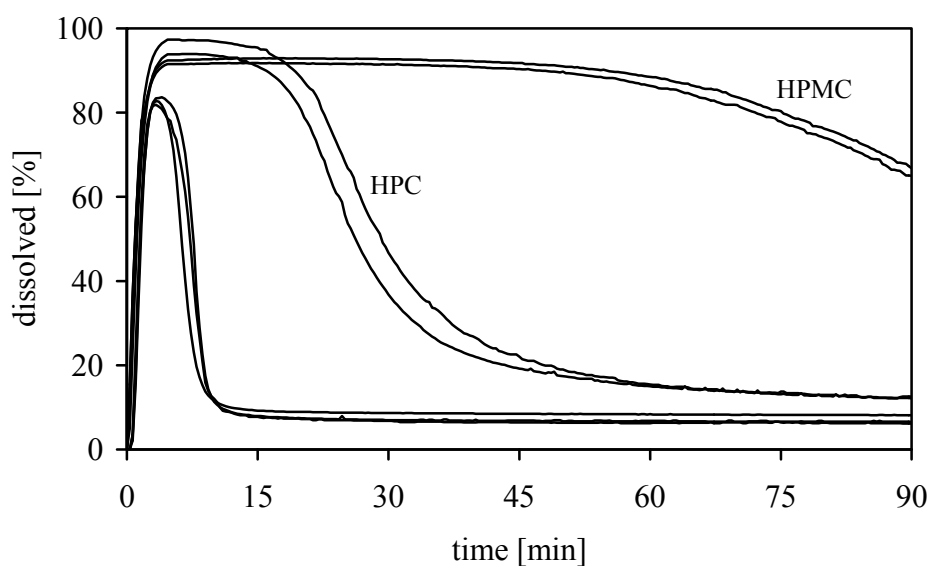
Figure 4.81: Dissolution profiles of glassy solid solutions of CEL/aPMMA; 200 mg drug; 0.1 N HCl, 0.1 N HCl + 40 mg HPC, 0.1 N HCl + 40 mg HPMC; non-sink conditions, 37 °C, paddle, 50 rpm, 250 nm

94

To test the efficacy as solution-state stabilizer, 10% HPMC or HPC related to the entire extrudate sample, were added to the dissolution medium. Figure 4.81 shows the dissolution profile of the glassy solid solution in non-sink conditions. Within the first five minutes the drug release resulted in a supersaturated solution which recrystallized after ten minutes. Adding HPMC to the dissolution medium prevented the supersaturated solution from recrystallization for at least one hour, which might be sufficient to allow absorption of the drug from the gastrointestinal tract.

Similar results were obtained with HPC, but the stabilization of the supersaturated solution could be maintained for about 20 min only. Further excipients like crospovidone, croscarmellose sodium, xanthan gum, tragacanth, locust bean gum, guar gum, tara gum, and conjac gum, all in a concentration of 10% related to the sample, did not act as stabilizers. Cellulose derivatives are able to form a hydrodynamic boundary layer around the drug molecules being released from the glassy solid solution. The other gel-forming substances failed to stabilize the solution-state related to their gel-forming properties. Plant extracts like tragacanth are highly branched hydrocolloids and need to be added in high concentrations. Locust bean gum, guar gum, tara gum, and conjac gum represent elongated hydrocolloids like the cellulose derivatives, but need to be processed to temperatures >37 °C for a complete gel-formation. These substances can have a synergistic effect in combination with other gel-forming substances (Chowhan & Chen 2007), but are insufficient to increase the viscosity in the dissolution step as simple dispersions.

For the formulation of solid dosage forms from glassy solid solutions use was made of the stabilizing progress with HPMC.

4.6.4   Comparison with originator

CEL is marketed as a capsule formulation under the brand name Celebrex[TM] by its innovator company, Pharmacia Upjohn. The label claims the qualitative formula as lactose monohydrate, povidone, sodium lauryl sulphate, croscarmellose sodium, and magnesium stearate. Figure 4.82 demonstrates that CEL is present in its crystalline form in the original product.
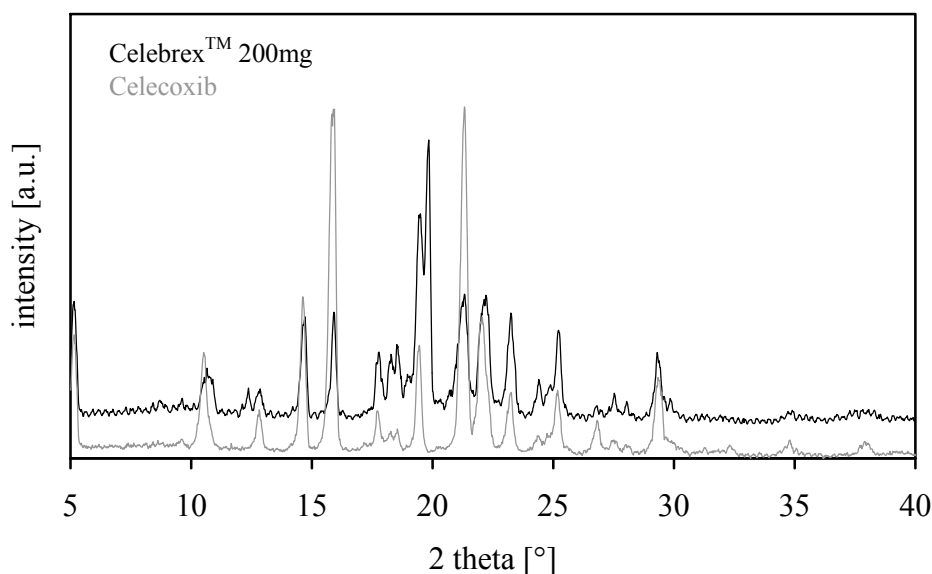
Figure 4.82: XRPD pattern of original product Celebrex™ and the drug CEL

In this case, another method of solubility enhancement is chosen. The surfactant SDS is added as wetting agent and increases the solubility of CEL in the dissolution medium. The pure drug and the simple mixture of the drug with SDS both float on the surface of the dissolution medium. As the contents of the reference formulation are found to wet quickly, the drug might be high-shear mixed with SDS (Bansal et al. 2006).

Under non-sink conditions, drug release from the original product is very slow (Figure 4.83). In contrast, drug release from capsules containing glassy solid solutions is fast and results in a supersaturated solution. In the first minutes, dissolving of the capsule only takes place resulting in a lag time. In all, about 50% drug are released from the capsule, and the supersaturated solution is kept constant for at least 90 min. The capsule does not dissolve completely and sticks together, possibly due to interaction between the ingredients and the gelatin. Additionally, the glassy solid solution becomes slightly sticky when getting into contact with the dissolution medium. Thus, a part of the formulation remains trapped in the capsule and cannot be dissolved. Due to the poor hydrodynamic in the basket apparatus, this problem may be related to the dissolution method only and can be overcome by dissolving the capsule employing the paddle method with a sinker.

One possibility ensuring a complete drug release from the capsule might be the addition of further excipients to the extrudate formulation in order to reduce the stickiness of the glassy solid solutions in solution-state.
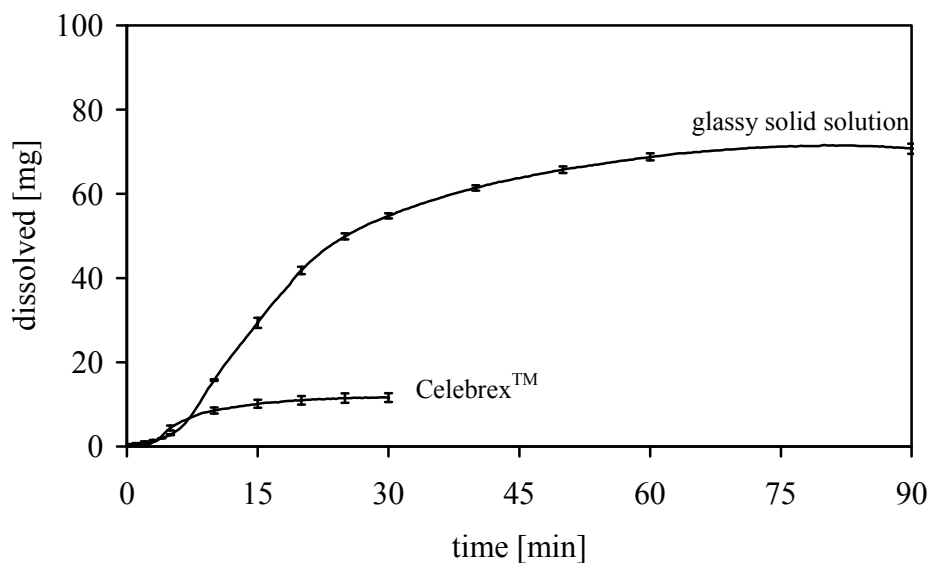
Figure 4.83: Dissolution profiles of gelatin capsules with CEL/aPMMA glassy solid solution + 10% HPMC and of original product Celebrex[TM]; 150 mg drug (glassy solid solution), 200 mg (Celebrex[TM]); 0.1 N HCl, non-sink conditions, 37 °C, basket, 100 rpm, 250 nm; mean ± SD, n=3

Experiments with HPMC capsules did not solve this problem. Enhancement of the dissolution rate and the formation of a supersaturated solution could not be observed.

In all, the results show that the processing of glassy solid solutions to capsules is a promising step to produce solid dosage forms from hot-melt extrudates.

4.6.5 Tabletting

For many pharmaceutical applications a tablet is the final dosage form. The downstream processing of extrudates to tablets can be realized by extruding a broad ribbon and cooling it by pulling it through a set of calender rolls with special tablet profiles (Breitenbach 2002, Rosenberg 2007). This preparation method has, on the one hand, the advantage that the systems are not strained with mechanical energy input and are thus prevented from physical stability problems. On the other hand, however, the cooling of the tablets might take a lot of time depending on the tablet size which could initiate an early recrystallization. Furthermore the variability in solid dosage form production is restricted as no further excipients can be added externally to the tablet formulation.

Therefore, it is useful to downstream the extrudates to powders via milling and processing them into tablets. During tabletting the glassy solid solution is faced with mechanical energy input which might have a negative impact on the physical stability of the amorphous systems. In this study, extrudates were milled, compressed into tablets and finally characterized as to the tablet properties, solid state characteristics, and dissolution behaviour.

97

The following samples were compressed into tablets (chapter 7.2.1.6) with a compression force of 13 to 14 kN (Figure 4.84). The formulations for tabletting did not contain any other excipients in order to facilitate the detection of the solid state in XRPD analysis.

Figure 4.84: Glassy solid solutions compressed into tablets

The compression force was chosen because tablets have to meet the demands for tablet crushing strength. If tablets have to be coated or blistered they need a certain crushing strength to withstand the processing forces. For the different samples the compression force was kept constant in order to enable a comparison of the compaction behaviour of the different materials. The tablets of the CEL and NAP formulations were characterized regarding tablet properties, solid state characteristics and dissolution behaviour. For the formulations of aPMMA with OXC and ACE, only the solid state characteristics were examined because there was a lack of material from the extrusion process.

The first four formulations of Figure 4.84 allow tablet production with a compression force of 13 to 14 kN. All materials show good tabletting behaviour. The tablets differ mainly in their crushing strengths, which range from 67 N for COP/CEL tablets to 126 N for PEG-PVA/CEL tablets (Table 4.19).

Table 4.19: Tablet characteristics

	PEG-PVA CEL 50%	COP CEL 50%	aPMMA CEL 50%	aPMMA NAP 50%
Compression force [kN]	13.5 ± 0.1 n=10	13.5 ± 0.4 n=10	13.4 ± 0.1 n=10	13.7 ± 0.2 n=5
Weight [mg]	300.8 ± 0.5 n=10	299.7 ± 0.2 n=10	299.3 ± 0.5 n=10	299.2 ± 0.9 n=5
Height [mm]	2.134 ± 0.0 n=10	2.283 ± 0.0 n=10	2.352 ± 0.0 n=10	2.467 ± 0.0 n=5
Volume [cm³]	0.24 ± 0.0 n=10	0.26 ± 0.0 n=10	0.27 ± 0.0 n=10	0.28 ± 0.0 n=5
Density [g/cm³]	1.25 ± 0.0 n=10	1.16 ± 0.0 n=10	1.13 ± 0.0 n=10	1.07 ± 0.0 n=5
Crushing strength [N]	126 ± 2.0 n=6	67 ± 1.2 n=6	75 ± 8.0 n=6	120 ± 2.9 n=3
Friability [%]	0.16 ± 0.1 n=3	0.31 ± 0.1 n=3	0.42 ± 0.2 n=3	0.30 ± 0.1 n=3
Disintegration time [min]	30-60 n=3	>60 n=3 slightly sticking	>60 n=3 sticking	>60 n=3 strongly sticking

Conspicuously, the crushing strength of the aPMMA/CEL tablets varies decisively whereas the others show relatively low standard deviations. The friability of all tablets is smaller than 1% which is in accordance with the demands of the Ph.Eur.

One great disadvantage is the long disintegration time, especially for tablets with aPMMA and COP. As hot-melt extruded glassy solid solutions have a very low porosity and as they form tablets with a very low porosity, too, the dissolution medium cannot infiltrate the compact. Therefore, drug release is guided only by dissolution from the tablet surface. Due to the low porosity and the stickiness when getting into contact with the dissolution medium, tablets produced from glassy solid solutions do not disintegrate. The long disintegration time leads to a poor dissolution.

Figure 4.86 shows the XRPD patterns of the six tablet formulations. In each diagram the pattern of the tablet is compared to the pattern of the pure crystalline drug. None of the glassy solid solution diffractograms shows a peak. This proves that the mechanical energy input emerging from the tabletting process has no influence on the solid state of the glassy solid solutions.
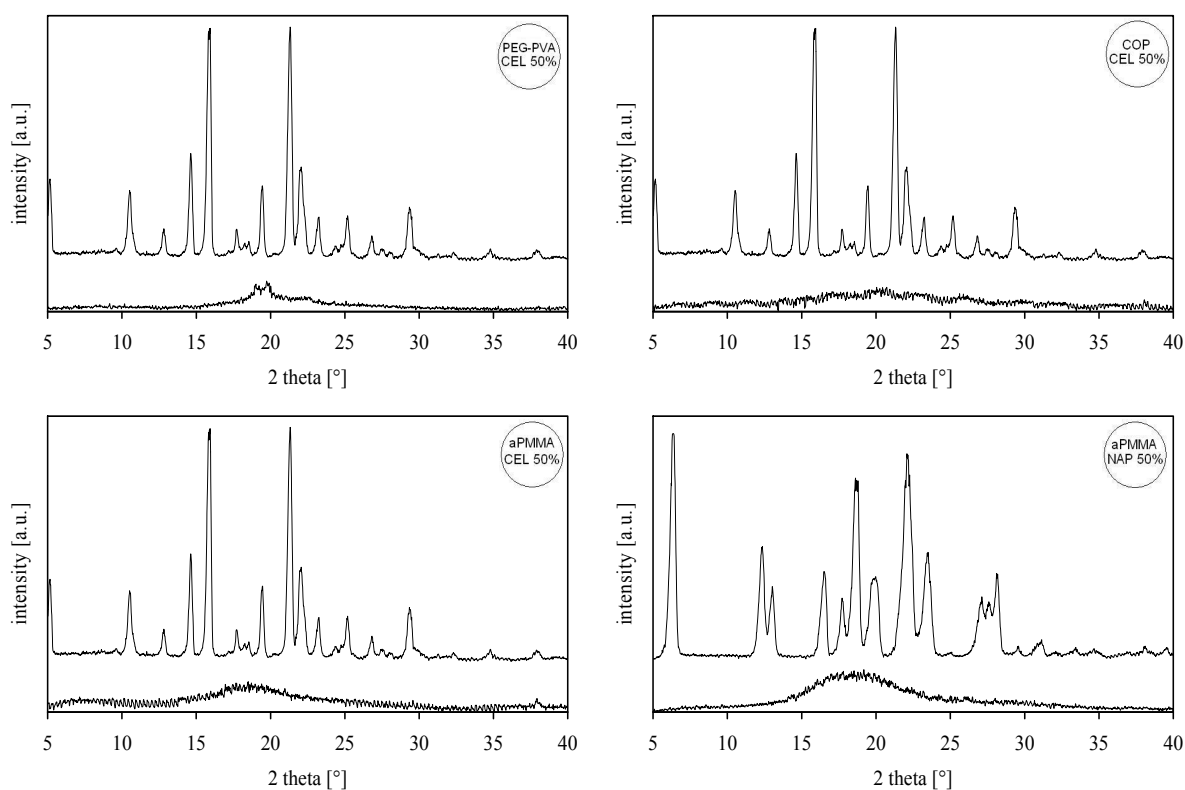
Figure 4.85: XRPD patterns of tablets from glassy solid solutions; each figure represents the comparison of tablet and pure drug

99
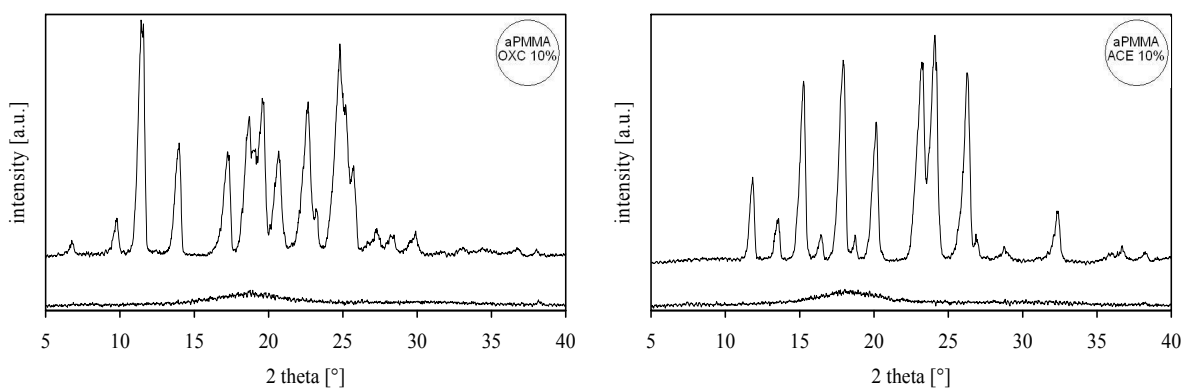
Figure 4.86: XRPD patterns of tablets from glassy solid solutions; each figure represents the comparison of tablet and pure drug continued

Drug release from tablets was determined under sink conditions and was compared to the results of the pure drug and the milled extrudates. In comparison with the milled extrudates and the pure drug, the drug release from copovidone tablets is very slow (Figure 4.87).
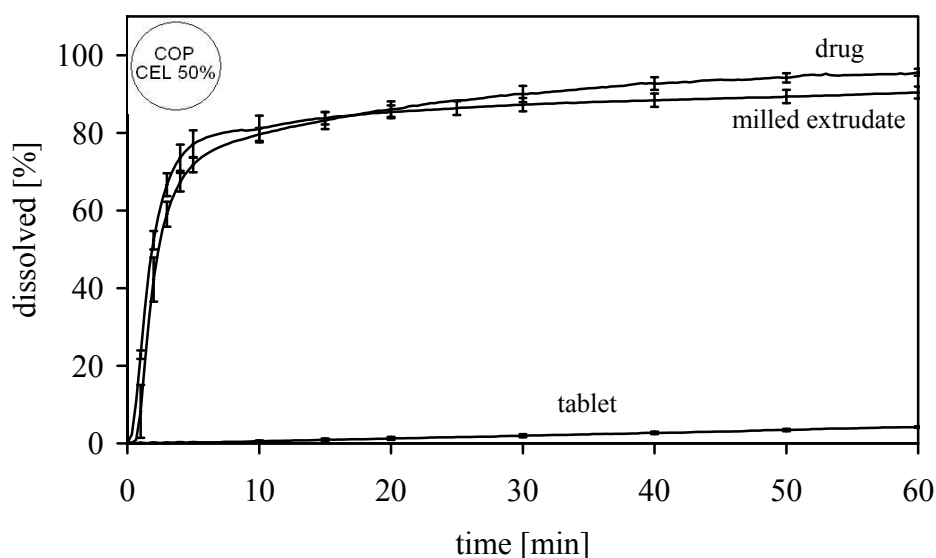
Figure 4.87: Dissolution profiles of pure drug, CEL/COP milled extrudates and CEL/COP tablet; 150 mg drug; 0.1N HCl + 0.3% cetrimid, sink conditions, 37 °C, paddle/basket, 50/100 rpm, 250 nm; mean ± SD, n=3

Contrary to the drug release from PEG-PVA (data not shown) and COP tablets, drug release from aPMMA tablets is much faster (Figure 4.88). 80% of the drug are released after 32 min. In comparison with the pure drug and the milled extrudates, drug release from tablets is slower.
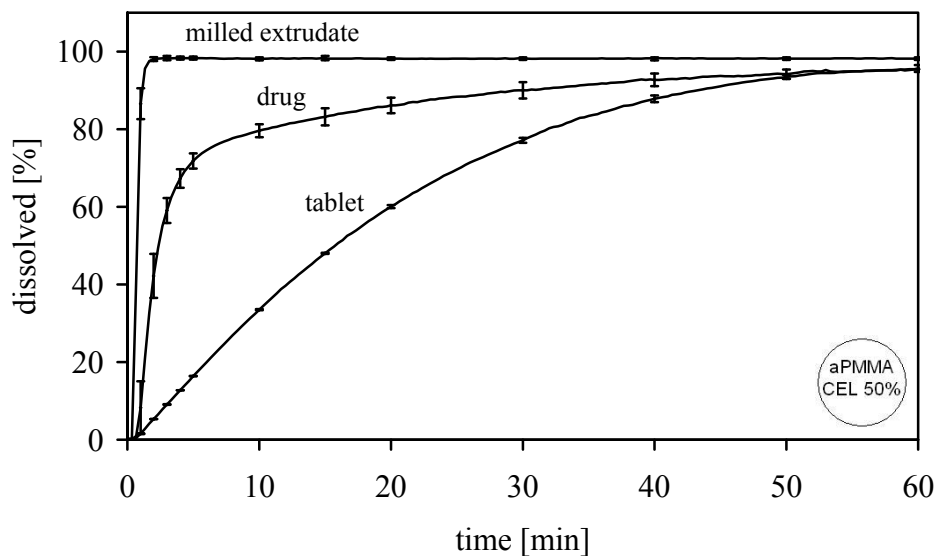
Figure 4.88: Dissolution profiles of pure drug, CEL/aPMMA milled extrudates and CEL/aPMMA tablet; 150 mg drug; 0.1 N HCl + 0.3% cetrimid, sink conditions, 37 °C, paddle, 50 rpm, 250 nm; mean ± SD, n=3

Tablets made from glassy solid solutions have a long disintegration time, which has a negative influence on the drug release. Therefore, superdisintegrants need to be added to the formulation, which support the disintegration of the tablets due to their swelling or capillary forces. Crospovidone, a superdisintegrant with a high swelling force, was used in this case.

Table 4.20: Tablet characteristics of aPMMA/CEL glassy solid solutions compressed with and without HPMC/crospovidone

	aPMMA/CEL50%	aPMMA/CEL 50% HPMC 10% crospovidone 1%
Compression force [kN]	13.4 ± 0.1 n=10	13.6 ± 0.1 n=10
Weight [mg]	299.3 ± 0.5 n=10	299.8 ± 0.3 n=10
Height [mm]	2.352 ± 0.0 n=10	2.353 ± 0.0 n=10
Volume [cm³]	0.27 ± 0.0 n=10	0.27 ± 0.0 n=10
Density [g/cm³]	1.13 ± 0.0 n=10	1.13 ± 0.0 n=10
Crushing strength [N]	75 ± 8.0 n=6	15 ± 0.5 n=6
Friability [%]	0.42 ± 0.2 n=3	2.67 ± 0.3 n=3
Disintegration time [min]	>60 n=3	19 ± 0.5 n=3

In order to shorten the disintegration time and to increase the solution-state stability, tablets with HPMC and crospovidone were compressed with a compression force of 14 kN. As the disintegrant has a negative effect on the crushing strength of the tablet, the amount of crospovidone was kept at a minimum of 1% only.

Table 4.20 shows that adding HPMC and crospovidone to the formulation leads to a distinct decrease of the crushing strength which is accompanied by a friability that does not fulfil the demands of the Ph.Eur. However, the disintegration time of the tablets was markedly shorter.

Tablets consisting of glassy solid solutions from aPMMA and CEL 50% were dissolved under non-sink conditions. The dissolution profiles of tablets with and without HPMC/crospovidone are shown in Figure 4.89. The dissolution profile of the aPMMA/CEL tablet resembles the dissolution profile of the milled aPMMA/CEL extrudates, but the supersaturation is much lower. As the tablet has a long disintegration time due to the low porosity and the sticking effect, the dissolution medium has a much smaller contact surface than given by the particles of the milled extrudates. The tablet with HPMC/crospovidone has a shorter disintegration time and, therefore, a larger contact surface for the dissolution medium. Drug release from this tablet results in a higher supersaturation, and the stabilizing effect of HPMC can be maintained for at least 60 min.
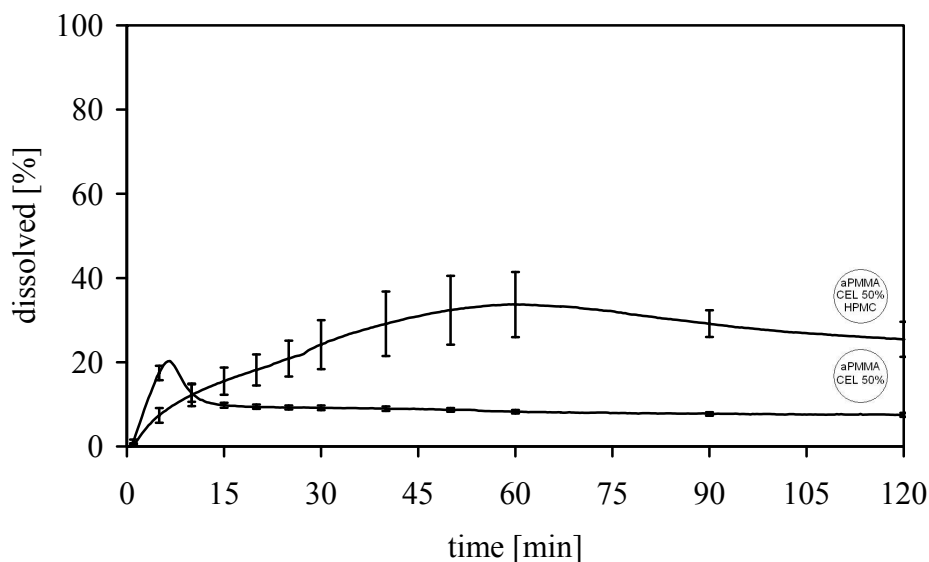
Figure 4.89: Dissolution profiles of CEL/aPMMA tablet and CEL/aPMMA+HPMC/crospovidone tablet; 150 mg drug; 0.1 N HCl, non-sink conditions, 37 °C, paddle, 50 rpm, 250 nm; mean ± SD, n=3

Compared to the formulation of the milled extrudates the supersaturation is lower. This lower supersaturation might be caused by the matrix former properties of HPMC in tabletting. Additionally, the reproducibility of the dissolution is worse, which might be caused by an irregular disintegration of the tablet due to sticking particles.

4.6.6   Summary

Hot-melt extruded glassy solid solutions can be processed into solid dosage forms. The mechanical energy input through milling and tabletting has no influence on the solid-state stability. The solution-state stability can be realized by adding HPMC to the external phase. Solubility enhancement by glassy solid solution formation results in a better dissolution than the improvement by surfactant addition as used in the original product. The low porosity and the stickiness of the glassy solid solutions are two problems that have to be overcome in order to obtain a complete drug release from capsules and tablets. The filling of capsules with milled hot-melt extrudates is a promising technique to obtain solid dosage forms from glassy solid solutions.

5   Summary

Hot-melt extrusion with poorly soluble drugs is a challenging method to enhance the solubility. The formation of solid dispersions, specifically of glassy solid solutions, wherein the drug is dispersed on a molecular basis in an inert carrier, leads to metastable systems that have advantageous dissolution behaviour but suffer from physical stability problems. To date, there is poor understanding of the solid state structure, the mechanism by which dissolution enhancement occurs, the stability on storage and in dissolution, and the processing to solid dosage forms.

The hot-melt extrusion process is influenced by several parameters. The right coordination of these parameters is decisive for the production of solid dispersions and thus, the success in solubility enhancement. The solid state and the viscosity of the extrudates can be controlled by the temperature of the barrels. Besides the configuration of the screw and the temperature profile of the barrel, the design of the die plate represents the third important extrusion parameter. By keeping the dead storage capacity at a minimum, an early solidification and thus a blockage of the dies can be prevented. Due to shear forces evolving in the extruder barrel and the ability of the drug to dissolve in the molten carrier before reaching the melting temperature, the process temperature can be kept below the melting point of the substances.

Basic butylated methacrylate copolymer is a suitable carrier to enhance the solubility of the poorly water-soluble drug celecoxib in a hot-melt extrusion process. The best solubility enhancement can be obtained by dispersing the drug in the molten carrier on a molecular basis and thus, to form glassy solid solutions. The solid state characteristics of the solid dispersion can be revealed by DSC analysis and interpretation of the corresponding glass transitions.

Such systems may contain a drug load of up to 60% and are stable at increased temperature and humidity which is due to the very low water uptake of the components. Glassy solid solutions of celecoxib and basic butylated methacrylate copolymer have a fast dissolution rate and result in a 58 fold supersaturated solution. The mechanism of drug release from these glassy solid solutions is carrier-controlled and governed by dissolution. The enhancement of the dissolution rate is based on improved solubility and wettability. Basic butylated methacrylate copolymer interacts chemically with celecoxib in an acid-base reaction.

The hot-melt extrusion process is highly dependent on the physicochemical properties of the compounds and their miscibility in the molten state.

The use of basic butylated methacrylate copolymer as solubility enhancing carrier in hot-melt extrusion cannot be transferred easily to all drugs. Depending on the properties of the drug, specifically the melting point and the pK_a, basic butylated methacrylate copolymer can be a useful carrier in glassy solid solution formation, but might be insufficient for solubility improvement. The formation of a glassy solid solution evolves from interactions between the drug and the carrier. Bonds can differ in their strength and can be advantageous or disadvantageous for a fast dissolution. Furthermore, decomposition processes can occur, when processing the drug at high temperatures. Thus, each formulation has to be analyzed separately.

The interpretation of the chemical structure, the calculation of solubility parameters, the determination of melting temperatures and enthalpies, and the performance of molecular dynamics simulations are tools to predict the miscibility of drugs and carriers for the formulation of solid dispersions. A combined approach of tools predicting miscibility is highly appropriate, as no single technique may yield all the required information. Nevertheless, the evaluation of the melting behaviour via DSC has the highest impact.

Hot-melt extruded glassy solid solutions can be processed into solid dosage forms. The mechanical energy input through milling and tabletting has no influence on the solid-state stability. The solution-state stability can be achieved by adding HPMC to the external phase. The filling of capsules with milled hot-melt extrudates is a promising technique to obtain solid dosage forms from glassy solid solutions.

By the extensive analysis of the hot-melt extrusion process, the interactions of the compounds, the thermal characteristics, and the dissolution mechanism of the resulting systems, it is possible to predict the extrusion process in an early stage of development and to improve the dissolution of poorly soluble drugs.

6 Zusammenfassung

Schmelzextrusion mit schwerlöslichen Arzneistoffen ist eine erfolgreiche Methode, um die Löslichkeit von Arzneistoffen zu verbessern. Die Formulierung von festen Dispersionen, speziell von glasartigen festen Lösungen, in denen der Arzneistoff molekulardispers im inerten Träger verteilt ist, führt zu metastabilen Systemen, die ein vorteilhaftes Freisetzungsverhalten zeigen, aber eine geringe Stabilität haben. Bis heute sind die solid state Eigenschaften, der Freisetzungsmechanismus, der zur Löslichkeitsverbesserung führt, die Stabilität bei der Lagerung und während der Freisetzung und die Weiterverarbeitung zu festen Arzneiformen nicht vollständig aufgeklärt.

Der Schmelzextrusionsprozess wird durch verschiedene Parameter beeinflusst. Die richtige Koordinierung dieser Parameter ist ausschlaggebend für die Herstellung fester Dispersionen und somit für den Erfolg der Löslichkeitsverbesserung. Der solid state und die Viskosität des Extrudats können über die Temperatur des Extruderzylinders geregelt werden. Neben der Schneckenkonfiguration und des Temperaturprofils, stellt das Design der Düsenplatte den dritten wichtigen Parameter dar. Ein frühzeitiges Erstarren und somit eine Blockade der Düsen kann durch eine Minimierung des Totraums vor der Düsenplatte verhindert werden. Durch Scherkräfte, die im Extruder entstehen, und die Fähigkeit des Arzneistoffs, sich im geschmolzenen Träger zu lösen bevor die Schmelztemperatur des Arzneistoffs erreicht wird, kann der Prozess unterhalb der Schmelztemperatur der Substanzen gefahren werden.

Eudragit® E ist ein geeigneter Träger, um die Löslichkeit des schwer wasserlöslichen Arzneistoffs Celecoxib mit Hilfe der Schmelzextrusion zu verbessern. Die beste Löslichkeitsverbesserung kann durch molekulardisperse Verteilung des Arzneistoffs im geschmolzenen Träger, d.h. der Bildung einer glasartigen festen Lösung, erreicht werden. Die solid state Eigenschaften der festen Dispersion können mittels DSC Analyse offenbart werden. Solche Systeme mit Celecoxib können bis zu 60% Arzneistoff enthalten und sind stabil während der Lagerung bei hohen Temperaturen und hoher relativer Feuchte, was durch die geringe Wasseraufnahme der Substanzen bedingt ist. Glasartige feste Lösungen aus Celecoxib und Eudragit® E haben eine schnelle Freisetzungsgeschwindigkeit und erreichen eine 58 fach übersättigte Lösung. Der Mechanismus der Freisetzung aus diesen glasartigen festen Lösungen ist Träger-kontrolliert und bestimmt durch Auflösung. Die Erhöhung der Freisetzungsgeschwindigkeit basiert auf erhöhter Löslichkeit und Benetzbarkeit des Arzneistoffs. Eudragit® E geht mit Celecoxib eine chemische Wechselwirkung in Form einer Säure-Base-Reaktion ein.

Der Schmelzextrusionsprozess ist stark abhängig von den physikochemischen Eigenschaften der Substanzen und ihrer Mischbarkeit im geschmolzenen Zustand. Die Verwendung von Eudragit® E als löslichkeitsverbessernder Träger im Schmelzextrusionsprozess kann nicht einfach auf alle Arzneistoffe übertragen werden. Abhängig von den Eigenschaften der Arzneistoffe, speziell, dem Schmelzpunkt und dem pK_s-Wert, stellt Eudragit® E einen nützlichen Hlfsstoff zur Bildung glasartiger fester Lösungen dar, kann aber die Löskichkeit des Arzneistoffs nicht verbessern. Die Bildung von glasartigen festen Lösungen entsteht durch Wechselwirkung zwischen Arzneistoff und Träger. Bindungen können in ihrer Stärke variieren und somit einen positiven oder negativen Effekt auf die Freisetzungsgeschwindigkeit haben. Des Weiteren können Zersetzungsprozesse auftreten, wenn Arzneistoffe bei hohen Temperaturen verarbeitet werden. Deshalb muss jede Formulierung separat analysiert werden.

Die Interpretation der chemischen Struktur, die Berechnung der Löslichkeitsparameter, die Bestimmung der Schmelztemperaturen und Schmelzenthalpien und die Durchführung von Moleküldynamik Simulationen werden als Methoden eingesetzt, um die Mischbarkeit von Arzneistoff und Träger für die Herstellung fester Dispersionen vorherzusagen. Eine Kombination dieser Methoden ist unumgänglich, da eine einzelne Technik nicht alle benötigten Informationen zu liefern vermag. Dennoch hat die Untersuchung des Schmelzverhaltens die größte Bedeutung.

Schmelzextrudierte glasartige feste Lösungen können zu festen Darreichungsformen weiterverarbeitet werden. Der mechanische Energieeintrag durch Mahlung und Tablettierung hat keinen Einfluss auf die physikalische Stabilität. Die Stabilität während der Freisetzung kann durch Zugabe von HPMC zur externen Phase ehöht werden. Die Abfüllung der gemahlenen glasartigen festen Lösungen in Kapseln ist ein viel versprechender Ansatz, um feste Arzneiformen mit schneller Freisetzungsgeschwindigkeit herzustellen.

Durch die umfassende Analyse des Schmelzextrusionsprozesses, der Interaktionen der Substanzen im geschmolzenen Zustand, der thermischen Eigenschaften und des Freisetzungsverhaltens der resultierenden Systeme, ist es möglich, bereits in einem frühen Stadium der Entwicklung mit kleinen Substanzmengen den Extrusionsprozess vorauszusagen und die Freisetzung schwerlöslicher Arzneistoffe gezielt zu verbessern.

7   Experimental part

7.1   Materials

7.1.1   Drugs

Experiments were performed with the poorly water-soluble drugs CEL, NAP, OXC, and IBU. The other drugs listed in Table 7.1 have a good aqueous solubility and were chosen because of their chemical and physical properties.

Table 7.1: Drugs used for manufacturing solid dispersions

drug	abbreviation	batch no.	source
acetaminophen	ACE	AEPP034	BASF, Ludwigshafen, Germany
caffeine anhydrate	CAF	001P34AX1B	BASF, Ludwigshafen, Germany
celecoxib	CEL	CBX508026	Aarti Drugs Limited, Mumbai, India
etofylline	ETO	17986	BASF, Ludwigshafen, Germany
ibuprofen	IBU	IB1Q0016	BASF, Ludwigshafen, Germany
lidocaine HCl	LID	2005051808	ratiopharm, Ulm, Germany
naproxen	NAP	R000232	ratiopharm, Ulm, Germany
oxcarbazepine	OXC	WE2381	ratiopharm, Ulm, Germany
pentoxyfylline	PEN	B141	Sanofi-Aventis Group, Frankfurt, Germany

The molecular weight, the melting behaviour, the solid state, the lipophilicity, the ability of forming H-bonds, and the acidity are main properties that have an effect on the solubility of the drugs. The indication is listed for the sake of completeness only and is of no further importance for the investigations (Table 7.2).

Table 7.2: Chemical and physical properties of drugs investigated in this study (source: Merck Index, DAB commentary)

drug	chemical structure	molecular weight	melting point [°C]	T_g or T_m [°C] 2nd heating	total solubility parameter	Hbond acceptor	Hbond donor	logP	pK_a a=acidic b=basic	solubility in water at RT [mg/L]	indication
ACE		151	169	23 T_g 157 T_m	24.61	3	2	0.339	9.86a 1.72b	14000	analgesic, antipyretic
CAF		194	236	236 T_m	29.13	6	0	-0.131	0.73b	21600	psycho stimulant
CEL		381	162	57 T_g	25.10	5	2	4.213	9.68a -6.12b	3	selective COX-2-inhibitor
ETO		224	163	146 T_m 162 T_m	33.86	7	1	-0.551	14.41a 0.50b		bronchial dilator
IBU		206	76	-45 T_g	19.36	2	1	3.722	4.41a	21	analgesic
LID HCl		271	72	36 T_g	(13.57 for LID)						anaesthetic
NAP		230	157	156 T_m	22.47	3	1	2.998	4.84a	16	analgesic
OXC		252	231	62 T_g 167 T_g	26.91	4	2	1.246	13.73a -0.53b		antiepileptic
PEN		278	105	-16 T_g	25.10	7	0	0.322	0.76b	77000	haemorheologic

7.1.2 Carriers

Several excipients were evaluated for the use in solid dispersion formation to improve the solubility of poorly water-soluble drugs (Table 7.3).

Table 7.3: Carriers used for manufacturing solid dispersions

substance	name	purity	batch no.	source
basic butylated methacrylate-copolymer	Eudragit E PO	Ph.Eur., JPE	G060431060	Evonik, Darmstadt, Germany
carbomer copolymer	Pemulen	USP/NF	CC378CT810	Noveon, Raubling, Germany
carbomer homopolymer	Carbopol BF	Ph.Eur., USP/NF, JPE	AB006N3	Goodrich, Cleveland OH, USA
CMCNa	Tylopur C 300 P2		DEAC 097557	Shin Etsu, Wiesbaden, Germany
copovidone	Kollidon VA64		07-4919	BASF, Ludwigshafen, Germany
crospovidone	Kollidon CL	Ph.Eur., USP/NF, JPE	50-1422	BASF, Ludwigshafen, Germany
ethylenglycol-, PEG6-, PEG32-stearate	Tefose		102257	Gattefossé, Weil am Rhein, Germany
HPC	Klucel HF Pharm		65900	Hercules, Wilmington, USA
HPMC	Pharmacoat 606		603146301565	Syntapharm, Mülheim, Germany
HPMCAS	Aqoat AS-MF	JPE	41007	Syntapharm, Mülheim, Germany
isomalt	galen IQ^{TM} 800	Ph.Eur., USP/NF	L547	Palatinit, Mannheim, Germany
lactitol anhydrate	Lactitol	food grade	N120T4615A	Danisco, Bönningstedt, Germany
macrogolglycerol-laurate	Gelucire 44/14	Ph.Eur.	101012	Gattefossé, Weil am Rhein, Germany
PEG 10000	Polyglycol 10000		DEGE024184	Clariant GmbH, Sulzbach, Germany
PEG 4000	Polyglycol 4000		DEGE122662	Clariant GmbH, Sulzbach, Germany
polydextrose refined powder FCC	Litesse Ultra		LS028S-3	Danisco, Bönningstedt, Germany
Polyox	Polyox WSR N10	NF	TG1355S5H1	Dow Chemical, Midland MI, USA
polyvinyl alcohol	Polyviol 05/20	USP	33360	Serva Feinbiochemica, Heidelberg, Germany
polyvinyl alcohol-polyethylene glycol-copolymer	Kollicoat IR		63767524 U0 91449856 P0	BASF, Ludwigshafen, Germany
PVP K30	Kollidon 30		49-0064	BASF, Ludwigshafen, Germany

Other excipients were used for producing solid dosage forms, testing recrystallization inhibition, and characterizing the extrudates and solid dosage forms (Table 7.4).

Table 7.4: Other chemicals and laboratory supplies used for manufacturing and characterizing solid dispersions and the corresponding solid dosage forms

substance	purity	batch no	source
cetrimid	Ph.Eur.	0511A098	Fagron, Barsbüttel, Germany
Texapon K 1296, sodium dodecyl sulphate	DAB	33043	Henkel KGaA, Düsseldorf, Germany
magnesium stearate		3043	Baerlocher GmbH, Unterschleißheim, Germany
crospovidone		20653188Q0	BASF, Ludwigshafen, Germany
xanthan gum		-	Schöner GmbH, Achim-Uphusen, Germany
tragacanth		-	Merck KGaA, Darmstadt, Germany
locust bean gum		15052-4343	König & Wiegand, Düsseldorf, Germany
guar gum		1603-4023	König & Wiegand, Düsseldorf, Germany
tara gum		1430-4067	König & Wiegand, Düsseldorf, Germany
conjac gum		1553-4013	König & Wiegand, Düsseldorf, Germany
gelatin capsules size 0		05CS	Capsugel, Colmar, France
HPMC capsules size 0		05VC	Capsugel, Colmar, France
potassium bromide	IR grade	50910	Riedel de Haën, Buchs SG, Switzerland
HCl		various	Merck KGaA, Darmstadt, Germany
purified water	Ph.Eur.		purified with reverse osmosis
silica gel		51575491	Carl Roth GmbH, Karlsruhe, Germany

7.2 Methods

7.2.1 Manufacturing methods

7.2.1.1 Preparation of melts

For preliminary testing approximately 2-4 g of the drug or the drug/carrier blend were molten. All blends were prepared with mortar and pestle. The substances were molten at their corresponding melting temperatures (Table 7.2) in a drying oven (Heraeus Vacutherm type VT

6025, Kendro Laboratory Products, Hanau, Germany) under vacuum, cooled at room temperature, and milled in the analytic mill A10 (Janke & Kunkel, IKA-Labortechnik, Staufen, Germany).

7.2.1.2 Preparation of evaporates

The physical mixture of CEL/aPMMA 1:1 was prepared with mortar and pestle. After dissolving the blend in ethanol, the solvent was removed with the rotary evaporator RV05 (IKA-Labortechnik, Staufen, Germany) at 50 °C under vacuum. After removal of the solvent, the residue was stored in a drying oven (Heraeus Vacutherm type VT 6025, Kendro Laboratory Products, Hanau, Germany) at 50 °C under vacuum to ensure the absence of ethanol.

7.2.1.3 Hot-melt extrusion

Blends of drug and carrier with a batch size of 1-2 kg were prepared by mixing accurately weighed quantities of both components in a Turbula mixer (T10B, W.A. Bachofen AG, Basel, Switzerland) for 15 min. Extrusion was performed using a co-rotating twin-screw extruder with a diameter of 18 mm and a L/D ratio of 30 (Leistritz Micro 18PH 30D, Nuremberg, Germany). The heating barrel is divided into six temperature zones of length 5D whereas the first zone cannot be heated and serves as feeding zone only. The die plate and the flange respectively, can be heated additionally. Figure 7.1 shows the configuration of the extruder and the screws. The screws consist of different screw element types, namely conveying elements (GFF and GFA), combing mixer elements (GFM), and kneading blocks (KB) which are described in more detail by Djuric and Kleinebudde (2008). The abbreviations GFF, GFA, GFM, and KB according to the terminology of the supplier Leistritz were adopted. In the abbreviations of the conveying and combing mixer elements the first number describes the number of starts, the second number the pitch of the screw, and the third number the length of the element. In the abbreviations of the kneading elements the first number stands for the number of kneading segments, the second number for the number of starts, the third for the length of the kneading block, and the fourth for the advance angle of the single kneading segment. F signifies conveying.
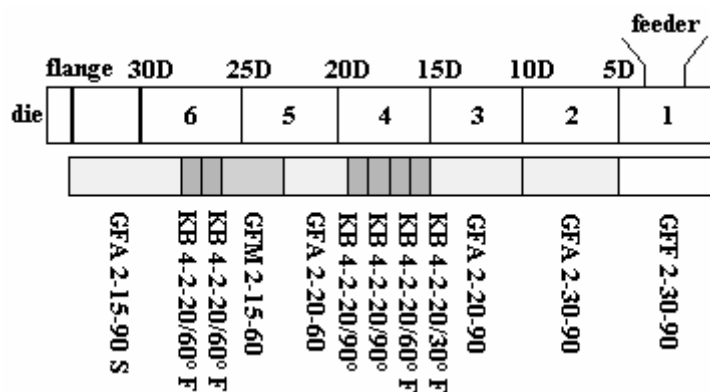
112

Figure 7.1: Configuration of the extruder and the screw

The temperature profile of the extruder barrel varied for each formulation as described below (Table 7.5).

Table 7.5: Temperature profiles of the extruder barrel for extruded blends

drug	drug load [%]	carrier	temperature of the heating zones [°C]						die plate
			zone 1	zone 2	zone 3	zone 4	zone 5	zone 6	
ACE	30	aPMMA	20	70	130	168	168	140	130
ACE	50	COP	20	70	130	155	155	125	125
CAF	50	aPMMA	20	70	150	233	233	180	150
CEL	50	aPMMA	20	70	130	157	157	140	125
CEL	62.5	aPMMA	20	70	130	157	157	140	125
CEL	50	COP	20	70	130	157	157	140	130
CEL	50	PEG-PVA	20	70	130	157	157	160	160
ETO	50	aPMMA	20	70	130	153	153	150	150
ETO	50	COP	20	70	130	153	153	140	140
ETO	50	PEG-PVA	20	70	130	153	153	140	140
IBU	50	aPMMA	20	50	60	70	70	70	70
LID HCl	50	aPMMA	20	30	40	60	60	60	60
NAP	50	aPMMA	20	70	90	100	100	100	100
NAP	50	PEG-PVA	20	70	130	155	155	155	155
OXC	10	aPMMA	20	70	150	210	210	170	140
OXC	50	aPMMA	20	70	150	215	215	170	140
PEN	50	aPMMA	20	70	85	100	100	95	95

The screw rotation speed was kept constant at 140 rpm. The feeding rate changed with the carrier (Table 7.6). The current intensity, the pressure at the die plate, and the mass temperature at the die plate were measured for each extrusion process (Table 7.6). During extrusion the temperature of zone four and five (Figure 7.1) were varied to obtain transparent strands. The temperatures of zone six and of the die plate were adapted to obtain semisolid strands.

Therefore, the current intensity had to be kept as small as possible. If the pressure at the die plate was too small, the viscosity of the melt was too low, if it was too high, the melt dammed up before the dies. A suitable viscosity of the melt could be obtained at a pressure of about 10-20 bar measured at the die plate.

Table 7.6: Extrusion parameters

drug	drug load [%]	carrier	feeding rate [kg/h]	current intensity [%]	pressure at the die plate [bar]	mass temperature at the die plate [°C]
ACE	30	aPMMA	0.5	20-40	5-20	156
ACE	50	COP	1.0	35-45	12-16	154
CAF	50	aPMMA	0.6	30-45	10-16	153
CEL	50	aPMMA	0.6	19-32	8-9	120
CEL	62.5	aPMMA	0.6	30-45	9-75	125
CEL	50	COP	1.0	12-24	20-34	130
CEL	50	PEG-PVA	0.3	25-35	30-40	161
ETO	50	aPMMA	0.6	40-59	5-10	160
ETO	50	COP	1.0	20-40	30-40	140
ETO	50	PEG-PVA	0.3	20-40	35-45	140
IBU	50	aPMMA	0.6	46-61	14-37	68
LID HCl	50	aPMMA	0.6	18-35	40-50	65
NAP	50	aPMMA	0.6	25-45	20-40	96
NAP	50	PEG-PVA	0.3	25-35	20-37	155
OXC	10	aPMMA	0.6	25-50	8-10	145
OXC	50	aPMMA	0.6	25-50	15-20	150
PEN	50	aPMMA	0.6	19-33	4-10	107

Semisolid strands leaving the die plate are collected manually and cooled at room temperature. Solidified strands are broken into small fragments and finally investigated, processed or stored.

7.2.1.4 Milling

Extrudates were grinded with a centrifugal mill (Ultra Centrifugal Mill ZM 200, Retsch, Haan, Germany) with a ring sieve of size 1 mm. Extrudates were milled with a rotating speed of 6000 rpm.

7.2.1.5 Capsule filling

The milled extrudates were filled into size zero hard-gelatin or HPMC capsules. Since these experiments focused on the ability to prepare solid dosage forms and to examine the dissolution behaviour of solid dispersions from capsules, the powder blends were weighed into the capsule bodies manually.

7.2.1.6 Tabletting

Tablets were prepared using an instrumented pneumohydraulic single punch tablet press (FlexiTab[TM], Röltgen, Solingen, Germany) (Albers et al. 2006). Milled extrudates were compressed without any tabletting aids to keep the formulation as simple as possible. The punches were lubricated externally by compressing a magnesium stearate tablet before each tabletting step. Glassy solid solution samples of 300 mg were weighed and compressed in the manual mode at a constant compression force of 13 to 14 kN.

10 g of the blend of CEL, aPMMA, HPMC, and crospovidone were mixed in a Turbula mixer for 10 min. Tabletting of this blend was performed as described above.

7.2.2 Analytical methods

7.2.2.1 Bagley plot

Bagley introduced the combined solubility parameter δ_v to achieve a projection of the three-dimensional solubility parameter space into a two-dimensional plot.

$$\delta_v = \sqrt{\delta_d^2 + \delta_p^2}$$

Equation 4: Calculation of combined solubility parameter δ_v, δ_d = partial solubility parameter for dispersion components, δ_p = partial solubility parameter for polar components

7.2.2.2 Calculation of solubility parameters

Three-dimensional solubility parameters for polar systems by Hansen (1967) were calculated by the computer program SPWin, version 2.1 (Breitkreutz 1998), which contains an advanced parameter set that is based on the group contribution methods of Fedors (1974) and Van Krevelen and Hoftyzer (1976). Group contributions by Fedors and Van Krevelen and Hoftyzer were combined by Braun and Gröning (1996) and were modified and optimized by Breitkreutz for the software SPWin 2.1.

For the calculation the structures of the drugs and carriers have to be divided into functional groups, wherein each atom may only occur once (Table 7.7). The deciding factor for the affiliation to a group is its priority in chemical nomenclature.

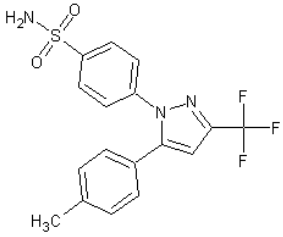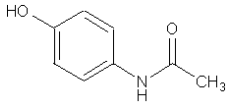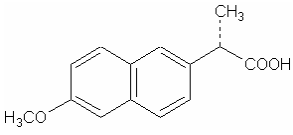Table 7.7: Chemical structure and functional groups of drugs used for solubility parameter calculation
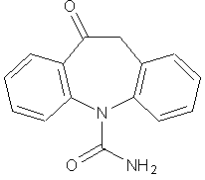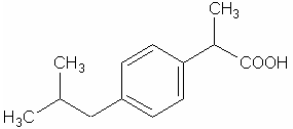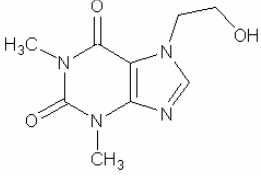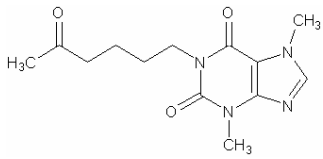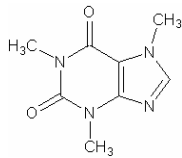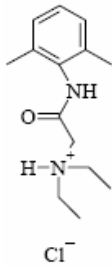
drug	structure	MW	groups	frequency
CEL		381	-CH$_3$	1
			>C<	1
			-CH=	1
			>C=	2
			phenylene	2
			ring $\geq$ 5	1
			conjugated db	2
			-NH$_2$	1
			-N= (planar)	2
			-SO$_2$-	1
			-F	3
ACE		151	-CH$_3$	1
			phenylene	1
			>C=O (ketone)	1
			-OH (not adjacent)	1
			-NH	1
NAP		230	-CH$_3$	2
			>CH-	1
			-CH=	6
			>C=	4
			ring $\geq$ 5	2
			conjugated db	5
			-COOH	1
			-O- (not adjacent)	1
OXC		252	-CH$_2$-	1
			phenylene	2
			ring $\geq$ 5	1
			>C=O (ketone)	2
			-NH$_2$	1
			-N= (planar)	1
IBU		206	-CH$_3$	3
			-CH$_2$-	1
			>CH-	2
			phenylene	1
			-COOH	1
ETO		224	-CH$_3$	2
			-CH$_2$-	2
			-CH=	1
			>C=	2
			ring $\geq$ 5	2
			conjugated db	2
			>C=O (ketone)	2
			-OH (not adjacent)	1
			-N= (planar)	4
PEN		278	-CH$_3$	3
			-CH$_2$-	4
			-CH=	1
			>C=	2
			ring $\geq$ 5	2
			conjugated db	2
			>C=O (ketone)	3
			-N= (planar)	4

Table 7.8: Chemical structure and functional groups of drugs used for solubility parameter calculation continued

drug	structure	MW	groups	frequency
CAF		194	-CH$_3$	3
			-CH=	1
			>C=	2
			ring ≥ 5	2
			conjugated db	2
			>C=O (ketone)	2
			-N= (planar)	4
LID HCl		271	-CH$_3$	4
			-CH$_2$-	3
			-CH=	3
			>C=	3
			ring ≥ 5	1
			conjugated db	3
			>C=O (ketone)	1
			-NH-	1
			>N- (tetraeder)	1
			solubility parameter was calculated for the free base as the package does not set aside for the calculation of salts	

Solubility parameters of polymers always relate to a certain molecular weight which is given in the following table (Table 7.9). From the molecular weight of the polymer and the structure of one single monomer the frequencies of the groups can be determined.

For polymers whose precise distribution of substituents is not known, like in HPMCAS, one structure that occurs mainly in the mixture is assumed. For polymers with unknown molecular weight, e.g. crospovidone or Gelucire, the calculation of solubility parameters was not possible.

Table 7.9: Chemical structure and functional groups of carriers used for solubility parameter calculation
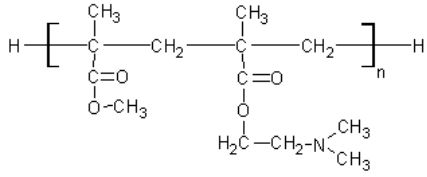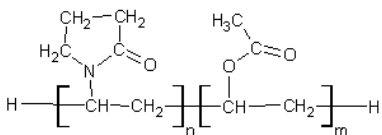
carrier	structure	MW	groups	frequency
aPMMA	C: 13 H: 23 N: 1 O: 4 => Σ 257	150000 (257 x n) n = 584	-CH$_3$	2921
			-CH$_2$-	2335
			>CH-	1
			>C<	1167
			-COOR	1168
			>N-	584
copovidone	C: 6 + 4 H: 9 + 6 N: 1 O: 1 + 2 => Σ 111 / Σ 86	45000 (111 x n + 86 x m) n = 244 m = 209	-CH$_3$	210
			-CH$_2$-	1185
			>CH-	452
			ring ≥ 5	244
			-COOR	209
			>C=O (ketone)	244
			-N= (planar)	244

Table 7.10: Chemical structure and functional groups of carriers used for solubility parameter calculation continued
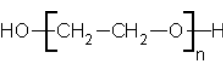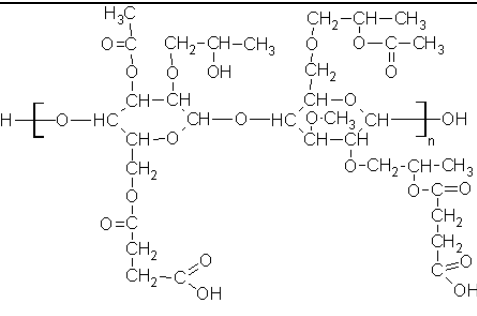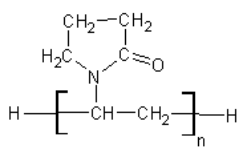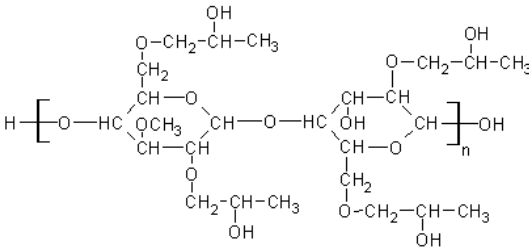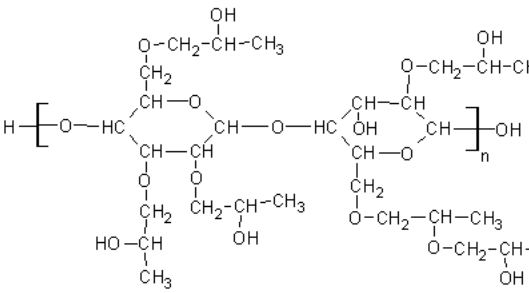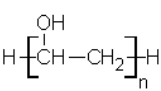
carrier	structure	MW	groups	frequency
PEG-PVA	C: 18 H: 34 O: 9 => Σ 218 / Σ 72	44946 (11250 PEG + 33750 PVA) (218 x n + 2 x 72 x m) n = 52 m = 234	$-CH_2-$ >CH- -OH (not adjacent) -OH (adjacent) -O- (adjacent)	1354 1038 936 2 259
isomalt		344	$-CH_2-$ >CH- ring ≥ 5 -OH (adjacent) -O- (adjacent)	3 9 1 9 2
lactitol		344	$-CH_2-$ >CH- ring ≥ 5 -OH (adjacent) -O- (adjacent)	3 9 1 9 2
polydextrose	C: 6 H: 10 O: 5 => Σ 162	1314 (162 x n) n = 8	$-CH_2-$ >CH- ring ≥ 5 -OH (adjacent) -O- (adjacent)	8 40 8 26 15
PEG 4000	C: 2 H: 4 O: 1 => Σ 44	3978 (44 x n) n = 90	$-CH_2-$ -OH (adjacent) -O- (adjacent)	180 2 89
HPMCAS	C: 34 H: 52 O: 21 => Σ 796	18000 (796 x n) n = 23	$-CH_3$ $-CH_2-$ >CH- ring ≥ 5 -COOH -COOR -OH (adjacent) -O- (adjacent)	138 207 299 46 46 92 25 183

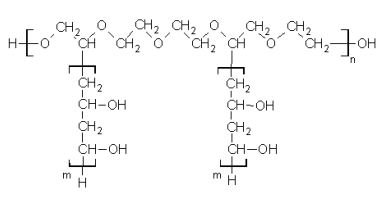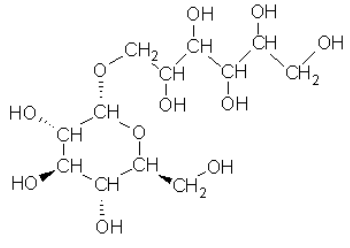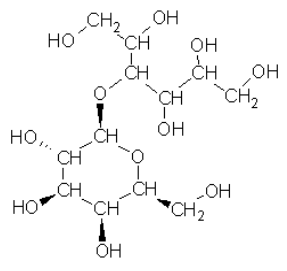Table 7.11: Chemical structure and functional groups of carriers used for solubility parameter calculation continued
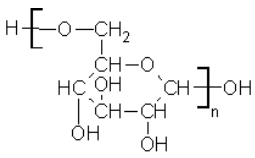
carrier	structure	MW	groups	frequency
PVP K30	CH_2-CH_2, H_2C, $C=O$, N, $H-[CH-CH_2]_n-H$ C: 6 H: 9 N: 1 O: 1 => Σ 450	50000 (111 x n) n = 450	-CH_3 -CH_2- >CH- ring ≥ 5 >C=O (ketone) >N- (tetraeder)	1 1800 449 450 450 450
HPMC	(structure) C: 25 H: 46 O: 14 => Σ 570	10000 (570 x n) n = 18	-CH_3 -CH_2- >CH- ring ≥ 5 -OH (adjacent) -O- (adjacent)	90 108 252 36 92 161
HPC	(structure) C: 30 H: 56 O: 16 => Σ 672	1150000 (672 x n) n = 1711	-CH_3 -CH_2- >CH- ring ≥ 5 -OH (adjacent) -O- (adjacent)	10266 13688 27376 3422 10268 17109
PVA	OH, $H-[CH-CH_2]_n-H$ C: 2 H: 4 O: 1 => Σ 44	22000 (44 x n) n = 500	-CH_3 -CH_2- >CH- -OH (not adjacent)	1 500 499 500

7.2.2.3 Calculation of distances in Bagley and DSC plot

Drugs and carriers are predicted as miscible when the corresponding solubility parameters δ are similar, i.e. the difference Δδ is small. In the Bagley plot three-dimensional solubility parameters are combined to achieve a projection of the three-dimensional solubility parameter space into a two-dimensional plot. In order to determine the Δδ in this two-dimensional plot, the distance between a drug and a carrier was calculated by the Pythagorean Theorem. The same method was used to determine the distances in the DSC plot.

7.2.2.4 Calibration UV spectroscopy

The concentration of the drug in the dissolution studies was detected via UV spectroscopy. Calibrations for CEL, NAP, and OXC were provided as described in Figure 7.2 to Figure 7.5.
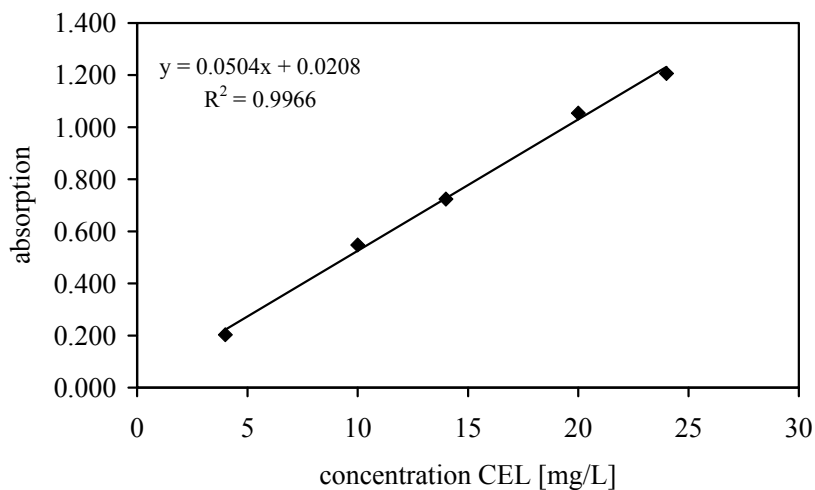
Figure 7.2: UV calibration of CEL in 0.1 N HCl + 10% ethanol, 37 °C; wavelength 250 nm, cuvette 1 cm
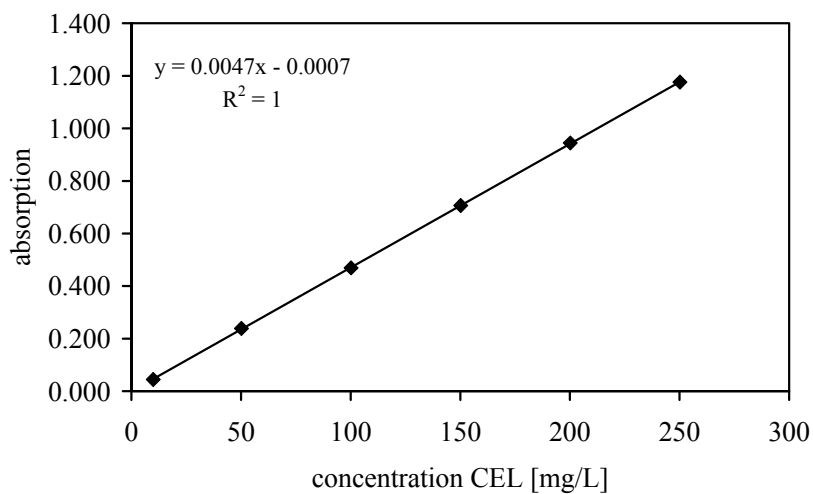
Figure 7.3: UV calibration of CEL in 0.1 N HCl + 0.3% Cetrimid, 37 °C; wavelength 250 nm, cuvette 1 mm
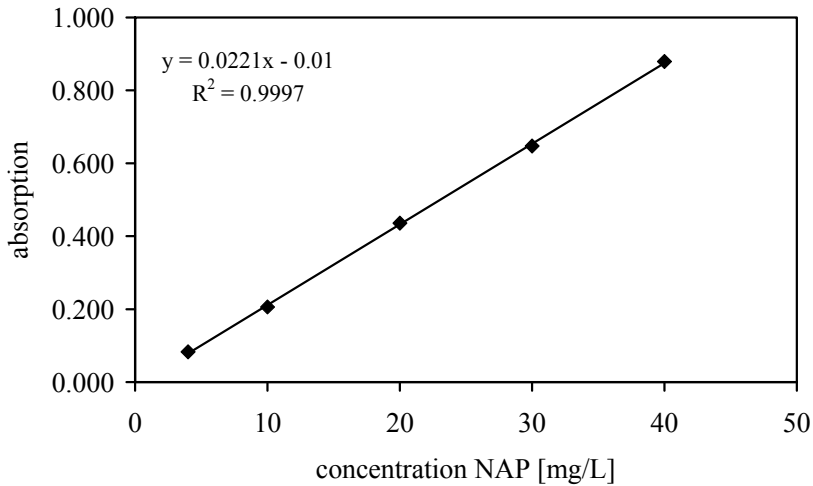
Figure 7.4: UV calibration of NAP in 0.1 N HCl, 37 °C; wavelength 272 nm, cuvette 1 cm
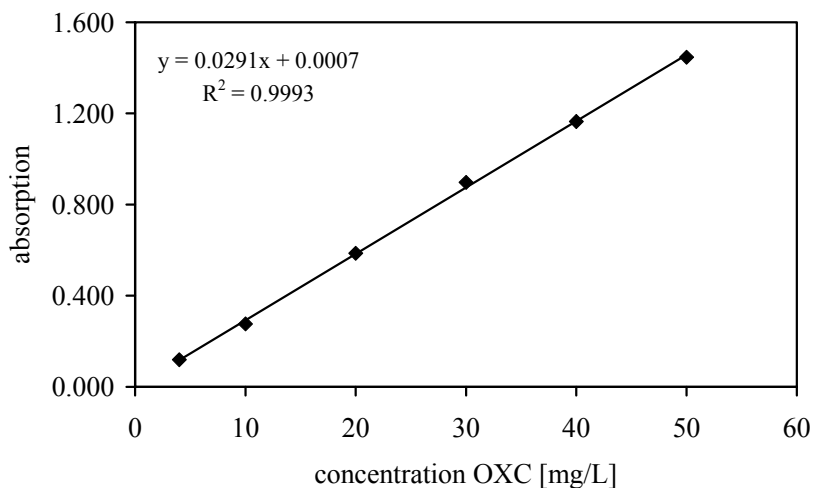
Figure 7.5: UV calibration of OXC in 0.1 N HCl, 37 °C; wavelength 256 nm, cuvette 1 cm

7.2.2.5 Contact angle

Contact angles were measured with a drop shape analysis system (DSA100, Krüss, Hamburg, Germany) at room temperature. Samples of the powders and the physical mixtures with a smooth surface were prepared with a hydraulic press (Perkin Elmer, Überlingen, Germany) with a pressure of 8.8 t/cm² and a diameter of 13 mm. For the preparation of smooth melts the powders were molten and filled into aluminum frames. Extrudates were stuck onto cards to fix their position during the measurement.

Droplets of demineralised water of 0.5 µL for the extrudates and 2.5 µL for the melts and compacted powders were placed on five different positions of each surface with a dropping speed of 1500 µL/min (Hamilton Microlitre Syringe 750, Hamilton, Bonaduz, Switzerland). The average value was defined as measured contact angle. For the powders and melts the

contact angle was determined with the height/width method, for the extrudates with the circle-fitting method employing the drop shape analysis software DSA 3 (Krüss, Hamburg, Germany).

7.2.2.6 Crushing strength

The crushing strength of the tablets was determined with a hardness tester (HT1, Sotax, Basel, Switzerland) in the mode constant speed with 1.00 mm/s.

7.2.2.7 Differential scanning calorimetry

Differential Scanning Calorimetry was used to determine the T_g of individual components and the drug/carrier blends, and to examine the solid-state characteristics of the extrudates. Measurements were carried out using a DSC 821e (Mettler-Toledo, Gießen, Germany). Samples of approximately 2-3 mg were sealed in pierced aluminum pans of 40 μL and were measured at a scanning speed of 10 K/min over a temperature range, which was adjusted to the melting point of each individual drug. The samples were cycled twice to remove the effects of moisture and thermal history. The glass transition temperature was measured in the second cycle as the step transition in the plot of heat flow versus temperature. The solid-state characteristics were surveyed in the first heating cycle by observing the melting enthalpy and the onset melting temperature of the drug. Miscibility of drug and carrier is detected by changes in the melting endotherms of the drug and by the temperature of the glass transition of the blend in comparison with the single T_g of drug and carrier. An empty pan served as reference.

The calibrations of temperature and enthalpy were performed with indium, zinc, and cyclohexane.

7.2.2.8 Disintegration time

Disintegration time was determined for three single tablets with an apparatus consisting of a basket-rack assembly with six tubes and disks (ZT 2, Erweka, Sulzbach-Laufen, Germany), a thermostatic arrangement for heating (Julabo Paratherm IM heating), and a device for raising and lowering the basket (Ph.Eur.). The immersion fluid was water at a temperature of 37 °C.

7.2.2.9 Dissolution

Drug release (BTWS 600, Pharmatest, Hainburg, Germany) from extrudates, milled extrudates, and tablets was conducted in 900 mL of 0.1 N HCl with (sink conditions) or without (non-sink conditions) surfactant cetrimid using the paddle method (USP apparatus 2). The rotational speed of the paddles was set at 50 rpm. Drug release from capsules was examined using the basket method (USP apparatus 1) at a rotational speed of 100 rpm. The respective maximum UV wavelength of each drug was selected for the spectrophotometrical detection (Lambda-2, Perkin-Elmer, Überlingen, Germany), which was free from interference with the carrier and cetrimid spectra. Measurements were performed in triplicate. Samples for the scanning electron microscopy were released for 2 min in 0.1 N HCl, washed with demineralised water, and dried at room temperature.

7.2.2.10 Fourier-transform infrared spectroscopy

FT-IR spectra of the carriers, the drugs, and the solid dispersions were obtained on a Nicolet FT-IR 100 spectrophotometer (Thermo Electron Corporation, Waltham, USA). Sample-KBr-blends were compressed into potassium bromide disks in a hydraulic press (Perkin-Elmer, Überlingen, Germany).

7.2.2.11 Friability

Friability was determined according to the European Pharmacopeia in a friability tester (TAP, Erweka, Sulzbach-Laufen, Germany). The test was performed with one tablet at a time (n=3).

7.2.2.12 Helium-pycnometry

The particle density of the amorphous drugs and carriers was measured by gas pycnometry with helium as test gas (Accu PycTM 1330, Micromeritics, Norcross, GA, USA). The solid state of the compounds was transferred into the amorphous form by the melting method.

7.2.2.13 Hot stage microscopy

A polarisation microscope (Leica DM LB, Leica, Cambridge, United Kingdom) was used to investigate drug/carrier miscibility. Samples were prepared on a temperature controlled microscope stage (THMS 600, Linkam Scientific Instruments, Surrey, United Kingdom) and were heated with the temperature control system TMS 94 (Linkam Scientific Instruments, Surrey, United Kingdom) at a heating rate of 10 K/min.

7.2.2.14 Intrinsic dissolution

For the determination of the intrinsic dissolution according to Ph.Eur. 5.4 300 mg of the physical mixture were molten, cooled at room temperature, milled and compacted with a hydraulic press for 90 s with a load of 1 t. Samples with a well-defined surface (diameter 13 mm) were placed in 900 mL 0.1 N HCl + 0.3% cetrimid (rotating speed 100 rpm). To calculate the intrinsic dissolution rate, the cumulative amount of sample dissolved was plotted against time until 10% dissolved. Linear regression was performed on data points up to and including the time point beyond when 10% was dissolved. The intrinsic dissolution rate is given by the slope of the regression line (mg/min). The amount of drug dissolved was detected photometrically (Lambda-2, Perkin-Elmer, Überlingen, Germany).

7.2.2.15 Karl-Fischer titration

The water contents of CEL melts, carrier melts, and their solid dispersions with a drug load of 50% were determined by Karl-Fischer titration (Mettler DL 18, Mettler-Toledo, Gießen, Germany).

7.2.2.16 Laser light diffraction

For the determination of the particle size distribution and the median particle size, powder samples were brought into the beam of a laser diffractometer (Sympatec, Clausthal-Zellerfeld, Germany) through a dry dispersion device (RODOS, Sympatec) with a pressure of 2 bar and a feed rate of 80%. A lens sized 0.25/0.45-87.5 µm was used for the micronized powders aPMMA, CEL, NAP, and OXC, a lense sized 0.5/1.8-350 µm for ACE, and a lense sized 0.5/4.5-875 µm for IBU and ETO. Analysis was performed with the program HELOS (Sympatec, Clausthal-Zellerfeld, Germany). The x_{50} value describes the median of the particle size distribution.

7.2.2.17 Molecular modelling

Molecular modelling was performed using the GROMACS 3.1 package (Berendsen et al. 1995, Lindahl et al. 2001). Molecular dynamics simulations were computed for the carriers isomalt (ISO) and aPMMA in form of ethyldimethylamine (aPMMA*). To investigate the interactions of drugs with the carriers, small carrier models existing of 34 ISO molecules or 287 aPMMA* molecules are built with the computer. These carrier entities are heated to 373 K (ISO) and 336 K (aPMMA*) respectively, and conveyed to the liquid state. An adequate number of carrier

molecules is removed from the centre of the entity and replaced by a drug molecule. Drug-carrier interactions can then be calculated whereas drug-drug interactions are not taken into account. For each drug/carrier mixture a 2 ns simulation was performed.

In this study hydrogen bond interactions as well as other electrostatic short-range interactions are summarized in the Coulomb interaction term C. The van der Waals forces include attractive and repulsive forces. The calculation of the Lennard-Jones potential LJ is used to describe the attractive dispersion forces and the repulsive components of the van der Waals interaction energy.

7.2.2.18 Prediction of glass transition temperature

The Gordon-Taylor (Gordon & Taylor 1952) equation simplified by application of the Simha-Boyer (Simha & Boyer 1962) rule describes the glass transition of a binary mixture (Equation 5).

$$Tg = \frac{w_1 Tg_1 + K w_2 Tg_2}{w_1 + K w_2} \qquad K \approx \frac{\rho_1 Tg_1}{\rho_2 Tg_2}$$

Equation 5: Gordon-Taylor equation simplified by application of the Simha-Boyer rule; w_i = weight fractions of the components, K = parameter, ρ_i = densities of the amorphous components, subscript 2 = compound with the higher T_g

The correspondence of experimental data with the Gordon-Taylor equation serves as a criterion of ideality for mixing of the two components (Forster et al. 2003).

7.2.2.19 Saturation solubility

For the determination of the saturation solubility solutions with a surplus of drug were prepared and shaken at 37 °C for seven days. Afterwards the solutions were filtered, and the drug concentration was measured via UV-spectroscopy at 37 °C.

7.2.2.20 Scanning electron microscopy

Samples were coated with gold for 180 s under argon atmosphere using an Agar Manual Sputter Coater (Agar Scientific, Stansted, UK). Coated samples were mounted onto specimen stubs with double-sided carbon tape and scanned under high vacuum with a LEO VP 1430 (Carl Zeiss, Jena, Germany). The measurements were operated with a voltage of 10 to 20 kV. The morphologies of the extrudates and the extrudates exposed to dissolution were observed at magnifications of 100 x and 500 x.

7.2.2.21 Thermogravimetric analysis

The decomposition of substances was determined by thermogravimetric analyis (TGA SDTA 851^e, Mettler-Toledo, Gießen, Germany). Samples of 5 mg were heated from 25 to 250 °C with a heating rate of 5 K/min.

7.2.2.22 X-ray powder diffraction

The crystallinity of the milled extrudates, extrudates, and tablets was measured using a Miniflex apparatus (Rigaku, Munich, Germany) with CuKα radiation. Samples were prepared into aluminum frames. For the preparation the front of the frames was mounted on a smooth Teflon plate. The samples were filled into the window and were compressed with a slide. This procedure avoided a preferential orientation of the particles.

Diffraction patterns were obtained at a voltage of 45 kV and a current of 40 mA. Samples were scanned in a 2Θ range from 5° to 40° with a scanning speed of 2 °/min and an intensity of 1000 cps.

7.2.3 Storage conditions for stability testing

Stability tests (Table 7.12) according to the ICH harmonised tripartite guidelines "Stability testing of new drug substances and products Q1A (R2)" (2003) were performed to determine the physical stability of the solid dispersions under the influence of the environmental factors temperature and humidity. Samples were stored in a conditioning cabinet (KBF 240, Binder, Tuttlingen, Germany) for storage at accelerated conditions.

Table 7.12: Storage conditions for stability testing of solid dispersions

study	storage condition	period
long-term	25 °C and 60% RH open	6 months
accelerated	40 °C and 75% RH aluminum foil	6 months

As the storage conditions and the lengths of studies chosen should be sufficient to cover storage, shipment, and subsequent use, long-term testing should cover a minimum of 12 months' duration. Data from the accelerated storage conditions can be used to evaluate the effect of short term excursions outside the label storage conditions, such as might occur during shipping.

In this study stability data for six months are presented as the tests are still ongoing.

8 Appendix

8.1 Characterization of model drug
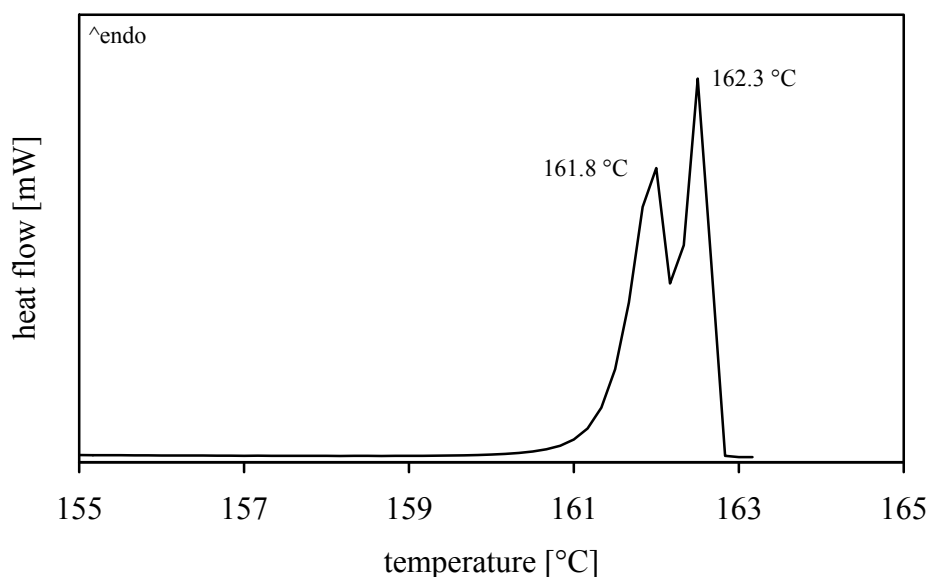
Figure 8.1: DSC analysis (chapter 7.2.2.7) of celecoxib, which shows a DSC melting transition when scanned at 0.5 °C/min

Table 8.1: Saturation solubility (chapter 7.2.2.19) of celecoxib in different media; since celecoxib has a higher solubility in cetrimid solutions than in SDS solutions, cetrimid was chosen as surfactant for dissolution studies.

Medium	c_s [mg/L]
H_2O	2.58
0.1 N HCl	3.15
0.1 N HCl + 0.30 % cetrimid	254.19
0.1 N HCl + 0.50 % cetrimid	328.34
0.1 N HCl + 0.30 % SDS	83.28
0.1 N HCl + 0.50 % SDS	141.12
0.1 N HCl + 0.75 % SDS	215.79
0.1 N HCl + 1.00 % SDS	290.01

Figure 8.2: TGA analysis (chapter 7.2.2.21) of aPMMA, celecoxib, and aPMMA/celecoxib 1:1 physical mixture; heating rate 5 K/min; black line shows weight loss of substances during heating >200 °C revealing decomposition processes

8.2 Selection of suitable carrier for solubility enhancement

Table 8.2: DSC analysis (chapter 7.2.2.7) of different carriers

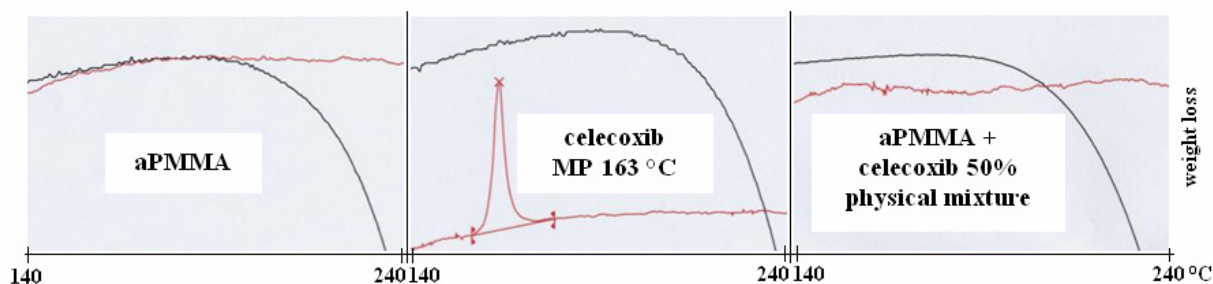| carrier	1st heating				2nd heating		
	T_g or T_m	T_{onset} [°C]	$T_{peak\ or\ mean}$ [°C]	H [J/g]	T_g or T_m	T_{onset} [°C]	$T_{peak\ or\ mean}$ [°C]
isomalt	T_m	91.9	99.1	128.2	T_g	58.6	61.0
	T_m	145.5	150.0	118.5			
lactitol	T_m	65.2	79.8	14.8	T_g	62.7	64.5
	T_m	114.7	123.2	5.5			
	T_m	152.0	155.3	154.7			
polydextrose	T_g	62.5	65.6	-	T_g	89.9	99.4
polyox	T_m	61.9	67.8	190.6	T_m	59.4	62.7
PEG 10000	T_m	60.2	62.5	197.6	T_m	60.3	62.4
PEG 4000	T_m	56.6	60.2	195.8	T_m	55.0	57.4
					T_m	57.9	61.1
aPMMA	T_g	57.9	60.1	-	T_g	32.9*	43.6*
PEG-PVA	T_g	45.7	51.9	-	T_g	25.6	36.0
PVP K30	T_g	157.6	161.8	-	T_g	156.7	162.0
crospovidone	T_m	131.8	135.3	0.5	T_m	142.6	145.0
copovidone	-	-	-	-	T_g	101.5	106.9
PVA	-	-	-	-	T_g	67.8	75.6
HPMCAS	T_g	115.5	125.5	-	T_g	114.1	119.3
HPMC	T_g	175.7	177.8	-	T_g	131.7	141.5
HPC	-	-	-	-	T_g	96.4*	102.1*
CMCNa	-	-	-	-	T_g	78.3	98.0
Gelucire	T_m	43.7	46.5	116.5	T_m	40.4	44.2
Tefose	T_m	30.0	36.2	86.7	T_m	24.6	31.3
	T_m	44.4	53.0	18.9	T_m	32.9	36.2
					T_m	33.8	41.0
					T_m	46.0	52.3
Carbopol	T_g	128.1	130.5	-	T_g	125.5	128.7
					T_g	143.1*	144.2*
Pemulen	T_g	127.9	129.9	-	T_g	126.6	129.7
					T_g	139.9*	140.8*

Table 8.3: Three-dimensional (δ_d, δ_p, δ_h), combined (δ_v), total (δ_t) solubility parameters, and molar volume of different carriers calculated with the computer program SPWin (chapter 7.2.2.2)

| carrier	δ_d [MPa$^{0.5}$]	δ_p [MPa$^{0.5}$]	δ_h [MPa$^{0.5}$]	δ_v [MPa$^{0.5}$]	δ_t [MPa$^{0.5}$]	molar volume [cm^3/mol]
isomalt	21.24	8.52	32.12	22.88	39.43	181
lactitol	21.24	8.52	32.12	22.88	39.43	181
polydextrose	22.72	4.95	30.33	23.25	38.22	622
PEG 4000	17.96	1.52	10.28	18.02	20.75	3325
aPMMA	17.41	0.20	9.28	17.41	19.73	128808
PEG-PVA	21.61	0.58	26.23	21.62	33.99	31313
PVP K30	20.43	0.64	9.28	20.44	22.45	36575
copovidone	17.42	0.5	9.23	17.43	19.73	37183
PVA	22.28	0.92	29.57	22.30	37.03	12585
HPMCAS	18.71	0.74	13.40	18.72	23.02	12508
HPMC	18.95	1.14	18.53	18.98	26.53	6998
HPC	18.77	0.10	18.18	18.77	26.13	802138

128
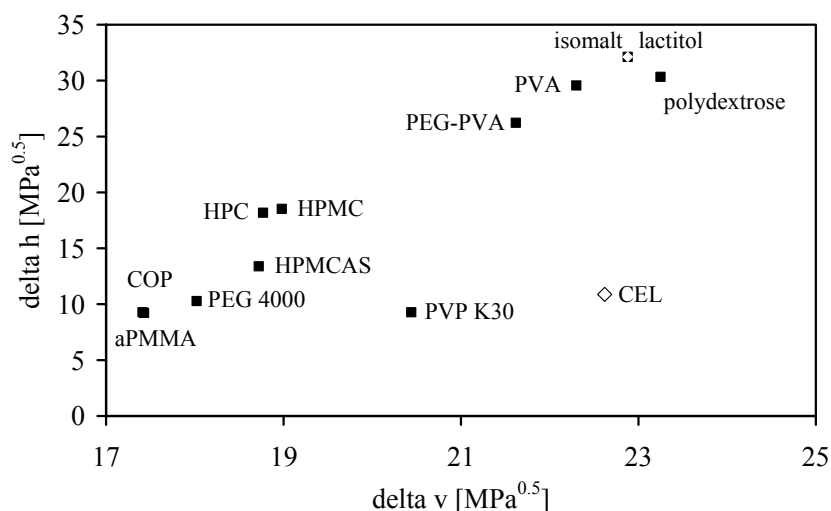
Figure 8.3: Bagley plot (chapter 7.2.2.1) representing celecoxib and carriers

Table 8.4: Prediction of miscibility by comparing experimentally determined T_g of single components, blends, and theoretically calculated (chapter 7.2.2.18) blends; GT = Gordon-Taylor

| drug / carrier	$T_{g\,mean}$ / $T_{m\,peak}$ 2nd [°C] single compound	$T_{g\,mean}$ 2nd [°C] blend	enthalpy 1st [J/g] CEL in blend	density [g/cm³] amorphous compound	T_g [°C] GT	miscible
CEL	57.5 T_g	-	102	1.399	-	/
isomalt	61.0 T_g	55.3 T_g 162.7 T_m	100	-	-	-
lactitol	64.5 T_g	57.9 T_g 60.4 T_g 65.6 T_g 162.4 T_m	93	-	-	-
polydextrose	99.4 T_g	56.9 T_g	93	-	-	-
polyox	62.7 T_m	36.8 T_g	0	-	-	+
PEG 4000	57.4 T_m 61.1 T_m	30.1 T_g	0	-	-	+
aPMMA	43.6 T_g	56.9 T_g	85	1.114	40.2	+
PEG-PVA	36.0 T_g	39.4 T_g*	54	1.060	33.4	+
PVP K30	162.0 T_g	100.3 T_g	71	1.215	85.0	+
crospovidone	145.0 T_m	132.6 T_m	85	-	-	+
copovidone	106.9 T_g	91.7 T_g	63	1.235	73.2	+
PVA	75.6 T_g	59.0 T_g	92	1.308	61.3	+
HPMCAS	119.3 T_g	72.9 T_g	81	1.306	75.7	+
HPMC	141.5 T_g	82.2 T_g	77	1.292	79.5	+
HPC	102.1 T_g	46.1 T_g	84	1.198	72.1	±
CMCNa	98.0 T_g	60.0 T_g	96	1.599	64.3	+
PEGglycerol laurate	44.2 T_m	-	51*	-	-	+
PEOstearates	31.3 T_m 36.2 T_m 41.0 T_m 52.3 T_m	not detectable	9	-	-	+
Carbopol	128.7 T_g	57.4 T_g 129.4 T_g	91	1.470	76.4	-
Pemulen	129.7 T_g	57.2 T_g 163.8 T_m	154	1.431	77.0	-
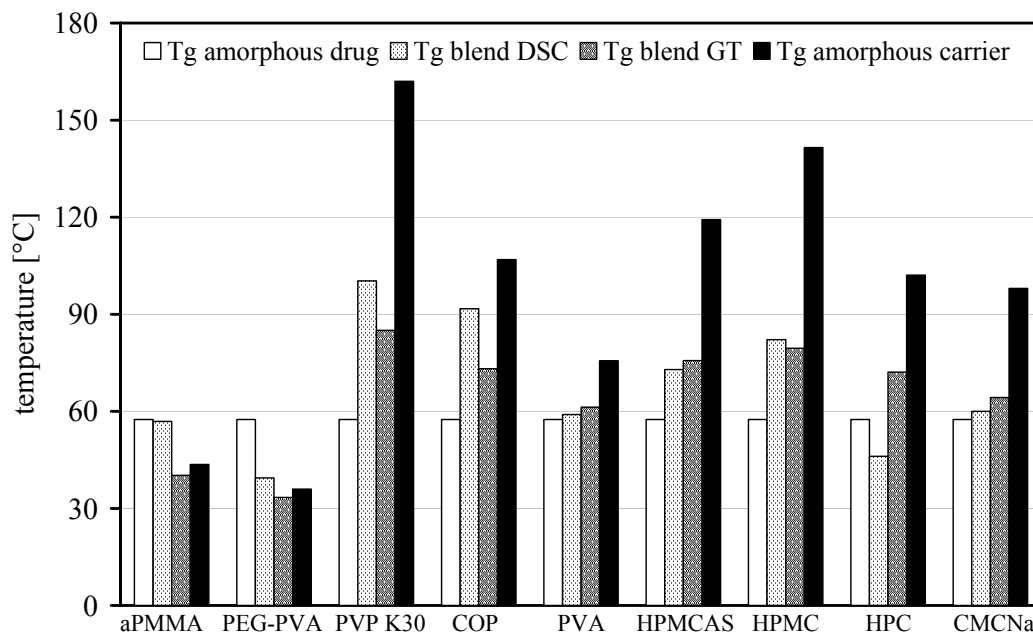
Figure 8.4: Prediction of miscibility by comparing T_g of single components with experimentally determined and theoretically calculated (chapter 7.2.2.18) T_g of blends
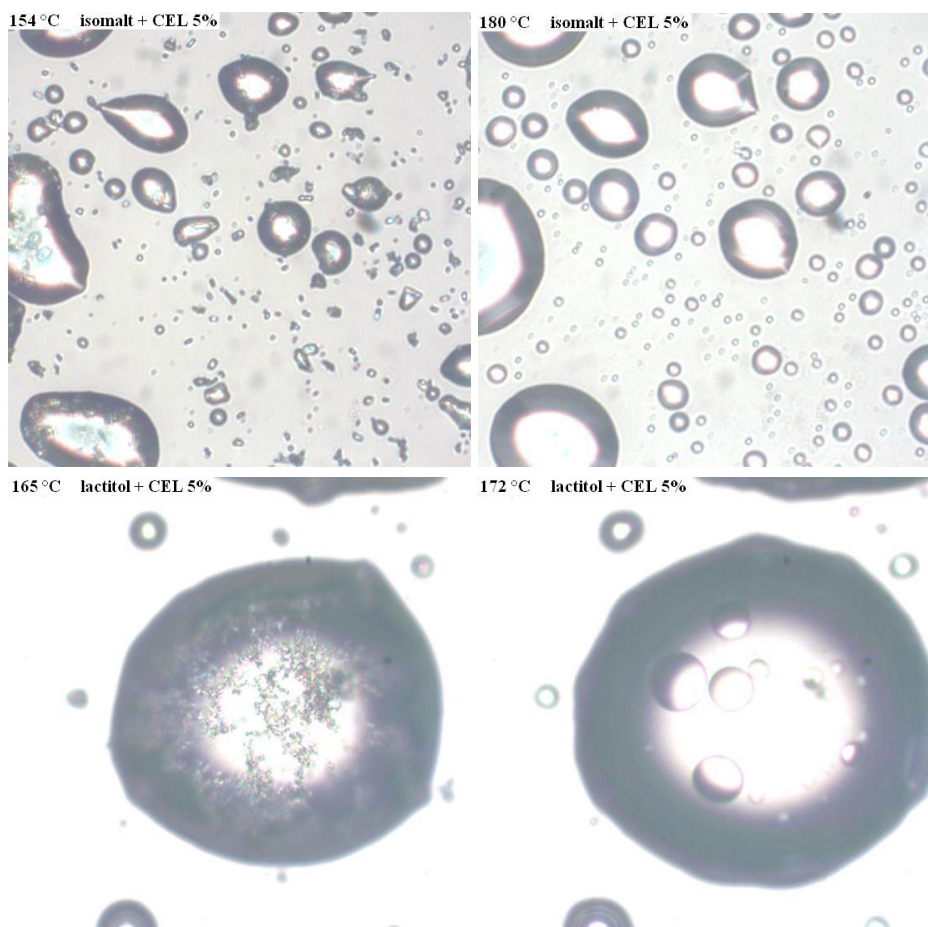

Figure 8.5: Examination of the miscibility of celecoxib with isomalt and lactitol in the molten state by hot stage microscopy (chapter 7.2.2.13); two-phase systems indicate immiscibility of the substances
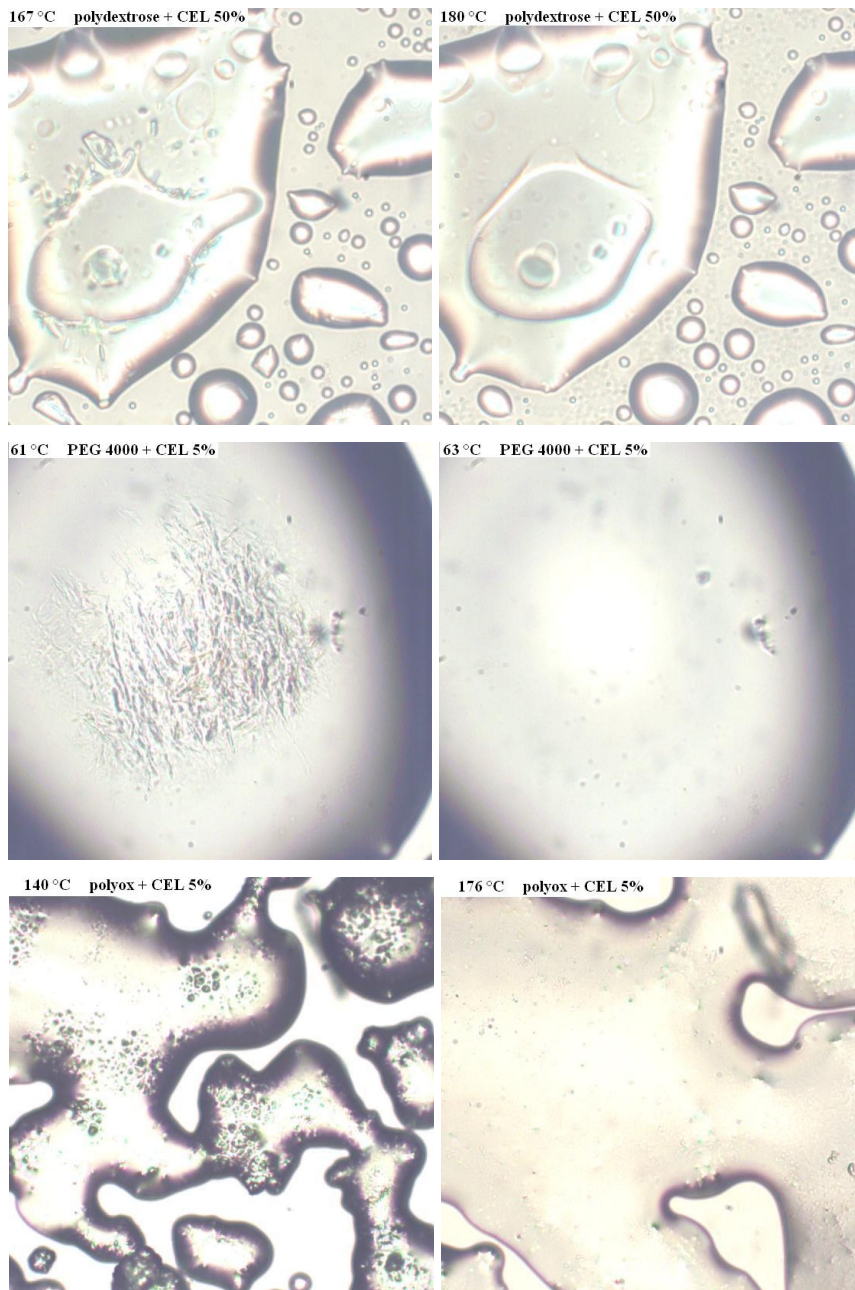
Figure 8.6: Examination of the miscibility of celecoxib with polydextrose, PEG, and polyox in the molten state by hot stage microscopy (chapter 7.2.2.13); two-phase systems indicate immiscibility of the substances
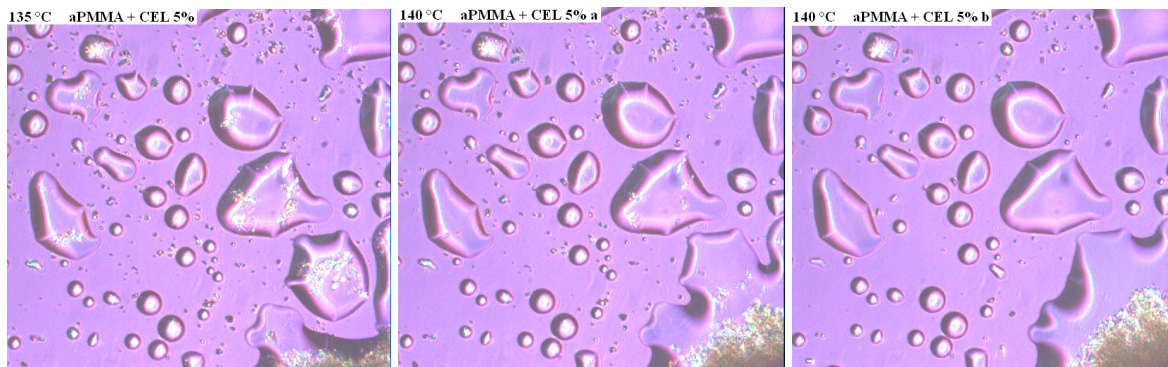

Figure 8.7: Examination of the miscibility of celecoxib with aPMMA in the molten state by hot stage microscopy (chapter 7.2.2.13); miscibility is dependent on the heating rate

Table 8.5: Intrinsic dissolution (chapter 7.2.2.14) of physical mixtures and melts with 50% celecoxib; intrinsic dissolution of celecoxib is 0.013 mg/min

carrier	physical mixtures		melts	
	dissolution rate [mg/min]	R²	dissolution rate [mg/min]	R²
isomalt	0.013 ± 0.00	0.998 ± 0.00	0.035 ± 0.00	0.983 ± 0.01
lactitol	0.014 ± 0.00	1.000 ± 0.00	0.038 ± 0.00	0.974 ± 0.01
polydextrose	0.016 ± 0.00	1.000 ± 0.00	0.017 ± 0.00	0.995 ± 0.00
polyox	0.017 ± 0.00	0.992 ± 0.00	0.014 ± 0.00	0.990 ± 0.00
PEG 10000	0.016 ± 0.00	0.993 ± 0.00	0.022 ± 0.00	0.980 ± 0.01
PEG 4000	0.016 ± 0.00	0.992 ± 0.00	0.019 ± 0.00	0.990 ± 0.01
aPMMA	0.024 ± 0.00	0.999 ± 0.00	2.601 ± 0.02	0.996 ± 0.00
PEG-PVA	0.261 ± 0.01	0.984 ± 0.01	4.517 ± 0.64	0.915 ± 0.01
crospovidone	0.531 ± 0.09	0.756 ± 0.06	0.160 ± 0.03	0.976 ± 0.01
HPMCAS	0.006 ± 0.00	0.937 ± 0.01	0.003 ± 0.00	0.907 ± 0.04
Gelucire	0.014 ± 0.00	0.998 ± 0.00	-	
Tefose	0.181 ± 0.02	0.997 ± 0.00	-	
Carbopol	0.033 ± 0.00	0.983 ± 0.00	0.005 ± 0.00	0.959 ± 0.02
Pemulen	0.002 ± 0.00	0.394 ± 0.04	0.005 ± 0.00	0.802 ± 0.01

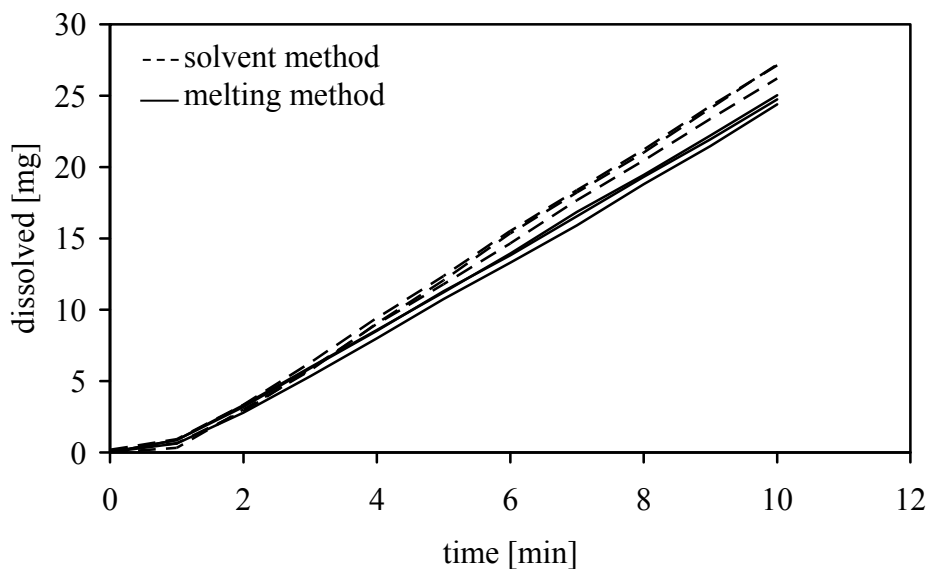## 8.3 Selection of suitable technique for solid dispersion formation

Figure 8.8: Comparison of intrinsic dissolution profiles of aPMMA/celecoxib 1:1 solid dispersions prepared by the solvent (chapter 7.2.1.2) and the melting (chapter 7.2.1.1) method
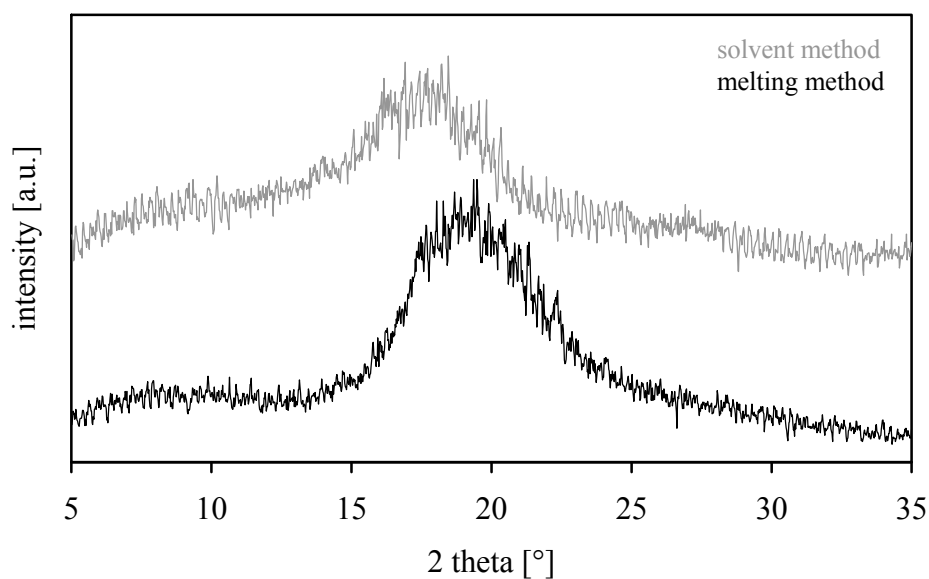
Figure 8.9: XRPD (chapter 7.2.2.22) patterns of aPMMA/celecoxib 1:1 solid dispersions prepared by the solvent and the melting method

8.4   Investigation of powder properties

Table 8.6: Particle density (chapter 7.2.2.12) of amorphous celecoxib and carriers for prediction of the glass transition temperature according to Gordon-Taylor and Simha-Boyer (chapter 7.2.2.18); n=3

substance	mean density [g/cm³]	SD density [g/cm³]
celecoxib	1.399	0.004
aPMMA	1.114	0.001
carbomer copolymer	1.428	0.002
carbomer homopolymer	1.474	0.004
CMC Na	1.599	0.001
COP	1.235	0.002
HPC	1.198	0.001
HPMC	1.292	0.003
HPMCAS	1.306	0.001
PEG-PVA	1.060	0.035
polyox	1.241	0.000
PVA	1.308	0.001
PVP K30	1.215	0.005

Table 8.7: Particle size (chapter 7.2.2.16) of drugs and aPMMA; n=3

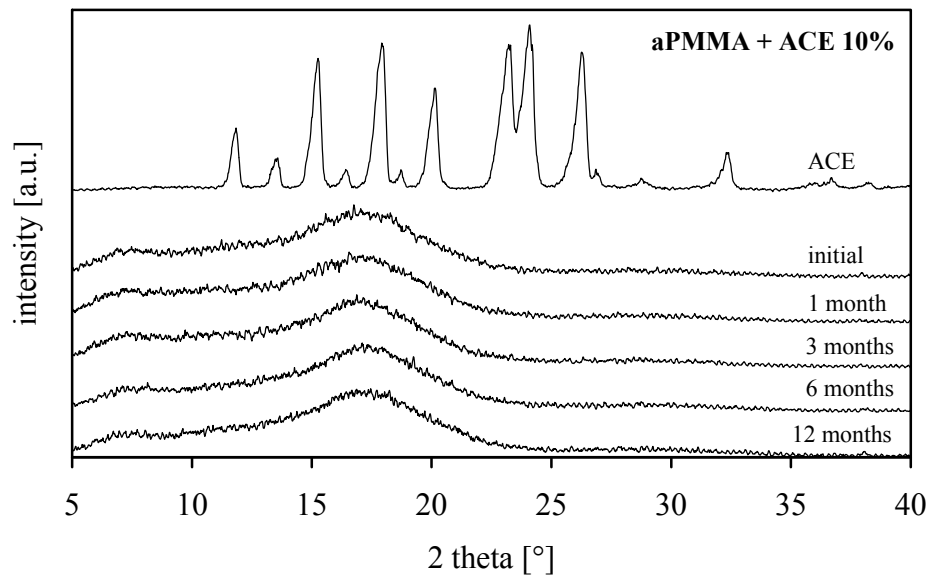| drug	x10 [µm]	x50 [µm]	x90 [µm]
ACE	3.4 ± 0.1	16.3 ± 0.2	69.6 ± 2.1
CEL	1.2 ± 0.0	5.8 ± 0.1	17.0 ± 0.0
ETO	8.0 ± 0.0	24.9 ± 0.1	104.2 ± 0.9
IBU	13.8 ± 0.1	90.7 ± 2.3	220.8 ± 10.4
NAP	9.7 ± 0.4	24.8 ± 0.3	48.4 ± 1.4
OXC	0.7 ± 0.0	1.5 ± 0.0	2.9 ± 0.0
aPMMA	2.5 ± 0.0	9.3 ± 0.0	15.1 ± 0.0

8.5 Stability of solid dispersions

Figure 8.10: Stability of aPMMA/acetaminophen 9:1 (w/w) extrudates at 25 °C over silica gel
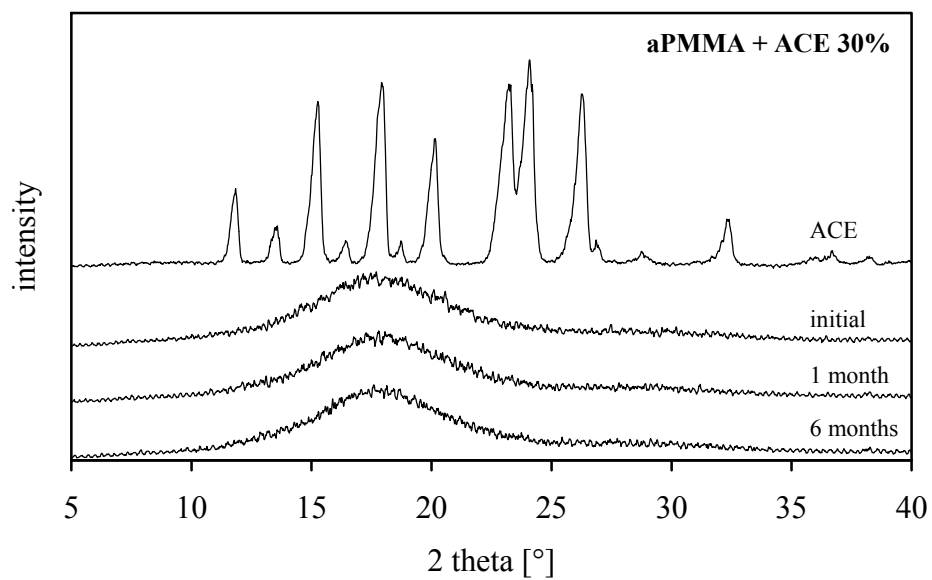

Figure 8.11: Stability of aPMMA/acetaminophen 7:3 (w/w) extrudates at 25 °C over silica gel
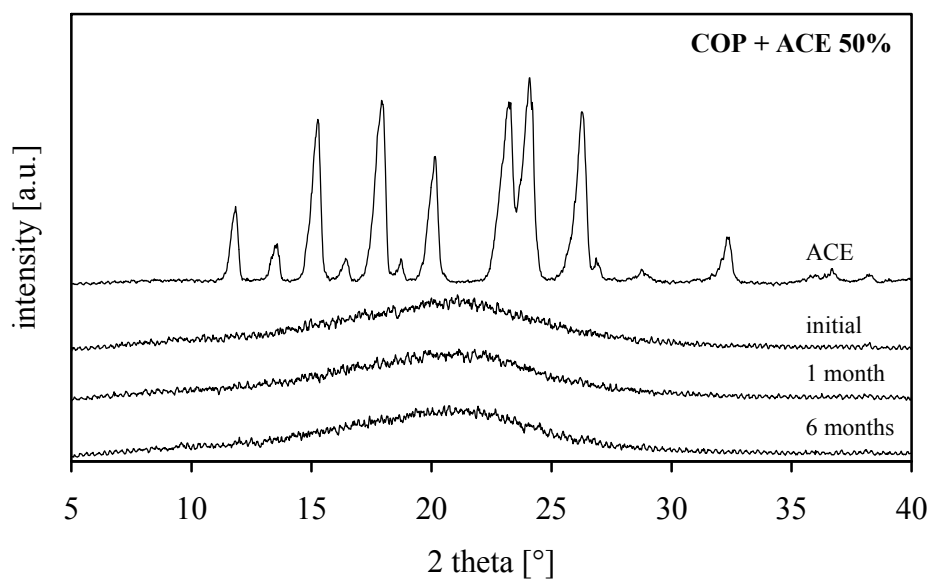
Figure 8.12: Stability of COP/acetaminophen 1:1 (w/w) extrudates at 25 °C over silica gel
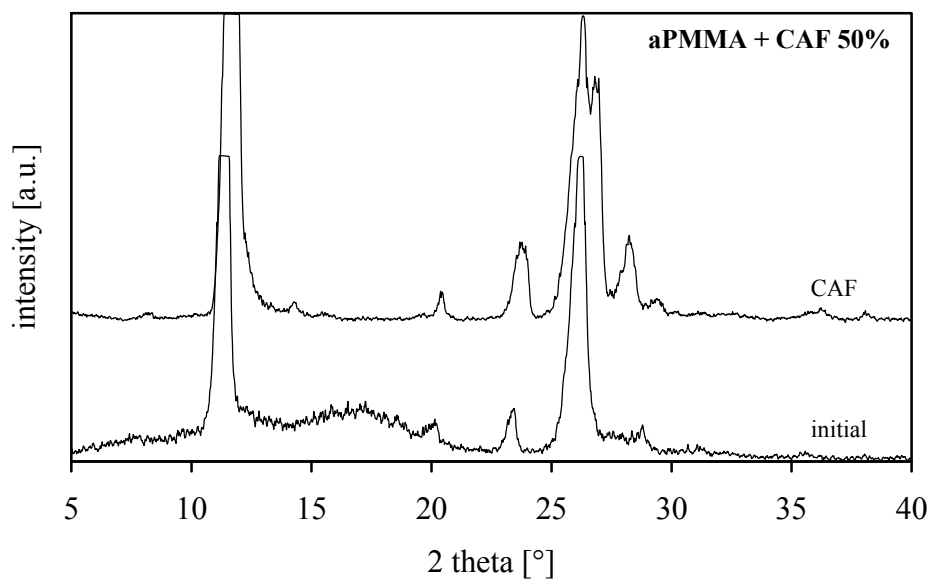

Figure 8.13: Stability of aPMMA/caffeine 1:1 (w/w) extrudates at 25 °C over silica gel

Figure 8.14: Stability of aPMMA/etofylline 1:1 (w/w) extrudates at 25 °C over silica gel

Figure 8.15: Stability of COP/etofylline 1:1 (w/w) extrudates at 25 °C over silica gel

136

Figure 8.16: Stability of PEG-PVA/etofylline 1:1 (w/w) extrudates at 25 °C over silica gel

Figure 8.17: Stability of aPMMA/ibuprofen 1:1 (w/w) extrudates at 25 °C over silica gel

Figure 8.18: Stability of PEG-PVA/naproxen 1:1 (w/w) extrudates at 25 °C over silica gel

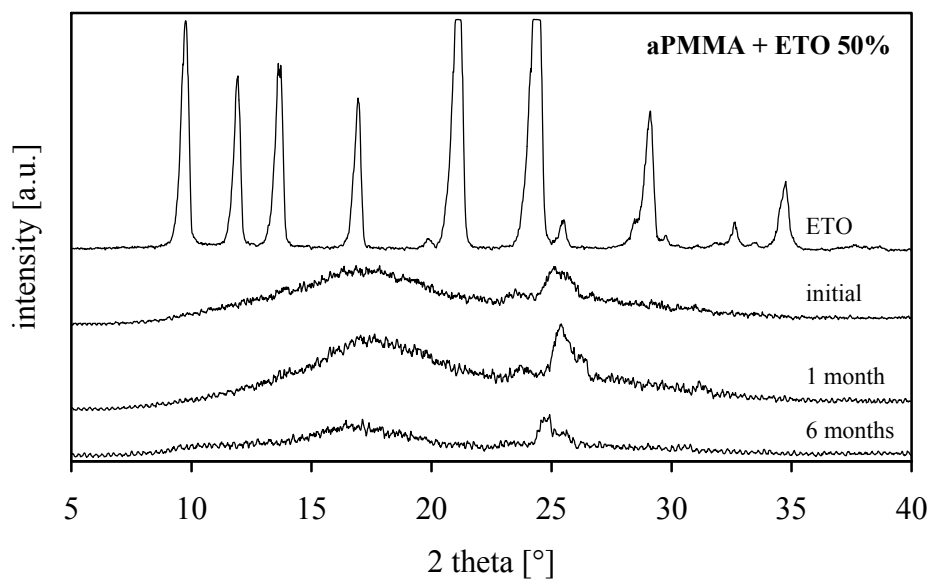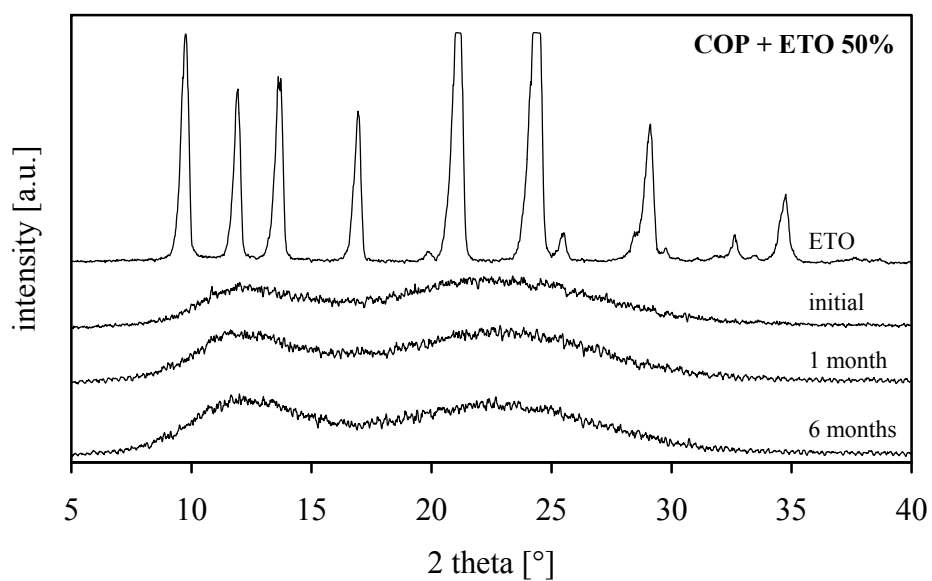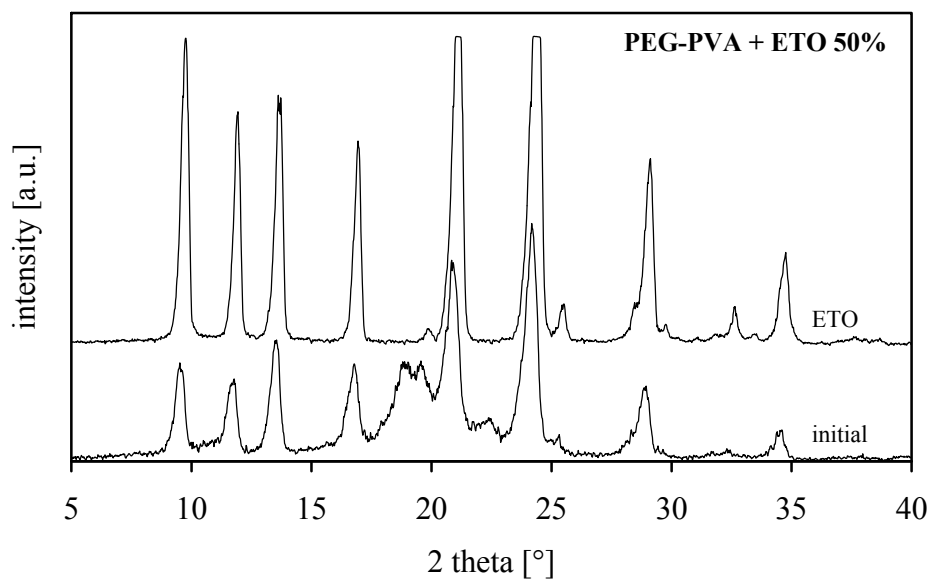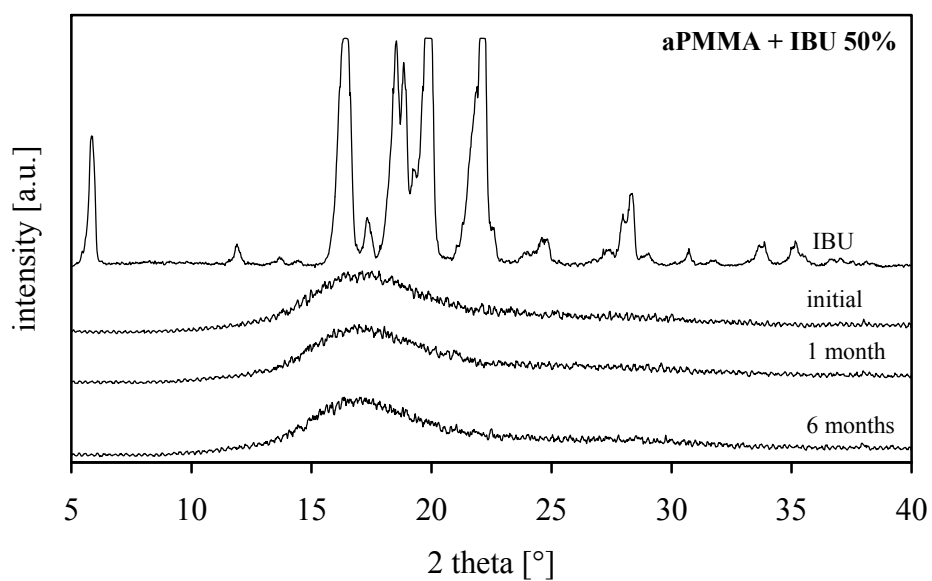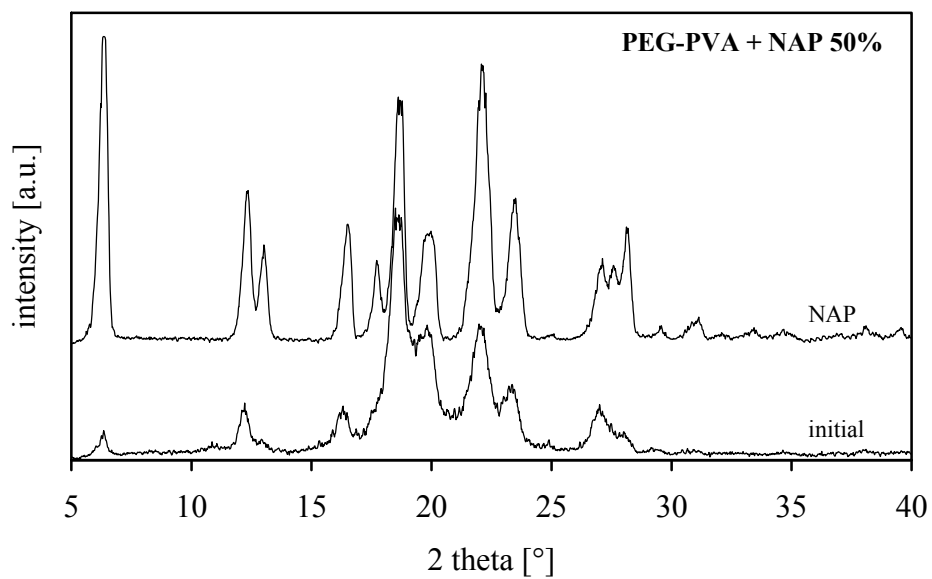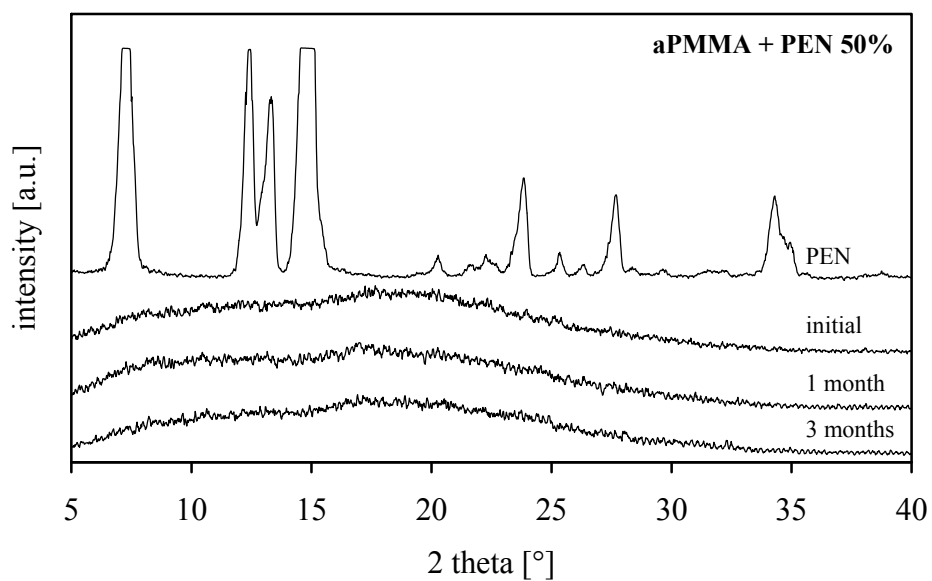Figure 8.19: Stability of aPMMA/pentoxyfylline 1:1 (w/w) extrudates at 25 °C over silica gel

9   Bibliography

Albers J, Knop K & Kleinebudde P. Brand-to-brand and batch-to-batch uniformity of microcrystalline cellulose in direct tableting with a pneumohydraulic tablet press. *Pharm Ind* 68 (2006) 1420-1428.

Amidon GL, Lennernäs H, Shah VP & Crison JR. A Theoretical basis for a biopharmaceutic drug classification - the correlation of in-vitro drug product dissolution and in-vivo bioavailability. *Pharm Res* 12 (1995) 413-420.

Bagley EB, Nelson TP & Scigliano JM. Three-dimensional solubility parameters and their relationship to internal pressure measurements in polar and hydrogen bonding solvents. *J Paint Technol* 43 (1971) 35-42.

Banga S, Chawla G, Varandani D, Mehta BR & Bansal AK. Modification of the crystal habit of celecoxib for improved processability. *J Pharm Pharmacol* 59 (2007) 29-39.

Bansal AK, Mulla M & Kakumanu VK. Criticality of functional excipients and decoding methods during generic product development. *Pharm Technol Eur* (2006) 34-38.

Berendsen HJC, van der Spoel D & van Drunen R. GROMACS: a message-passing parallel molecular dynamics implementation. *Comp Phys Commun* 91 (1995) 43-56.

Breitenbach J. Melt extrusion: from process to drug delivery technology. *Eur J Pharm Biopharm* 54 (2002) 107-117.

Breitkreutz J. Prediction of intestinal drug absorption properties by three-dimensional solubility parameters. *Pharm Res* 15 (1998) 1370-1375.

Chawla G Gupta P Thilagavathi R Chakraborti AK, Bansal AK. Characterization of solid-state forms of celecoxib. *Eur J Pharm Sci* 20 (2003) 305-317.

Chiou WL & Riegelman S. Pharmaceutical applications of solid dispersion systems. *J Pharm Sci* 60 (1971) 1281-1302.

Chowhan MA & Chen H. Ophthalmic compositions containing a synergistic combination of three polymers. *US patent 7306802* (2007).

Constantinides PP. Lipid microemulsions for improving drug dissolution and dral absorption - physical and biopharmaceutical aspects. *Pharm Res* 12 (1995) 1561-1572.

Corrigan OI. Mechanisms of dissolution of fast release solid dispersions. *Drug Dev Ind Pharm* 11 (1985) 697-724.

Craig DQM, Royall PG, Kett VL & Hopton ML. The relevance of the amorphous state to pharmaceutical dosage forms: glassy drugs and freeze dried systems. *Int J Pharm* 179 (1999) 179-207.

Craig DQM. The mechanisms of drug release from solid dispersions in water-soluble polymers. *Int J Pharm* 231 (2002) 131-144.

Crowley MM, Zhang F, Repka MA, Thumma S, Upadhye SB, Battu SK, McGinity JW & Martin C. Pharmaceutical applications of hot-melt extrusion: Part I. *Drug Dev Ind Pharm* 33 (2007) 909-926.

Debenedetti PG & Stillinger FH. Supercooled liquids and the glass transition. Nature 410 (2001) 259-267.

Djuric D & Kleinebudde P. Impact of screw elements on continuous granulation with a twin-screw extruder. *J Pharm Sci* 25 (2008) 1-9.

Doelker M, Adel El-Egakey M, Soliva M & Speiser P. Hot extruded dosage forms. *Pharm Acta Helv* 46 (1971) 31-52.

Dressman JB, Butler J, Hempenstall J & Reppas C. The BCS: Where do we go from here? *Pharm Technol* 25 (2001) 68-76.

Fedors RF. A method for estimating both the solubility parameters and molar volumes of liquids. *Pol Eng Sci* 14 (1974) 147-154.

Ferro LJ & Miyake PJ. Polymorphic crystalline forms of celecoxib. *WO 01/42222 A1* (2001).

Forster A, Hempenstall J & Rades T. Characterization of glass solutions of poorly water-soluble drugs produced by melt extrusion with hydrophilic amorphous polymers. *J Pharm Pharmacol* 53 (2001a) 303-315.

Forster A, Hempenstall J, Tucker I & Rades T. Selection of excipients for melt extrusion with two poorly water-soluble drugs by solubility parameter calculation and thermal analysis. *Int J Pharm* 226 (2001b) 147-161.

Forster A, Hempenstall J, Tucker I & Rades T. The potential of small-scale fusion experiments and the Gordon-Taylor equation to predict the suitablity of drug/polymer blends for melt extrusion. *Drug Dev Ind Pharm* 27 (2001c) 549-560.

Forster A, Hempenstall J & Rades T. Comparison of the Gordon-Taylor and Couchman-Karasz equations for prediction of the glass transition temperature of glass solutions of drug and polyvinylpyrrolidone prepared by melt extrusion. *Pharmazie* 58 (2003) 838-839.

Gordon M & Taylor JS. Ideal copolymers and the second-order transitions of synthetic rubbers. I. Non-crystalline copolymers. J Appl Chem 2 (1952) 493-500.

Govindarajan R & Suryanarayanan R. Processing-induced transformations and their implications on pharmaceutical product quality. In *Hilfiker R (Ed). Polymorphism: In the Pharmaceutical Industry*. Weinheim: Wiley-VCH. (2006) 333-364.

Greenhalgh DJ, Williams AC, Timmins P & York P. Solubility parameters as predictors of miscibility in solid dispersions. *J Pharm Sci* 88 (1999) 1182-1190.

Gröning R & Braun FJ. Threedimensional solubility parameters and their use in characterising the permeation of drugs through the skin. *Pharmazie* 51 (1996) 337-341.

Gryczke A. Downstream processing of extrudates via pelletisation, granulation and milling. *APV Experts' Workshop on Hot melt extrusion and its use in the manufacturing of pharmaceutical dosage forms.* Ludwigshafen (2008).

Gupta P Thilagavathi R, Chakraborti, AK & Bansal AK. Differential molecular interactions between the crystalline and the amorphous phases of celecoxib. *J Pharm Pharmacol* 57 (2005) 1271-1278.

Hancock BC, Shamblin SL & Zografi G. Molecular mobility of amorphous pharmaceutical solids below their glass transition temperatures. *Pharm Res* 12 (1995) 799-806.

Hancock BC & Zografi G. Characteristics and significance of the amorphous state in pharmaceutical systems. *J Pharm Sci* 86 (1997) 1-12.

Hancock BC & Christensen K. Estimating the critical molecular mobility temperature (T_K) of amorphous pharmaceuticals. *Pharm Res* 15 (1998) 1649-1651.

Hansen CM. The universality of the solubility parameter. *Ind Eng Chem Res Dev* 8 (1969) 2-11.

ICH Harmonised tripartite guideline. Stability testing of new drug substances and products Q1A(R2). *International Conference on Harmonisation* (2003).

Janssens S, de Armas HN, Remon JP & Van den Mooter G. The use of a new hydrophilic polymer, Kollicoat IR[®], in the formulation of solid dispersions of itraconazole. *Eur J Pharm Sci* 30 (2007) 288-294.

Kakumanu VK & Bansal AK. Enthalpy relaxation studies of celecoxib amorphous mixtures. Pharm *Res* 19 (2002) 1873-1878.

Kaushal AM, Gupta P & Bansal AK. Amorphous Drug Delivery Systems: Molecular aspects, design, and performance. *Crit Rev Ther Drug Carrier Syst* 21 (2004) 133-193.

Kerns EH. High throughput physicochemical profiling for drug discovery. *J Pharm Sci* 90 (2001) 1838-1858.

Langer M. Glasartige feste Lösungen schwerlöslicher Arzneistoffe in Zuckeralkoholen. *Dissertation University Düsseldorf* (2003).

Langer M, Holtje M, Urbanetz NA, Brandt B, Holtje HD & Lippold BC. Investigations on the predictability of the formation of glassy solid solutions of drugs in sugar alcohols. *Int J Pharm* 252 (2003b) 167-179.

Law D, Krill SL, Schmitt EA, Fort JJ, Qiu Y, Wang W & Porter WR. Physicochemical considerations in the preparation of amorphous ritonavir-poly (ethylene glycol) 8000 solid dispersions. *J Pharm Sci* 90 (2001) 1015-1025.

Leuner C. Verbesserung des Freisetzungsverhaltens von Itraconazol durch feste Dispersionen. *Dissertation university Frankfurt* (2004).

Leuner C & Dressman J. Improving drug solubility for oral delivery using solid dispersions. *Eur J Pharm Biopharm* 50 (2000) 47-60.

Lindahl E, Hess B & van der Spoel D. GROMACS 3.0: a package for molecular simulation and trajectory analysis. *J Mol Model* 7 (2001) 306-317.

Maegerlein M. Solid dispersions of poorly water soluble substances – a challenge for analytical development. *Innovative Drug Delivery Technologien zur Verbesserung der Bioverfügbarkeit APV-Kurs* Ludwigshafen (2005).

McGinity JW & Zhang F. Melt-extruded controlled-release dosage forms. In *Ghebre-Sellassie I & Martin C (Eds). Pharmaceutical extrusion technology*. New York: Marcel Dekker. 133 (2003) 183-208.

Meylan WM & Howard PH. Atom/fragment contribution method for estimating octanol-water partition coefficient. *J Pharm Sci* 84 (1995) 83-92.

Meylan WM & Howard PH. Estimating log P with atom/fragments and water solubility with log P. *Persp Drug Disc Des* 19 (2000) 67-84.

Mittwollen JP, Solution polymers for melt extrusion applications. *APV Experts' Workshop on Hot melt extrusion and its use in the manufacturing of pharmaceutical dosage forms*. Ludwigshafen (2008).

Moneghini M, Carcano A, Zingone G & Perissutti B. Studies in dissolution enhancement of atenolol. *Int J Pharm* 175 (1998) 177-183.

Müller RH, Jacobs C & Kayser O. Nanosuspensions as particulate drug formulations in therapy Rationale for development and what we can expect for the future. *Adv Drug Del Rev* 47 (2001) 3-19.

Nakamichi K, Nakano T, Yasuura H, Izumi S & Kawashima Y. The role of the kneading paddle and the effects of screw revolution speed and water content on the preparation of solid dispersions using a twin-screw extruder. *Int J Pharm* 241 (2002) 203-211.

Neil JM, Fell AF & Smith G. Evaluation of the stability of frusemide in intravenous infusions by reversed-phase high-performance liquid-chromatography. *Int J Pharm* 22 (1984) 105-126.

Nollenberger K. Solubility enhancement of felodipine by melt extrusion. *International Symposium on Hot Melt Extrusion Frankfurt* (2007).

Noyes AA & Whitney WR. The rate of solution of solid substances in their own solutions. *J Am Chem Soc* 19 (1897) 930-934.

Oladiran GS & Batchelor HK. Determination of ibuprofen solubility in wax: A comparison of microscopic, thermal and release rate techniques. *Eur J Pharm Biopharm* 67 (2007) 106-111.

Palzer S. The effect of glass transition on the desired and undesired agglomeration of amorphous food powders. *Chem Eng Sci* 60 (2005) 3959-3968.

Paulson S, Vaughn M, Jessen S, Lawal Y, Gresk C, Yan B, Maziasz T, Cook C & Karim A. Pharmacokinetics of celecoxib after oral administration in dogs and humans: effect of food and site of absorption. *J Pharmacol Exp Ther* 297 (2001) 638-645.

Phuapradit W. Controlled release of a poorly water-soluble drug from hot-melt extrudates containing acrylic polymers. *International Symposium on Hot Melt Extrusion Frankfurt* (2007).

Pouton CW. Formulation of self-emulsifying drug delivery systems. *Adv Drug Del Rev* 25 (1997) 47-58.

Qui S, Gryczke A, Belton P & Craig DQM. Characterisation of solid dispersions of paracetamol and Eudragit® E prepared by hot-melt extrusion using thermal, microthermal and spectroscopic analysis. *Int J Pharm* 354 (2008) 158-167.

Quinteros DA, Rigo VR, Kairuz AFJ, Olivera ME, Manzo RH & Allemandi DA. Interaction between a cationic polymethacrylate (Eudragit E) and anionic drugs. *Eur J Pharm Sci* 33 (2008) 72-79.

Repka MA, Gerding TG, Repka SL & McGinity JW. Influence of plasticizers and drugs on the physical-mechanical properties of hydroxypropylcellulose films prepared by hot melt extrusion. *Drug Dev Ind Pharm* 25 (1999) 625-633.

Repka MA, Battu SK, Upadhye SB, Thumma S, Crowley MM, Zhang F, Martin C & McGinity JW. Pharmaceutical applications of hot-melt extrusion: Part II. *Drug Dev Ind Pharm* 33 (2007) 1043-1057.

Rosenberg J. Manufacturing of pharmaceutical dosage forms using melt-extrusion technology. In *Bröckel U, Meier W & Wagner G (Eds). Product Design and Engeneering: Best Practices*. Weinheim: Wiley-VCH. (2007) 247-257.

Schamp K. Lipidartige Formulierungen zur Verbesserung der Bioverfügbarkeit schwer löslicher Arzneistoffe. *Dissertation University Frankfurt* 2002.

Scharf M. Rheological design of extrusion dies. *APV Experts' Workshop on Hot melt extrusion and its use in the manufacturing of pharmaceutical dosage forms*. Ludwigshafen (2008).

Sekiguchi K & Obi N. Studies on absorption of eutectic mixtures I. a comparison of the behaviour of eutectic mixtures of sulphathiazole and that of ordinary sulphathiazole in man. *Chem Pharm Bull* 9 (1961) 866-872.

Sethia S & Squillante E. Solid dispersions: Revival with greater possibilities and applications in oral drug delivery. *Crit Rev Ther Drug Carrier Syst* 20 (2003) 215-247.

Shah VP, Konecny JJ, Everett RL, McCullough B, Noorizadeh AC & Selly JP. In-vitro dissolution profile of water-insoluble drug dosage forms in the presence of surfactants. *Pharm Res* 6 (1989) 612-618.

Simha R & Boyer RF. On a general relation involving the glass temperatures and coefficient of expansion of polymers. J Chem Phys 37 (1962) 1003-1017.

Six K, Berghmans H, Leuner C, Dressman J, Van Werde K, Mullens J, Benoist L, Thimon M, Meublat L, Verreck G, Peeters J, Brewster M & Van den Mooter G. Characterization of solid dispersions of itraconazole and hydroxypropylmethylcellulose prepared by melt extrusion, Part II. *Pharm Res* 20 (2003) 1047-1054.

Six K, Verreck G, Peeters J, Brewster M & Van den Mooter G. Increased physical stability and improved dissolution properties of itraconazole, a class II drug, by solid dispersions that combine fast- and slow-dissolving polymers. *J Pharm Sci* 93 (2004) 124-131.

Suzuki H & Sunada H. Influence of water-soluble polymers on the dissolution of nifedipine solid dispersions with combined carriers. *Chem Pharm Bull* 46 (1998) 482-487.

Szente L & Szejtli J. Highly soluble cyclodextrin derivatives: chemistry, properties, and trends in development. *Adv Drug Del Rev* 36 (1999) 17-28.

Tachibana T & Nakamura A. A method for preparing an aqueous colloidal dispersion of organic materials by using water-soluble polymers: dispersion of beta-carotene by polyvinylpyrrolidone. *Kolloid-Z Polym* 203 (1965) 130-133.

Theeuwes F, Hussain A & Higuchi T. Quantitative analytical method for determination of drug dispersed in polymers using differential scanning calorimetry. *J Pharm Sci* 63 (1974) 427-429.

Urbanetz NA. Stabilität und Stabilisierung fester Dispersionen auf der Basis von Polyethylenglykol. *Dissertation University Düsseldorf* (1999).

Van Krevelen DW & Hoftyzer PJ. Properties of polymers. Their estimation and correlation with chemical structures. *Amsterdam: Elsevier*. (1976).

Van Lengerich B, Meuser F & Ng C. Extrusion technology for product design. *Product Design and Engeneering: Best Practices*. Weinheim: Wiley-VCH. (2007) 215-245.

Verreck G, Six K, Van den Mooter G, Baert L, Peeters J & Brewster ME. Characterization of solid dispersions of itraconazole and hydroxypropylmethylcellulose prepared by melt extrusion - part I. *Int J Pharm* 251 (2003) 165-174.

Verreck G, Decorte A, Heymans K, Adriaensen J, Cleeren D, Jacobs A, Liu D, Tomasko D, Arien A, Peeters J, Rombaut P, Van den Mooter G & Brewster ME. The effect of pressurized carbon dioxide as a temporary plasticizer and foaming agent on the hot melt extrusion process and extrudate properties of solid dispersions of itraconazole with PVP-VA64. *Eur J Pharm Sci* 26 (2005) 349-358.

Verreck G, Decorte A, Heymans K, Adriaensen J, Liu D, Tomasko D, Arien A, Peeters J, Van den Mooter G & Brewster ME. Hot stage extrusion of p-amino salicylic acid with EC using CO_2 as a temporary platicizer. *Int J Pharm* 327 (2006a) 45-50.

Verreck G, Decorte A, Li HB, Tomasko D, Arien A, Peeters J, Rombaut P, Van den Mooter G & Brewster ME. The effect of pressurized carbon dioxide as a plasticizer and foaming agent on the hot melt extrusion process and extrudate properties of pharmaceutical polymers. *J Supercrit Fluids* 38 (2006b) 383-391.

Yazdanian M, Briggs K, Jankovsky C & Hawi A. The "high solubility" definition of the current FDA guidance on Biopharmaceutical Classification System may be too strict for acidic drugs. *Pharm Res* 21 (2004) 293-299.

Yoshinaga M, Katsuki S, Miyazaki M, Liu L, Kihara S-I & Funatsu K. Mixing mechanism of three-tip kneading block in twin screw extruders. *Pol Eng Sci* 40 (2000) 168-178.

Zhou D, Zhang GGZ, Law D, Grant DJW & Schmitt EA. Physical stability of amorphous pharmaceuticals: Importance of configurational thermodynamic quantities and molecular mobility. *J Pharm Sci* 91 (2002) 1863-1872.

Zhu Y, Shah NH, Malick AW, Infeld MH & McGinity JW. Solid-state plasticization of an acrylic polymer with chlorpheniramine maleate and triethyl citrate. *Int J Pharm* 241 (2002) 301-310.

Zingone G & Rubessa F. Release of carbamazepine from solid dispersions with pylivinylpyrrolidone/vinylacetate copolymer (PVP/VA). *STP Pharm Sci* 4 (1994) 122-127.

Danksagung

Die vorliegende Arbeit wurde unter Leitung von Prof. Dr. P. Kleinebudde während meiner Tätigkeit als wissenschaftliche Mitarbeiterin am Institut für Pharmazeutische Technologie und Biopharmazie der Heinrich-Heine-Universität Düsseldorf in Zusammenarbeit mit der Gen-Plus GmbH & Co KG durchgeführt.

Mein besonderer Dank gilt

…meinem Doktorvater Prof. Dr. P. Kleinebudde für die Überlassung des interessanten Forschungsthemas, ebenso wie für seine fachliche Unterstützung und anregende Diskussionen. Insbesondere möchte ich mich für die Möglichkeit der Teilnahme an internationalen Kongressen, Symposien und Seminaren bedanken.

…der Firma Gen-Plus GmbH & Co KG in München, insbesondere Dr. Julia Schulze Nahrup und Dr. Peter Kraahs, für die fruchtbare Zusammenarbeit, fachliche Diskussionen, finanzielle und materielle Unterstützung und die Bereitstellung des Extruders für Versuche in München. Besonderen Dank schulde ich Rainer Alles, der mich mit seinen Erfahrungen auf dem Gebiet der Schmelzextrusion beraten und tatkräftig unterstützt hat.

…Dr. Klaus Knop, der mich mit seiner engagierten Betreuung und steten Hilfsbereitschaft während der gesamten Promotion begleitet hat.

…Prof. Dr. J. Breitkreutz für die Übernahme des Koreferats, seine stete Hilfsbereitschaft und zahlreiche Diskussionen über Löslichkeitsparameter und Molecular Modelling.

…Karin Matthée für die unermüdliche praktische Durchführung von DSC und Karl-Fischer Messungen, sowie die Aufnahme von rasterelektronenmikroskopischen Bildern.

…Prof. Dr. Dr. H.-D. Höltje vom Institut für Medizinische Chemie der Heinrich-Heine-Universität Düsseldorf, unter dessen Leitung die Moleküldynamik-Simulationen durchgeführt wurden. Ganz herzlich bedanken möchte ich mich bei Birte Schmitz für die schnelle Durchführung der Simulationen und die Erstellung der Grafiken.

…meinen Wahlpflichtstudenten Jekaterina Frenkel, Maya Petrova, Moritz Derix und Martin Köster für die FT-IR- und Kontaktwinkelmessungen, sowie die Aufnahme der Extrudatfotos.

…Dr. Andrea Burgenmeister der Firma ratiopharm in Ulm für anregende und interessante Telefonate zum Thema Schmelzextrusion.

…Kathrin Nollenberger und Christian Brunnengräber der Firma Evonik in Darmstadt für die erste Einarbeitung am Extruder und die Einweihung in die Geheimnisse der Schmelzextrusion.

…Stefan Stich und der Feinmechanik für die schnelle Anfertigung spezieller Probenbehältnisse und Geräte.

…Kristina Bräunig der Firma BASF in Ludwigshafen für die freundliche Zusammenarbeit und die Unterstützung bei Fragen zu Hilfsstoffen und Prozessen.

…allen Mitarbeitern des Instituts für Pharmazeutische Technologie und Biopharmazie und der Firma Gen-Plus für die kollegiale Zusammenarbeit, sowie gemeinsame Unternehmungen, Fahrten und Erlebnisse.

…Barbara Voß, Rieke Draheim und Joshua Müller für ihren Einsatz beim Korrekturlesen und ihre Unterstützung, insbesondere beim Abschluss der Arbeit.

…meiner Familie, ohne deren Hilfe ich dieses Ziel nicht erreicht hätte.